Politecnico di Torino

Master of Science program in
Architecture for Sustainability Design
Academic year 2021/2022
Graduation Session July 2022

Master Degree Thesis

Rhino-Grasshopper EnergyPlus Interfaces

Development of a simple input compiler to study technological strategies for low-energy buildings

Supervisor:
Giacomo Chiesa

Candidate:
Eleonora Vignani s275254

To my friends and beloved ones

To Concreto

CONTENTS

LIST OF FIGURES

LIST OF TABLES

LIST OF ABBREVIATIONS

EU	European Union
GHGs	Green House Gasses
EPBD	Energy Performance of Building Directive
EPB	Energy Performance of Building (standards)
MEPS	Minimum Energy Performance Standard
EPC	Energy Performance Certificate
CEN	Comité Européen de Normalisation
DEPC	Dynamic Energy Performance Certification
AC	Air Conditioning
CAD	Computer Aided Design
GA	Genetic Algorithm
GH	Grasshopper
VC	Ventilative Cooling
IEA	International Energy Agency
EBC	Energy in Buildings and Communities program
EP	EnergyPlus
LB	Ladybug
HB	Honeybee
GUI	Graphical User Interfaces
DOE	U.S. Department of Energy

BTO	Building Technologies Office
IDF	Input Data File
IDD	Input Data Dictionary
BESOS	Building and Energy Simulation, Optimization and Surrogate-modelling
PREDYCE	Python semi-Realtime Energy DYnamics and Climate Evaluation
KPI	Key Performance Indicator
OS	OpenStudio
SDK	Software Development Kit
OSM	OpenStudio Model
ECM	Energy Conservation Measure
PAT	Parametric Analysis Tool (from OpenStudio)
SDI	Spatial Daylight Illumination
DLA	Daylight Autonomy
UDLI	Useful Daylight Illuminance
ASE	Annual Sun Exposure
sDA	Spatial Daylight Autonomy
WWR	Window-to-Wall Ratio
HVAC	Heating, Ventilation and Air Conditioning
NV	Natural Ventilation
g-value	Solar energy transmittance

ρ_e	Solar energy reflection
τ_v	Light or visible transmittance
ρ_v	Light or visible reflection
λ	Thermal conductivity
U-value	Thermal transmittance
SRES	Special Report on Emissions Scenarios
EPW	EnergyPlus Weather
CSV	Comma Separated Variable
EIO	EnergyPlus Invariant Output
RDD	Report (variable) Data Dictionary
PMV	Predicted Mean Vote
PPD	Predicted Percent of Dissatisfied
RH	Relative Humidity
DGI	Daylight Glare Index
DGP	Daylight Glare Probability
SPEA-2	Strength Pareto Evolutionary Algorithm 2
HypE	Hypervolume Estimation algorithm
HOY	Hour Of the Year
COP	Coefficient Of Performance
also	Conference Of the Parties (if followed by a number)
IAQ	Indoor Air Quality
EUI	Energy Usage Intensity

CEUI	Cooling Energy Usage Intensity
HEUI	Heating Energy Usage Intensity
TEUI	Thermal Energy Usage Intensity
LEUI	Lighting Energy Usage Intensity
RCM	Regional Climate Models
IGU	Insulated Glass Unit

ABSTRACT

ENGLISH

Recent strong impacts of global warming have brought awareness on the topic to spread and climate change issues to be put on top of the international political agenda. The urge for a step-change able to lead to a GHGs emissions reduction is getting increasingly stronger, affecting particularly the building sector, which is responsible for 40% of the European energy consumption and 36% of emissions. To this end, leveraging EU incentives and global technological advancements (Big Data, genetic algorithms, etc.) is crucial to implement a methodological renovation towards a more integrated, conscious and sustainable architectural design. The tool developed in this research harnesses the potential of Rhino-Grasshopper parametric environment to establish a link between 3D modeling and performance analysis engines such as EnergyPlus and Radiance, with the purpose of assessing building performance and, on the basis of this, optimizing formal and technical decisions made during early-design stage. Through Honeybee and Ladybug plug-ins, thermal and daylight comfort metrics are evaluated in free-running mode (without cooling/heating nor mechanical ventilation or artificial lighting systems turned on) and maximized by means of Octopus evolutionary simulator, in order to find optimal configurations of selected design variables. Minimization of glare, predicted by the LEED ASE index, is also accounted for in the multi-objective optimization process. Once the "best" optimal solution is selected, the tool identifies wherever discomfort periods are still present, in accordance with the adaptive comfort model used, and generates HVAC control schedules to be applied to the building when simulated in mixed-mode, so that heating and cooling systems are only turned on when really needed. Hence, energy savings that derive from the application of the proposed methodology are assessed. The tool is tested in ten European and Italian locations (Kemi, Aalborg, Geneva, Turin, Athens, Bari, Paphos, Palermo, Rome, Trieste) under present and 2050 climatic conditions. The optimization processes carried out resulted in satisfying visual and thermal comfort levels, as well as good energy savings (over 90% of thermal

energy saved in Palermo and Paphos) in optimized solutions, although the tool was found to be less effective in colder climates such as Kemi or Aalborg. The developed workflow is finally applied to two case studies, a school classroom in Torre Pellice and an apartment in Turin. With respect to the simulated actual situations, thermal comfort improved in both cases (by 15% in the classroom and by almost 40% in the apartment) and TEUI savings reached 90% and over under present conditions as well as in 2050. Visual comfort, and so LEUI savings, were discovered more difficult to optimize. To conclude, the tool has proven to be a valid instrument to support an important methodological change in the design process. Further analyses and developments will contribute to better investigate the tool's potentialities and to overcome its limitations found within the presented research.

ITALIANO

I recenti forti impatti del riscaldamento globale hanno portato alla diffusione della sensibilizzazione sul tema e all'interesse da parte dei governi internazionali a combattere il cambiamento climatico. La necessità di un cambio di passo capace di portare alla diminuzione delle emissioni di gas serra sta diventando sempre più imperante, investendo in particolar modo il settore edilizio, responsabile del 40% del consumo energetico europeo e del 36% delle emissioni climalteranti. A tal fine, risulta fondamentale sfruttare gli incentivi dell'Unione Europea e i progressi in campo tecnologico (*Big Data*, algoritmi genetici, ecc.) per attuare un rinnovamento metodologico volto ad una progettazione architettonica più integrata, consapevole e sostenibile. Il tool sviluppato nella presente ricerca sfrutta le potenzialità dell'ambiente parametrico di Rhino-Grasshopper per stabilire un collegamento tra la modellazione 3D e software di analisi come EnergyPlus e Radiance, con lo scopo di valutare la performance dell'edificio e, sulla base di questa, ottimizzare le scelte formali e tecniche stabilite nelle prime fasi del progetto. Mediante i *plug-in* Honeybee e Ladybug, vengono stimati i parametri di comfort termico e visivo in *free-running* (in assenza impianti di riscaldamento/raffrescamento, ventilazione meccanica e illuminazione artificiale) e massimizzati attraverso il solutore evolutivo Octopus, al fine di trovare le configurazioni ottimali di determinate variabili di progetto. La minimizzazione dell'abbagliamento, predetto mediante l'indice LEED ASE, è inoltre presa in considerazione all'interno del processo di ottimizzazione multi-obiettivo. Selezionata la "migliore" soluzione ottimale, il tool identifica se e quando sono ancora presenti periodi di discomfort, in accordo con il modello di comfort adattivo utilizzato, e genera *schedules* di accensione e spegnimento del sistema di HVAC da applicare nella simulazione dell'edificio in *mixed-mode*, cosicché gli impianti di riscaldamento e raffrescamento si accendano solo quando realmente necessario. Conseguentemente, vengono valutati i risparmi energetici che derivano dall'applicazione della metodologia proposta. Il tool è stato testato in dieci località europee e italiane (Kemi, Aalborg, Ginevra, Torino, Atene, Bari, Paphos, Palermo, Roma, Trieste) considerando condizioni climatiche presenti e future (2050). Le ottimizzazioni condotte hanno portato a livelli di comfort termico e visivo soddisfacenti e a buoni risultati di risparmio energetico nelle soluzioni ottimizzate (oltre il 90% di energia termica risparmiata a Palermo e Paphos), anche se il tool si è rivelato meno efficiente in climi più freddi come quelli di Kemi e Aalborg. Il workflow sviluppato è infine applicato a due casi studio, un'aula scolastica a Torre Pellice e un appartamento a Torino. Rispetto alle situazioni attuali simulate, il comfort termico è aumentato in entrambi i casi (del 15% nell'aula e del 40% circa nell'appartamento) e la TEUI risparmiata ha raggiunto il 90% e oltre, sia in condizioni climatiche presenti sia future. Il comfort visivo, e quindi il risparmio di LEUI, si sono rivelati più complessi da ottimizzare. In conclusione, il tool ha dato prova di essere un valido strumento di supporto per migliorare la metodologia di progetto. Ulteriori analisi e sviluppi contribuiranno a indagare meglio le potenzialità del tool e a superare i limiti riscontrati nella presente ricerca.

1. INTRODUCTION

1. INTRODUCTION

«L'aria irrespirabile della nostra città, il consumo disastroso del nostro pianeta, l'inconsistente progetto di futuro per le nuove generazioni resteranno lì, sotto gli occhi di tutti, come da sempre, invisibili. Tutto questo non è più possibile»

(Eugenio in via Di Gioia via Instagram, 2022)

1.1 Background

In the last decades, awareness on climate change has spread and the urgency for a renovation has become a matter of public concern. According to Eurobarometer's survey, in 2021 93% of EU citizens consider climate change as the most serious problem facing the world [1]. Nowadays it is common to see people, especially young, taking to the streets demanding for concrete action to limit global warming and declaring their love to Earth[1]. In this sense, young Swedish activist Greta Thunberg, who founded the climate strike movement known as Fridays For Future (FFF) in 2018, has had great impact on climate change attitude. The movement's call for action has been able to raise consent between students all over the world, agitating for their own future. Although environmental activism has reached overall dimensions in the past few years, also thanks to the power of social media, its roots date back to the early 1970s. In these years, climate change emerged as a political issue. In 1972, for the first time, environmental problems were addressed in a major conference that took place in Stockholm, Sweden: the UN Conference on the Human Environment (UNCHE). The

[1] It Is worth mentioning the venture by the Italian band Eugenio in Via DI Gioia that took place during the night between the 28th and the 29th March 2022 in Turin. A group of 150 people reunited in Piazza San Carlo and wrote in capital letters *TI AMO ANCORA* (*I still love you*) with chalk on the ground.

counties that took part in it agreed on the need of a global-scale and cooperative action to tackle climate change [1].

Since then, many conferences have been held[2], but the problem has been put off, passing the torch to future generations [1, 3]. Thus far, climate crisis has been perceived as «a distant danger, a case scenario that we can deal with tomorrow» ([4], p. 1), an issue that can wait to be solved while troubleshooting short-term problems, such as financial and economic ones[3] [1]. But now humankind is paying the price of this governments' decision. According to NASA/GISS [5], the global temperature increased by 1,01°C in the period 1880-2021 and 2020 has been declared to be the hottest year ever recorded since the XIX century. Earth is warming at an alarming rate, as well as the level of carbon dioxide in the air is increasing. Heat waves are becoming more frequent, temperatures and humidity are rising, especially in anthropized areas (the highest temperature ever recorded in Europe has been registered in Syracuse, Sicily, in August 2021 – 48,8°C). Artic sea ice is shrinking, accelerating the rise of ocean level thus endangering life in coastal cities by causing floods. Besides, the thawing of the permafrost could lead to the release of carbon dioxide and methane trapped into ice, increasing the already high levels of GHGs (Green House Gasses) in the atmosphere [6]. Drought and wildfires are devastating entire countries, such as California and Australia and fields of Amazon Rainforest are burnt down every year, endangering wildlife. Human-caused climate changes are inducing environmental disruptions that mainly damage already fragile people and ecosystems, leading to significant consequences for nature, but also for human health and wellness. The problem is no longer only related to environment and economy but is turning into an actual social challenge and time available to act is running out [1, 7].

Therefore, today climate issues are at the top of the international political agenda. The 21st Conference of the Parties (COP21) that took place in Paris in 2015 marked a change

---

[2] Some noteworthy are the UN Conference on Environment and Development (UNCED) held in Rio de Janeiro in June 1992, the World Summit on Sustainable Development held in Johannesburg (South Africa) in 2002 and the Conferences of the Parties (COPs), international meetings that are held every year since 1995, when the first one took place in Berlin - Germany (COP1) [2].

[3] i.e. 2008-2009 economic crisis.

in pace. In December of that same year, the 196 attending parties managed to define common objectives and signed the Paris Agreement, which represents the «first-ever universal, legally binding global climate change» treaty [8]. A two-pronged strategy to counter global warming was presented, through adaptation and mitigation policies. Adaptation relates to the reduction of societies' vulnerability towards climate change expected impacts, increasing the ability to adapt to adverse conditions. Mitigation refers to the aim of «holding the increase in global average temperature to well below 2°C above pre-industrial levels and pursuing efforts to limit the temperature increase to 1,5°C [...] recognizing that this would significantly reduce the risk and impacts of climate change» ([9], p. 3). In order to limit global warming, huge reduction of GHGs emissions is necessary, seeking to reach the zero-emission scenario. To fall in line with what is required by the treaty, every country should outline and communicate every five years to the UNFCCC secretariat its own nationally determined contribution (NDC), defining the objectives that intends to achieve (Article 4, paragraph 2– [9]). For example, European Union's initial NDC was the commitment to reduce GHGs emissions by 40% by 2030, compared to 1990 levels, Then, in December 2020 EU updated its NDC and set itself the target of reducing emissions by at least 55% by 2030[4], moving toward decarbonization and climate neutrality.

Among the most impacting sectors in terms of emissions there is power generation and heat production, accounting for nearly 39% of global carbon dioxide emissions in 2020 and 46% in 2021 [10, 11]. During 2020, due to restrictions enacted to contain the spread of COVID-19 disease, energy demand decreased, and CO_2 emissions experienced a drastic decline. The pandemic offered Governments the opportunity to reconsider priorities and start a green recovery, rebuilding a worldwide economy that invests on low-carbon technologies, slows down global warming and allows meeting Paris Agreement's goals. As Rosen and Forster pointed out [4], a strong green economic recovery could cut the rate of warming by up to half in coming decades, giving the chance of keeping the temperature increase below the goal of 1,5°C.

[4] Climate Target Plan 2030, proposed by the Commission on 14 July 2021.

However, as the world started rebounding from health crisis, it became clear that a sustainable restoration was not being pursued. Carbon dioxide emissions, especially ones originating from coal combustion[5], raised again, reaching 36.3 billion tons in 2021, the highest level ever registered in history [11]. According to the European Commission [13], in 2021 40% of EU energy consumption and 36% of the energy-related GHGs emissions are accounted to buildings, largely caused by existing building stock, 75% of which is not energy efficient. Poor efficiency affects the environment as well as human quality of living. The higher the energy consumptions, the higher the bills, weighing on household budget thus resulting in energy poverty becoming a widespread problem. Moreover, inefficient buildings do not allow to have adequate indoor comfort and sanitary conditions in living and working places, leading to health problems and productivity reduction [14]. In the light of this evidence, clearly emerges the urge for a radical innovation of the construction sector, not only in the way buildings are made, but also in the way they are conceived during the very early-design stage, with the aim of reducing resources exploitation, pollution, social inequalities and improving present and future health and quality of life in a sustainable development perspective [3, 15].

1.2 EU incentives for change

Climate action is currently a burning issue in the European context. With the aim of reaching climate neutrality by 2050, legislative framework concerning the subject constantly keeps being updated and different funding programmes are being established. It has been estimated – see for example [14] – that EU allocates nearly 40% of world-wide investments for building energy efficiency improvement every year. So far, progress in energy performance has been achieved at some level, succeeding in cutting new buildings' energy consumptions by half with respect to similar buildings

[5] The recourse to coal as an energy source increased mainly due to the high prices of natural gas because of high energy demand in post-COVID-19 recovery. Russia's invasion of Ukraine (24 February 2022) and sanctions imposed to the Country aggravated energy crisis even further, as Russia provides around 45% of EU's total gas imports [12]. Investing on renewables and innovative strategies to reduce energy demand is the answer to the crisis in place, allowing to disengage from the use of fossil fuels for energy production.

twenty years ago [14]. Nevertheless, the main challenge is represented by building stock. Retrofit rate keeps being lower than what would be needed to meet European decarbonization and reduced consumptions goals [14, 16]. One reason lies in the fact that renovation processes are often unattractive to investors, considering that they are usually expensive, time-consuming and not cost-effective in the short-term. Therefore, in order to encourage building retrofit, some EU Countries have established tax reliefs. For instance, Italy introduced next to other fiscal facilitations already existing the "Superbonus 110%" [6], which enables contributors to fulfill energy efficiency improvement, static consolidation and renewables installation, allowing to deduce 110% of the intervention costs. Albeit commendable, the Superbonus 110% potential is still not fully exploited. As the Legambiente report underlines [15], this economic measure is more likely to benefit wealthy users rather than vulnerable families, who should instead become the primary target for the purpose of eradicating energy poverty and pursuing a large-scale building renovation. It is clear that some effort is still to put into fund management and programming.

Another reason lies in the persistence of barriers and disinformation, especially among end-users. Without a clear framework, actual benefits that could result from energy savings are hard to understand, measure and translate into monetization [14]. To boost building refurbishment and promote policies concerning energy efficiency, investments and savings, EU relies on its main legislative instrument, the Energy Performance of Building Directive (EPBD). First published in 2002 (Directive 2002/91/EC), then recast in 2010 (Directive 2010/31/EU on the energy performance of buildings) and in 2018 (Directive 2018/844/EU), a new revision of EPBD has been proposed for 2022 as part of the "Fit for 55" package [17], in order to update objectives[7] and upgrade existing regulatory framework. The last EPBD revision proposal aims to

[6] Superbonus 110% was introduced in July 2020 and then extended up to the end of 2025 through the "Legge di Bilancio 2022". More on Superbonus on Agenzia delle Entrate official website, https://www.agenziaentrate.gov.it/portale/web/guest/superbonus-110%25. Accessed 07 April 2022.

[7] EU target regarding GHGs emissions has changed in 2020. See footnote 4. Directive 2010/31/EU required all new buildings to be NZEB (Net-Zero Energy Building) by the end of 2020. The 2022 EPBD revision proposal aims to go further, moving towards ZEB (Zero-Emission Building) as of January 2030 for new constructions and by the end of 2050 for existing stock.

enhance clarity and reliability of energy performance calculation methodologies and certifications. In this respect, in 2022 European Commission will submit the introduction of mandatory minimum energy performance standards (MEPS) and a stronger obligation to provide Energy Performance Certificates (EPCs), establishing common criteria on which to base performance classes [18]. As a support to the EPBD directive, a set of standards called Energy Performance of Building Standards or "set of EPB standards", developed by CEN[8], is established. The set of EPB standards enables to assess the overall energy performance of both new and existing (and then renovated) buildings, using a holistic approach that considers several complementary aspects [19]. As stated in the mandate M480, «the use of European standards increases the accessibility, transparency and objectivity of energy performance assessment [...] facilitating the comparison of best practices and supporting the internal market for construction products» ([20], p.1). Moving in this direction, EU's funding programme Horizon 2020[9] published a call for tenders titled "Building a low-carbon, climate resilient future" (H2020-LC-SC3-2018-2019-2020 [10]) as part of the H2020 SC3 Societal Challenge – Secure, Clean and Efficient Energy. Of particular interest is the topic LC-SC3-EE-5-2018-2019-2020, titled "Next-generation of Energy Performance Assessment and Certification". The call [16] invites participants to present innovative assessment and certification systems compliant with EPBD and EPB standards, in order to go beyond fragmentation in evaluation methodologies and to ensure a higher level of application of EPCs. Providing a shared framework makes assessment and certification more reliable, comparable on EU scale as well as

[8] European Committee for Standardization (CEN from the French Comité Européen de Normalisation). CEN website: https://www.cencenelec.eu/. Accessed 06 April 2022.

[9] Horizon 2020, also known as H2020, was the EU's research and innovation funding programme for seven years (from 2014-2020) with a budget of nearly €80 billion, among the highest in the world. Funds were on direct management. H2020 has been succeeded by Horizon Europe, the new financial program for the next seven years (2021-2027) with a budget of €95.5 billion. Horizon Europe, and Horizon 2020 before, publish calls for proposals and tenders related to five main missions, aiming at financing projects for scientific and technological development. More on Horizon 2020 at https://horizon2020.apre.it/ and on Horizon Europe at https://ec.europa.eu/info/research-and-innovation/funding/funding-opportunities/funding-programmes-and-open-calls/horizon-europe_en. Accessed 07 April 2022.

[10] A full list and description of the H2020-LC-SC3-2018-2019-2020 call topics is provided in [16].

understandable, enabling users to make more informed choices and overcoming the aforementioned barriers.

1.3 A new perspective

Horizon 2020 funded projects pave the way for a profound innovation in performance evaluation and in the development of sustainable strategies, recognizing that a new digital era has already started. With the spread of ICT (Information and Communication Technologies) and IT (Information Technologies) and computers being ordinarily accessible, the world is currently experiencing a massive technological revolution that is leading to breakthrough in all fields [21-27]. The conventional disjunction between digital and real worlds crumbles on behalf of a dynamic and continuous interrelation and hybridization between the two realities [21, 27]. By building up smart-sensors grids at various levels of the constructed environment, it becomes possible to control the real world through digitalization as well as influencing virtual models starting from actual measured data [21]. Sensors gather an inconceivable quantity of real-time data and computers make it possible to manage it and search through it, while this abundance of information would rather be impossible to handle for humans unless a simplification is operated [11]. Inevitably, the small-data logic of accuracy must be forsaken as sensors' single-measurement precision cannot be ensured: abundance of readings provides instead a better understanding of the phenomenon and allows forecasting [21]. Hence, applications of these big sets of data are endless. Actual energy related measurements could be used in the process for the definition of a new-generation of building performance assessment (as suggested by H2020 LC-SC3-EE-5 call [16]), as well as performance and indoor comfort certification, increasing their quality and reliability. In particular, this is the main objective of H2020 funded project E-DYCE (Energy flexible DYnamic building Certification), which proposes DEPC (Dynamic Energy Performance

[11] According to Mario Carpo [22], the Google slogan "search don't sort" well represents the difference between computers and human approach towards data. «Humans need a lot of sorting because they can manage only a few data at a time; computers need less sorting – or, indeed, no sorting» ([22], p. 96). Thus, the use of machines opens to new possibilities.

Certification) as an evolution of conventional EPCs closer to building real operation condition [23]. Monitored data can also provide a better knowledge of actual energy use in buildings, which enables a more aware planification of energy consumption [24]. This finds application in advanced control systems targeted at improving building smartness as means of creating healthier and more comfortable indoor environments while reducing energy consumption, carbon footprint and optimizing the use of renewable energy resources. To concretely apply these technologies on large scale, simpler, more interactive and cheaper solutions should be implemented. EU funded project PRELUDE (H2020 LC-EEB-07-2020 call), for example, works in this direction – see [24-26].

Big data has also implications for design process and modelling, leading to the need of modernization in the designer's role and method. In the first digital turn that happened in 1990s, architects immediately recognized the new tools' potential and accepted digital change in their professional practices earlier than any other trade [22]. Now most of them appear to deny the new way of thinking and making that the ICT revolution has brought along, inviting their "extinction" [21, 28]. As Carpo says, «design professionals tend to think that they cannot be replaced by a machine, and (that) their own expertise», based on traditionally consolidated knowledge, «has a unique value and cost» ([22], p. 161). But in an era in which information data multiplies, requirements change, and in which the design process becomes more complex and demands new management models «in a transparent, inclusive and bottom-up ecological system» [29, 30], the architect as it is conventionally conceived loses his authority. To achieve overall quality and sustainability of the project, a holistic perspective is required, crossing traditional boundaries of expertise [31] and overcoming fragmentation in practice. As Geymonat claims [32], «specialism must […] be reinterpreted not denied […] (it must be), in a certain sense, denied but also accepted, as the starting point for its overcoming». Thereby, In the contemporary world designers cease to be solo players and become part of many active participants, each contributing with their own sectoral knowledge, and evolves into a supervisor of the whole design process [22]. In view of an interdisciplinary aggregation, communication and transparency are crucial elements: the designer must now explicate and share information about the project choices and strategies, which has been made easier through the use of BIM (Building Information Modelling) software. Form and performance in buildings must reflect this multidisciplinary approach [33].

1.4 Form form-making to form-finding

Design profession has always been dedicated to shaping reality, giving form to the environment that human inhabits. In early 1990s new computational tools, such as CAD (computer-aided design) software, have been made available: architects initially adopted them to simply replace paper-based drawing without affecting the design method [21, 33, 34]. These digital instruments brought along the possibility to effortlessly handle complex shapes like splines, free-form curves that hitherto were only mathematical elements, and designers started to play with them [22]. This first generation of digital architects mainly focused their efforts on creating objects with high aesthetic value and spatial complexity, constantly seeking for modernity. The rise of the so-called *style of the blob* or *blob architecture* [12] resulted in isolated streamlined structures that stand out ì as mere *landmarks* [3] and icons of innovation. Their curve, almost naturalistic, shape has no justification, does not really consider the context in which the building is located and it is end to itself. An approach like this can no longer be followed in a view of development of a greener and more sustainable construction sector. Contemporary architecture should imitate nature not only in its shapes, but also in its way of functioning [3] and its ability to adapt to different, sometimes extreme, conditions and environments. «Nature fits form to function» [36] and so design must do, heading towards a bio-inspired approach that can profoundly change the way we build and inhabit spaces.

[12] The term *blob architecture* (also *blobitecture*) was coined in 1996 by architect Greg Lynn in the article "Blobs, or Why Tectonics Is Square and Topology Is Groovy" written for the journal *ANY: Architecture New York*, no. 14, pp. 58-61. The expression identifies an architecture style made of curvilinear and smooth objects that arose in 1990s thanks to the use of CAD and other digital tools. Among the most iconic blobitecture buildings Frank Ghery's Guggenheim Museum in Bilbao is the most iconic.

Form must be searched, not made. Design process is comparable to a problem whose solution is to find within a context or *environmental system* that establishes a need-performance-based framework [21, 31, 34, 37-40]. In simple terms, form originates from the fulfillment of a list of requirements that is achieved providing a certain level of performance through technical choices. Thus, form assumes a meaningful sense, a justification, resulting as the materialization in the constructed environment of answers given to needs [41], both human and environmental. This concept underlies the "metodo esigenziale-prestazionale" (*requirement-driven approach*) developed in Italy between the 60s and the 70s [e.g. 39-41], which today finds full application as *performance-driven design* or *performative design*. In the performance-driven design method, performance evaluation is used since early-design phases as a guiding factor to assess if the initial conceptual idea performs in compliance with expectations. The process is not linear yet leads to backtrack and to a continuous iterative requirement-performance check throughout the entire design process, with the aim of finding the optimal solution that meets an established set of (sometimes conflicting) objectives. As building is a complex system made of a several interdependent components and functions, technological choices acting on one of these variables could affect others, generating different configurations of the same geometric components [21, 31], which means different design solutions. Exploring and comparing a large number of design alternatives in the preliminary phase, «when the possibility to change is higher and its cost is lower» [42], provides architects with the opportunity to better understand the effect of their formal decisions on overall building future quality, functional efficiency and environmental impact [21, 31, 34]. Traditionally, designers explored only a very small number of design solutions, mostly due to their cognitive limits [31, 43] in managing complexity and large amount of data. Neither CAD nor 3D modelers could solve the problem, as they simply allow to set up building models with geometric information only, while performance analyses is delegated to other simulation tools used by external professionals (e.g. engineers or other consultants) [35, 44]. Instead, a parametric and algorithmic approach allows to establish a clear design method, directly integrating performance simulation in the workflow and using its outputs for investigating and comparing acceptable design solutions that are generated by manipulating specific parameters. With respect to this, the application of evolutionary algorithms (e.g. genetic algorithms – GAs) in form-finding and form-optimization issues, especially within environmental design, is becoming increasingly present in professional practice.

1.5 Research objective and methodology

The main objective of this research is the development of a simplified and user-friendly script within Rhinoceros-Grasshopper environment aimed at optimizing building envelope design choices made in early-design stage, that have been proven to have the largest impact on final quality and efficiency of the building [31, 35]. Ladybug and Honeybee plug-ins for Grasshopper allow to establish a link between 3D geometry and energy/daylight simulations through the implementation of analysis engines such as EnergyPlus, Radiance and Daysim. By applying the proposed optimization tool, designers can put up an integrated building model and get rapid and iterative performance feedback on their decisions. The goal is to optimize formal parameters (e.g., orientation, window-to-wall ratio, insulation, shading devices, etc.) of a free-running single-zone spatial unit, with the aim of improving users' indoor thermal and visual comfort while minimizing energy demand related to heating, cooling and artificial lighting. The research studies the application of passive strategies (e.g. natural ventilation) that harness the potential of the boundary conditions in which the building lies. Applicability and resilience of the workflow under different Italian and European environmental conditions, both present and future, is tested. For each location and climatic condition, the geometric configuration of the examined thermal zone that better meets the requirements is found. Lastly, optimal solutions are further analyzed to quantitatively estimate the reduction of energy demand and the energy savings that derive from the application of the proposed methodology. Annual-based simulations outputs visualization through interactive graphics is provided. The workflow is then applied to two real case studies in Italy: a school classroom in Torre Pellice and a residential apartment located in Turin.

2. STATE OF THE ART

2. STATE OF THE ART

This chapter discusses the general background and the inspirations of the work. The simple GH tool proposed by the paper stands as a parametric and optimizing graphical user interface (GUI) for EnergyPlus analysis engine, ranking among a lengthy list of available tools that perform similar functions. Similarities and differences of these tools and the proposed one are investigated. A brief literature review of related analysis and optimization experiences with HB and LB tools are discussed. Other specific states of the art can be found along the next chapters.

2.1 EP parametric and optimizing interfaces

EnergyPlus (EP) is a free, open-source and cross-platform whole building simulation software developed by the U.S. Department of Energy's (DOE) Building Technologies Office (BTO) in 1997 [45]. It is one of the most widely used tool to execute performance-driven energy analyses and to carry out optimization processes. EP file format is the IDF, a text-based file that contains all the building data needed to run an energy simulation. Each IDF consists of a number of ordered string fields, all conform to an associated IDD (*Input Data Dictionary*) file which is related to a specific EP release. The IDD contains a detailed list of all possible EnergyPlus objects and a specification of the data each object requires [46], so describing how EP should read an IDF file. EnergyPlus does not have any interface, making it difficult to use the program, especially for non-experts. For this reason, several tools that provide interfaces for EP have been created, allowing parametric energy simulations and optimizations. Parametric interfaces can be divided into scripting-based and GUIs. An example of scripting-based interface is BESOS (Building and Energy Simulation, Optimization and Surrogate-modelling). First launched in July 2019, BESOS is a cloud-based and open-source platform based on Python code and Jupiter Notebooks «that seeks to provide a single interface to interact with traditional modelling tools and make use of novel optimization and machine learning techniques» [47, p. 5]. It consists in a collection of modules that allow parametric building energy simulations through EP via Eppy[13] or EnergyHub, and multi-objective optimizations using evolutionary algorithms through Platypus library [48]. BESOS Platform provides a powerful way to run large-scale energy analyses. However, it requires a certain level of knowledge of coding and file formats from the user. From this point of view, graphical interfaces are usually more user-friendly and require less expertise on programming. This does not happen with jEPlus [49], an open-source project written in Java that was originally introduced in 2009. It provides a parametric GUI for EP for «defining design parameters, editing models, manage simulation runs, and collecting results» [49]. When paired with an evolutionary algorithm, jEPlus can efficiently perform building design optimizations, both single-objective and multi-objective [50]. Nevertheless, for this tool, as well as for script-based ones, a basic knowledge on «EnergyPlus modelling process and the text input files» [49] is still required.

More accessible than jEPlus is PREDYCE (Python semi-Realtime Energy DYnamics and Climate Evaluation) tool, a Python library developed by POLITO researchers in the context of EU funded project EDYCE [51]. It provides «a simple GUI to launch (parametric) simulations and choose among the list of pre-built actions» [52], not requiring any knowledge of Python, and produces highly-graphic outputs. PRELUDE is composed of three main independent modules (IDF editor, Key Performance Indicators calculator and runner) and other additional ones (e.g. EPW compiler) that can be combined together into «task-oriented scripts (named scenarios)» [51]. KPIs are, for example, thermal comfort, indoor air quality, ventilative cooling, etc. The tool is meant to be used particularly for free-running building simulations and optimizations. However, in this kind of GUI a connection with a 3D modeler is completely absent and simulations are only limited to energy ones. Instead, the proposed tool provides, through Rhino-GH 3D modeling software, a highly graphic interface for EP and other analysis engines, such as Radiance and Daysim, allowing to also run daylight simulations and thus to consider all aspects of comfort when optimizing building

[13] Eppy is a scripting language written in Python for IDF files and other EP output files. More on Eppy at https://pypi.org/project/eppy/.

design. In addition, as it is made of simple and intuitive components in which a Python code is already set up, it does not require any expertise on programming nor on input and output files, which are automatically edited, read and translated into values and/or into visual outputs (bar charts, annual hourly charts, etc.).

Similar to the workflow here presented are OpenStudio and DesignBuilder tools. EP graphical interface OpenStudio (OS) [53] is one of the most diffused and consists in a free-license software development kit (SDK) that works as a user-friendly and flexible interface to EP. A direct link with SketchUP 3D modeler is possible thanks to the dedicated plug-in. «The most powerful feature of the OpenStudio platform and the core of its value proposition» [54, p. 322] are OS Measures, which are «set of programmatic instructions [...] that makes changes to an energy model» [55] (an OpenStudio Model – OSM) in order to implement an *energy conservation measure* (ECM). To learn more about OS Measures, reader can make reference to *OpenStudio Measure Writer's Reference Guide* [56]. Measures can be used to set up building models parametrically from scratch. This "procedural modeling" [54] is very similar to Grasshopper-Honeybee functioning, which creates models by linking together various components, each one adding a specific feature to the building. Parametric analysis can be performed with OpenStudio PAT (Parametric Analysis Tool), applying «programmatically and systematically» [54, p. 323] combinations of Measures in a defined order to the OSM, in order to generate and compare various design alternatives and assess their energy performance. Measures options (values) can be manually specified, requiring a lot of time and effort from the user, or can be automatically chosen between a specified range of variation using selected algorithms (e.g. optimization), allowing the exploration of larger sets of solutions [57]. OS PAT is very similar to the tool developed in this paper: both provide a graphical parametric interface to EP and can perform multi-objective optimizations (thanks to the implementation of algorithms such as SPEA2) of free-running or conditioned building design; it also can perform daylight analysis through Radiance engine. However, PAT algorithmic optimizations cannot be run on local on personal computers due to their complexity, yet they need to be run in the cloud (Amazon cloud) or other dedicated servers. This consistently reduces the time for the simulation, but makes it more difficult to obtain detailed results, as they are usually very large files and must be downloaded from the server right after the simulation, with the risk of losing data if the server is shut down [57]. Instead, Octopus plug-in used by the presented tool can only be run on local memory. This could significantly increase the simulation time, but it allows to periodically save on the optimization results during the simulation and to store them within the saved GH document. Then, solutions can be directly reinstated into GH environment so that it is much simpler to analyze the obtained data.

DesignBuilder [58] is one of the most reliable and employed tools in the professional practice by architects as well as engineers. A 3D modeler is the hearth of the tool: every kind of building geometries, even complex ones, can be created within DesignBuilder environment. 3D models generated using other BIM/CAD tools can also be imported, achieving high levels of interoperability. This is possible in the presented tool as well. Full integration between different analysis tools (EP, Radiance, ecc.) provides a holistic view of performance and parametric analysis allows to create design curve outputs adjusting up to two variables [59], so that to quickly see the impacts of designs decisions on performance level and compare solutions [58]. Through a genetic algorithm, the tool is able to perform optimization processes aimed at searching for the optimal combination of selected design variables «that give the highest or lowest values of the objective KPI» [60]. Multi-objective optimization is allowed, but number of objectives is limited to two. Unlike DesignBuilder, the proposed tool, trough Octopus plug-in, is capable of considering a minimum of two and a maximum of theoretically unlimited number of goals at once [61].

Within Rhino-Grasshopper environment, besides Ladybug Legacy plug-in Honeybee, there are other plug-ins that are able to establish a link with EP, Radiance and Daysim simulation engines and run parametric performance analyses. ClimateStudio [62] is one such example. It is a fully parametric «advanced daylighting, electric lighting, and conceptual thermal simulation software developed by Solemma LLC» [63]. It is easy to use and to understand and is very similar to Honeybee+Ladybug in terms of functionalities and time spent for energy and daylight analyses. Optimizations are made possible when such plug-ins are in combination with tools like Galapagos or the aforementioned Octopus.

2.2 Related works

The tool developed in the presented work falls within a framework of numerous previous studies in which parametric modeling is integrated with building performance assessment and in which GAs are used to perform fully-automated design optimizations. In this regard, several papers have been reviewed with the aim of investigating the research progresses in this field. Focus is placed on those works in which Honeybee and Ladybug plug-ins for Grasshopper are used together with GH optimization add-ons, such as Galapagos and Octopus.

Galapagos is a simple GH plug-in that allows to perform single-objective optimizations through the use of an evolutionary algorithm, being able to only consider one objective at a time. Since optimization objectives (e.g. daylight and energy performance) are usually interdependent and influence each other, this kind of tool is progressively being replaced with more advanced multi-objective optimization GH plug-ins like Octopus. This issue is evident in Qingsong and Fukuda's research [64]. A simple office box building located in Beijing (China) is considered with the goal of finding the optimal window configuration (height, width and area) on each of the four cardinal directions that maximizes useful daylight illuminance (percentage of the time illuminance is more than 300 lx on the analysis plane) and minimizes total thermal energy. Galapagos plug-in was used and two separated processes were run, one for daylight and the other for energy optimization. The optimal window dimensions on each wall resulted to be different for daylight and energy goals. So, using an optimization tool that only considers one objective at a time, although useful for identifying a design strategy, requires a further effort from the designer, who has to interpret the results and find a solution that balances the usually conflicting targets. Multi-objective optimization using Octopus tool is able to solve this «contradictive relationship between daylighting and energy performance» ([65], p. 3597), as Toutou et al. [65] demonstrated. In this case, Spatial Daylight Illumination (SDI) and Energy

Use Intensity (EUI) are considered in the optimization process as a function of seven variables, which include south window-to-wall ratio, window material, wall construction, and shading angle and dimensions. Toutou et al. concluded that optimal design solutions from the daylight and energetic points of view do not correspond. This divergence is also evident in Fang PhD thesis [66]. In his dissertation, the author performs two single-objective optimizations through Galapagos plug-in, the first one aimed at finding the solution that better maximizes UDLI, and the second one with the goal of minimizing EUI. Then, an Octopus multi-objective optimization process is run to find trade-off solutions that optimize both objectives. This workflow is applied under four different US specific climatic conditions. Running the optimizations in different climates is a valuable way to test the applicability of the established workflow and can also be found in [67, 68].

Other examples of the use of Octopus plug-in to optimize conflicting design goals can be found in [69, 70, 71]. In Zhang and Ji paper [69], multi-objective optimization considered the minimization of cooling energy consumption and the simultaneous maximization of DLA and wind speed as goals for the simulations, varying WWRs on the four façades of the studied building. Zhang A. et. al [70] optimized several design parameters (orientation, spaces depth, WWR of different facades, glazing materials and shading types) for a school building in China, with the aim of maximizing $UDLI_{100-2000lx}$ while reducing heating and lighting energy need and summer discomfort. Pilechiha et al. [71] proposed an innovative «approach for quantifying Quality of View in office buildings in balance with energy performance and daylighting» [71], and optimized window location and dimensions through Octopus, using sDA, ASE, EUI and QV as design goals.

Multi-objective optimization is often used for finding the optimal shading configuration that optimizes occupants' comfort, as well as energy consumption. For example, Bahdad et al. [72] employed Octopus to find the optimal configuration of light-shelves design that ensured minimum EUI, maximum UDLI and minimum DGP. Octopus application for this purpose can be found in other papers – see e.g. [73, 74].

Glare is also considered in Bakmohammadi and Noorzai [75]. A greater number of objectives, with respect to the aforementioned paper, is here taken into account, addressing both occupants' thermal and visual comfort and energy consumption. In particular, five goal parameters - Useful Daylight Illuminance between 100 and 2000 lx ($UDLI_{100-2000}$), Daylight Autonomy (DA), Thermal Energy Use Intensity (TEUI), Lighting Energy Use Intensity (LEUI) and occupants' thermal comfort - were considered to find the best design option for a primary school classroom in Tehran. Adaptive thermal comfort model was adopted, even though the space is considered conditioned, as EP analysis outputs TEUI and LEUI values. Glare probability is here taken into account through DGP in a second moment, after the optimization process, as a measure to choose the final optimal solution.

Multi-objective optimization is also applied to find trade-off solutions between comfort/energy consumption and other variables such as material cost (see for example Sun et al. [76], where the minimization of envelope cost was introduced among the optimization objectives) and emissions (see Manni et al. [77]).

Reviewing existing relevant articles, it emerged that Octopus optimization is almost always used for fully conditioned building, as energy use intensity (total EUI or thermal and lighting separately) is included among the objectives of the simulation in order to be minimized. Apparently, the method has never been used to find optimal design configuration of free-running buildings. Instead, the proposed tool performs the optimization considering thermal and visual comfort metrics calculated without any mechanical system in function, with the aim of reducing discomfort as much as possible only harnessing the potential of the building design. Only in a second phase, the approach takes into account HVAC and lighting systems, suggesting control schedules with the aim of completely eliminating discomfort while reducing energy consumption. In line with some reviewed papers, the developed workflow optimizes a significant number of variables, examining various design aspects (e.g. windows position and configuration, insulation, shadings, natural ventilation), with the goal of improving all aspects of comfort, both visual and thermal. As in examples [66, 67, 68], the tool's applicability is tested in various real climate conditions.

As pointed out by Manni and Nicolini in [78], research works that take into account climate change effects in their multi-objective optimizations are very rare, although future climatic conditions could make present optimal design solutions obsolete. Hence, besides running the developed tool under different European climates, resilience of the workflow is tested under 2050 weather, comparing present and future optimal building designs.

3. WORKFLOW

3. WORKFLOW

The proposed methodology is based on a predictive model of users' thermal and visual comfort in a free-running space and aimed at finding, under different climatic conditions, building design choices that improve performance and minimize energy needs for heating, cooling and artificial lighting. Rhino-Grasshopper is selected as the platform for the development of the tool, as it provides an open-source user-friendly 3D interface for energy and daylight dynamic performance simulation engines. A nine-step approach is presented. It has been defined using Honeybee and Ladybug plug-ins for environmental analysis and using Octopus evolutionary simulator for the multi-objective optimization process. Figure 1 schematizes the workflow, identifying the methodological phases and the tools used in each of them.

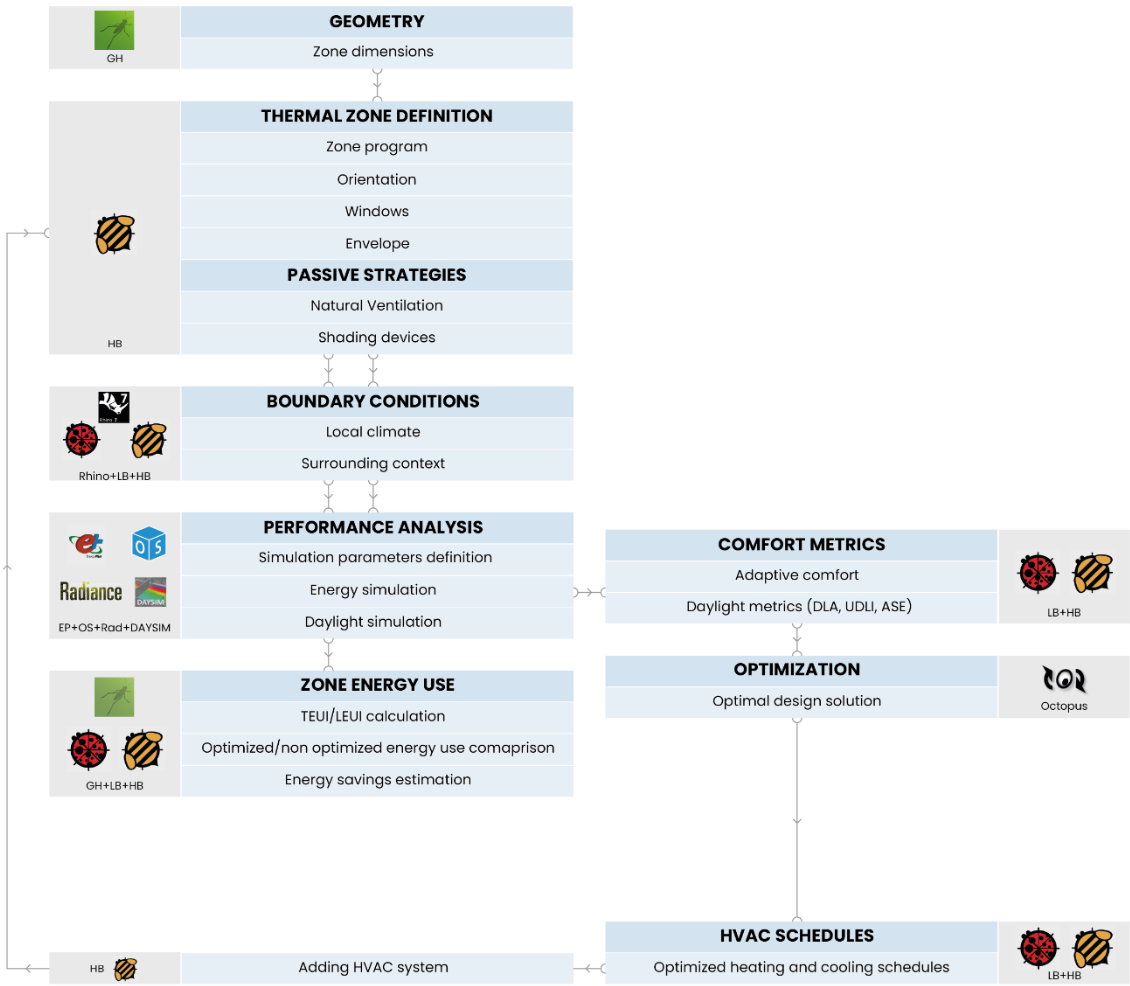

Figure 1 - Grasshopper workflow schematization.

The followed path is not linear, yet it is "circular", iterative. First, the geometry is parametrically modeled and characterized in its features. It is of primary importance to give particular attention to architectural design choices, especially when seeking to enhance the best from the application of passive strategies, such as ventilative cooling. To this end, it has been decided to optimize several design variables that have been proven to have a significant effect on cooling potential [79]. These include building orientation, location, size and opening configuration of windows, envelope insulation and shading devices position. After defining boundary conditions, performance analysis is carried out through EnergyPlus and OpenStudio, Radiance and Daysim engines. Performance level of the zone without any mechanical conditioning nor heating systems on is evaluated using specific thermal and visual comfort indicators: percentage of the time comfortable (adaptive comfort method), Daylight Autonomy (DLA), Useful Daylight Intensity (UDLI) and Annual Sunlight Exposure (ASE) are considered in the presented case. Optimization of these parameters allows to search for the optimal configuration of the design variables mentioned above. Through Octopus algorithm, several optimal solutions are found. Designer's action is required to interpret these design options and choose between them "the best" alternative, which is the one that maximizes users' comfort, both thermal and visual. Once the optimal solution is selected, the tool identifies wherever discomfort is still present during the analysis period for that design option and generates two schedules for the HVAC system control, one for cooling and the other for heating. Hence, the optimal solution is further analyzed, running the building in a mixed-mode[14], to estimate how much energy could be potentially saved by applying these custom HVAC schedules instead of using default fixed schedules that provide nearly always active systems, even when it may be unnecessary. The optimal solution to which optimized schedules are applied will be called from now on "optimized zone"; instead, the optimal solution to which default schedules are applied will be called

[14] Mixed-mode means that the building is conditioned both naturally and mechanically, integrating AC with natural ventilation from operable windows, thus reducing energy use for HVAC and increasing occupants' indoor comfort [80].

"non-optimized zone". Figure 2 provides a schematization of the inputs (in grey), the main tasks (in blue) and the outputs (in light blue) of each task of the developed tool.

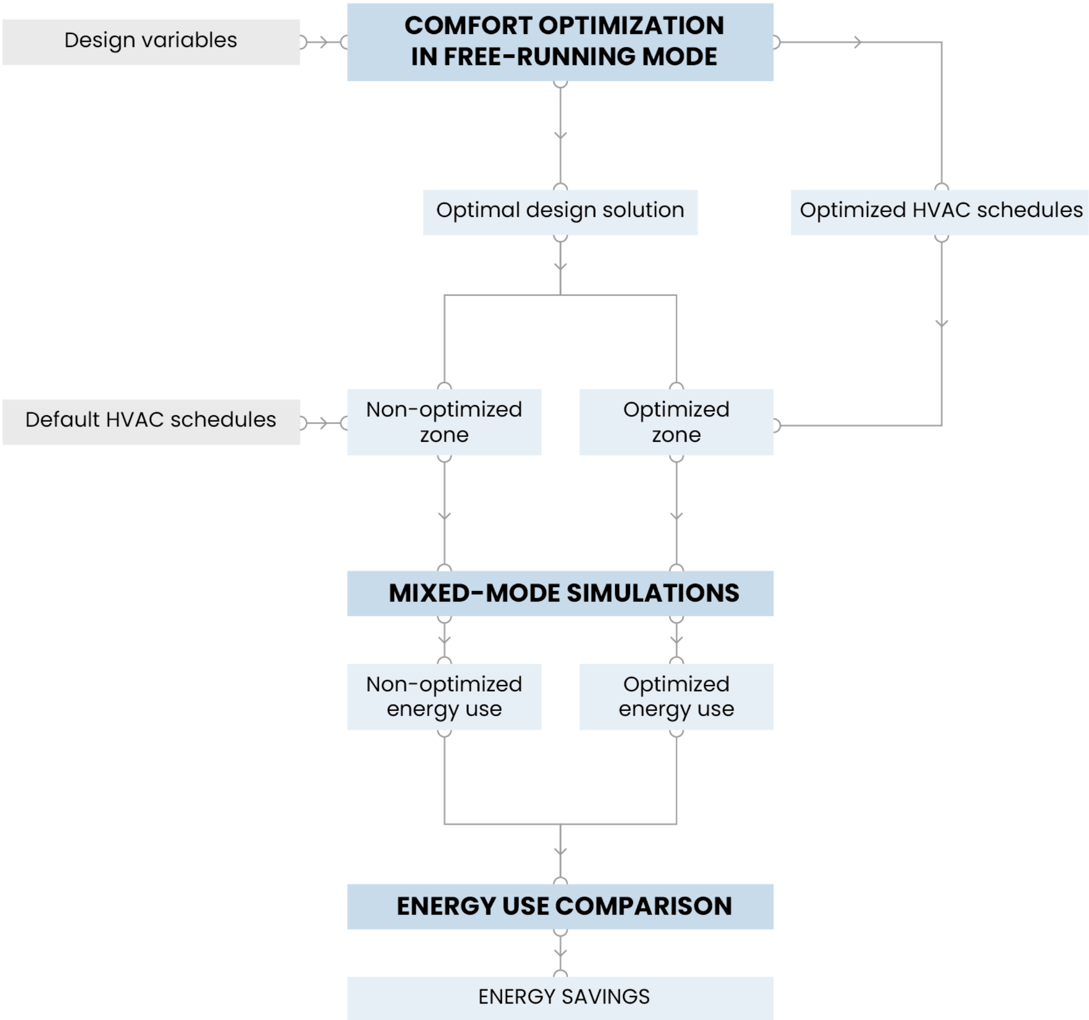

Figure 2 - Tool schematization.

This workflow proves to be an essential tool for the preliminary stage of the project in a view of environmental sustainability and conscious design, as it assists architects in exploring a large number of design options at one time by comparing their level of performance and its effects on comfort. Furthermore, the tool allows to reach satisfying comfort levels in the indoor environment without any mechanical cooling or heating system, assessing the building's free-running potential.

Each of the following sections focuses on one of the nine phases of the discussed method and illustrates more in detail the developed approach. For a visualization of the GH workflow structure, reader is referred to ANNEX 1.

3.1 Geometry

A simplified single-zone geometry is considered and modeled within Rhino-Grasshopper parametric 3D environment. Similar to the existing analysis software DIAL+ [81], the tool gives the possibility to choose among three different plan shapes: rectangular, L-shaped and trapezoidal. However, unlike DIAL+, GH parametric environment allow to easily change the dimensions (width, depth and height) for each configuration using simple number sliders. Default geometries given by the tool can be easily replaced with custom building geometries by importing Rhino 3D objects as Breps[15] into GH.

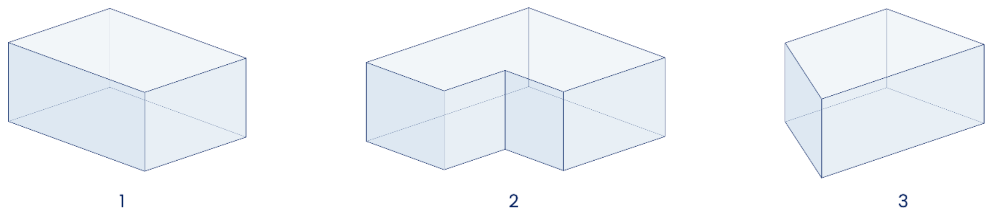

Figure 3 - Axonometric schematization of the three possible geometric configurations among which to choose for the analyses. (1) rectangular; (2) L-shaped; (3) trapezoidal.

In this case, a simple box shape unit with a 5 x 7 m rectangular floor plan (35 m^2 floor area), 3 m high and no interior partitions is considered.

3.1.1 Single-zone model

Although the tool could be capable of dealing with both mono-zone and multi-zone analysis, the simplified model is recognized as the most suitable for the analysis purpose. Single-zone models are usually preferred to more accurate multi-zone models when it comes to performance assessment as they are less complex, simpler and quicker to analyze, improving computational cost. In addition, they normally lead to results with comparable accuracy. For instance, Johari et al. [82] demonstrated that

[15] Brep is a term that stands for Boundary REPresentation and describes a way of defining solid objects using their outside boundaries [33].

the relative difference between analysis results of a mono and a multi-zone model did not go beyond ± 5%.

When dealing with a building, especially of large size, in which requirements change in between individual zones and throughout time, mono-zone models can help setting up more efficient, healthier and less expensive systems that can provide higher level of occupants' comfort. Donald and Wulfinghoff [83] pointed out the shortcomings of most widely used multiple-zone HVAC systems and identified single-zone optimized systems as a better alternative. In order to bring actual advantages, such systems must be accurately designed and tailored to the requirements of each building area so that to improve efficiency and reduce costs and energy waste. Using a single-zone model for performance simulation during early building design stages moves in this direction.

3.2 Thermal zone definition

After establishing the desired geometry and setting its dimensions, thermal zone is defined through Honeybee plug-in, creating a *HB zone*. In this section, key aspects of building design on which it is possible to intervene and their impact on passive strategies potential are discussed.

3.2.1 Zone program and conditioning

First step consists in choosing the zone program, that is its intended use, from a given list. Among selectable zone programs there are residential, office, retail, school, hotel, hospital and others, and each class of use include other sub-classes. A closed office program (sedentary activity) is applied to the HB zone and used to assign EP schedules and loads for occupancy and internal electronics, thus defining the zone energy need. Next, HB requires information about if the indoor space is conditioned or not. For the analysis purpose, the building is considered not conditioned, operating in a *free-running* mode. A free-running building (also naturally-conditioned or naturally-ventilated) is a building in which neither heating nor cooling systems are in operation, although non-conditioning mechanical ventilation system could be in function. This condition is defined as essential for the application of the adaptive comfort model from both the American (ASHRAE-55) and the European (UNI EN 15251:2008 and UNI EN 16798:2019) adaptive standards. Honeybee zone is thus created and needs to be further characterized.

3.2.2 Orientation

Building orientation plays an important role in defining indoor thermal and visual comfort, as it establishes the exposure of surfaces, especially transparent openings, with respect to wind and radiation. Therefore, changing the orientation of the building means modifying the amount of solar energy and light that hit the envelope and that can potentially reach the indoor environment, as well as the rate of air flow useful for ventilative cooling[16] [79, 84]. Control over these parameters results in control over indoor temperatures and visual comfort, minimizing the amount of energy needed for conditioning and artificial lighting.

Zone orientation is defined through HB component *rotateHBObject*. To the selected geometry, the possibility to rotate counterclockwise around its center point of a defined angle is given. Possible orientation angles happen every 45° between 0 and 360 degrees, as displayed in Figure 4. Y-axis is considered as the north direction, which corresponds to 0°, while 180° corresponds to the south.

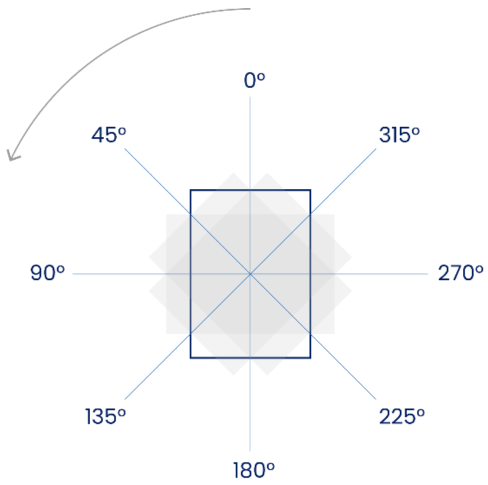

Figure 4 - Possible building orientations.

[16] For instance, according to Grosso [84] and Givoni [79], better ventilation conditions are provided by oblique wind, when the incident angle of the air flow is not perpendicular to the apertures' surfaces.

3.2.3 Windows

Windows have different functions and can bring numerous benefits to the indoor environment (e.g. solar gains, natural lighting, visual contact with the outdoors, ventilation, etc. [79]). However, if not designed properly, they could become a source of discomfort, resulting in increased glare probability and causing overheating or, on the other hand, high heat dissipation. Hence, control over windows position and size is crucial.

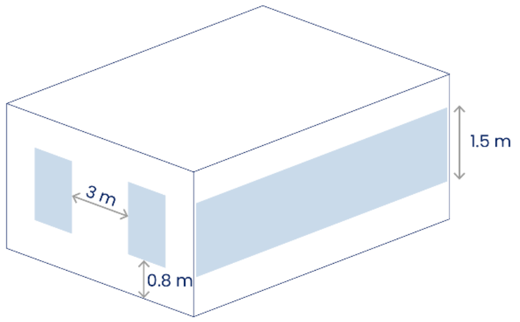

Figure 5 – Axonometric representation generated with GH-HB illustrative of one possible glazing configuration for the zone and windows fixed dimensions. WWR is 0,5 on east façade and 0,3 on south façade.

The proposed parametric tool allows to generate glazed openings based on desired window-to-wall ratios, defined for each of the four primary cardinal directions. Influence of WWR on energy needs for heating and cooling is discussed in [42]. Window-to-wall ratios can vary from 0 (0%) to 1 (100%) and can be easily established in the parametric environment using number sliders, one for each façade. HB *glazingCreator* based on ratio also provides a high level of control over windows geometry. It is possible to create either one single window or a distributed set of multiple apertures for each vertical surface. As HB suggests, generating one single glazing on wall surfaces is recommended to decrease simulation run time, while multiple windows are better for increasing simulation accuracy and output resolution. In addition, having more than one opening on different walls provides a better chance to achieve effective natural cross-ventilation. For these reasons, multiple glazing surfaces configuration was chosen. Aside from WWR, windows are generated on the basis of other dimensions that can be established by the user. In particular, apertures height was set at 1.5 m, distance between individual windows at 3 m and distance from sill to floor at 0.8 m. On this subject, it is worth mentioning the influence of vertical positioning of windows [79, 84] on ventilation. If placed too high with respect to the level of occupancy, the beneficial effect of external air flows could be limited.

Assuming a work plane height of 0.75-0.80 m and the level of a man sitting at around 1.10-1.20 m, the considered sill height appears ideal.

The tool also provides the possibility to split the glazed area into two parts by setting a vertical distance between them. For this study, windows are considered as a one-pieces without internal divisions. It is worth noting that for small WWR custom input dimensions are respected, but in the case of high values of glazing ratios, WWR takes priority over them. Figure 5 shows an example of how user input dimensions can be overridden by high WWR. On the east façade of the zone, a glazing ratio of 0.5 (50%) makes that distance between windows is no longer respected, creating one single extended aperture on the wall surface. Instead, preset window height and sill height are preserved.

3.2.4 Envelope

As the building envelope is considered the main barrier between the outdoors and the indoors, it is one of the most important elements for comfort preservation [85]. Therefore, it is of great importance to put effort to design it appropriately with respect to local climate and surrounding context.

The geometry considered for the simulation operates as a stand-alone space unit. As shown in Figure 6, five of the six surfaces of the zone are exposed to the external conditions, allowing heat transfer between the inside and the outside. The floor slab is not exposed to the external environment, yet it is in contact with the ground.

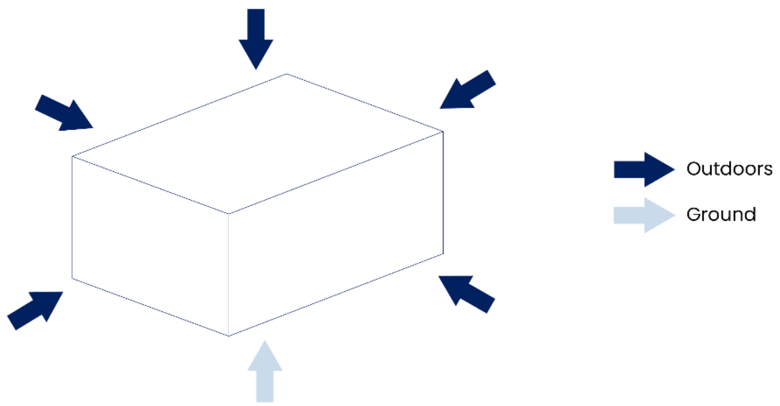

Figure 6 – Visualization of how the office unit is exposed to the exterior.

Opaque envelope is then defined using default materials from the EP construction library, combining them into custom EnergyPlus constructions. Only the insulation material (the XPS) is created from scratch, generating a custom EP opaque material and then adding it to the Honeybee material library. The insulation characteristics (see Table 1) are specified as HB inputs for the material definition.

INSULATION MATERIAL	COMMERCIAL NAME	ROUGHNESS	THICKNESS [m]	CONDUCTIVITY [W/m K]	DENSITY [kg/m³]	SPECIFIC HEAT [J/kg K]
	XPS Styrodur 2500 C	Medium	Variable	0.035	100	1450

Table 1 – XPS insulation technical data used to define the material in HB.

Adequate insulation of the envelope is a key parameter for both cold and hot weather conditions, as it reduces thermal loss from the inside towards the outside in the former case, while delays heat penetration from the outside into the indoor environment in the latter. However, excessive insulation could cause overheating, especially in hot climates. Hence, the insulation layer must be appropriately designed. For this simulation, thickness is conceived as a variable number, as it will be one of the parameters to be considered for the multi-objective optimization process. Possible insulation thicknesses range from 0.15 m (15 cm) to 0.45 m (45 cm).

Assuming a framed structure (e.g. steel framed) for the considered zone, walls stratigraphy has been conceived as a lightweight closing element without any bearing capacity. A metal roofing superiorly closes the space; internally, ceiling is paneled in acoustic tyles, very common in offices. Floor is conceived as an inferior horizontal closing element, facing the ground. Walls, ceiling and floor are insulated.

As far as transparent envelope is concerned, window construction has been defined using custom materials. With the help of ACG Glass Configurator [86], a double-glazing window is created by pairing a 6 mm low-e[17] single glass pane with a 6 mm

[17] Low-e glass is a glass on which a thin layer of low-emissivity coating is applied to reduce heat dissipation, while not limiting the amount of light that enters the indoors. Low-e coatings are made of metal oxides and are usually applied on the inner side of the glass pane.

clear single glass pane, introducing a 20 mm air gap in between the two. The most important light and energy properties of the two glass pane types are provided in Table 2.

GLASS	THICKNESS [mm]	g-value [-]	ρ_e [-]	τ_v [-]	ρ_v [-]	λ [W/m K]
LOW-E	6	0.68	0.20	0.90	0.05	0.30
CLEAR	6	0.86	0.08	0.89	0.07	0.90

Table 2 – Glass panes technical details used as inputs for the creation of the EP glass materials. Source: AGC Glass Configurator.

This glazing construction is applied to all windows. Table 3 displays the light and energy properties of the final window construction. Window U-value is 1.4 W/m² K, which corresponds to a thermal conduction of 0.045 W/m K as the glass construction thickness is 0.032 m.

	THICKNESS [mm]	g-value [-]	ρ_e [-]	τ_v [-]	ρ_v [-]	λ [W/m K]
WINDOW	32	0.64	0.25	0.81	0.12	0.045

Table 3 – Windows light and energy properties. Source: AGC Glass Configurator.

EP opaque and transparent constructions used in this analysis represent only some of the numerous configurations that can be created combining default and customized materials and assigned to the desired building components.

3.3 Passive strategies

When seeking to enhance efficiency and minimize environmental impact of buildings, reduction of heating and cooling needs is crucial, as they account for more than 50% on building energy balance [18]. Reduction of heating energy need has been largely

[18] In residential buildings heating and cooling are responsible for 80% of energy consumption, as stated in [14]. Cooling on its own accounts for 10% of all global electricity consumption today [87].

discussed and investigated through the implementation of strategies, such as passive solar heating and improved envelope insulation [42, 85]. Only recently the focus has shifted towards reducing cooling energy demand, which seems to be constantly growing and is expected to triple by 2050, becoming particularly important especially in hotter regions [87]. Reasons to this must be searched in the occurrence of higher outdoor temperatures due to climate change, in increased indoor thermal comfort expectations [88] and in low ACs efficiency. Hence, the integration in the design process, since conceptual phase, of passive cooling solutions capable of thermal control and heat dissipation – see [79-89] – arises as an important challenge for modern designers. The goal is to create buildings that are able to take advantage of natural sources, such as the wind, to maintain acceptable temperatures within the indoors and improve indoor thermal comfort. Several natural and passive cooling techniques, either non-mechanical or mechanical, can be applied to a building to reduce energy consumption. Among these, ventilative cooling (which refers to the use of outside air in natural or mechanical ventilation strategies to cool indoor spaces during daytime or nighttime), radiant cooling, evaporative cooling and earth cooling strategies are some examples [79]. In this research, natural daytime ventilation through the opening of windows is considered. Natural ventilation (NV) in public buildings, such as offices, is still poorly discussed, despite the fact that it could considerably minimize the cooling load required for maintaining comfortable indoor conditions. Particular focus in this section is also given to shading, although it cannot be strictly defined as a cooling strategy in the true meaning of the expression.

3.3.1 Natural ventilation

Natural ventilation, also known as *comfort-ventilation* [79], is one of the simplest passive cooling strategies for improving comfort during occupancy period when indoor temperature is perceived as too warm. A tool for the evaluation of climate ventilation potential already exists. Refer is made to the *Ventilative Cooling potential tool* (*VC tool*), developed within IEA-EBC Annex 62 project [90-92]. This excel-based tool provides useful information for comparing in early-design stages the effectiveness of different low-energy cooling systems under different climatic conditions and building characteristics, supporting decision making. Starting from hourly based climate data, the tool calculates for a single-zone model wherever cooling is required and what type of ventilative strategy is the most suitable for each hour of the year. Instead, the proposed tool offers the possibility to model different common types of natural ventilation (window, chimney/cowl or fan-driven NV) through the dedicated HB component and identifies the hours of the year when it is required for cooling purpose. Moreover, an energy model obtained with EP such as the one used in this paper, is more accurate with respect to VC tool, which operates several simplifications in calculations that could result in overestimating or underestimating ventilative cooling usefulness, especially during summer period [92].

For the simulation, window daytime NV is selected. Cross-ventilation is allowed, assuming that windows on opposite walls can open simultaneously, thus generating a pressure gradient that increases ventilative cooling potential. Letting flow into the environment outdoor air, even when it is warmer than the indoor average temperature, produces a direct physiological cooling effect on users, as higher air speeds increase the upper temperature limit of comfort by raising sweat evaporation rate [79]. Air flow rate and interior speed depend on the size of the glazed surface that is operable for NV. It has been considered that all the windows of the zone are entirely operable in their height, while operable area fraction is variable between 0.50 (50%) and 1 (100%). This parameter will be improved through the optimization process. Air flow rate and speed can also be modified by the presence of fly screens. To account for additional friction caused by them, a *stack discharge coefficient* is considered by HB and multiplied by the area of the window. This number can range between 0 (no stack ventilation) and 1; default coefficient of 0.17 is assumed.

As NV is not desirable throughout the whole year, especially when heating is required, a temperature range for the application of this passive strategy is set. Glazing operable area can be opened only when outdoor temperature is above 12°C and indoor temperature is at least 25°C. This enhances the effectiveness of ventilative cooling, limiting its use exclusively when it is really needed.

3.3.2 Shading

According to Kamal [93], «the most important passive cooling strategy, regardless of mass, is shading». The reason to this statement lies in the fact that shading devices play a significant role in controlling inflows, both solar and wind, that enter the building through its apertures. They can be classified in different categories based on their geometry (vertical or horizontal shading), their position with respect to glazing (internal or external shading) and their control type (fixed or adjustable shading) [79, 84]. Using one shading type rather than the other depends on the desired level of performance and on the architectural result that the designer wants to achieve. External shading devices are usually preferred as they are more effective in solar controlling. Due to their position outside the windows, they are able to intercept sun rays before they reach the glass surface, preventing its overheating and hence minimizing peak heat gain and keeping indoor air temperatures lower than what would have been without any kind of shading [93, 94]. Consequently, cooling demand decreases and building performance is improved, also leading to the possibility to install smaller HVAC systems [93]. Furthermore, external shading also has implications on natural ventilation and visual comfort. With regard to NV, shading placed outside can control both air flow rate and its direction depending on their angle, potentially allowing ventilation to better reach occupancy zone and so raising ventilative cooling effectiveness. Meanwhile, with respect to visual comfort, external devices can control incoming light, block it whenever unwanted and reduce glare probability and associated discomfort.

External fixed horizontal shading devices are modeled in GH for all the HB zone windows. Venetian blinds are selected among the possible shading types, which also include shades (fabric roller shades or perforated metal screens) and switchable glazing (electrochromic glass). Horizontal shading has been proven to be the most effective in all orientations, as it allows more daylight penetration and provide wider external view with respect to vertical devices [94, 95]. Five slats per window are designed, with a depth of 10 cm and positioned at a distance of 20 cm from the glass surface. Shading material is not conceived as completely opaque, but slightly transmitting light (τ_v = 0.20), like a perforated shade.

Figure 7 - Illustrative 2D section of the zone with a focus on shading devices.

Then, shading angle is defined. It is represented by a number between -90° and +90° that specifies how much the slats of the venetian blinds are rotated with respect to the horizontal plane. For instance, an angle of 0° defines slats that are orthogonal to the window surface, while for an angle of 90° slats are parallel to the glass. Shading angle has been chosen as one of the design variables to be used for the optimization.

3.4 Boundary conditions

The term *boundary condition* is used to identify every element that defines the surrounding context of the building. Physical context and climate fall under this definition. To achieve a good building design, it is impossible to disregard these components. The following subparagraphs discuss the boundary conditions used for the simulations.

3.4.1 Local climate

Weather data is imported into GH environment through LB using EPW files. EnergyPlus Weather files are text files which contain hourly information about temperatures, relative humidity, wind speed and direction, solar radiation, illuminance and pressure for a given location. Along with these details, in the first eight lines of the file further information is displayed: location coordinates, design conditions, typical/extreme periods, ground temperatures, holidays/daylight savings, data periods and other comments [96]. The proposed method is implemented by considering ten Italian and European locations representative of different climatic conditions. Sites in question include Bari, Palermo, Rome, Turin and Trieste in Italy; Aalborg (Denmark), Athens (Greece), Paphos (Cyprus), Geneva (Switzerland) and Kemi (Finland) among other EU countries, as illustrated in Figure 8. EPW files applied in the analyses have been created with Meteonorm software (v7.11) [97, 98] using weather data recorded by meteorological ground stations located near the aforementioned cities.

Figure 8 - Europe map on which the ten locations considered for the definition of local climates in the analyses are illustrated.

Considered locations can be divided in three groups based on their weather condition, as it can be seen from Table 4. In compliance with Meteonorm handbook [97], climatic classification developed by Troll and Paffen [99] is applied. According to this classification, five climatic zones are defined based on irradiation, temperature, precipitation and vegetation parameters. These are further subdivided into 34 climate types to describe typical weather conditions expected in a specific area. Main zones are as follows:

I. polar and subpolar zone;
II. cold temperate boreal zone;
III. cool temperate zone;
IV. warm temperate, subtropical zone;
V. tropical zone.

CLIMATIC ZONES	LOCATION	CLIMATIC ZONE	CLIMATE TYPE
	Kemi	II 2	Continental boreal climate
	Aalborg Geneva Turin	III 3	Submaritime climate
	Athens Bari Palermo Paphos Rome Trieste	IV 1	Mediterranean climate with humid winters and dry summers

Table 4 - Identification of Troll and Paffen climatic zones for the considered European locations.

Zone II 2, to which Kemi belongs, is characterized by hard climatic conditions. It experiences long, cold and very snowy winters, while summers are short and relatively warm. In contrast, zone III 3 has milder weather conditions: moderately cold winters and modestly warm to warm and long summers are peculiarity of this climate. Maximum precipitation occurs during autumn and summer seasons. Last, sites located in the southern part of Europe belong to the zone IV 1, which experiences humid winters and dry summers [100].

After choosing the locations for which to carry out the analyses, EPW files are created. First tranche of simulations is run considering present climatic conditions and employing weather file generated for a typical year using solar radiation data from the period 1991-2010 and temperatures data from the period 2000-2009. To test the workflow resilience, a second tranche of simulations is performed with weather files that contains climate future projections for the year 2050, in accordance with A2 emissions scenario described in the Special Report on Emissions Scenarios (SRES) [101] and in other IPCC reports – see for example [102]. The SRES develops four storylines or scenario families (A1, A2, B1 and B2) that group together forty different scenarios. Each scenario outlines a different possible future world development up to 2100, considering several factors such as demographic change, social, economic and technological development, energy use and land-use change, that are the main driving forces of GHGs emissions. Among the four SRES scenarios, A2 describes a high-impact (although not the worst) future development, dominated by a significant and continuously increasing global population growth, a slow technological and economic (regionally oriented) development and a stark transition back to coal.

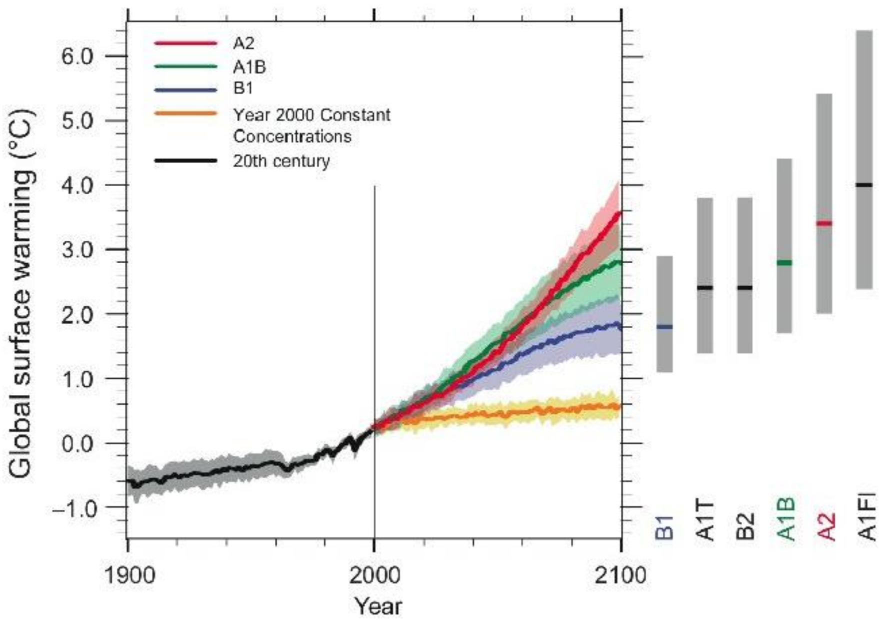

Figure 9 - Multi-model averages and assessed ranges for surface warming. Source: NARCCAP [103].

These driving forces lead to a continuous rise in GHGs emissions throughout the whole-time horizon to 2100 [101], the highest projection among the four scenarios. As expected, this scenario results in the highest temperature rise – see Figure 9.

Following the NARCCAP method [103], A2 was preferred because of its greater meaningfulness from an impacts and adaptation point of view, with respect to other SRES scenarios. Potentially, if adaptation is achieved in the case of a larger climate change, then it will be achieved even in the event of smaller changes in climatic conditions. Therefore, if the presented method is capable of finding optimized solutions for a more severe weather, it will be reliably able to deal with milder climatic conditions.

3.4.2 Context

Context geometries are modeled into Rhino and then imported to GH as Breps. It is supposed that the considered office space is located in a city environment. Surrounding buildings are generated randomly as solid blocks, as displayed in Figure 10. The context is kept always the same for all the locations. In addition, a ground surface is created as a HB surface directly into GH to improve daylight calculation accuracy.

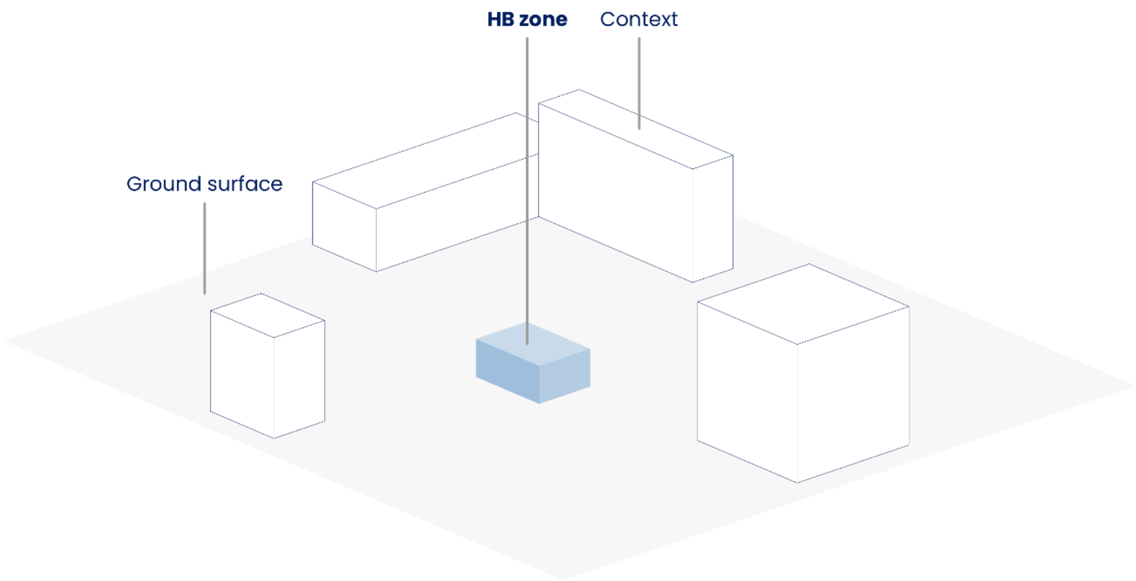

Figure 10 - HB zone context. S-E Axonometric view generated with Rhino-GH.

3.5 Performance simulations

Overall building performance is evaluated assessing two fundamental aspects that contribute to define indoor comfort and efficiency: energy and daylight. Two parallel detailed dynamic simulations are run using Honeybee plug-in (v0.0.66 – Legacy Plugins) as an interface with EnergyPlus, Radiance and Daysim engines. It should be recalled that, for this part of the research, the thermal zone operates in free-running. This paragraph contains information about the programs used, the simulation parameters set and the analyses output files formats. The definitions provided in this paragraph are mostly taken from HB components inputs and outputs descriptions.

3.5.1 Energy simulation

Energy analyses are performed through EnergyPlus (v9.6.0) along with OpenStudio (v2.9.1), which establishes a link between the tree-dimensional parametric model developed in Rhino-GH and the simulation engine. The proposed workflow uses HB component *exportToOpenStudio* to export the developed HB zone into an OSM (*OpenStudio Model*) file that is translated into an IDF (*Input Data File*) file and then run through EP. This component requires a collection of inputs (simulation parameters) and outputs several files of different formats.

Inputs

- *Weather file*: an EPW file imported to GH through Ladybug.
- *Analysis period*: an optional analysis period can be set using the corresponding LB component. In this case, no analysis period is specified, so that simulation is run for the entire year.
- *Energy Simulation Parameters*: HB component *EnergySimPar* allows to establish a series of simulation parameters:
  - Timestep: energy simulation is performed with a timestep of 10, which represents the number of times the simulation is run in an hour.
  - Shadow calculation: it is averaged over multiple days (instead of running it for every timestep) with a frequency of 30. This means that it is performed

every 30 days and the average over this period is used to represent all 30 days in the energy simulation. A maximum number of 3000 points is accounted for the shadow calculation.

- Solar distribution calculation: "full interior and exterior with reflections" distribution calculation is chosen, which represents the most accurate method as it accounts for light bounces that happen both on the outside and on the inside of the zone. However, if the L-shaped geometry is selected at the very beginning of the workflow, severe warnings can show up at this stage, as the concave geometry mess up with solar distribution calculation. In this case, it is recommended to use another calculation method among the ones proposed by the HB component: "minimal shadowing", "full exterior", "full interior and exterior" or "full exterior with reflections".
- Holydays: the days of the year in which a holiday occurs can be inputted as a list (e.g. JAN 01, DEC 25, etc.), in order to not consider them in the occupancy period.
- Simulation controls: optional EP simulation controls can be established using HB *simControl* component. In this case, because the zone does not have any conditioning system in function, HVAC sizing calculations are not performed. A Boolean toggle is set to False for zone, system and plant sizing calculations. Maximum and minimum warmup days [19] are left at default values, respectively 25 and 6 days.
- Heating and cooling sizing factors: HVAC is not considered in this part of the research, so sizing factors are not specified.
- Terrain: surrounding terrain of the building can be chosen among four options: city, suburbs, country and ocean. City is selected.

[19] Max and min warmup days represent the maximum and minimum number of days for which the simulation is run before EP starts recording result values. Default values are usually appropriate. However, it is possible that a severe warmup convergence warning shows up because, after the default max warmup days, the HB zone does not converge. This may be due to the fact that the zone experiences very dynamic conditions induced by natural ventilation settings. The warning may disappear if max and min warmup days values are increased. Though, the error does not prevent the simulation to give the requested results. For more see related discussions on dedicated forums, such as https://discourse.ladybug.tools/t/warmup-convergence-error/6643 and https://discourse.ladybug.tools/t/warmupconvergence/4857 (accessed 08 May 2022).

    - Monthly ground temperatures: HB default values are used. They are estimated starting from the values contained in the weather file. When EPW ground temperatures are below 18°C, 18°C is used as actual ground temperature. Instead, when monthly ground temperatures are above 24°C, this value is used as the actual temperature. Lastly, if monthly average falls between 18°C and 24°C, actual ground temperature is considered.
- *HB zone*: the Honeybee zone whose performance has to be simulated through OS+EP.
- *Context*: context geometry described in §3.4.2 is inputted.
- *Simulation outputs*: HB component *Generate EP Output* is employed to select output that are desired to be written by EP in the result files. For this part of the research, it is fundamental to have the *zoneComfortmetics* set to true, in order to get information about the zone's mean air temperature, mean radiant temperature, operative temperature and relative humidity, whose values will be applied in further comfort metrics calculation. Load type is set to Total.
- *File name and working directory*: it is possible to specify a name for the files and a custom folder on the system where the results will be placed. It is of paramount importance not to use any spaces in the input directory name, otherwise an error will occur.

Once set all the simulation parameters and connected all the essential inputs, the simulation is launched by setting to True the *runSimulation* field. Analysis may take up to some minutes.

Outputs

Outputs from the *exportToOpenStudio* component include:

- The generated IDF file, the EP file that contains the details of the model.
- The generated OSM file: an instance file of the OpenStudio data schema which is clear text and look very similar to IDF.

- A CSV file (*Comma Separated Variable*), a text file which contains the simulation results (EP standard outputs ESO + EP meter outputs MTR) structured in columns. This file format can be easily read using Excel.
- An EIO file (*EnergyPlus Invariant Output*). It represents a text file containing output that does not vary with time, like location information (latitude, longitude, time zone, altitude) [46].
- A RDD file (*Report - variable - Data Dictionary*), that is a text file listing the variables available for reporting [46].
- An HTML report, generated after running the simulation. It can be opened through a web browser to get an overview of the energy model results.

The CSV file is the one needed to obtain the desired information from the simulation. Its address is used as the input for the *readEPResult* Honeybee component which extract from the CSV file all the data related to the HB zone. In this component, the outputs displayed depend on the one selected from the *Generate EP Output* component previously described.

3.5.2 Daylight simulation

Annual daylight simulations are carried out using Radiance (v5.4) engine. Radiance is a free-license highly accurate ray-tracing software system developed by the U.S. Department Of Energy (DOE) with support from the Swiss Federal Government [104]. It is widely used by engineers and architects to predict and preview daylighting distribution and visual comfort during early-design stages. Using *runDaylightAnalysis* component, the zone is exported to a RAD file, which is a text format that translates HB geometries and materials into the main input file for Radiance. Most important inputs and outputs for this Honeybee component are discussed below.

Inputs

- *Honeybee objects*: required geometries include the HB zone, the context, the shading devices Breps and the ground surface created before – see §3.4.2.

- *Analysis recipe*: as Radiance can perform different kinds of simulations, HB provides several analysis recipes that can be connected to this input field. For instance, possible analyses include daylight factor simulation, grid-based or image-based lighting analyses and annual daylight simulation. The last mentioned is the one chosen for the research purpose. Therefore, *annualDaylightSimulation* recipe is built up using the EPW file and generating a test points grid and a test mesh that match the zone's floor area. The test grid has a size of 0.50 and is located at a height of 0.80 m from the base surface (the floor), as can be seen in Figure 11. This results in 140 points that will be used for the daylight analysis.

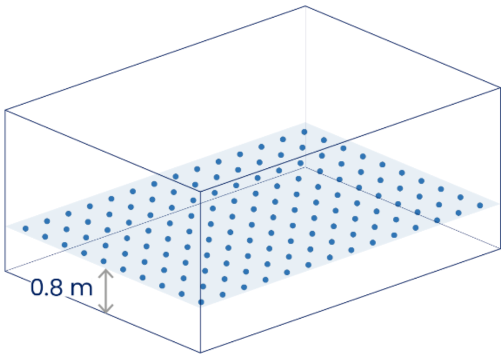

Figure 11 - Axonometric visualization of the test points grid and the test mesh generated for the daylight simulation.

- *Number of CPUs*: the number of CPUs to be used for the studies can be set.
- *File name and working directory*: as for energy simulation, the component allows to specify a name for the project and a directory where the result files will be written. Here too using spaces in the directory name is not permitted.

Daylight simulation is then run by setting to True the *writeRad* and the *runRad* fields. Radiance takes up a longer time (several minutes) with respect to EP to perform the analysis.

Outputs

Resulting files from the simulation include the RAD file previously generated and an ILL file (annual analysis file). The ILL file is then used by Daysim software (v4.0) to calculate daylight metrics, such as Daylight Autonomy (DLA) and Useful Daylight Illuminance (UDLI), through the *readAnnualResultsI* HB component. Based on Radiance backward ray-tracer, Daysim is a daylighting analysis software that estimates the annual daylight availability and lighting energy use in buildings on the basis of occupants' behavior [105, 106]. Advanced shading devices simulations can also be performed. A detailed description of the considered comfort metrics estimated through Daysim is provided in the following section.

3.6 Comfort metrics

Comfort is a primary indicator of human physical and mental wellbeing [107]. As users spend around 85% of their lifetime within the built environment [84], indoor microclimate is a core issue in building design, as it affects occupants' wellness, health, mood, productivity and work performance, and it also impacts on energy consumption. Indoor comfort results from the combination of several aspects, including thermal, visual and acoustic comfort, being influenced by a wide range of environmental factors (temperature, humidity, lighting, air quality, etc.). The model presented in this work is based on the prediction of occupants' thermal and visual comfort by means of assessing various parameters that attest the level of individual satisfaction and the compliance with normative thresholds. At first, only thermal comfort was taken into account to represent human wellbeing inside the zone, running only the EP energy simulation. However, thought has been given to the strong interdependence of the two issues. In fact, design strategies that could benefit thermal comfort could also result in visual discomfort, and vice versa. For instance, reducing WWR could represent a good choice to improve thermal performance of the building envelope, but, at the same time, it may lead to a reduction in the amount of daylight available within the environment throughout the year and, consequently, to higher energy needs for artificial lighting. Likewise, increasing WWR could enhance visual comfort yet increase heat transfer through the transparent surfaces, resulting in excessive thermal dissipation or overheating that determines higher energy consumption for heating/cooling. This makes clear that control on thermal and visual comfort cannot be separated from each other. Hence, both aspects are considered with the aim of giving a more complete overview of how indoor comfort is defined.

3.6.1 Adaptive thermal comfort

ASHRAE Standard-55 [108] describes thermal comfort as «that condition of mind that expresses satisfaction with the thermal environment and is assessed by subjective evaluation». Therefore, the feeling of thermal comfort highly depends on individual variables, among which age, physical characteristics, habits and adaptation to a certain climate. In short, the several parameters on which comfort depends may not produce the same responses and sensations in different persons. Yet it is possible to use well-established scientific approaches to predict the percentage of users' satisfaction/dissatisfaction with the conditions of a given environment. Two types of comfort models prevail in literature: *static* (or *steady-state*) and *adaptive* [109]. The first model, also called *rational* or *heat balance* [110], refers to the one developed by P. O. Fanger at the turn of 1970s [111]. This approach is the most widely employed in national and international standards (e.g. ISO-7730:2005 [112]) to assess indoor comfort. In accordance with Fanger's model, thermal sensation is the result of the «difference between the internal heat production and the heat loss to the actual environment for a man kept at the comfort values for skin temperature and sweat production at the actual activity level» [111]. Thermal comfort is a function of six variables, four of which depend on the environment (air temperature, mean radiant temperature, relative humidity and air speed) while the other two are physiological parameters (clothing insulation and activity level or metabolic rate). The combined effect of these variables on comfort can be investigated by providing the PMV index (*Predicted Mean Vote*), along with the PPD (*Predicted Percent of Dissatisfied*). PMV results from a complex mathematic equation developed on the basis of climate chamber experiments, under stationary conditions and controlled environmental (e.g. temperature, humidity, etc.) and physical variables (e.g. clothing). It represents the average mean vote on thermal sensation of a group of people in a given environment. Mean vote can be associated to a seven points scale that ranges from -3 (very cold) to +3 (very hot); 0 represents thermal neutrality. PPD, instead, is a statistical index that expresses the percent of people in that same environment who is not satisfied with the indoor thermal conditions. ISO 7730 regulation suggests that PPD should be kept around 10%, which corresponds to a PMV between -0.5 and +0.5.

For how it has been developed, the static comfort model previously described can be applied only in fully conditioned buildings, where a controlled and closely steady climate is maintained within the indoors, nearly independent from the highly variable outdoor conditions. In contrast, for naturally ventilated buildings, in which indoor temperatures continually change in time in relation to outdoor temperatures, Fanger's method is not applicable and could lead to errors in the assessment of occupants' thermal sensation. Significant discrepancy between calculated PMV and actual comfort votes in buildings with NV was found by De Dear et al. [113, 114] while putting together the ASHRAE RP-884 thermal comfort database [20]. Basically, in such buildings the PMV index tends to overestimate the dissatisfaction level of the occupants under warm conditions [110]. The interpretation to such trend may be found in the fact that people who live in naturally ventilated buildings under different climatic conditions can accept a larger range of comfort temperatures than what the *heat balance* model assumes – see for example [115]. Moreover, occupants are not inactive consumer of comfort, yet they are active participant and are able to adapt to internal/external dynamic thermal conditions, i.e. by changing their clothing or opening windows when temperatures are too warm. Given the adaptation capacity of users, it is clear that keeping indoor environments at constant and uniform temperatures defined by standards may result in unnecessary energy waste and even in uncomfortable conditions (overheating during winter and excessive coldness during summer due to the AC system). It has been pointed out that, even in buildings with sophisticated HVAC control, dissatisfaction of the thermal environment is widespread [110].

[20] RP-884 project represents a quality-controlled database built up assembling 21,000 samples from thermal comfort field studies in 160 buildings, both naturally ventilated and with HVAC systems, across different climate regions all over the world.

In response to the shortcomings of PMV method when applied to free-running buildings, *adaptive* comfort models were developed, built on a large number of field studies conducted on people in real environments. The main outcome from these surveys was that comfort (or neutral) temperature has a strong correlation with outdoor prevailing mean temperature, as can be seen in Figure 12. In fact, neutral temperature is related to indoor operative temperature, which in turn varies in accordance with the mean outdoor air temperature.

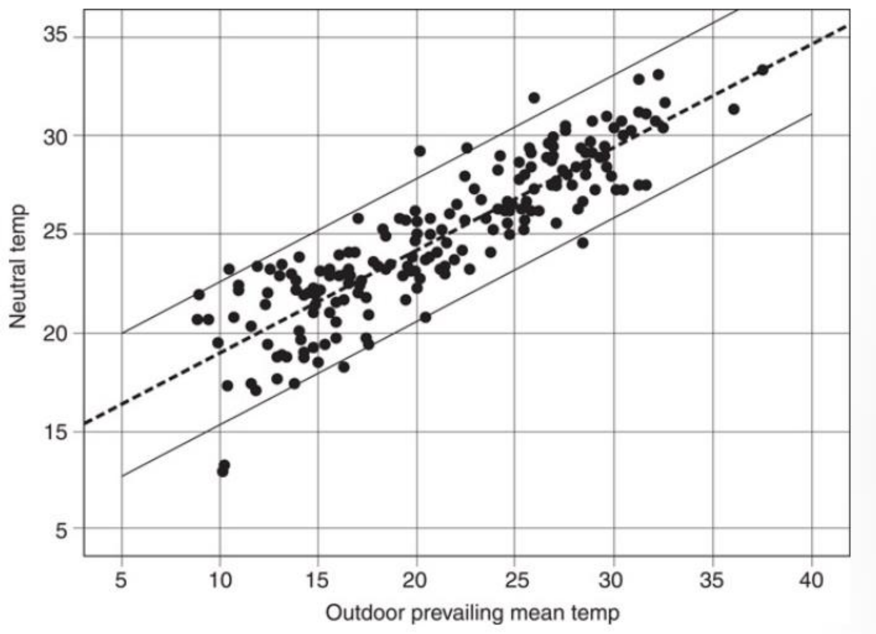

Figure 12 - Scatter plot of neutral temperatures and the prevailing mean outdoor temperatures in buildings in free-running mode, using data collected from field surveys since 1976 [116]. Source: [117].

Adaptive comfort components have been included in several national and international regulations, among them the American ASHRAE Standard-55 [108] and the European CEN Standard EN 15251 [118], now superseded by EN 16798-1:2019 [119]. The last-mentioned standard points out that this «adaptive method only applies for occupants with sedentary activities without strict clothing policies where thermal conditions are regulated primarily by the occupants through opening and closing of elements in the building envelope (e.g. windows, ventilation flaps, roof lights, etc.)» ([118] p. 19). So, in the definition of the adaptive comfort model, clothing insulation and metabolic rate are not considered. Neither relative humidity (RH) is taken into consideration, although the importance of this parameter on the perception of thermal comfort is widely investigated. The effect of RH has been reported to be small, not strong enough to influence comfort in a meaningful way. In this respect, Nicol [120] and De Dear [121] research works can be mentioned. «The effect of humidity is mainly a psychological one», comments Givoni in a personal communication in 2011 ([110], p. 58), and acclimatization of people in various climates plays a significant role in its perception. However, especially in naturally conditioned buildings, outdoor RH strongly influences internal humidity and, as it cannot be directly controlled by occupants, it should be expected to have some impact on their thermal sensation. Clear evidence of this is provided for the first time in Vellei et al. [109]. The research demonstrated that considering the RH in the adaptive model results in a comfort range shift. In particular, higher comfort temperatures and steeper gradients with respect to what ASHRAE standard predicts are found. High RH values (>60%) are discovered to have a strong impact, leading to lower comfort temperatures and a smaller acceptability range [109]. Nevertheless, as Ladybug Legacy Plug-ins do not provide the possibility to account for humidity, this parameter has been disregarded.

LB *AdaptiveComfortCalculator* component is used to calculate the adaptive comfort of the zone throughout the occupancy period. Since this research is developed within the European context, standard EN 15251 (now EN 16798-1) is preferred to the ASHRAE standard for the evaluation. The main difference lies in the database used to derive the adaptive standard: CEN regulations use the European SCATs project database, which collects comfort data measured in the same period from five European countries, using standard instruments and methodologies [110]. Standards EN 15251 and EN 16798 distinguish buildings based on their system (mechanically or naturally conditioned) and identify three categories (I, II, III). Category II, which corresponds to a «normal level of expectation and should be used for new buildings and renovations» [118], is considered for the tested building. For category II, upper and lower limits of comfort temperatures are calculated by means of formulas 1 and 2 [119]. The limits only apply when running mean outdoor temperature lies between 10°C and 30°C - Figure 13.

Upper limit: $$\Theta_o = 0{,}33\ \Theta_{rm} + 18{,}8 + 3 \quad (1)$$

Lower limit: $\Theta_o = 0{,}33\ \Theta_{rm} + 18{,}8 - 4$ (2)

where:

Θ_o = indoor operative temperature [°C]

Θ_{rm} = running mean outdoor temperature [°C]

Θ_c = optimal operative temperature [°C]

Optimal operative temperature is defined by formula 3 [119]:

$$\Theta_c = 0{,}33\ \Theta_{rm} + 18{,}8 \quad (3)$$

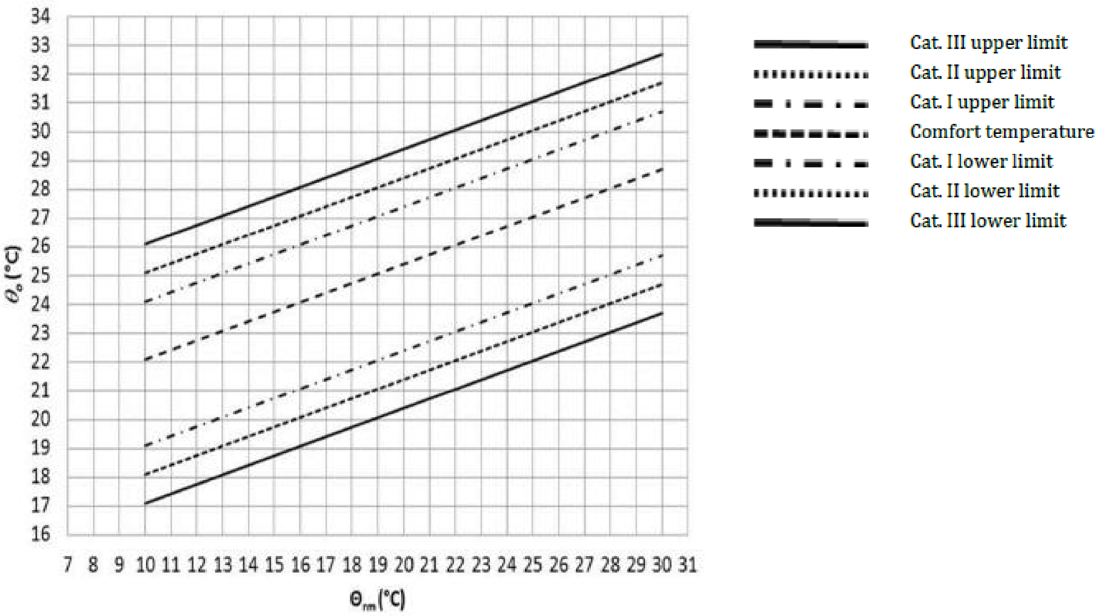

Figure 13 – Comfort temperatures ranges for free-running building categories I, II and III as a function of the exponentially-weighted running mean of the outdoor temperature. Upper and lower limits define design values for indoor temperature during summer and winter seasons. Source: EN 16798-1 [119].

In light of this, LB adaptive comfort calculator requires four main inputs:

- *indoor dry bulb temperature [°C]*: direct output from EP energy simulation;
- *indoor mean radiant temperature [°C]*: also direct output from EP simulation;
- *outdoor temperature*: direct output from the import EPW component;
- *wind speed*, which is assumed equal to 0.5 m/s. Effects of wind movement on comfort sensation have been discussed in §3.3.1. It should be pointed out that an air speed over 0.8 m/s could cause discomfort in workplaces, as it tends to move office papers from the desks [119].

The component calculates whether the environmental conditions defined by the input data are comfortable for the occupants or not: a stream of 0s (not comfortable) and 1s (comfortable) is provided, each number representing an hour of the analysis period. In addition, LB component outputs a list of values from -1 to +1 that correspond to each hour of the input data and indicate whether users feel cold (-1), comfortable (0) or hot (+1). Lastly, the percent of time hot, cold and comfortable are assessed. Maximizing this last parameter will be one of the objectives of the optimization process performed trough Octopus plug-in.

The developed GH script also allows to generate high-quality charts in the Rhino scene to support a clear visualization and understanding of the results. For instance, percent of time comfortable and hot/cold can be displayed as colored meshes on an annual graph using LB *3DChart* component. Figure 14 provides an example of such chart.

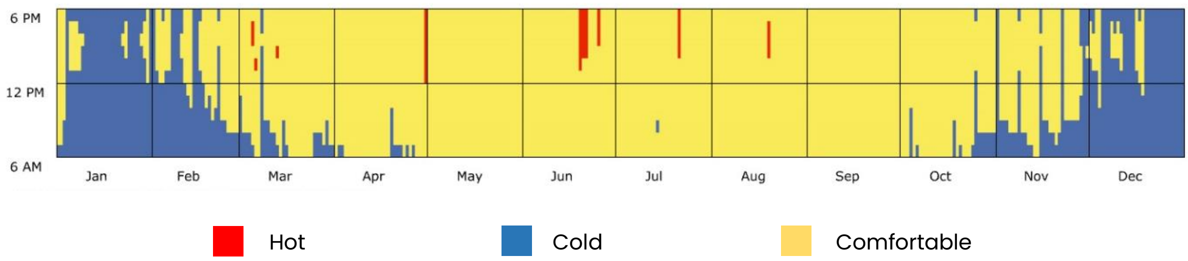

Figure 14 - 3D chart generated with Ladybug. It displays the percent of time comfortable, hot and cold that resulted from the simulation of the optimized solution for Turin (present). Percent hot = 0.75%; percent cold = 23.65%; percent comfortable = 75.59%.

Another meaningful output that can be generated using LB is the *Adaptive Chart*. This plot allows to visualize on a chart similar to the one presented in Figure 13 the number of hours of the considered occupancy period that lie in between the upper and lower limits of comfortable range of temperatures for a given set of input conditions. The hours are displayed as colored meshes, as can be seen in Figure 15. The colored "pixels" located in the chart area under the lower comfort limit represents the hours of the year in which occupants feel cold, while "pixels" above the upper limit represent the hours in which occupants feel hot.

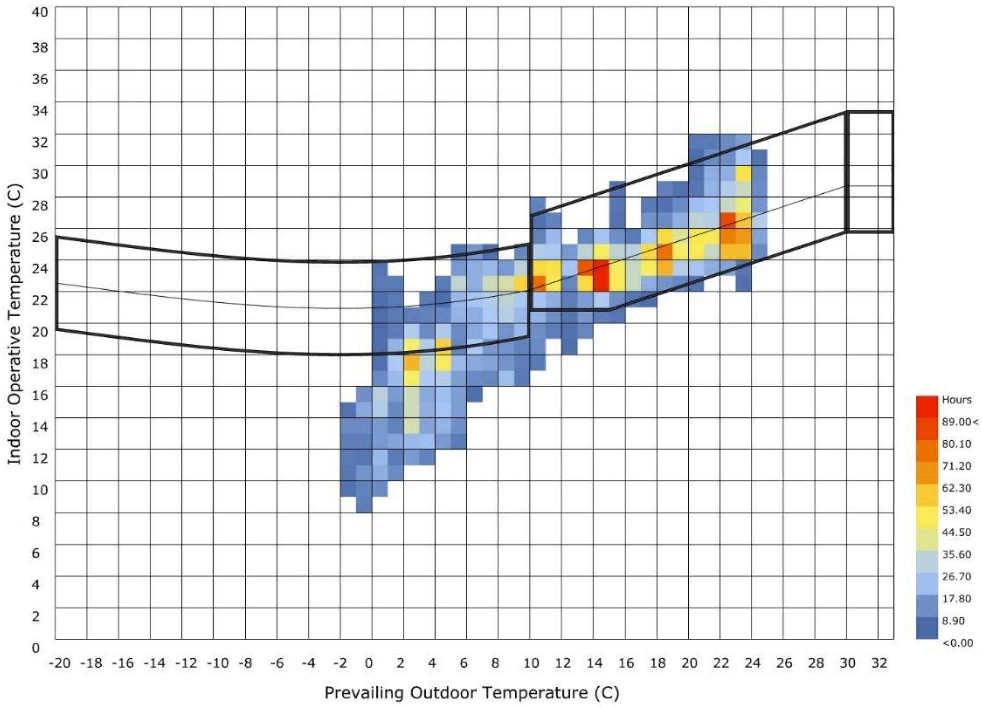

Figure 15 - LB adaptive chart for Turin's optimized solution (present).

3.6.2 Visual comfort

Visual comfort refers to «a subjective state of visual well-being caused by the visual surroundings» [122]. It is an important factor that involves various parameters, among which natural light, reduction of glare, external view and others. Although exposure to daylight is not strictly necessary to make human body function, it has been reported to have significant benefits on the occupants' physic and psychological health [123]. Indeed, natural light regulates human body's circadian rhythm, affecting mood, sleep quality, stress levels and, consequently, work performance and productivity. Moreover, improving daylight in buildings can lead to considerable energy savings, reducing electricity needs and influencing heating and cooling loads and so thermal comfort.

To assess visual comfort objectively, three parameters are considered: Daylight Autonomy (DLA), Useful Daylight Illuminance (UDLI) and Annual Sunlight Exposure (ASE). The first two metrics are calculated through Daysim, as previously mentioned in §3.5.2, while the last one is evaluated using Ladybug components and following a calculation method developed by Chris Mackey on Hydra [124]. Spatial Daylight Autonomy (sDA) is also observed. HB component *readAnnualResultsI* also outputs a

CSV file, that will be used as a custom lighting schedule for the final simulation of the optimized solution.

DAYLIGHT AMOUNT AND DISTRIBUTION - DLA, UDLI and sDA

Honeybee *readAnnualResultsI* allows to calculate several daylight metrics, among which DLA, UDLI and sDA. The component needs an ILL file from Radiance as main input, along with the test points used for the simulation (see §3.5.2). A custom occupancy file has to be inputted, so that Daysim calculates the outputs only for the hours during which the space is occupied. HB *occupancyGenerator* component is employed and an occupancy CSV file is generated. Occupancy period is the same considered as the analysis period for the adaptive comfort metrics calculation, that is from the 1st of January to the 31st of December, from 7 am to 6 pm. No daily off hours are considered, yet during weekend days (Saturday and Sunday) the space is treated as unoccupied. Illuminance threshold for Daylight Autonomy calculation is set at 500 lux to follow the EN 16798 European regulation for offices [119], instead of taking into account the default value of 300 lux. According to HB component description, resulting metrics can be defined as follows:

- DLA is the percentage of the time during the active occupancy hours that the test points receive more daylight than the illuminance threshold (set equal to 500 lx).
- UDLI is a daylight metric that represents the percentage of the occupied time in a year when daylight on test points falls within a specific range of illuminance. UDLI is calculated for three ranges of illuminances: less than 100 lux, between 100 and 2000 lux and over 2000 lux. Particularly meaningful is the $UDLI_{100-2000lx}$. This metric represents the percentage of time during the active occupancy hours that the test points receive between 100 and 2000 lux, which is the most desirable value range. Under 100 lux daylight is insufficient, while over 2000 lux overheating and glare problems may arise.
- sDA was introduced in 2012 by IES Lighting Measurement (LM) 83-12 [125] to represent a prediction of daylight sufficiency. It defines the percent of the analysis points that meets or exceeds the minimum daylight illuminance threshold value

for at least 50% of the working hours. This threshold is set to 300 lux for LEED (v4.1) calculation. To obtain the corresponding credits, sDA must be achieved for at least 55% of the area [126].

Ladybug provides the possibility to generate radiation analysis results visualization as colored meshes on the work plane area. Inputting the desired daylight index values (DLA or others) and the analysis mesh (as defined in §3.5.2) into the *reColorMesh* component, graphic outputs as shown in Figure 16 can be obtained.

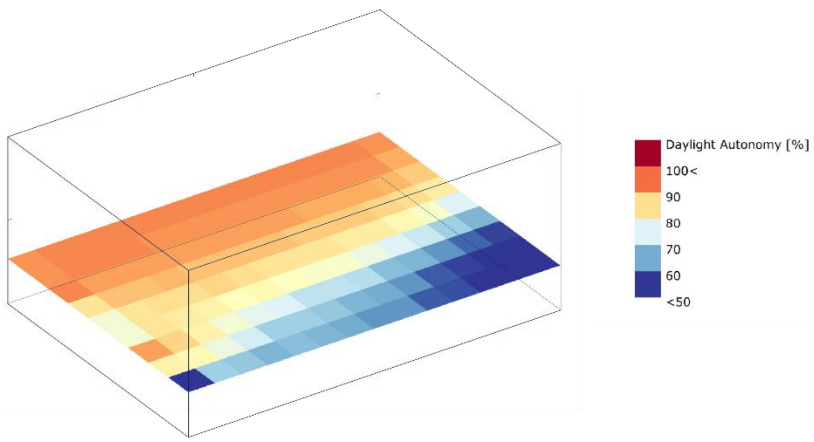

Figure 16 – Axonometric view of an illustrative Daylight Autonomy (DLA) colored mesh.

GLARE PREDICTION – ASE

Glare is defined by IES (Illuminating Engineering Society) as «the sensation produced by luminances within the visual field that are sufficiently greater than the luminance to which the eyes are adapted to cause annoyance, discomfort, or loss in visual performance or visibility. The magnitude of the sensation of glare depends on such factors as the size, position and luminance of a source; the number of sources; and the luminance to which the eyes are adapted» [127]. When designing windows size and position, as well as shading, control on glare is crucial since it can result in discomfort and distraction for the occupants. Several metrics can be used to evaluate the presence of daylight glare in a closed environment. Most commonly used current glare indexes are DGI (Daylight Glare Index) and DGP (Daylight Glare Probability). Both can be calculated through HB *Glare Analysis* that relies on Evaglare for Radiance. This component requires an HDR file that has to be generated through another daylight simulation, this time image-based (previous analysis, described in §3.5.2, was grid-based). Image-based analysis recipe also needs the specification of the position of the observer (through the creation of a Rhino view) for which glare presence will be estimated. However, since exact positions of occupants in the zone are still unknown during this phase of the design process, calculating DGI and DPG only for one or even some of the infinite possible views has been reckoned limitative and not much meaningful for the research purpose, besides being very time consuming as every view has to be rendered by the software. Instead, a method to evaluate the possible presence of glare for the entire floor area of the considered space is preferred. Ladybug Legacy plug-ins do not have any component to perform such analysis [21]. Thereby, ASE was chosen as the metric to predict annual glare within the tested environment.

ASE was introduced together with sDA in 2012 by the already mentioned IES LM-83-12 [125]. It «looks at direct sunlight as a potential source of visual discomfort, measuring the percentage of space that exceeds a specified direct sunlight illuminance level for a specified number of hours» [128]. Specifically, according to LEED v4 thresholds, ASE calculates the percent of the area that receives yearly too much direct sunlight (≥ 1000 lux) for at least 250 hours of the occupancy period at the work plane height (0.80 m). This excessive daylight could cause glare problems and/or overheating, so only ASE values that lie below 10% are considered acceptable for LEED v4 points attribution – see [126]. Although it is recognized that other sources of glare apart from direct sunlight may exist, ASE is here regarded as the simplest glare index to evaluate in light of the simulation's objective.

Calculation method is deduced from the existing methodology made available on Hydra sharing platform [124]; LB components are employed for this analysis. First,

[21] Actually, an imageless method to perform spatial and annual glare analysis has been developed by Jones N.L. in 2019 and is available at https://github.com/nljones/Accelerad/wiki/The-Imageless-Method-for-Spatial-and-Annual-Glare-Analysis (accessed 14 May 2022). However, these custom components are not available for Legacy plug-ins.

direct illuminance falling on the horizontal plane is found starting from direct normal and diffuse horizontal radiation hourly data (output from EPW file). Then, after averaging the values, sun vectors are generated using *sunPath* component, considering only those sun positions for which the horizontal illuminance is above 1000 lux. Resulting sun vectors are then employed to calculate, through the *sunlightHoursAnalysis* component, the number of the occupied hours during which each test point is exposed to excessive daylight. To enhance consistency, test points are the same already used for daylight analysis trough Radiance. Lastly, results are reported on the work plane to assess the percent of the considered area that meets the conditions of excessive illuminance (ASE index). The more the area exceeds the limit, the more probable glare and overheating become. Sunlight hours analysis also allows to create graphic visualizations, similar to the ones previously described for the other daylight metrics, in which the results are displayed on the analysis mesh. This is particularly useful to understand where the most critical areas of the zone are placed.

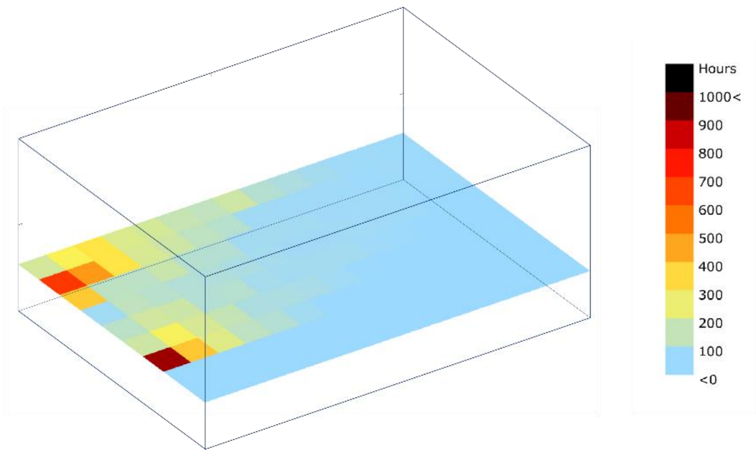

Figure 17 – Illustrative axonometric view of the zone with the analysis mesh, colored with hours results from the *sunlightHoursAnalysis* component.

3.7 Optimization

The purpose of the optimization is to find optimal configurations of a given set of parametric independent design parameters for which satisfying levels of occupants' thermal and visual comfort without mechanical conditioning are achieved. This process supports the exploration of a wide range of potential design solutions, both optimal and sub-optimal, gaining knowledge and awareness on construction choices and their consequences on overall building performance. Since indoor comfort depends on several interdependent, and usually conflicting, factors (see discussion in §3.6), a multi-objective complex problem is stated and solved using a GH plug-in called Octopus. Octopus evolutionary simulator is based on a genetic algorithm (GA, in this case SPEA-2 is used in combination with HypE algorithm) which has the ability to cross-reference multiple parameters simultaneously [129]. The best solutions to the problem will be the ones that are able to mediate the optimality of all the considered objectives. This paragraph discusses the theory that underlies Octopus functioning, along with the parameters and objectives chosen for the simulation and the criteria for the selection of optimal solutions.

3.7.1 Genetic algorithms (GAs)

GAs are among the most widely used evolutionary algorithms, applied in optimization processes of different kinds. They have been defined by Holland [130] as «computer programs that "evolve" in ways that resemble natural selection (and) can solve complex problems even their creators do not fully understand». Indeed, GAs operation is similar to Charles Darwin's natural selection theory, as they "kill" those options that do not correspond to optimal results and save those that do. The following procedure is put in practice by a GA:

1. First, a set of design parameters or *genes* is collected to construct the *cost function* or *genome*.
2. One or multiple objectives are chosen, thus defining the *fitness function*, which represents the selection criterium for the solutions (e.g. minimization or maximization of a given data).
3. After establishing the required *genes* and *fitness*, a first population of individuals, called *generation*, is created by randomly changing each *gene* value within its range of variation and evaluating the *fitness* for all the generated solutions. The population size, that is the number of solutions per generation, depends on custom settings.

4. New generations of individuals are created by applying various *genetic operators*, such as *crossover*, *mutation* and *selection*, whose role is to modify the offspring of each individual so that they perform better with respect to the *fitness function*. Genetic operators can be described as follows:
   - *Crossover*: consists in swapping parameters values between two subsequently generated solutions [61].
   - *Mutation*: randomly changes the parameters' values, «increases the diversity of the population and provides a mechanism for escaping from local optimum» [131].
   - *Selection criteria or elitism*: solutions with higher fitness values (the "best" solutions) are selected to pass to the next generation.

   So-generated new solutions replace part of the existing population, thus creating a generation that differs from the previous one. Then, iteration is repeated again using the new population as the starting point. These procedures can be potentially replicated endlessly for an infinite number of generations, unless otherwise specified by custom settings or unless a convergence criterium is reached [132].

3.7.2 Octopus optimization

Octopus solver component, shown in Figure 18 here aside, is used to perform the optimization. *Genes* must be connected to the G field, while the O field collects the objectives of the simulation (*fitness*) - minimum two. Both number and text parameters that defines respectively the values and the names of the objectives can be inputted here. It is recommended to group together these elements together in two separated lists, one for numbers and the other for names. An optional 3D mesh can also be connected to Octopus, defining the *phenotype* (P) and allowing visual assessment of the solutions [61]. Variations of the *phenotype* are collected into a tree and results as an output of Octopus component (Ps). In this case, no mesh is inputted to avoid overloading the simulation.

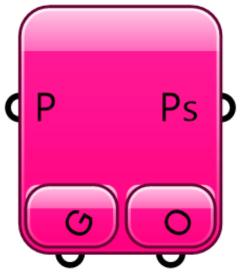

Figure 18 - Octopus component.

Figure 19 provides a list of the variables and the objectives that have been considered for the developed analysis. Eight parameters are selected to set up the *genome*: building orientation, WWR for the four main cardinal directions, thickness of the insulation layer of the opaque envelope, percent of glazed area operable for natural ventilation and shading devices inclination with respect to the horizontal plane. *Fitness function* for the optimization is defined by four objectives: annual percent of time during which the occupants feel comfortable in the free-running zone from a thermal point of view, DLA and $UDLI_{100-2000lx}$ must be maximized, while at the same time minimizing ASE. DLA and $UDLI_{100-2000lx}$ values are considered averaged on the analysis area. As Octopus can only solve minimization problems, values that needs to be maximized (comfort, DLA and $UDLI_{100-2000lx}$) are made negative by multiplying them for -1.

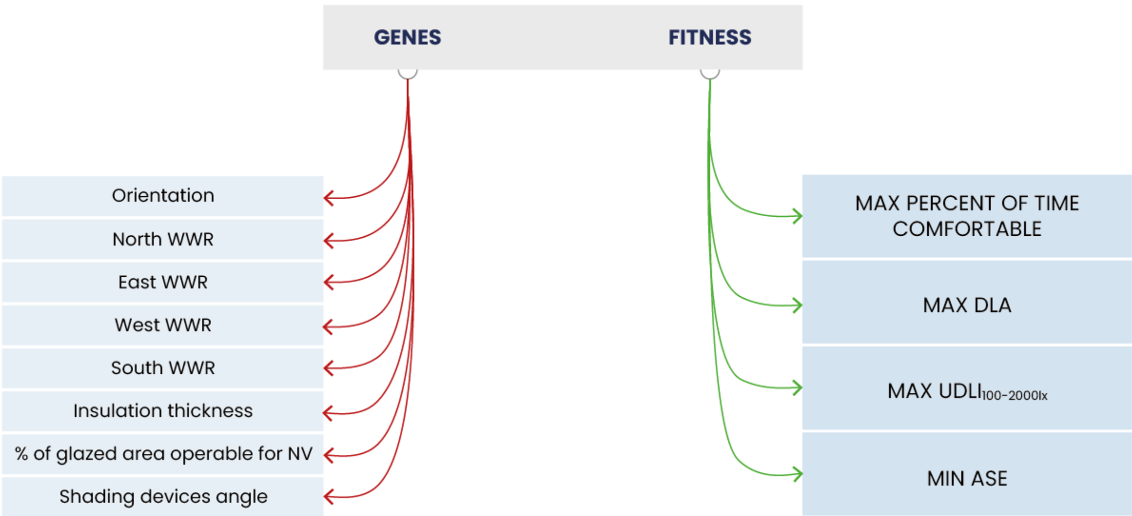

Figure 19 - Parameters and objectives for Octopus optimization.

Once the plug-in has collected all the required data, optimization can begin. By double-clicking on the solver component, the Octopus main window opens up, providing an interactive graphical user interface. The window appears as shown by Figure 20. Computed individuals of each generation appear as cubes on the 3D *Cube View* located in the center of the window. Comfort, DLA and UDLI objectives are displayed on the three Cartesian axes, respectively x-y-z, while different values of ASE are represented by the cubes' color, ranging from red (high ASE) to green (low ASE).

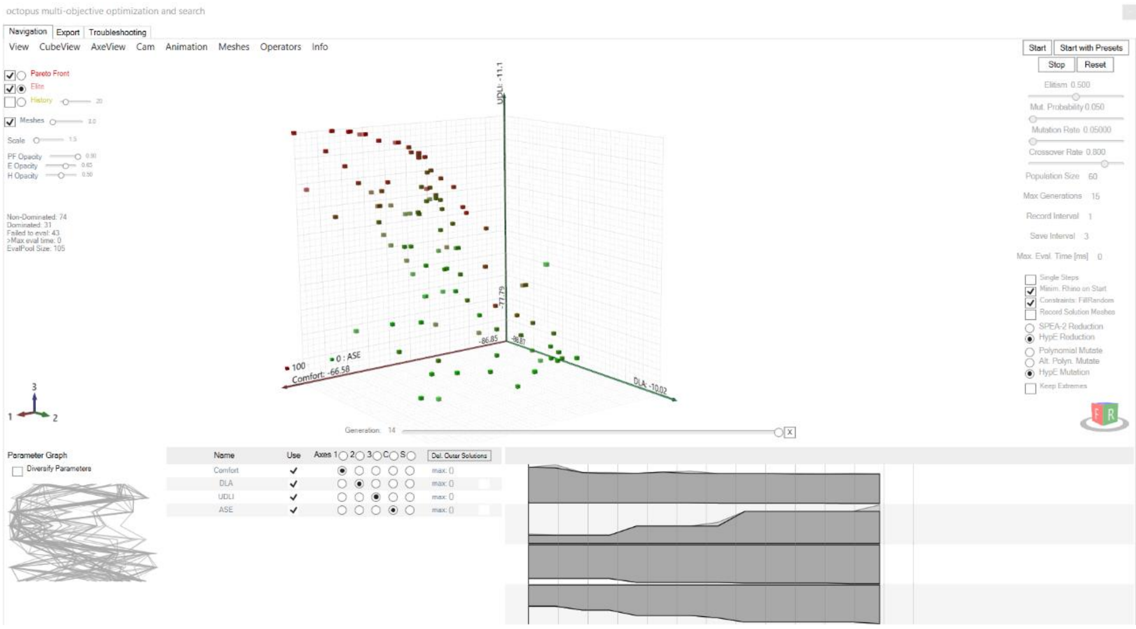

Figure 20 – Screen capture of Octopus window.

Left side of Octopus window contains the display settings for the results cubes, such as their scale and opacity, and the statistics generated during the optimization process. At the bottom of the interface, a «list of objectives by their name and in the order of how they are supplied to Octopus in Grasshopper» ([61], p. 4) is provided. In addition, two graphs are displayed: the one on the left is the parameters graph, while the one on the right is the convergence graph. For a detailed description of these charts, reader is referred to the Octopus manual [61]. Lastly, the right side of the plug-in window contains the control buttons (start, stop, reset) and the algorithm settings. Parameters for the optimization process have been set according to Table 5.

ALGORITHM SETTINGS	ELITISM	MUTATION PROBABILITY	MUTATION RATE	CROSSOVER RATE	POPULATION SIZE	MAXIMUM GENERATIONS
	0.500	0.050	0.050	0.800	60	15

Table 5 - Algorithm settings for Octopus optimization.

Considering what has been said in §3.7.1 and according to Octopus manual [61], parameters can be defined as follows:

- *Elitism*: as *Elite* consists of a fixed number of "best" solutions that are kept for the next generation, *Elitism* represents «the percentage of new solutions that are bred out of the Elite instead of the entire pool. When set high, more local optimization is performed» ([61], p. 3).
- *Mutation probability* gives the probability for each parameter to become mutated according to the *Mutation Rate*. «A low Mutation Rate means little changes to the parameters' values, a high rate means big changes» ([61], p. 3).
- *Crossover Rate* is the probability of two solutions to swap parameter values between each other.

Default HypE reduction and mutation strategies are applied. A population size of 60 and a maximum generations number of 15 are considered. This means that each generation will contain 60 random-generated individuals, with the exception of the first generation that always contains twice the population size (120 individuals), and that the optimization process stops after 15 generations. These numbers have been chosen with the aim of reducing the simulation time, that otherwise would have been far too much time consuming.

3.7.3 Optimal solutions selection criteria

Once the optimization process has finished, solutions are compared to find the optimal configuration of the *genes* that better meets the objectives. In a multi-objective optimization, a good set of solution is usually placed near or distributed on the approximative *Pareto front* generated by the software. Named after Vilfredo Pareto, who first used this concept in his studies at the turn of XIX and XX centuries, *Pareto front* (also called *Pareto set*) is described as «the set of non-dominated solutions, where each objective is considered as equally good» [133]. It is represented by a geometric entity that could be either bidimensional or three-dimensional, depending on the number of the considered *fitness values*. Non-dominated solutions, also called *Pareto optimal* or *Pareto efficient*, are those individuals for which «an optimal trade-off between two or more contradicting objectives» ([132], p. 31) is achieved and no change in the *genes* can lead to an improvement in some of the objectives results without degrading the others. In contrast, dominated solutions are so named because there is always a solution that is better than them in terms of goals values. The *Pareto front* concept is really helpful, as it allows the designers to restrict their attention to the set of solutions that are really optimal, rather than analyze every individual in search of the best ones.

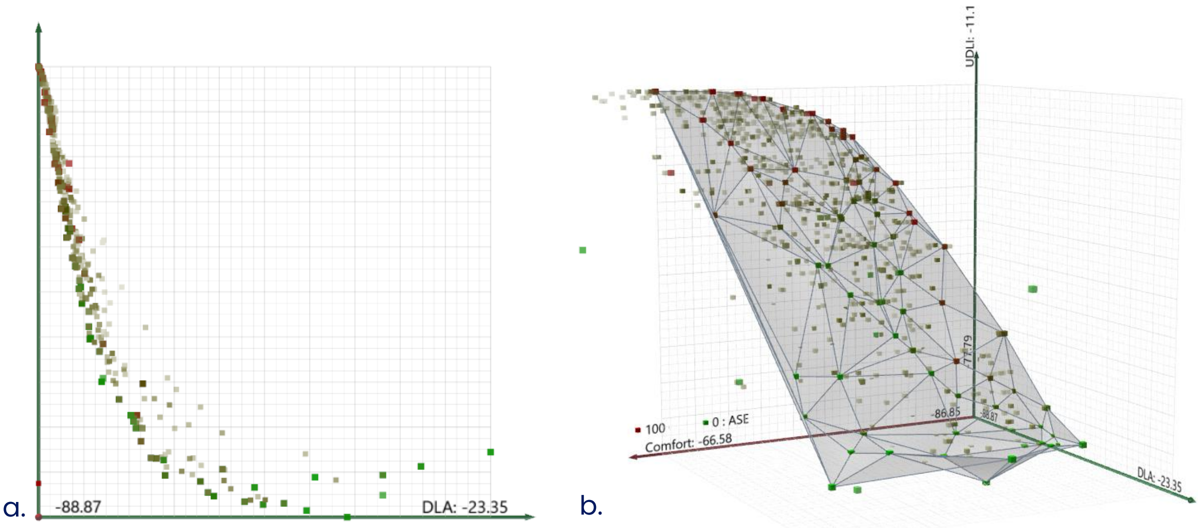

Figure 21 - Pareto front, Elite and History until generation 15 of Turin optimization under present climatic conditions – Octopus screen capture. Figure 20a represents Octopus cubeview from the side: opaque cubes are non-dominated solutions that define the *Pareto front*. Figure 20b shows a 3D view of the graph on which a 3D surface ("Delaunay front mesh") that approximates the *Pareto optimal* distribution is displayed.

Not all the *Pareto efficient* solutions can be considered optimal for the design purpose. In fact, as can be seen in Figure 21, these individuals have a wide distribution on the 3D cubeview diagram, also including extremes in data. However, it is probable that more than one optimal solution in this sense can be found: it is up to the designer to choose among them the "best" one. Optimal design solutions have to be searched between the individuals placed in the center of the graph, near the origin of the three Cartesian axes. Though, attention must be paid to the resulting cubes' color, which represents the fourth objective, because not all the solutions that are located in this position have satisfying ASE values. Figure 22 shows that, within the optimal solutions' circle, also dark green or even red cubes can be found. In fact, as pointed out in [129], «each of these solutions falls within the most desirable range of outcomes, but individually possesses its own advantages and disadvantages that would make it more or less favourable for further design development». The best design option (or options) that the designer is looking for will be the one (or the ones) that adequately balance all the four objectives (comfort, DLA, UDLI and ASE). The displayed preferred solution is chosen in virtue of its low ASE value, that should preferably be kept below 10%, and is reinstated into GH environment.

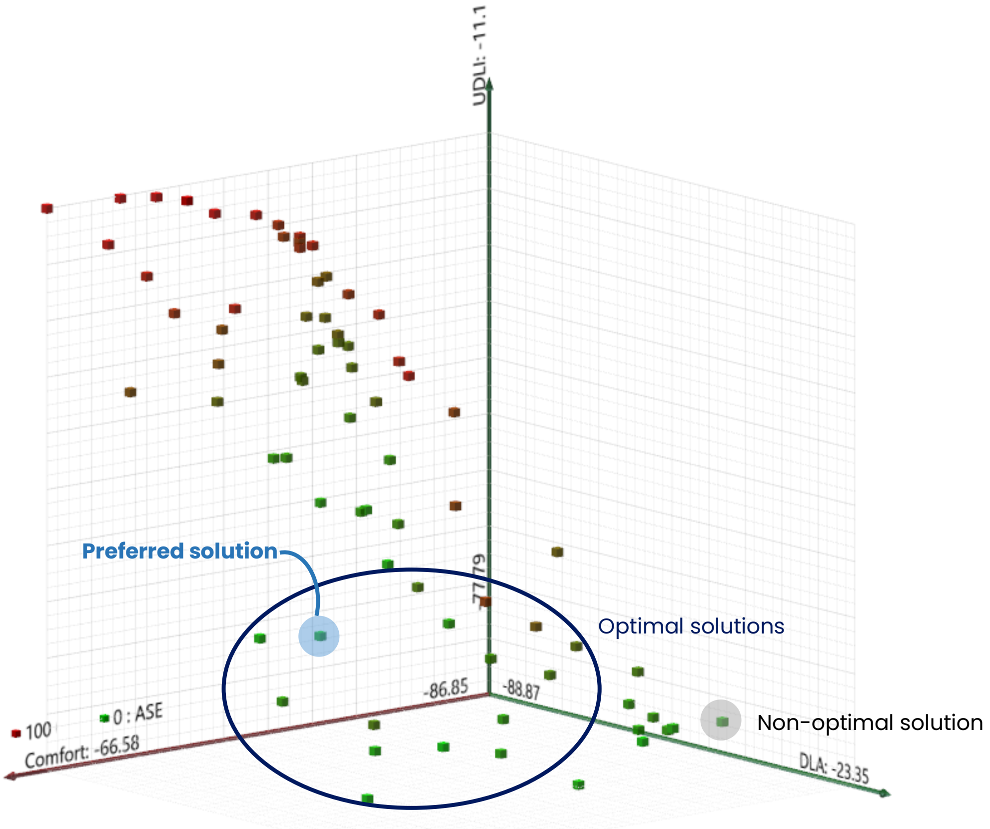

Figure 22 - Screen view of Turin's Pareto front with the indication of optimal solutions and preferred ones.

Design configurations that fall outside the optimal solutions' circle are not considered really optimal because, although one or two objectives could be greatly optimized, the other ones are negatively impacted. For instance, the non-optimal solution shown in Figure 22 corresponds to good values of comfort and UDLI, as well as to a small ASE value, but DLA is strongly sacrificed.

3.8 Optimized schedules

Next step of the workflow consists in generating optimized availability schedules that identify cooling and heating systems operating periods in order to eliminate discomfort wherever it persists during the year. These custom schedules are defined starting from occupants' thermal sensation without any conditioning system on (neither heating nor cooling) calculated for the optimal design solution through the LB Adaptive comfort component, as described in §3.6.1. The solution is chosen at the end of the optimization process by following the selection criteria discussed in §3.7.3.

To define the schedules, first step consists in finding the HOYs (Hours Of the Year) of the occupancy period. Occupied HOYs are listed as a set of 4380 values between 1 and 8760[22]. Each value of the occupants' condition list, made of -1s (cold), 0s (comfortable) and +1s (hot), is associated to the corresponding HOY of the analysis period previously found. Then, heating and cooling HOYs are separated into two different lists, while comfortable HOYs are removed. Afterwards, cooling and heating HOYs from these lists are introduced into two new lists that contain 8760 values of 0s and 1s, one list for cold and the other for hot conditions. 0s are associated to those hours of the year in which systems must be off because comfortable conditions are maintained into the building in free-running mode. Instead, 1s are associated to those hours in which occupants experience thermal discomfort (hot/cold) and so system must be in function. HB *Create CSV Schedule* is used to write the two availability schedules as CSV files for EnergyPlus. Input values are the previously described 0s and 1s lists, while unit is set dimensionless. Custom cooling and heating schedule are created for the entire year.

3.9 Zone energy use

The chosen optimal design solution is analyzed to assess the zone energy use. The workflow is replicated from step 2 (thermal zone definition - §3.2) to step 5 (energy simulation trough EP - §3.5.1) with the same parameters, but with one major difference.

[22] 8760 corresponds to the number of hours of a year.

While the initial zone was not conditioned at all and operated in a free-running mode, now the evaluation is performed allowing cooling and heating systems functioning. The *isConditioned* statement at the beginning of the workflow is set to True, and the zone is conditioned with an ideal air loads system. Consequently, an HVAC system must be specified. With the aim of comparing the energy savings that result from the application of the HVAC availability schedules created in the previous step (§3.8) with respect to a system that is always in function when the temperature setpoint is not met, two parallel EP simulations are run. One simulation is performed designing the HVAC system with default schedules assigned by HB, while the second one is run applying custom CSV schedules for heating, cooling and artificial lighting [23]. It must be pointed out that, when designing an ideal air loads system, coefficient of performance (COP) for both heating and cooling is considered equal to 1 (low efficiency) and cannot be modified from the Honeybee *HVAC Heating and Cooling Details* components. Different values for COP may be connected if a more detailed system is chosen among the ones suggested by the HVAC system list provided in the homonymous HB component. Realistic COPs will be accounted later on. As far as heating and cooling thermostat setpoints are concerned, default HB temperatures for the closed office zone program are kept (Table 6). In order to avoid the cooling system to turn on meanwhile windows are open, another temperature constraint for natural ventilation must be specified: maximum outdoor temperature for NV is set to 25°C. This number must always be kept under the cooling setpoint, so that when NV is not convenient anymore because outdoor air is too close to the setpoint, AC is turned on.

TEMP. SETPOINTS	HEATING SETPOINT	COOLING SETPOINT
	21°C	26.7°C

Table 6 - Heating and cooling setpoints.

Furthermore, *HVAC Air Details* component is used to set the ventilation system parameters. For both simulations, in addition to NV, a minimum mechanical

[23] Custom lighting CSV schedule is generated through HB component *readAnnualResultsI* based on daylight availability throughout the year estimated by Daysim starting from Radiance simulation – see §3.6.2.

ventilation rate is considered for indoor air quality (IAQ). Default ventilation loads are maintained (Table 7). Demand controlled variable ventilation is allowed. This means that the volume of air supplied to the zone through the mechanical system and its speed change depending upon the occupancy rate.

VENTILATION LOADS	VENTILATION PER AREA	VENTILATION PER PERSON
	0.0003 $m^3/s \cdot m^2$	0.0024 $m^3/s \cdot$person

Table 7 - Ventilation loads.

EP simulations output the zone total energy needs in kWh. In particular, for Ideal Air Loads, cooling energy need represents the sum of sensible and latent heat that must be removed from the zone; on the contrary, heating energy need represents the sum of sensible and latent heat that must be added to the zone. Heating and cooling loads are divided for the COPs of the systems, which are considered respectively equal to 3 and 6. These COPs provide a higher efficiency, lower energy consumption and thus lower emissions and functioning costs with respect to the default COP of 1. Then, to calculate the Energy Usage Intensity (EUI) of the zone in kWh/m^2, cooling, heating and artificial lighting needs from both simulations are normalized on the floor area. From this operation, Cooling Energy Usage Intensity (CEUI), Heating Energy Usage Intensity (HEUI) and Lighting Energy Usage Intensity (LEUI) are obtained. Summing the so-obtained CEUI and HEUI, total Thermal Energy Usage Intensity (TEUI) in kWh/m^2 is defined. Total thermal and lighting energy savings are expressed as percentages that result from formula 4:

$$\text{savings } [\%] = 100 - [(x/y) \cdot 100] \tag{4}$$

where:
x = optimized EUI
y = non-optimized EUI

3.9.1 Outputs visualization

Honeybee provides users with the possibility to build up the whole model energy balance starting from the results of the EP energy simulation. Ladybug allows to visualize through high-quality charts the outputs of the HB *energyBalance* component, averaged for each month. This supports not only the understanding of what are all the terms that come into play in defining the energy balance (loads, gains, etc.), but also «why it exists and what is driving it» [134]. Figure 23 shows by way of example the energy balance charts that resulted from the simulation of optimal design solution in Turin under present climatic conditions. As heating and cooling component the values divided for the actual COPs are considered for the energy balance instead of the values with COP = 1 from the EP simulation. It must be noted how simple is made the comparation between optimized and non-optimized terms of the energy balance.

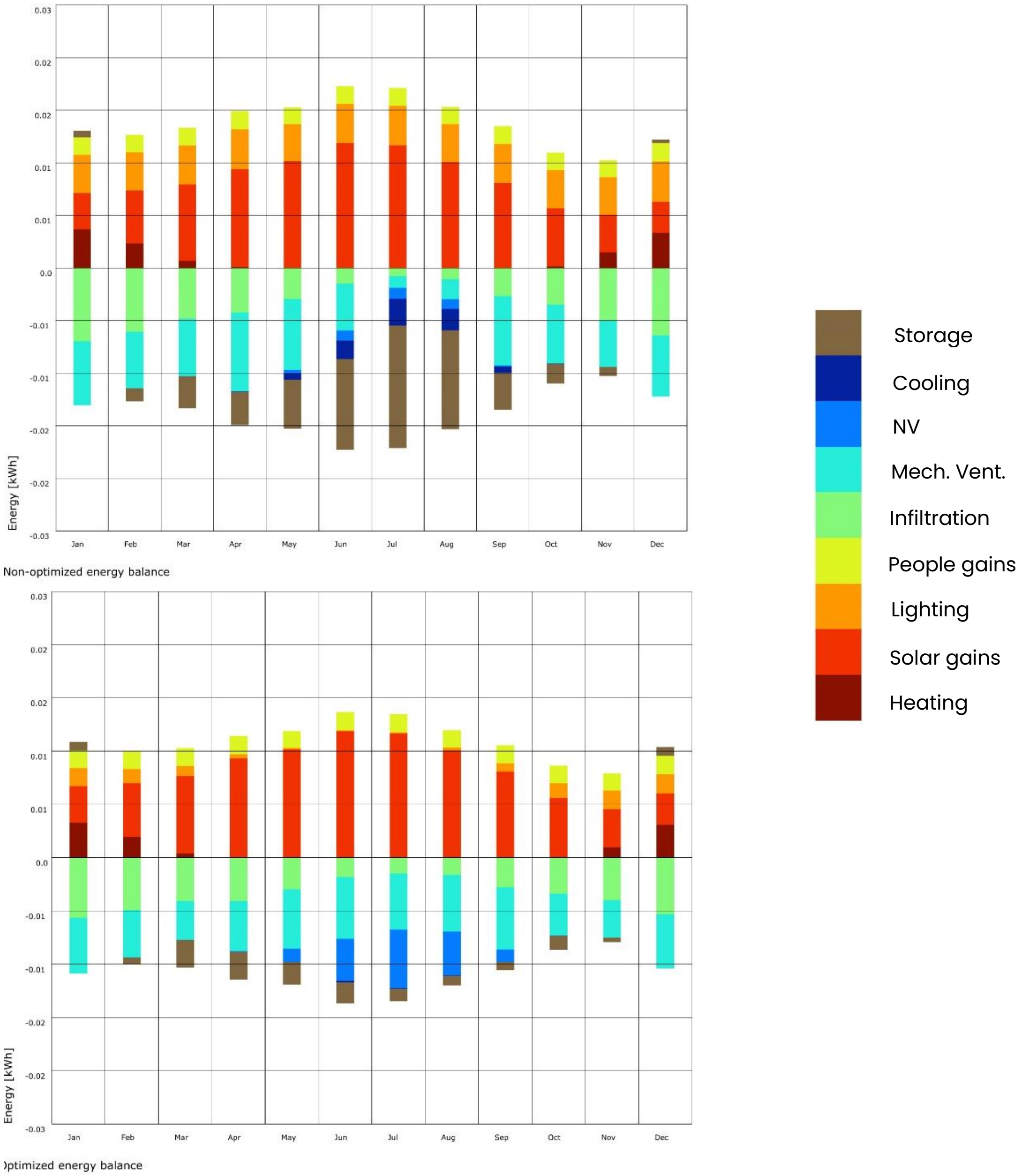

Figure 23 -Zone energy balance (non-optimized above and optimized below) for Turin's optimal solution under present climatic conditions.

Several considerations can be made starting from these charts. For example, it can be seen that some terms, such as solar and internal gains, remain the same in both cases, as they only depend on the zone design and program. Cooling and artificial lighting energy needs are strongly minimized, nearly removed, while heating need is still present, although reduced. In the solution with optimized schedules, it turns out that, during summer season, NV compensates for the reduced cooling energy use. The storage value represents the thermal energy that is stored in the building's mass and is calculated as the difference between gains (positive values) and losses (negative values). For this reason, it is higher when gains and losses are more unbalanced, for example during summer season in the solution with default schedules (non-optimized).

Energy balance terms can also be visualized individually on annual 3D charts. Examples are provided in Figure 24 and Figure 25; color scale for the charts is shown here aside. This allows to understand when a specific load is present during the year and how great it is. LB 3D charts are also useful to compare results.

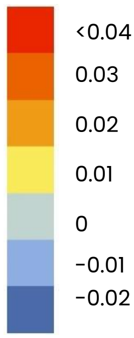

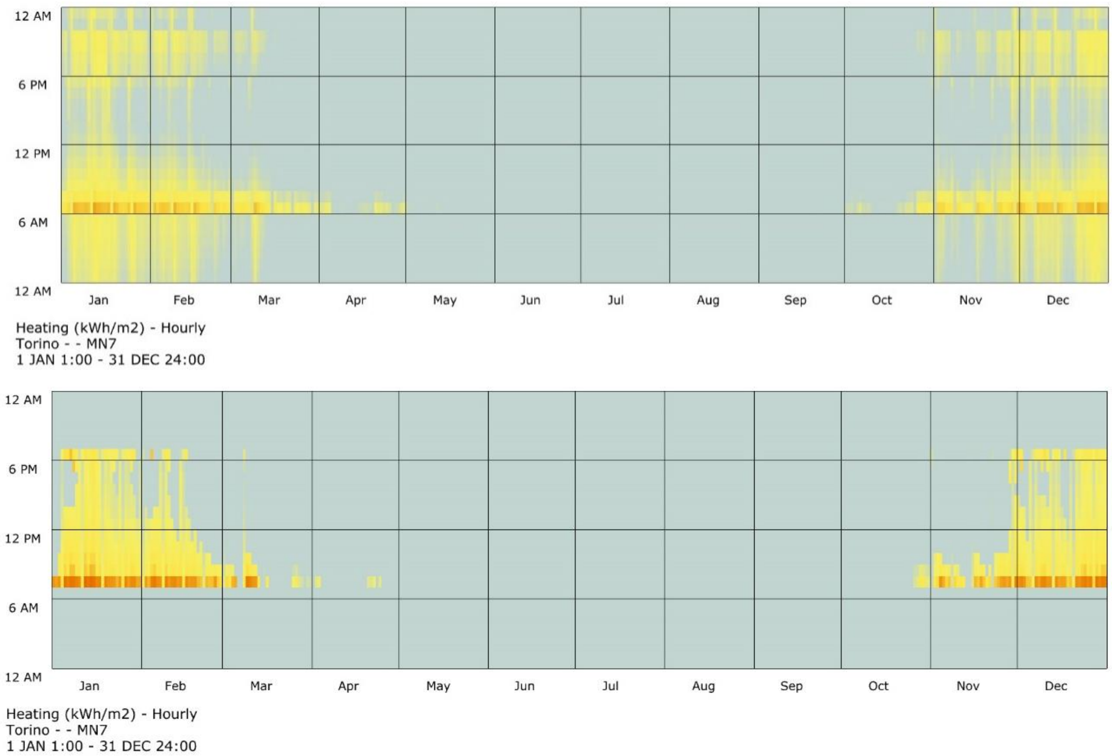

Figure 24 - LB 3D charts for heating load for the non-optimized (above) and the optimized solution (below) for Turin (present).

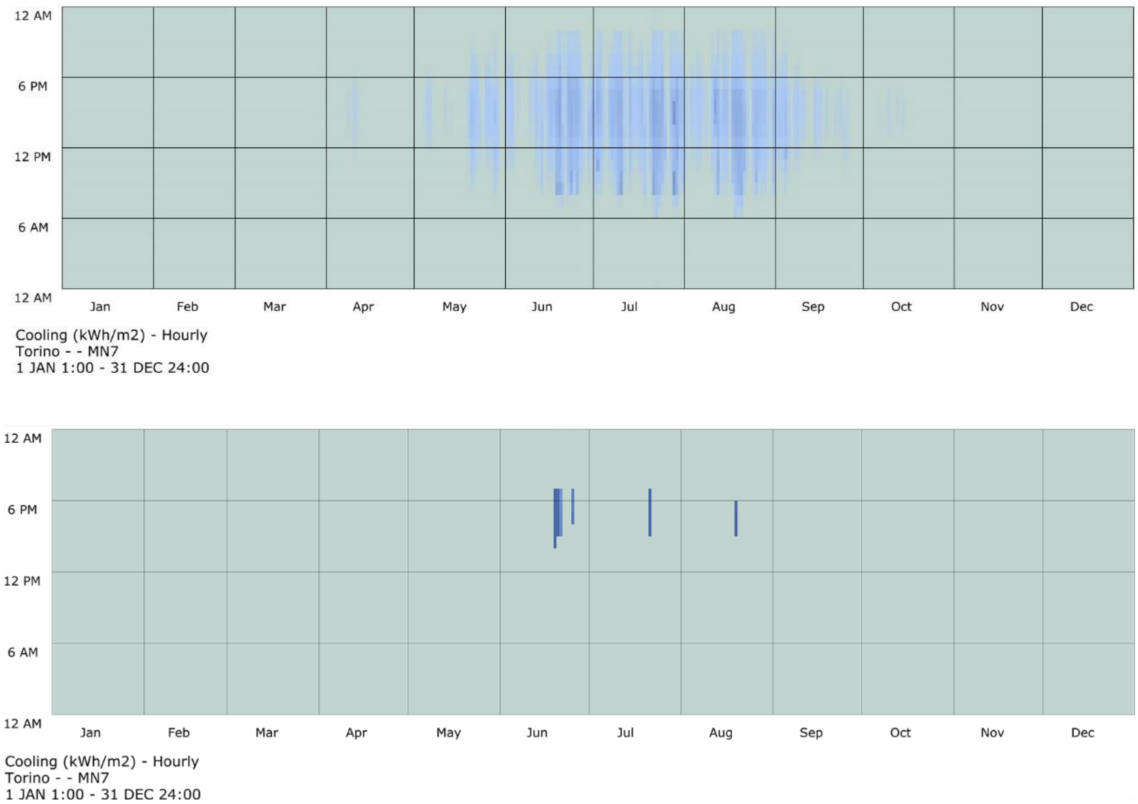

Figure 25 - LB 3D charts for cooling load for the non-optimized (above) and the optimized solution (below) for Turin (present).

Lastly, heating, cooling and lighting loads can be displayed on monthly bar charts, like the ones presented in Figure 26 and Figure 27.

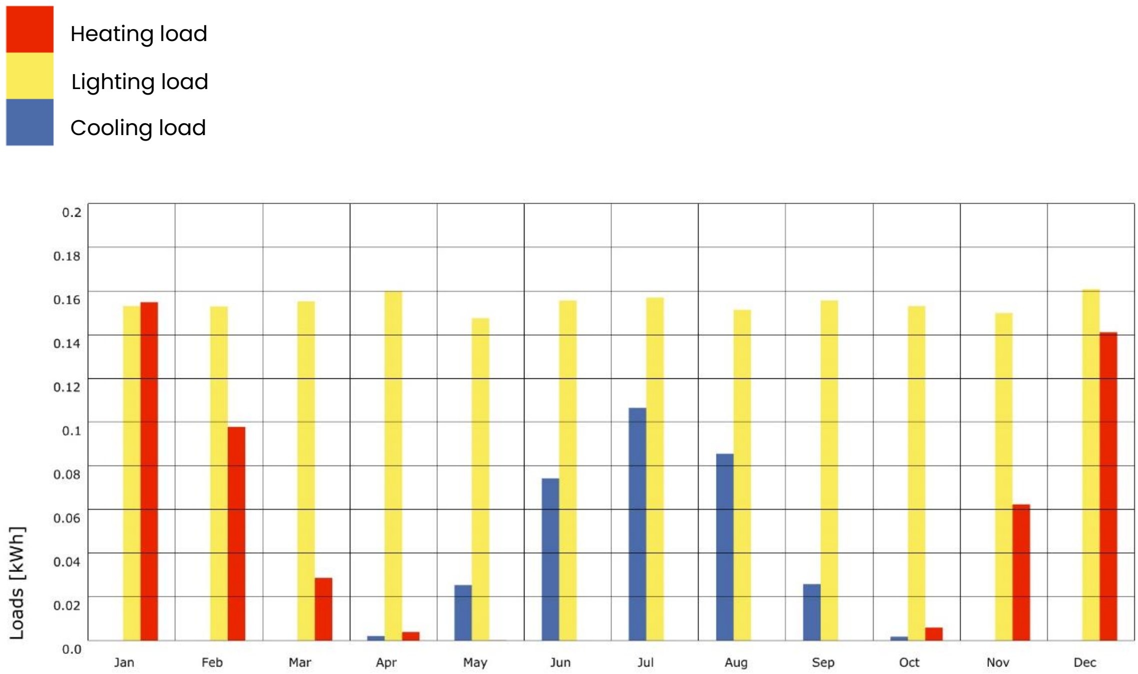

Figure 26 - Monthly bar chart displaying heating, cooling and lighting loads for Turin's non-optimized solution.

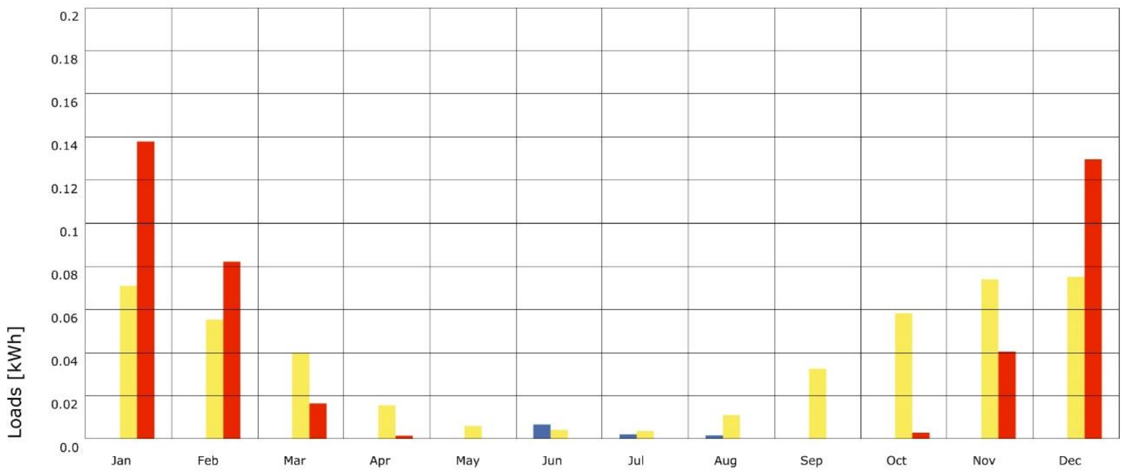

Figure 27 - Monthly bar chart displaying heating, cooling and lighting loads for Turin's optimized solution.

4. APPLICATION

4. APPLICATION

The presented workflow is applied to the ten European locations that have been discussed in §3.4.1: Aalborg, Athens, Bari, Geneva, Kemi, Palermo, Paphos, Rome, Turin and Trieste. Each location has been considered under present and future (A2 scenario for 2050) climatic conditions. A total of twenty simulations have been run on different GH files. Each Octopus optimization process took approximately 36 hours (1.5 days) to compute all the 15 generations of solutions. Several difficulties have been encountered during the optimization processes: the program crashed many times, making it challenging to complete the task. Moreover, when running Kemi's analysis under 2050 climatic conditions, an error in the EPW file from Meteonorm was discovered. Dew point temperature values for the first month of the year (January) were found completely incorrect, and so the horizontal irradiation values for the same period. Hence, the EPW file was edited manually, replacing wrong irradiation values with the ones from the present weather file and calculating dew point temperatures from RH and dry bulb temperature 2050 values. To do so, Excel was used, applying Meteonorm formula:

$$T_{dp} = \left(1/(T_{db}+273.15) - (1.85 \cdot 10^{-4}) \cdot \log(RH/100)\right)^{-1} - 273.15$$

where:

T_{dp} = dew point temperature

T_{db} = dry bulb temperature

RH = relative humidity

4.1 Climates comparation

A comparative analysis of the climatic conditions is performed with the aim of better understand how outdoor temperatures vary throughout the year and, in particular, how they change between the present and the year 2050 (A2 scenario). This analysis is an essential first step towards the further interpretation of the optimizations results. For each of the ten considered locations, monthly average dry bulb temperature, average global horizontal radiation and hourly wind speed/direction data from EPW files are used to compare outdoor boundary conditions. To visualize temperature and irradiation averaged data, LB bar charts are generated. Averaged monthly per hour values, which represent the average of each hour of each month, are also visualized in the bar charts. Instead, to visualize the prevailing direction of the wind, its speed and its temperature, LB wind roses are used. Wind data are analyzed only for warmer months (from May to September during occupancy period, which is 7 a.m. to 6 p.m.), which represent the period of the year during which NV is more desirable, due to higher outdoor temperatures. Analyzing the direction from which the wind comes may be useful to understand, for example, the reason for an optimal building orientation; or analyzing its speed may be interesting for understanding other NV parameters, such as the fraction of the glazed area operable for ventilation. Hereafter, results are presented and discussed for each location, grouping them based on Troll and Paffen climatic zones classification, as identified in Table 4.

4.1.1 Climatic zone II 2

KEMI (Finland)

Located in the northern part of Europe, Kemi is the coldest city among the ten considered. Figure 28 shows the temperature trend, comparing the present to the 2050 situations. Both now and in 2050, dry bulb temperatures remain way below 0°C during the winter period, especially from December to March. Higher temperatures are reached during summer, although maximum monthly average temperature does not reach 20°C. Overall temperatures in 2050 are expected to be higher than temperatures in the present, with an average difference of 2°C. The difference between the present and the future in hourly average data is most evident in February, March and June.

As far as global horizontal radiation is concerned, a reduction of its level in 2050 can be deduced from Figure 29. Radiation is greater during summer period, while it is very small, almost null, during winter (November, December and January in particular). Given Kemi's harsh climate and the paucity of radiation, a low comfort level achieved in free-running mode is expected: heating energy needs are expected to be high. In addition, optimal solution must harness radiation as much as possible, maximizing solar gains.

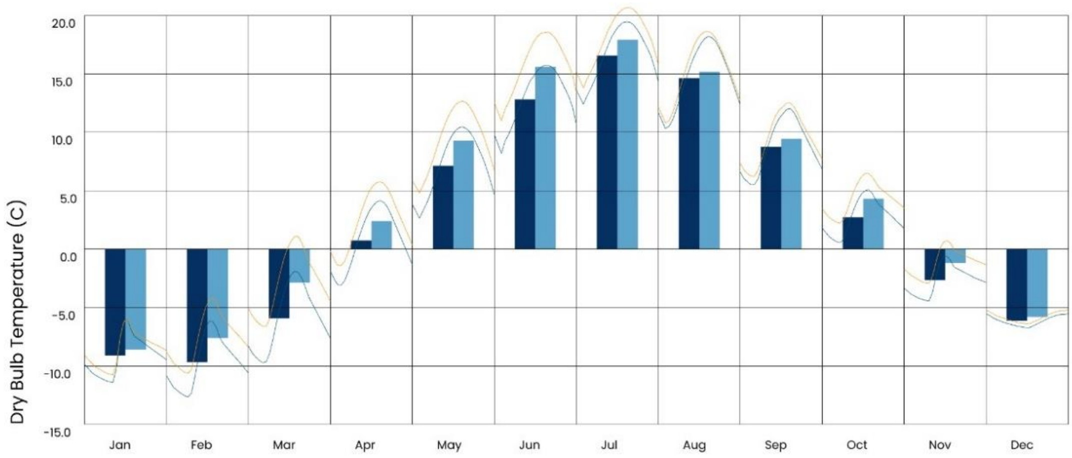

Present dry bulb temperature (monthly) | 2050 dry bulb temperature (monthly)

Present dry bulb temperature (hourly average) | 2050 dry bulb temperature (hourly average)

Figure 28 - LB bar chart showing Kemi's monthly average dry bulb temperatures annual trend, comparing present and 2050 values.

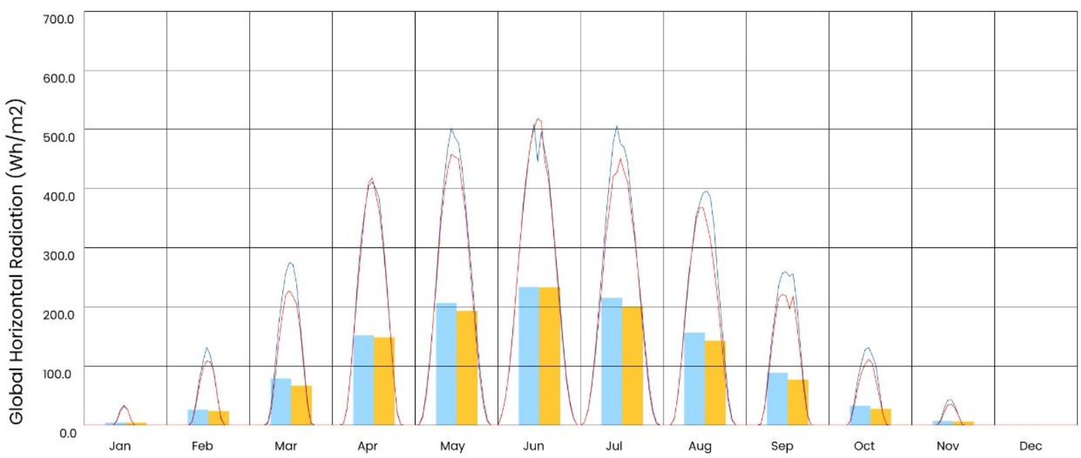

Present global horizontal radiation (monthly) | 2050 global horizontal radiation (monthly)

Present global hor. radiation (hourly average) | 2050 global hor. radiation (hourly average)

Figure 29 - LB bar chart showing Kemi's monthly average horizontal global radiation annual trend, comparing present and 2050 values.

Prevailing wind directions during summer are north-east (NE) and south-west (SW). Wind is mainly cool (0-15°C).

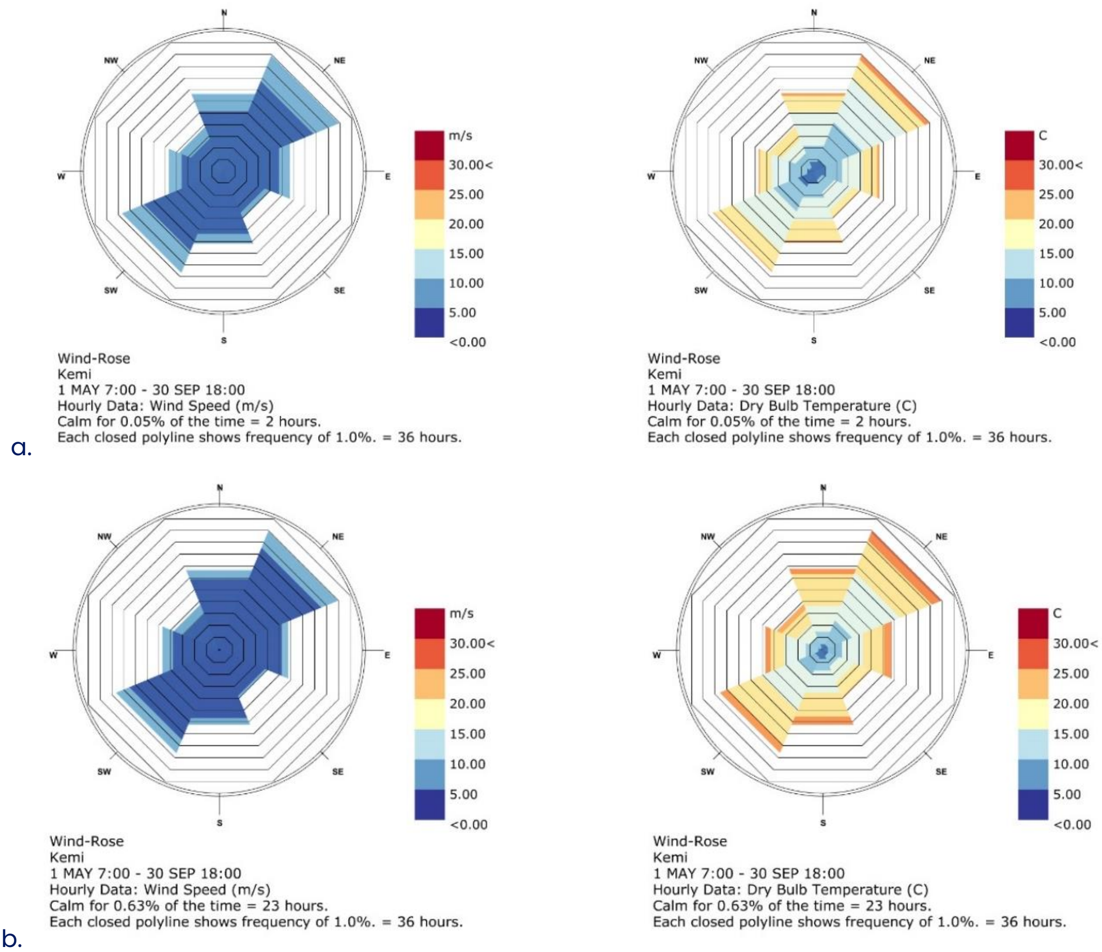

Figure 30 - Kemi's prevailing wind direction and speed (on the left) and temperature (on the right). 30a - present conditions; 30b - 2050.

4.1.2 Climatic zone III 3

AALBORG (Denmark)

After Kemi, it is the northernmost city considered. Aalborg's temperatures trend shows an increase during most part of the year in 2050 with respect to actual temperatures, while a slight decrease can be seen in April, July and August. In this case too, monthly average temperatures remain below 20°C, although during the central part of the day, especially during summer months, higher temperatures are reached – see Figure 31.

Like Kemi, global horizontal radiation is lower in 2050 than in the present. During winter months it is less intense with respect to the rest of the year. Although averaged values remain under 300 Wh/m^2, average hourly data for each months reach peaks of up to 600 Wh/m^2 in the central hours of the day (Figure 32).

Wind roses in Figure 33 show that prevailing wind direction is south-south-east. Wind roses for 2050 do not show particular changes in air flow directions with respect to present representation; slight differences could be noticed in speeds and air temperatures, that experience a little increase.

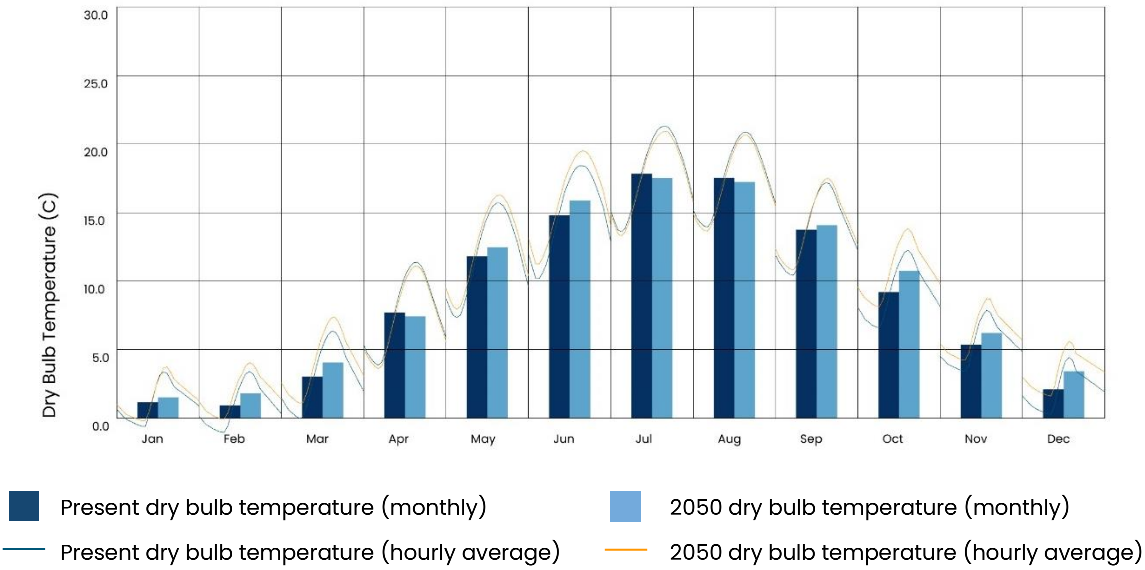

Figure 31 - LB bar chart showing Aalborg's monthly average dry bulb temperatures annual trend, comparing present and 2050 values.

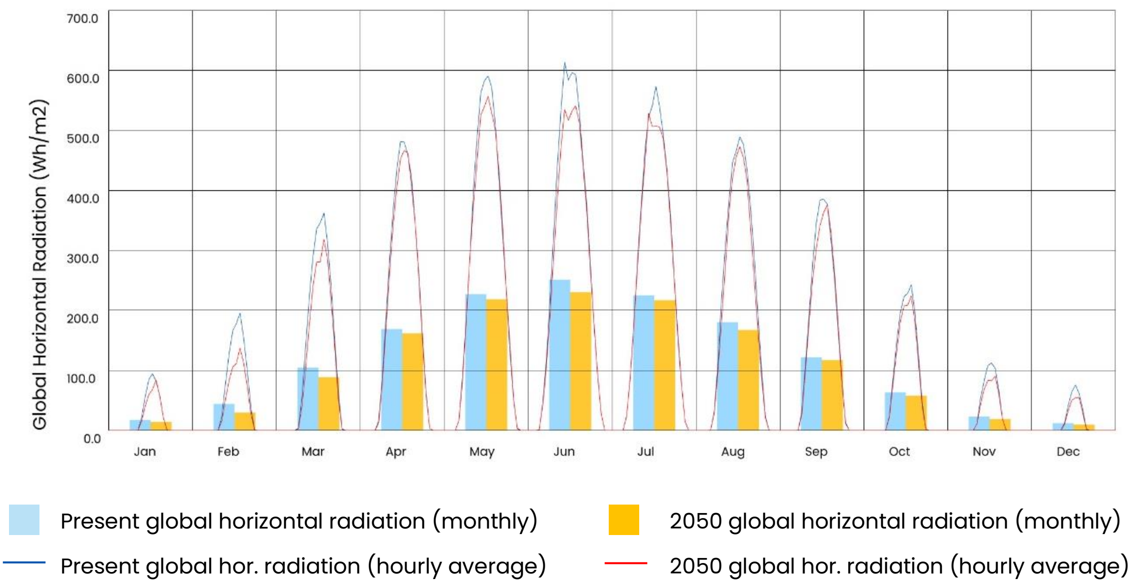

Figure 32 - LB bar chart showing Aalborg's monthly average horizontal global radiation annual trend, comparing present and 2050 values.

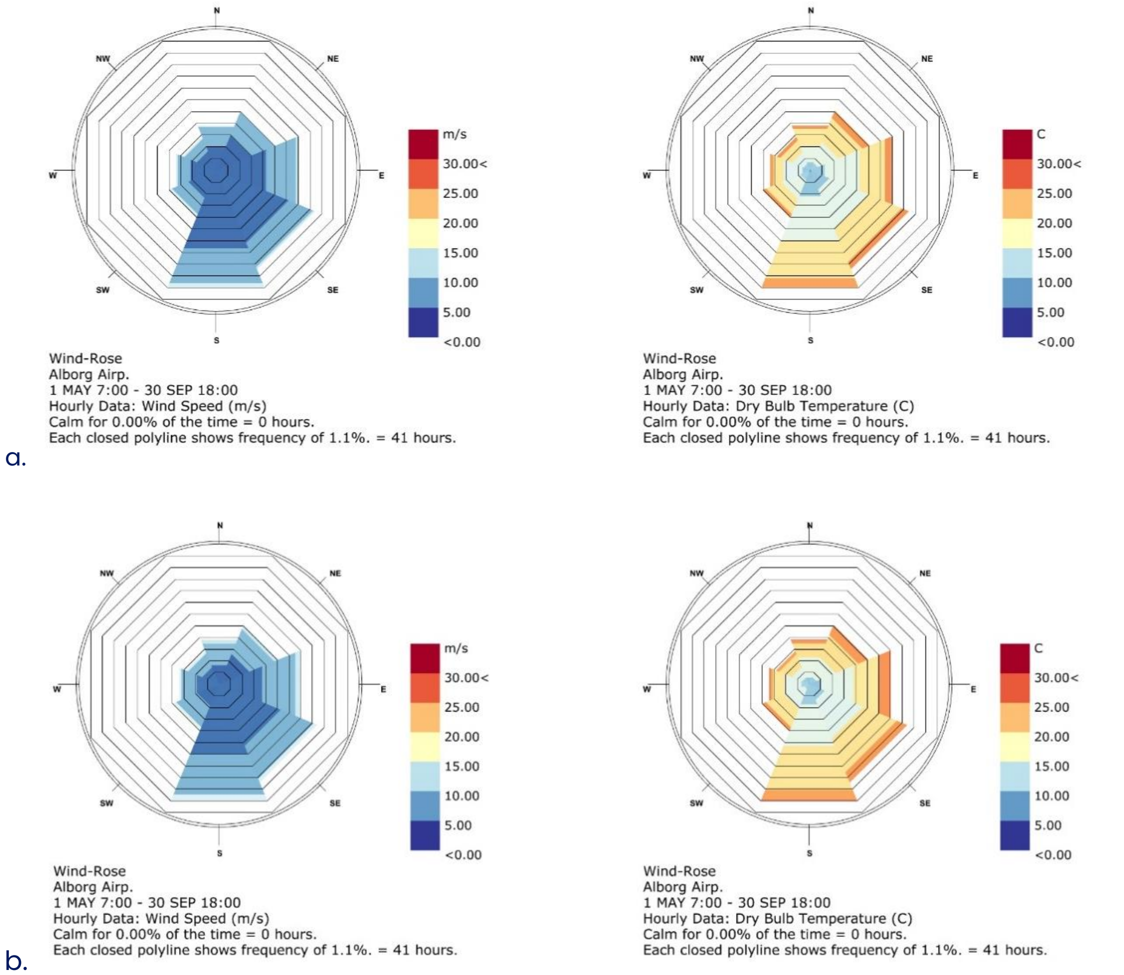

Figure 33 – Aalborg's prevailing wind direction and speed (on the left) and temperature (on the right). 33a - present conditions; 33b - 2050.

GENEVA (Switzerland)

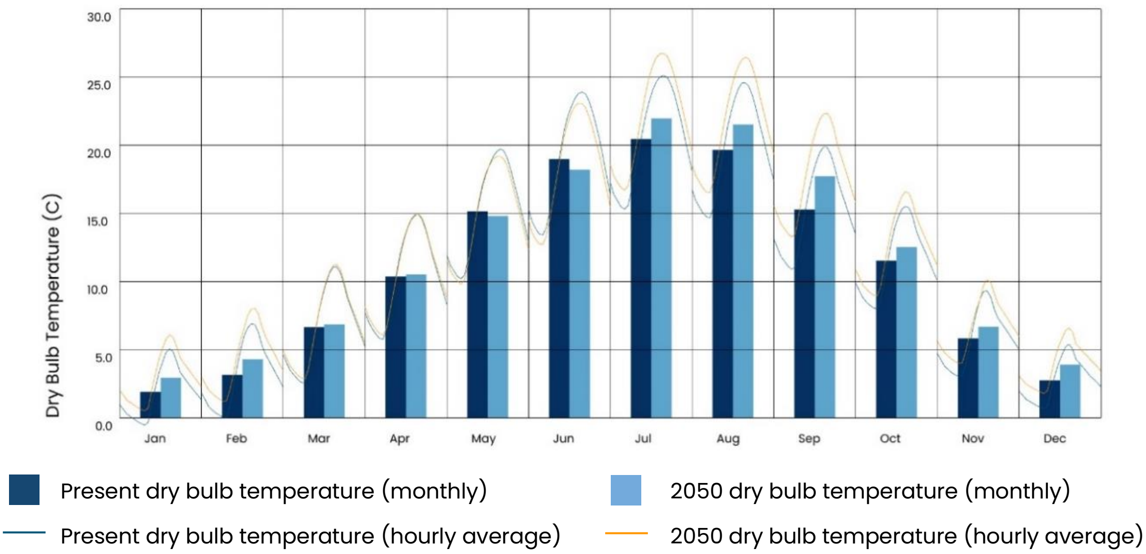

Figure 34 - LB bar chart showing Geneva's monthly average dry bulb temperatures annual trend, comparing present and 2050 values.

In Geneva, a general raise in monthly average temperatures between present and 2050 is registered, with the exception of June - Figure 34. Temperatures are higher than in Kemi's and Aalborg's cases, with hour average values that reach or exceed 25°C during summer. Lower average temperatures do not go below 0°C during winter.

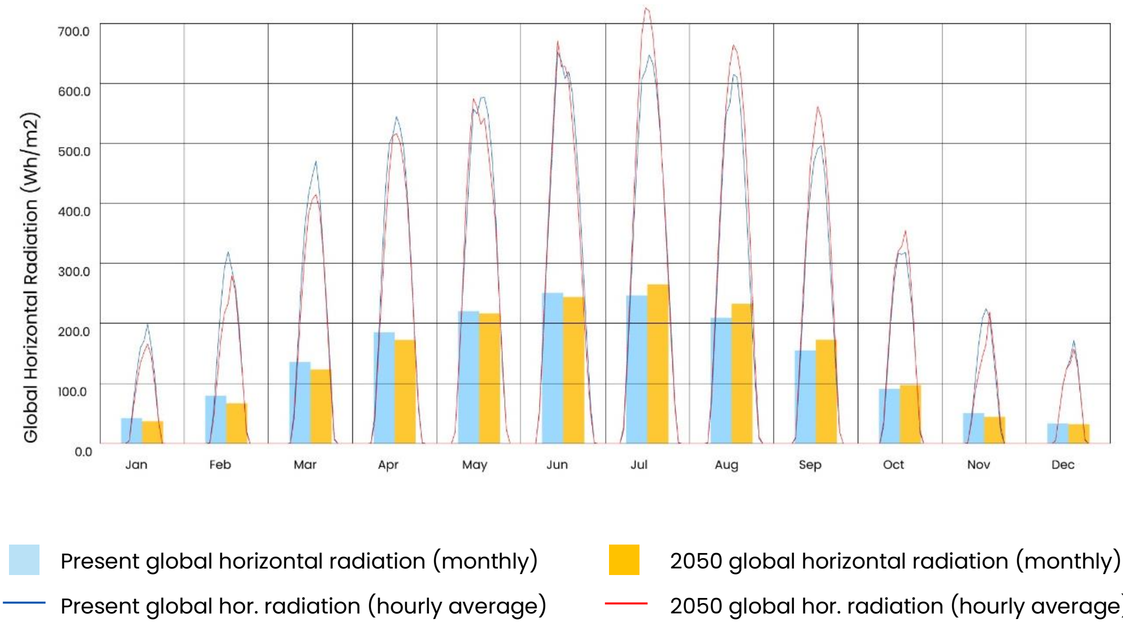

Figure 35 - LB bar chart showing Geneva's monthly average horizontal global radiation annual trend, comparing present and 2050 values.

Monthly average global horizontal radiation in 2050 is lower than in present years throughout all the year, except from July to October. Hourly average values reach up to 700 Wh/m² in July.

Prevailing wind direction is SE, although air flows also from north-NE and east directions. Wind speeds are low for most part of the analysis period, both in present and 2050 visualizations (see Figure 36), while temperatures reach up to 30°C or more in all the directions and are hotter in 2050 visualization.

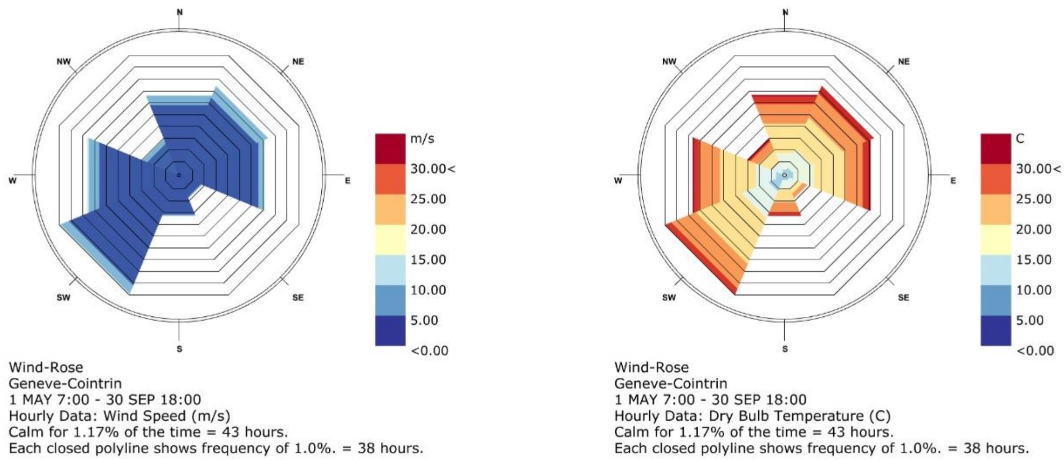

a.

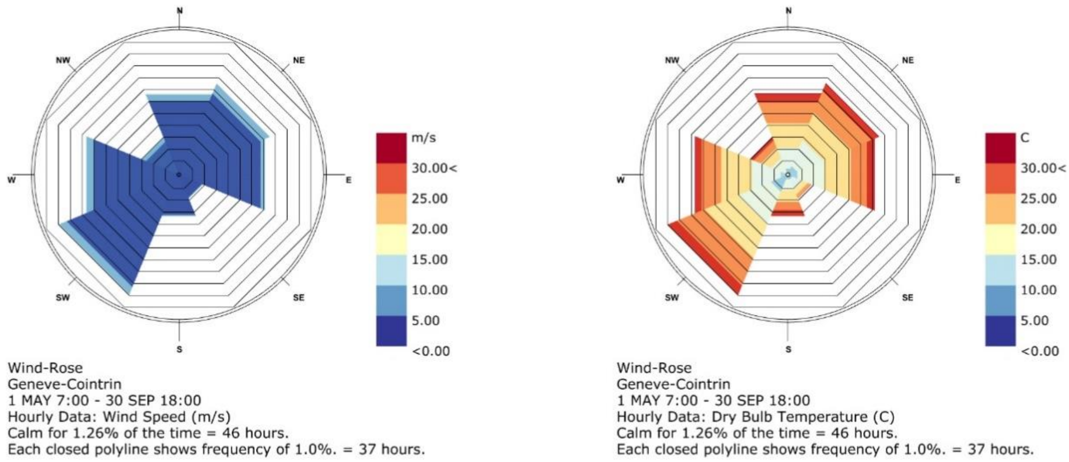

b.

Figure 36 – Geneva's prevailing wind direction and speed (on the left) and temperature (on the right). 36a - present conditions; 36b - 2050.

TURIN (Italy)

Turin is the only Italian location among the ones considered that is placed in climatic zone III 3 (submaritime climate), although temperatures are higher than in Aalborg or in Geneva. In 2050 a rise in temperatures is forecast, in particular during summer months when average monthly values go over 25ºC (July). During central hours of summer days in 2050, average temperatures reach 30ºC. Instead, winter average monthly temperatures, both present and future, do not fall below 0ºC, although hourly distribution shows that in December and January this happens during the first hours of the day – see Figure 37. Global horizontal radiation values are comparable to the ones of Geneva, due to their geographical proximity. In 2050, irradiation values are expected similar to the present ones, with a slight decrease from December to March and in July, and a slight increase in April, May, August-October periods. For radiation data see chart illustrated in Figure 38.

Turin receives weak wind from all the cardinal directions, especially from the east – see Figure 39. Air flows temperatures are hotter than in the previously described cases. In 2050, wind directions remain the same, but speed and temperatures increase.

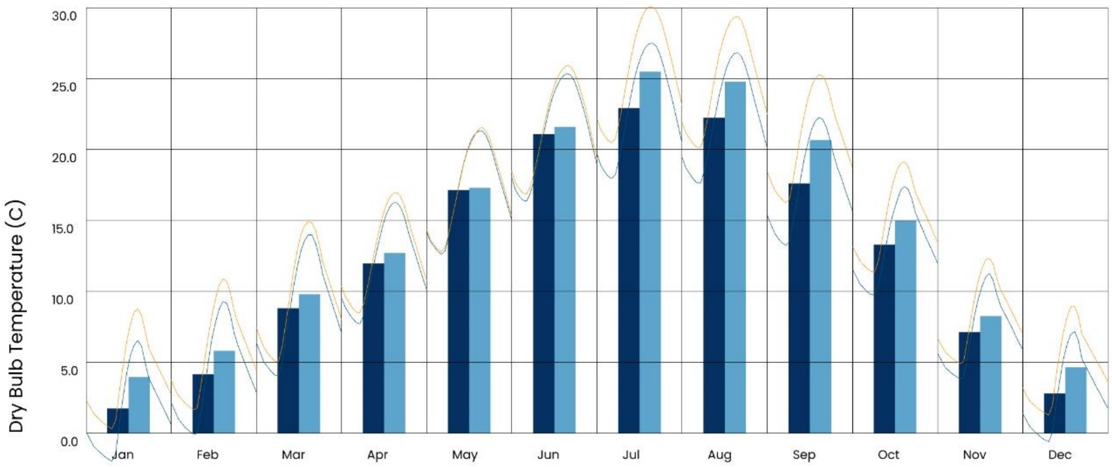

Present dry bulb temperature (monthly)

2050 dry bulb temperature (monthly)

Present dry bulb temperature (hourly average)

2050 dry bulb temperature (hourly average)

Figure 37 - LB bar chart showing Turin's monthly average dry bulb temperatures annual trend, comparing present and 2050 values.

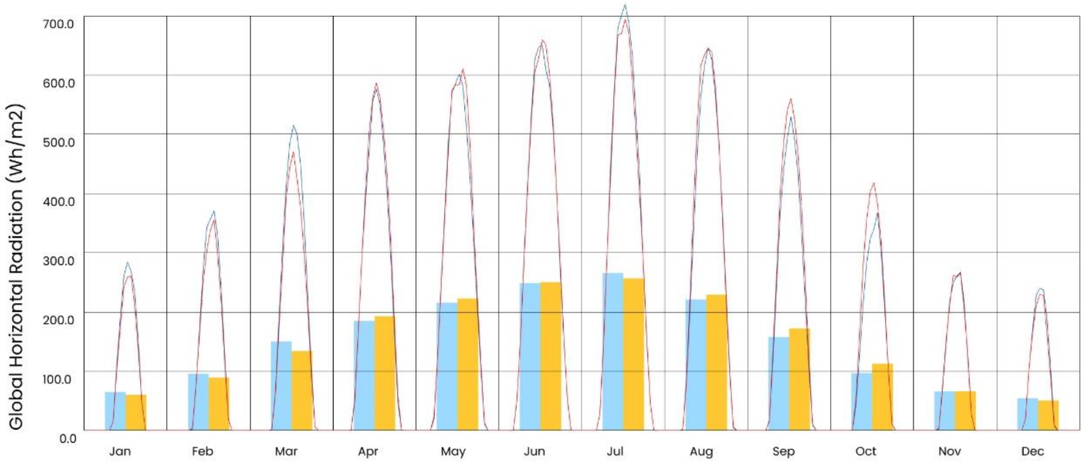

Present global horizontal radiation (monthly)

2050 global horizontal radiation (monthly)

Present global hor. radiation (hourly average)

2050 global hor. radiation (hourly average)

Figure 38 - LB bar chart showing Turin's monthly average horizontal global radiation annual trend, comparing present and 2050 values.

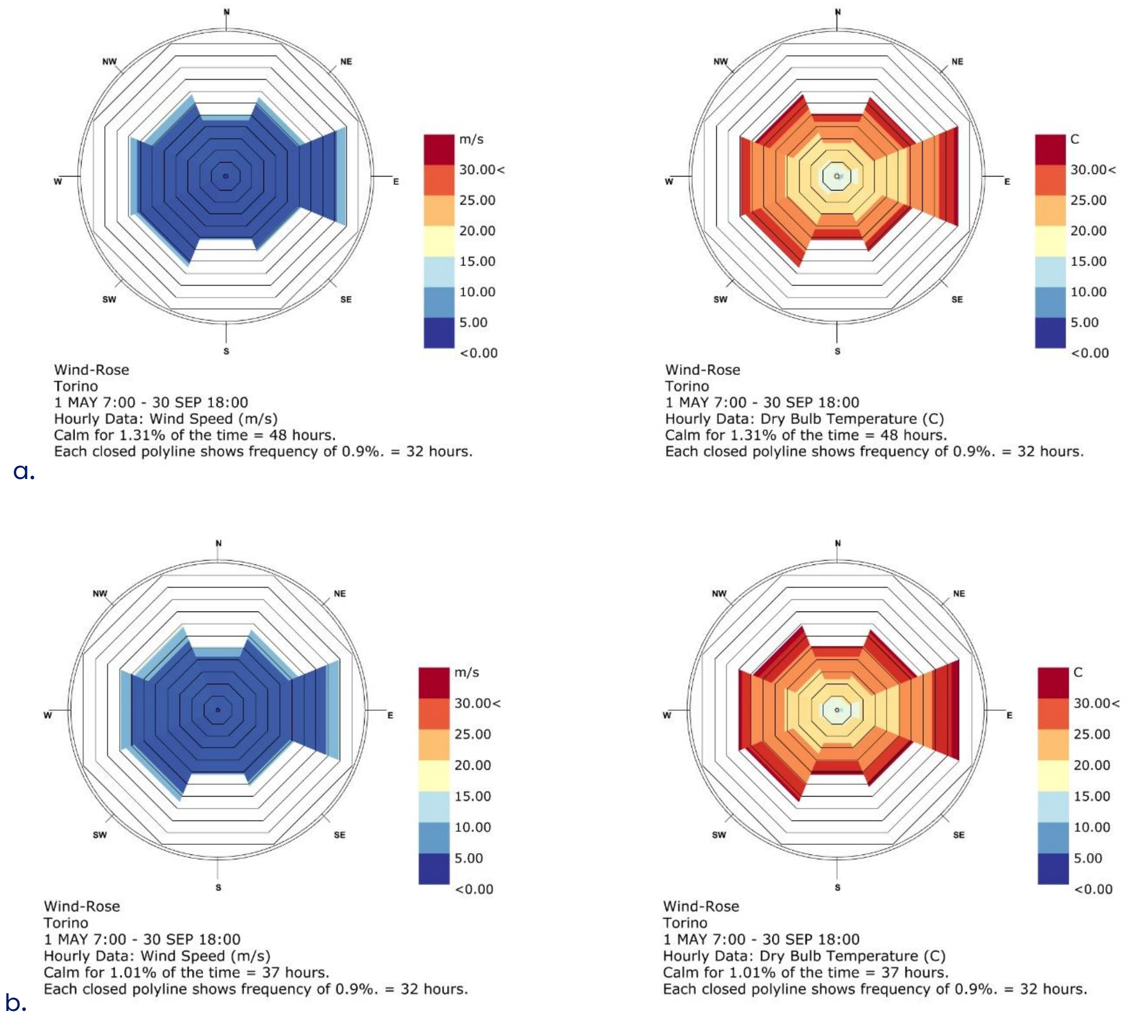

Figure 39 – Turin's prevailing wind direction and speed (on the left) and temperature (on the right). 39a - present conditions; 39b - 2050.

4.1.3 Climatic zone IV 1

ATHENS (Greece)

From Figure 40 it can be deduced that Athens has a warm climate, with mild winters and hot summers. In fact, average temperatures during winter season stand at nearly 10°C, with an increase of 1-1.5°C in 2050. In summer, monthly average values reach little less than 30°C, while hourly values reach up to 33-34°C in central hours of the day in July and August.

Solar radiation is generally very intense – see Figure 41. Average values in 2050 shows an overall decrease trend during all the months with respect to present irradiation, with the exception of September and October. Hourly values distribution does not differ much in the two periods, except during the central part of the day, when in 2050 values of nearly 900 Wh/m^2 are reached during summer.

Athens is less windy than the other locations discussed up to now. Prevailing wind direction is west, as can be deduced from wind roses displayed in Figure 42. Speeds remain low, although an increase may be observed in 2050, along with a rise in air temperatures.

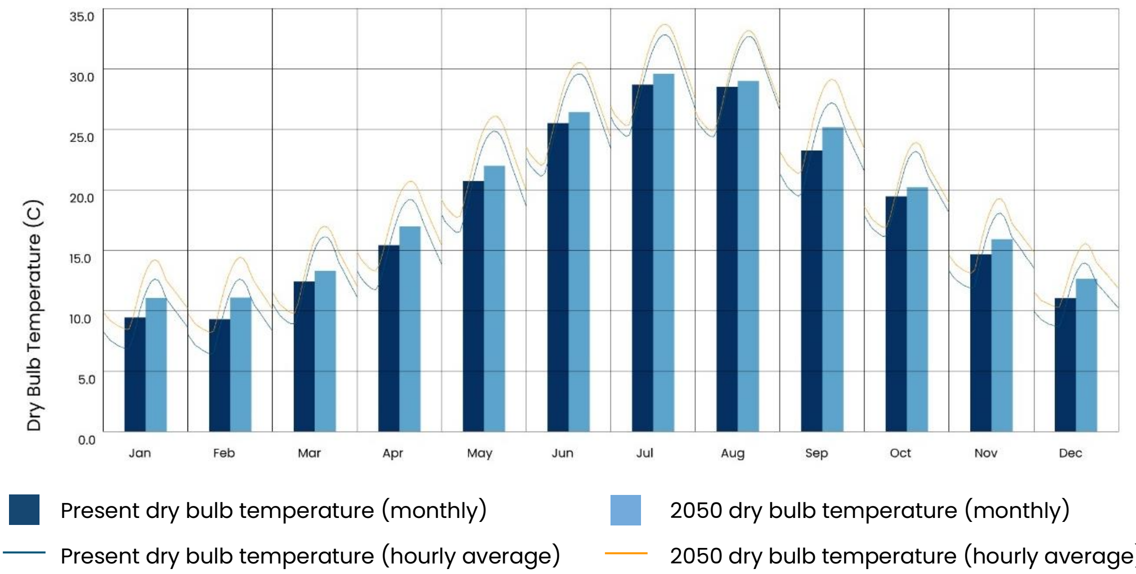

Figure 40 - LB bar chart showing Athens's monthly average dry bulb temperatures annual trend, comparing present and 2050 values.

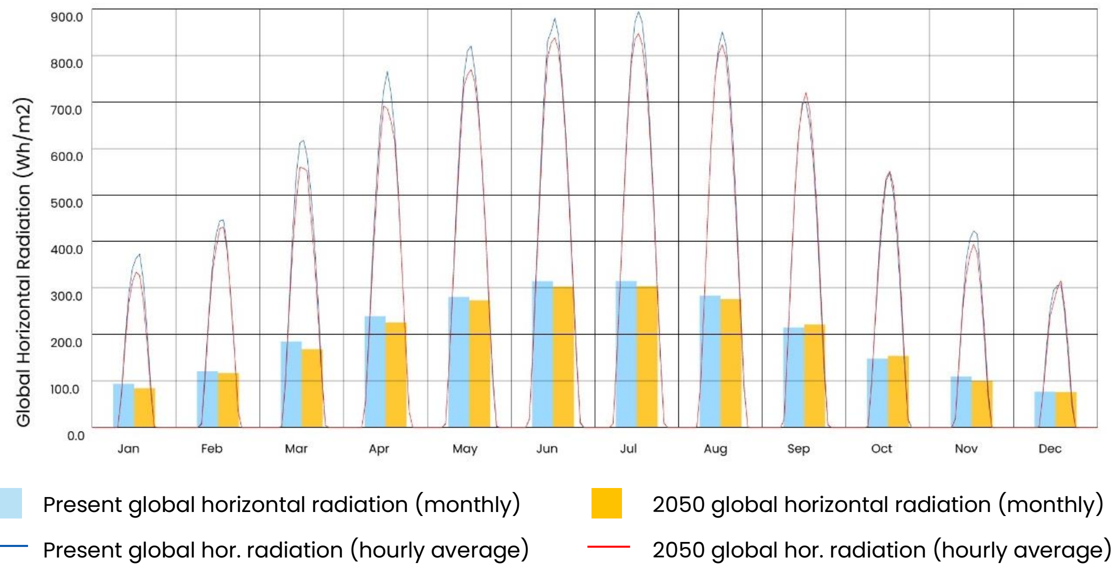

Figure 41 - LB bar chart showing Athens's monthly average horizontal global radiation annual trend, comparing present and 2050 values.

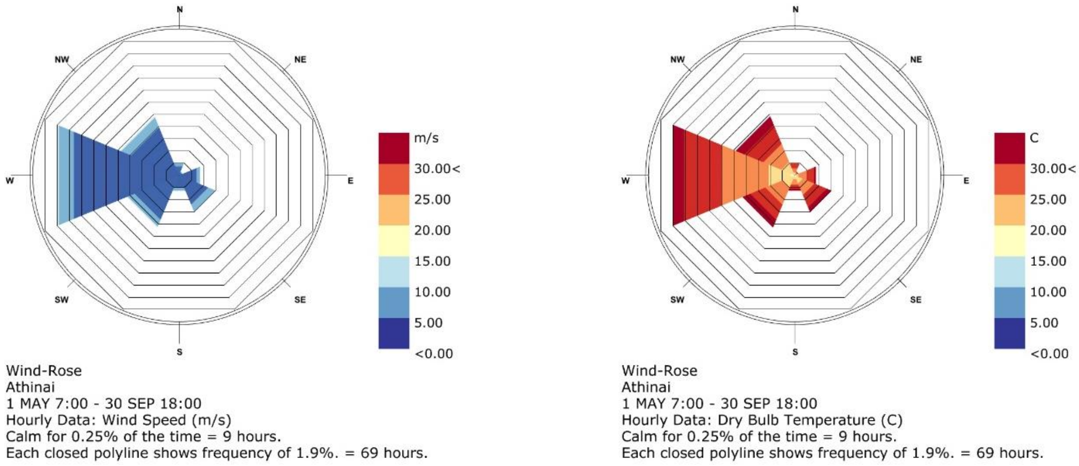

a.

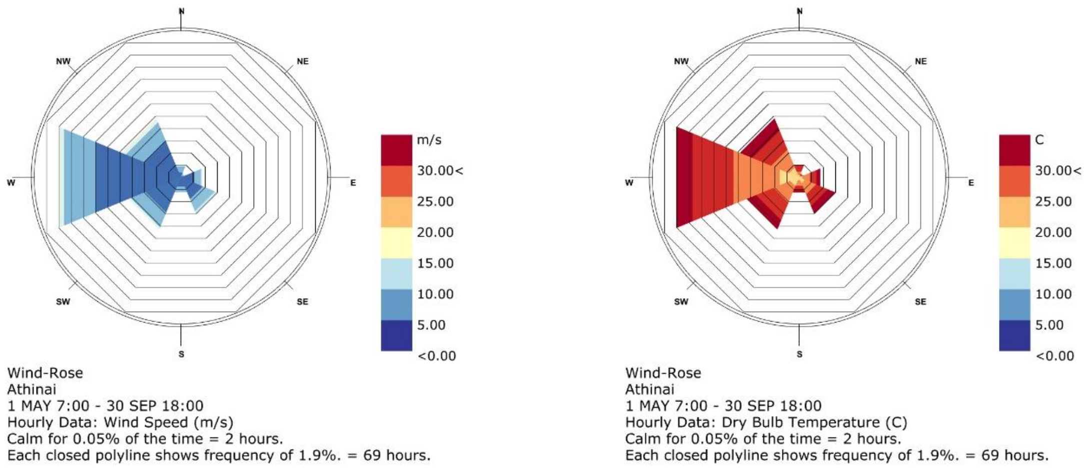

b.

Figure 42 – Athens's prevailing wind direction and speed (on the left) and temperature (on the right). 42a - present conditions; 42b - 2050.

BARI (Italy)

Bari and Athens have similar climatic conditions in terms of temperatures and global radiation fluctuation during the year. Though, global irradiation is less intense – see Figure 44. Also in this case, average temperatures in 2050 are higher; solar irradiation remains approximately the same.

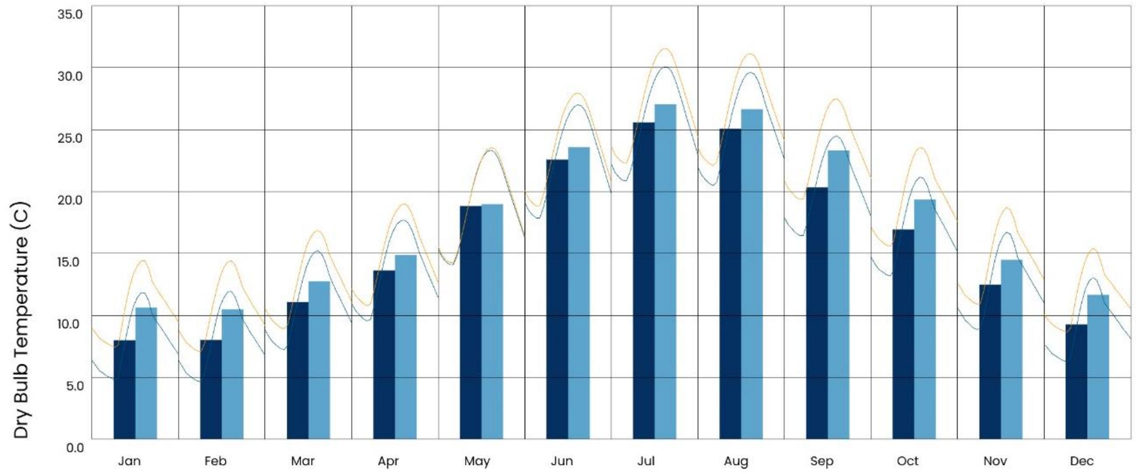

Present dry bulb temperature (monthly)

2050 dry bulb temperature (monthly)

Present dry bulb temperature (hourly average)

2050 dry bulb temperature (hourly average)

Figure 43 - LB bar chart showing Bari's monthly average dry bulb temperatures annual trend, comparing present and 2050 values.

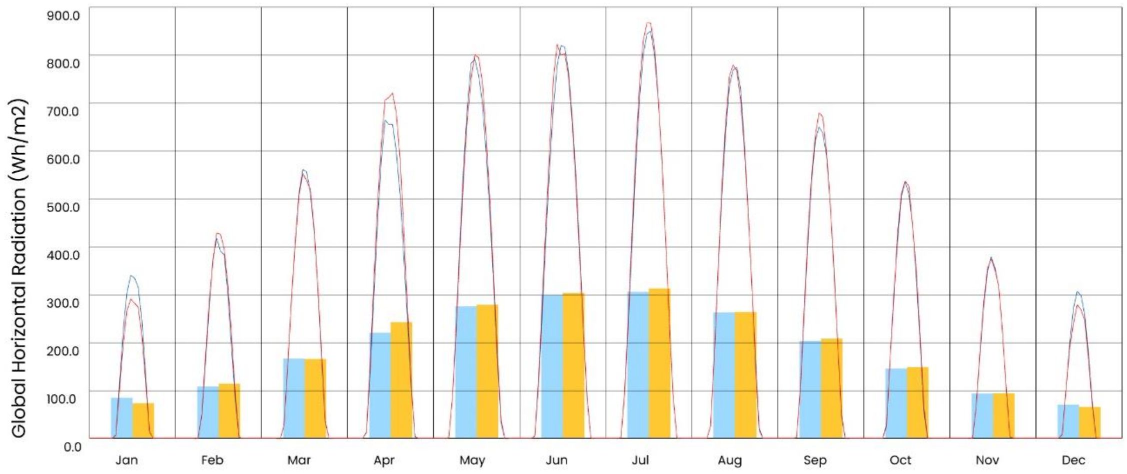

Present global horizontal radiation (monthly)

2050 global horizontal radiation (monthly)

Present global hor. radiation (hourly average)

2050 global hor. radiation (hourly average)

Figure 44 - LB bar chart showing Bari's monthly average horizontal global radiation annual trend, comparing present and 2050 values.

Figure 45 shows that Bari is very windy, with warm air flows that primarily come from east and north directions. Contrary to what observed in the previous locations, wind speed decreases in 2050. In accordance with the general trend, in 2050 air temperatures rise in all cardinal directions. Values reach up to 30°C or more under both present and future conditions.

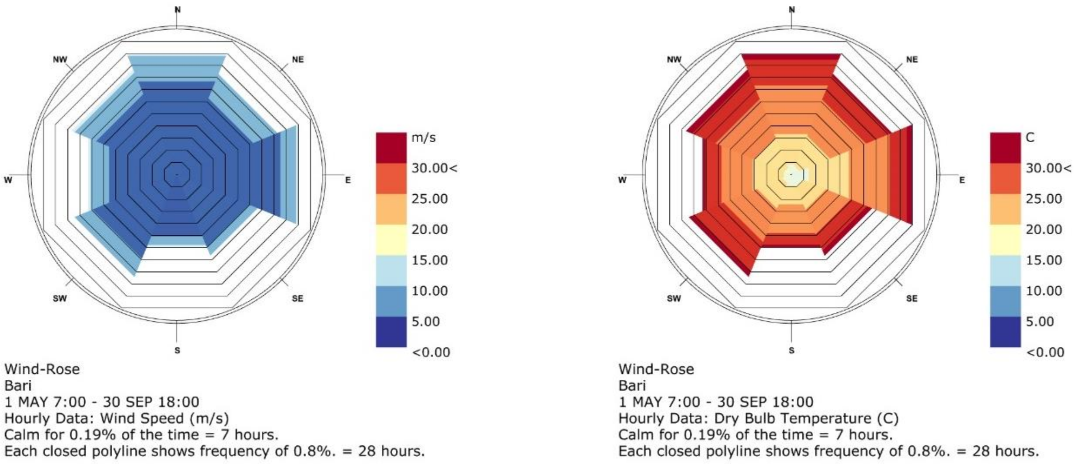

a.

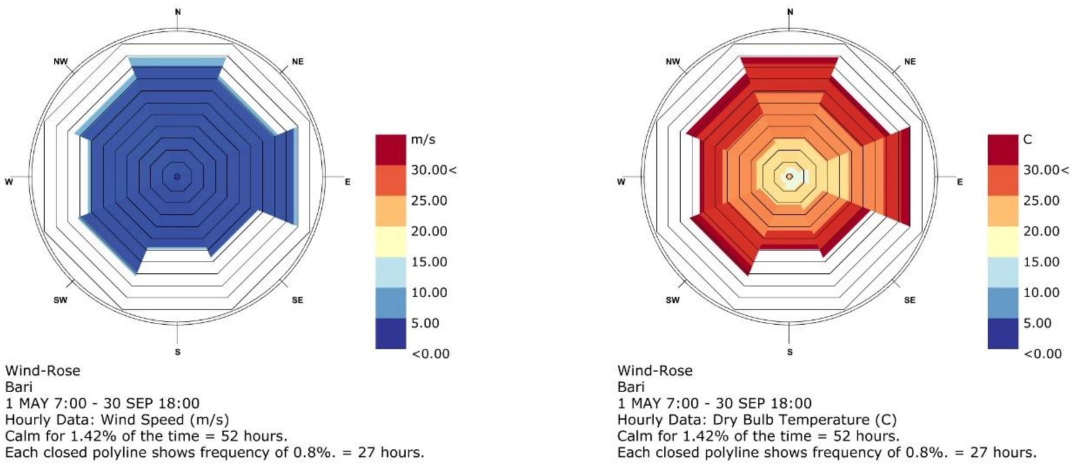

b.

Figure 45 – Bari's prevailing wind direction and speed (on the left) and temperature (on the right). 45a - present conditions; 45b - 2050.

PALERMO (Italy)

Palermo's climatic conditions are comparable to Bari's, with a major difference during the winter period. In this case, average temperatures exceed 10°C, reaching 15°C, defining a warmer climate – see Figure 46. 2050 contributes to make these temperatures hotter. Summer average temperatures fall mostly between 25°C and 30°C, while hourly values reach and exceed this limit. Global horizontal radiation, as it happens in Bari, remains basically the same between present and future conditions; its values are the highest see so far.

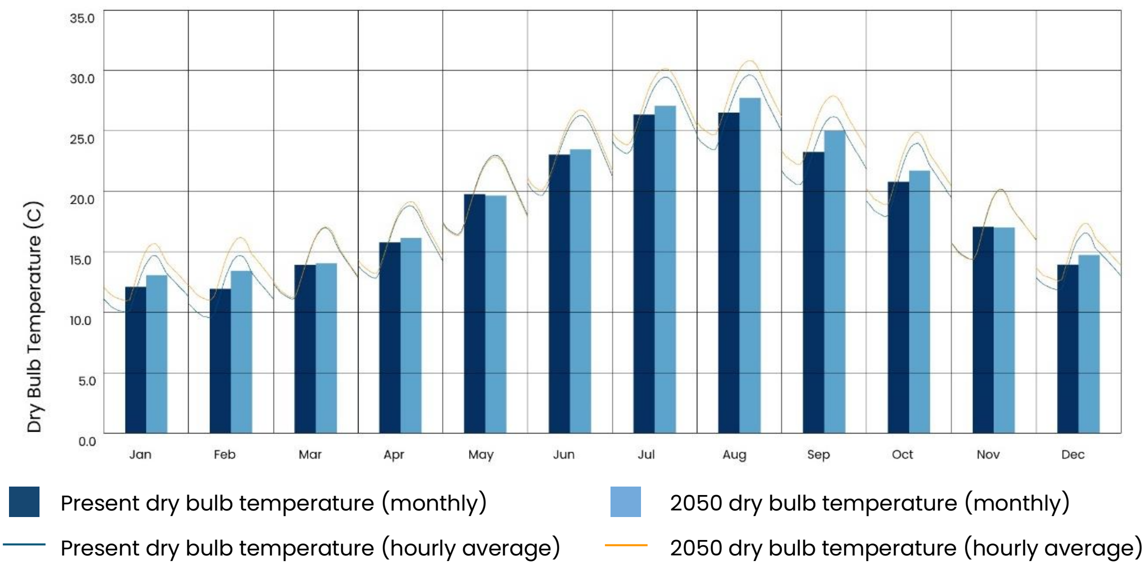

Figure 46 - LB bar chart showing Palermo's monthly average dry bulb temperatures annual trend, comparing present and 2050 values.

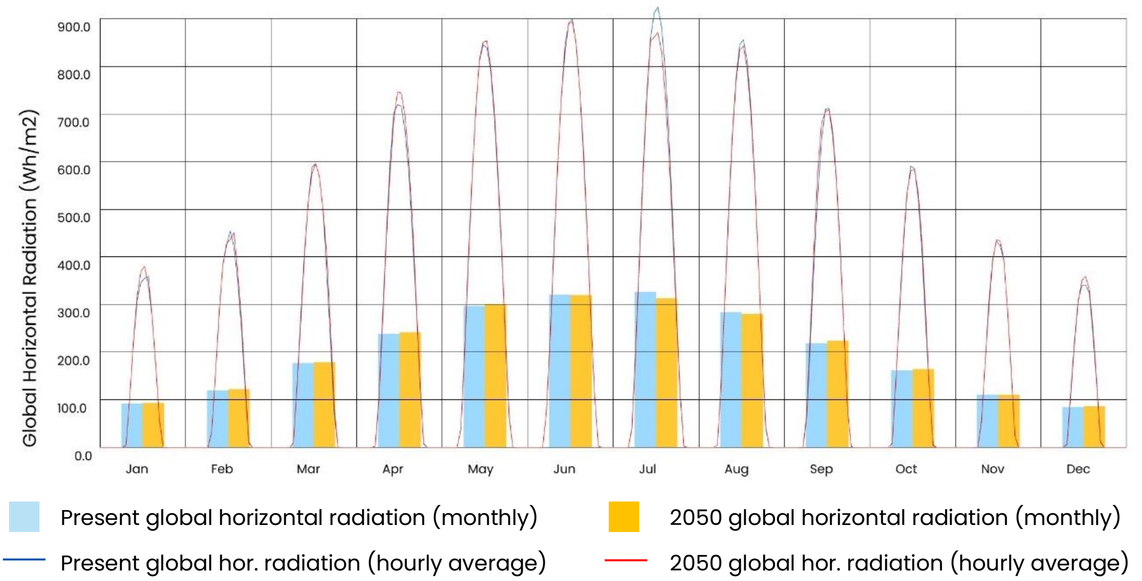

Figure 47 - LB bar chart showing Palermo's monthly average horizontal global radiation annual trend, comparing present and 2050 values.

Winds flows almost only from N-NE directions, as can be noticed from Figure 48. Then, by comparing present and 2050 wind roses, it can be noticed that directions, speeds and temperatures of the winds do not change particularly.

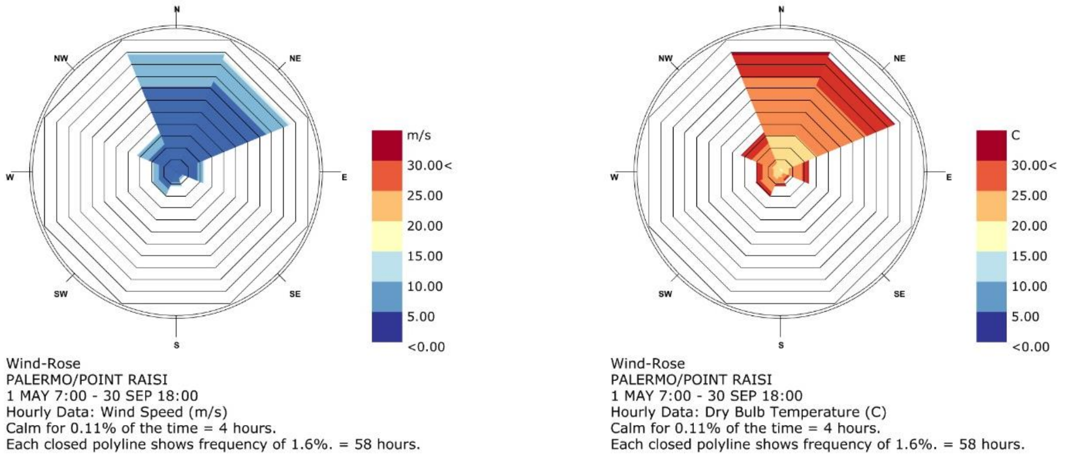

a.

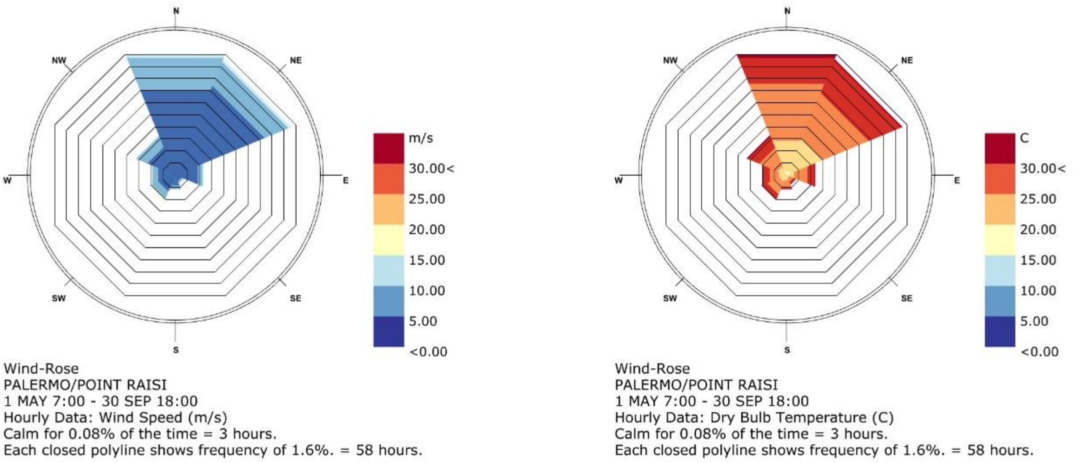

b.

Figure 48 – Palermo's prevailing wind direction and speed (on the left) and temperature (on the right). 48a - present conditions; 48b - 2050.

PAPHOS (Republic of Cyprus)

Paphos is located on the southwest coast of the island of Cyprus, in the Mediterranean Sea. Its average temperature trend is similar to Palermo's, with little higher values. The same may be said for radiation values (Figure 50). The only difference is that the most irradiated month is June and not July, as for all the previous cases. It can be stated that present and 2050 radiation values are almost the same.

Predominant wind comes from SW direction, but also, to a lesser extent, from south and west directions, as can be seen from Figure 51. Current wind speed does not exceed 10 m/s, while in 2050 this value is expected to increase, reaching 20 m/s from

W direction. Even wind temperatures during summer, already high, are expected to further increase, going over 30°C.

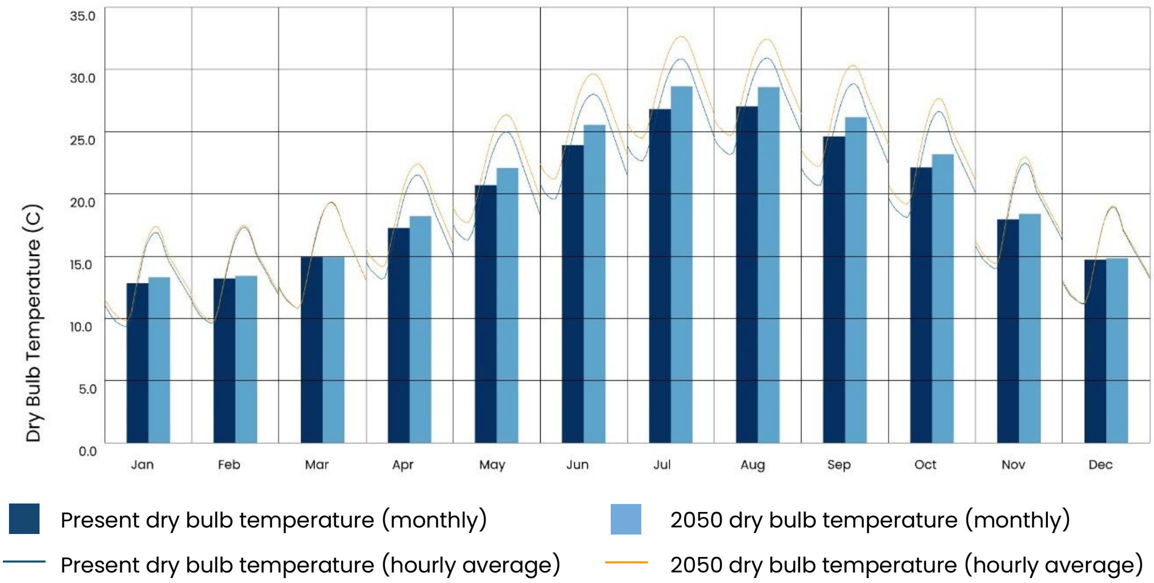

Figure 49 - LB bar chart showing Paphos's monthly average dry bulb temperatures annual trend, comparing present and 2050 values.

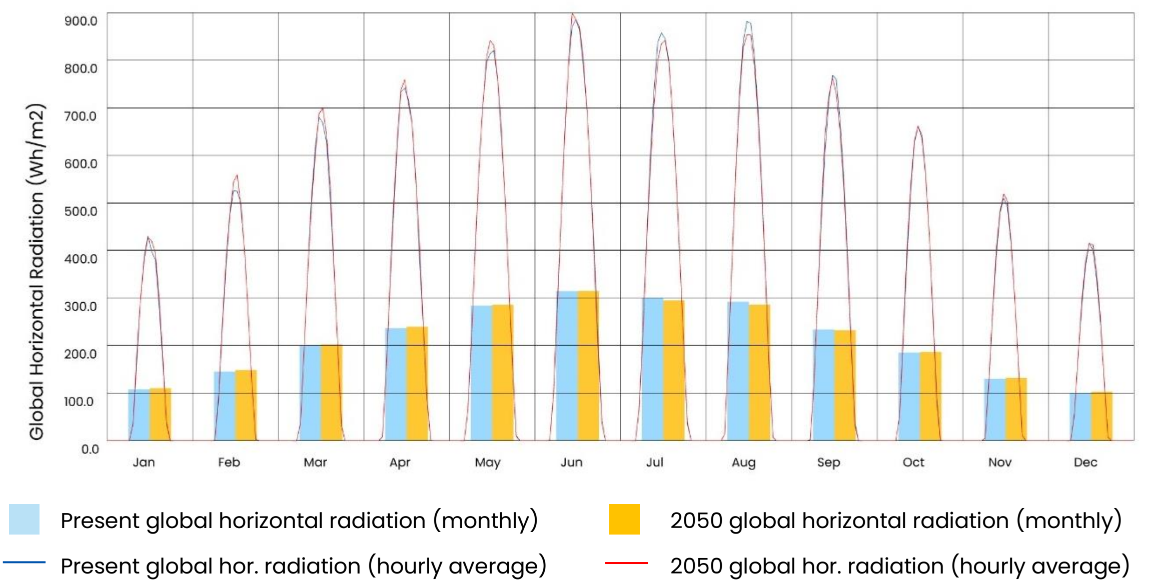

Figure 50 - LB bar chart showing Paphos's monthly average horizontal global radiation annual trend, comparing present and 2050 values.

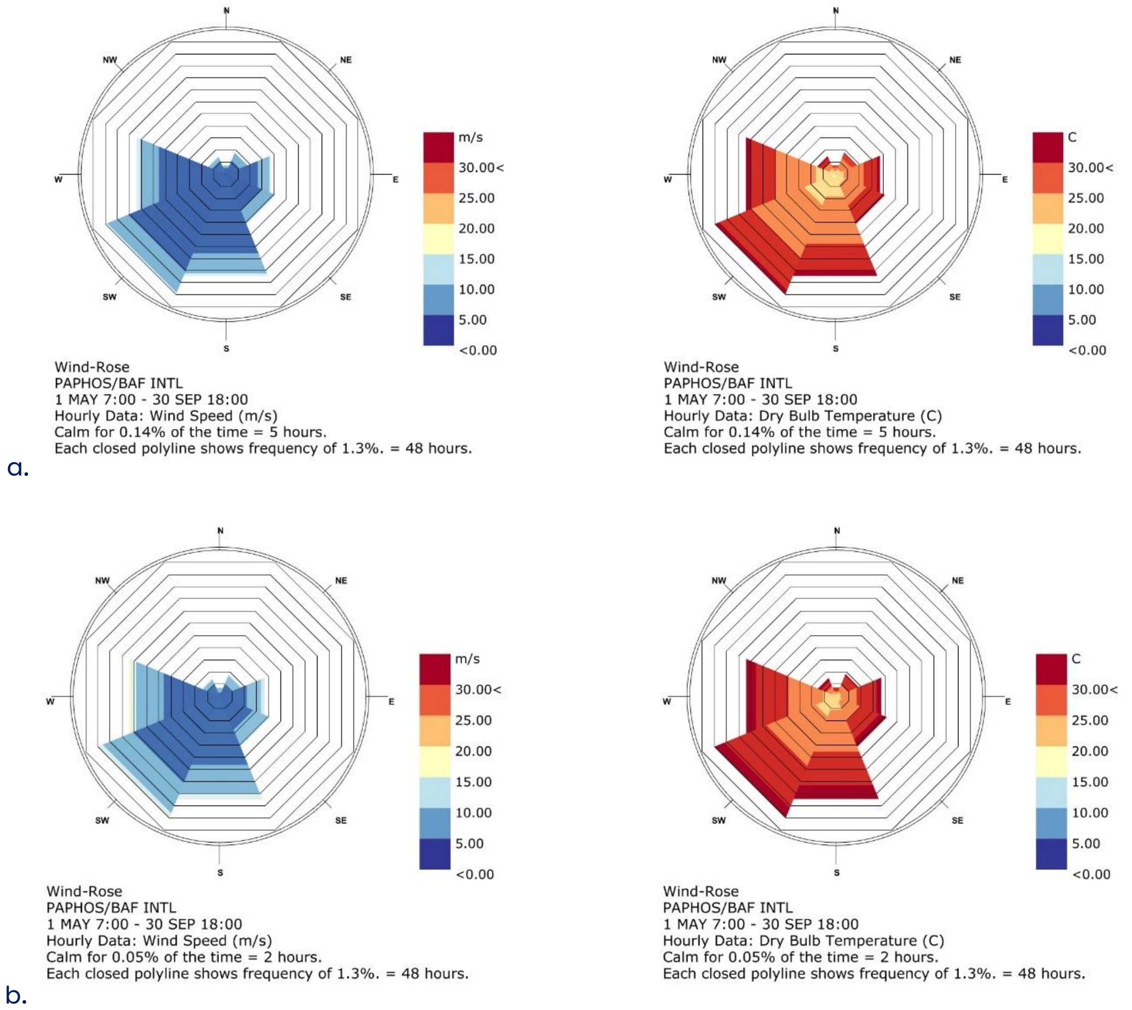

Figure 51 – Paphos's prevailing wind direction and speed (on the left) and temperature (on the right). 51a - present conditions; 51b - 2050.

ROME (Italy)

Average dry bulb temperatures' trend in Rome is similar to the one discussed for Bari. Winters are mild, while summers are hot (up to > 30°C for hourly data). Values for the year 2050 are higher than values recorded under current climatic conditions: evidence for this is provided in Figure 52. Then, as far as global horizontal radiation is concerned, Figure 53 shows that 2050 values will be higher than current values, with peaks in hourly average radiation over 850 Wh/m^2 during summer season.

During summer period, Rome receives warm air mostly from the SW, but also from NE and east – see Figure 54. Actual wind speeds are low and they further decrease under

2050 conditions. Air temperatures remain for the most part the same; a slight rise can be noticed looking at east and NE directions.

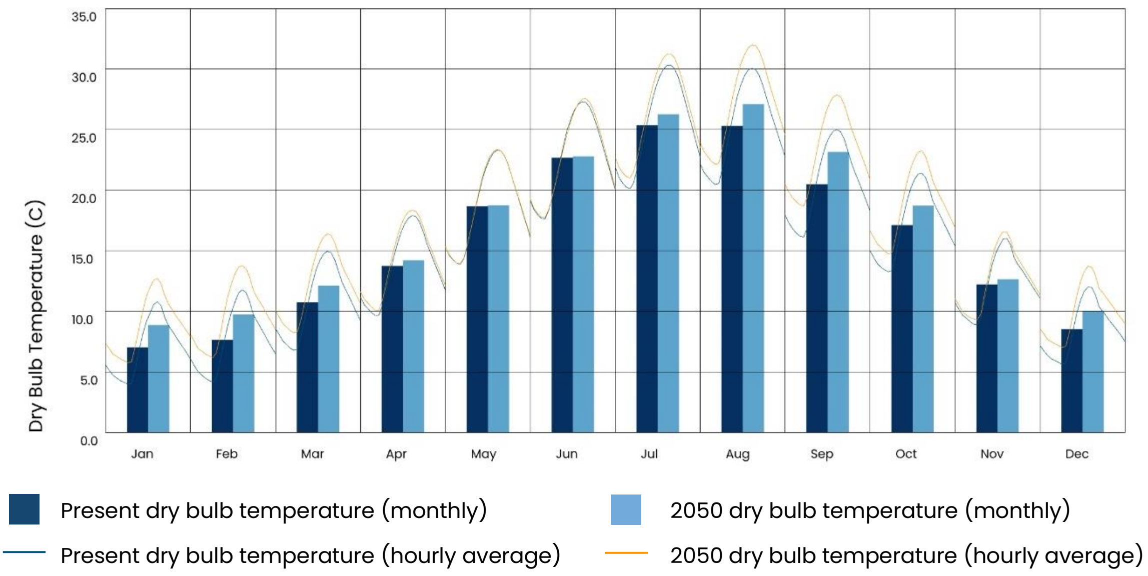

Figure 52 - LB bar chart showing Rome's monthly average dry bulb temperatures annual trend, comparing present and 2050 values.

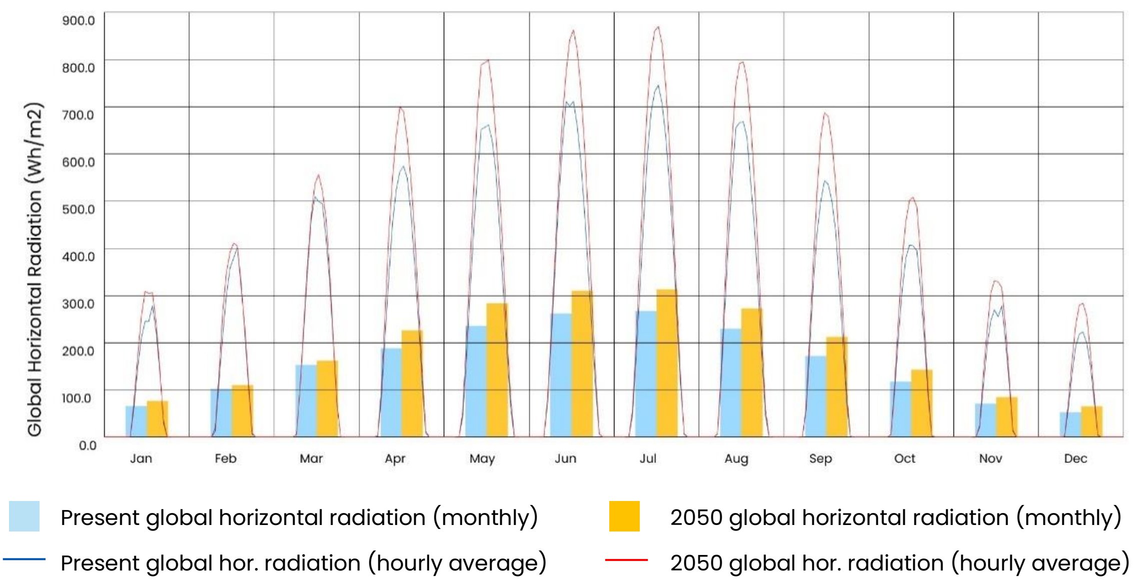

Figure 53 - LB bar chart showing Rome's monthly average horizontal global radiation annual trend, comparing present and 2050 values.

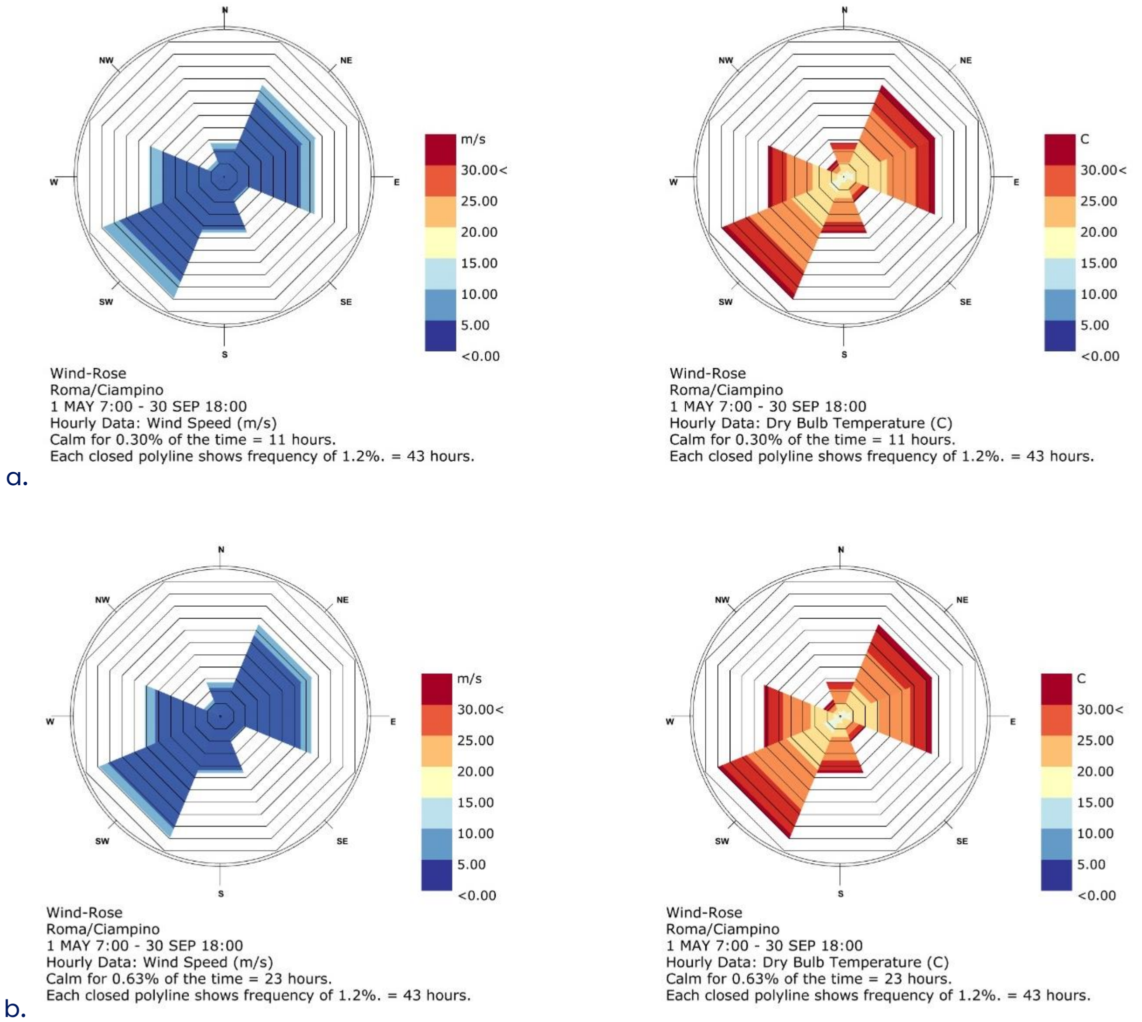

Figure 54 – Rome's prevailing wind direction and speed (on the left) and temperature (on the right). 54a - present conditions; 54b - 2050.

TRIESTE (Italy)

Although Trieste is located in the north of Italy, its climate is probably mitigated by its coastal position, facing the Adriatic Sea. Trieste's temperature trend throughout the year is comparable to the one showed in the previous paragraph (Rome), with slightly cooler winters. Also radiation trend is comparable. Under 2050 climatic conditions, average temperatures increase (or remain the same), as well as global irradiation. In this last case, exception is represented by the first three months of the year, in which average horizontal radiation diminishes.

As far as wind is concerned, Figure 57 illustrates that Trieste is typically windy during warm months. Prevailing directions from which the air flows are E-NE and SW. Air temperatures are warm, even hot, for the majority of the time. In 2050, wind speeds are expected to significantly rise, as well as temperatures. It is also predicted an increase in wind that comes from SW direction.

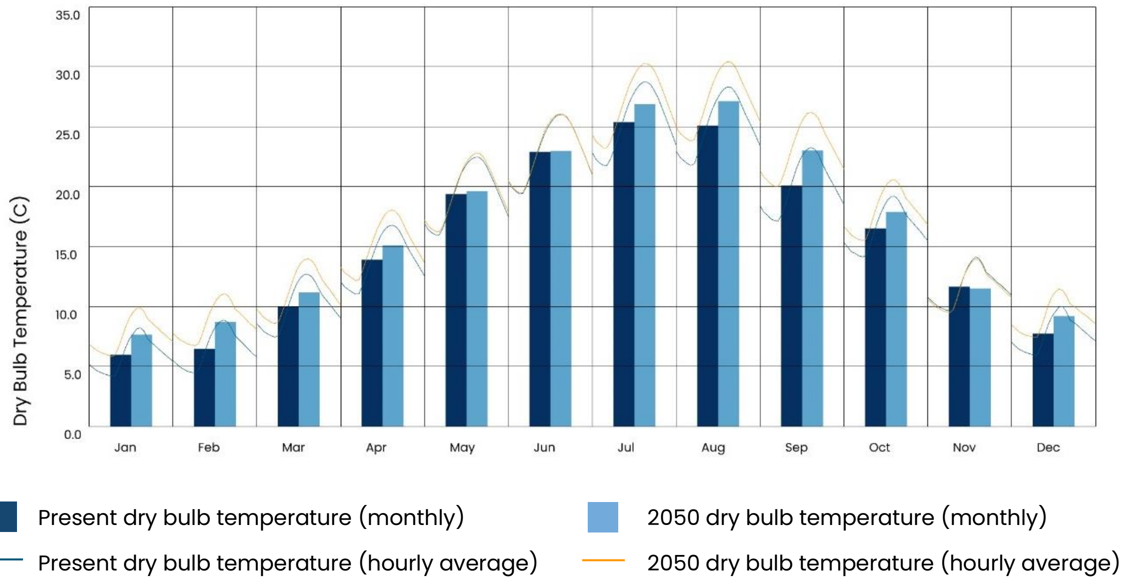

Figure 55 - LB bar chart showing Trieste's monthly average dry bulb temperatures annual trend, comparing present and 2050 values.

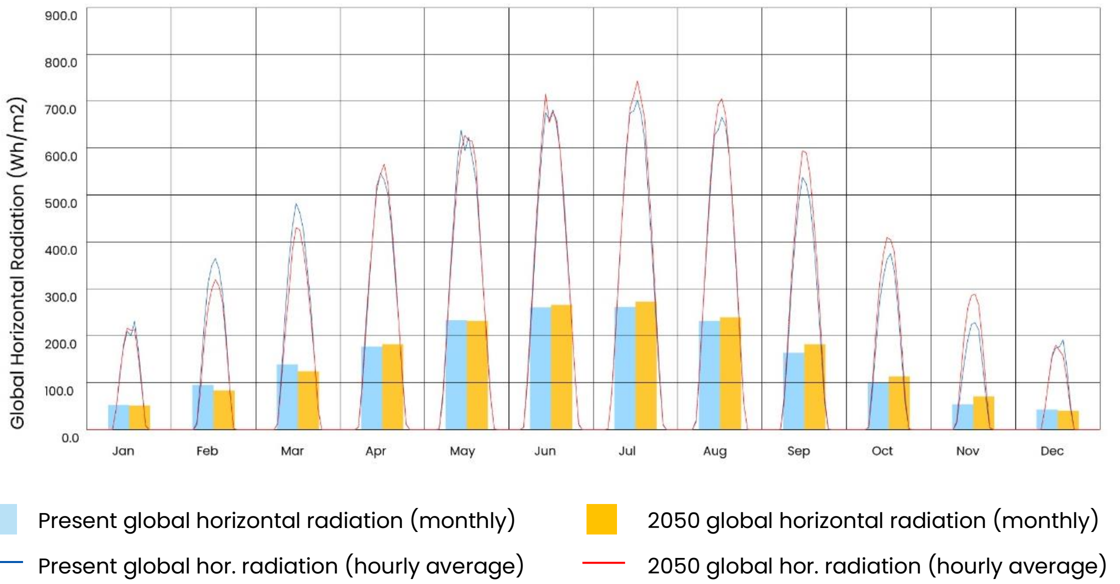

Figure 56 - LB bar chart showing Trieste's monthly average horizontal global radiation annual trend, comparing present and 2050 values.

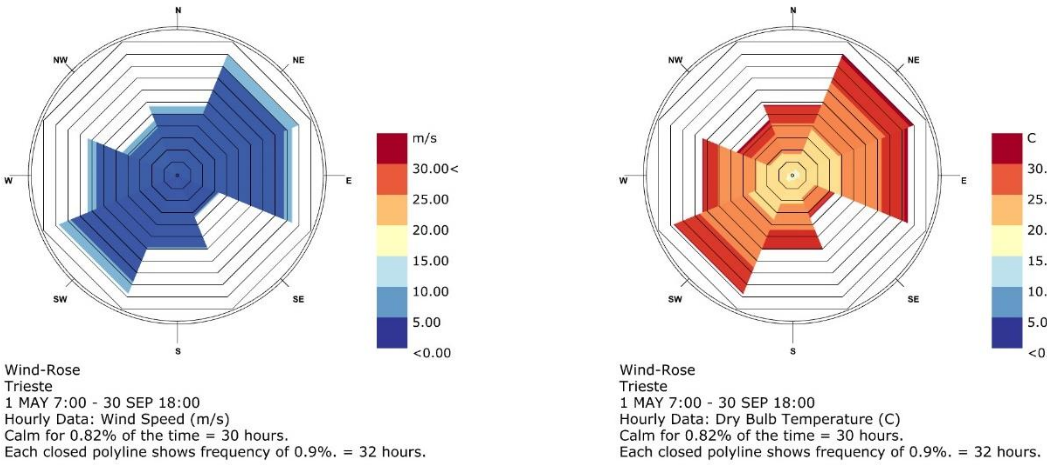

a.

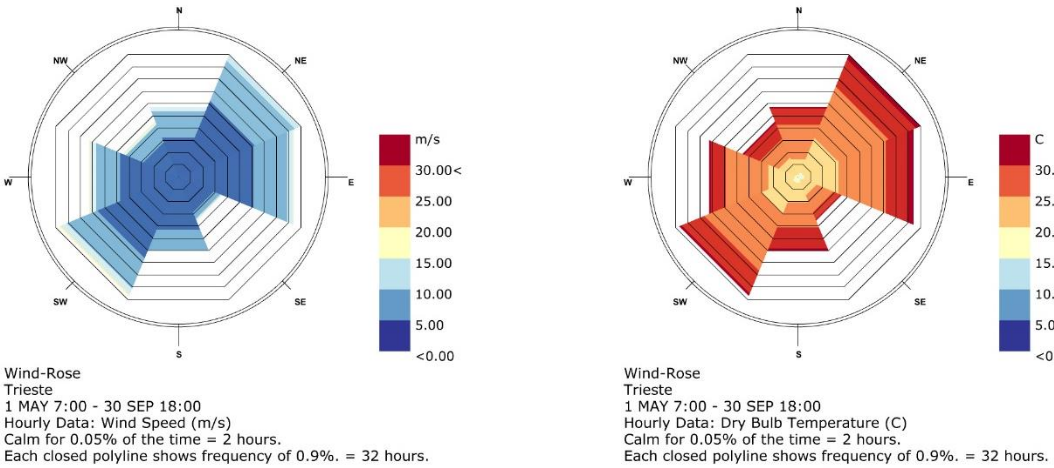

b.

Figure 57 – Trieste's prevailing wind direction and speed (on the left) and temperature (on the right). 57a - present conditions; 57b - 2050.

4.1.4 Climate analyses conclusions

On the basis of the previous analyses, general statements can be done. Among the ten considered locations, Kemi and Athens can be identified as the extreme cases. Kemi has the harshest climatic conditions: it is the coldest and less irradiated location, due to its northernmost position. In contrast, Athens is the hottest city and the one that receives the most intense global horizontal radiation throughout the year. Palermo and Paphos are similar cases. As far as the other locations are concerned, it can be stated that the more southern the location, the warmer the climate, with milder winters and hotter summers. Prevailing wind directions depend on the location.

In general, with respect to present conditions, in 2050 some changes can be noticed from LB climate analysis:

- Average dry bulb temperatures increase (ΔT up to 2-2.5°C).
- Average global horizontal radiation is generally lower or similar to current values, with the exception of some months in some locations. In marked contrast with this trend, Rome shows an increase in radiation, especially during summer months.
- While wind directions seem to remain the same in each location[24], variations can be observed in air temperatures and speeds. In general, both tend to increase; air temperatures rise is strongly linked to dry bulb temperatures increasing tendency. However, in Rome and Bari it is particularly evident that wind speeds decrease in 2050 with respect to actual conditions.

4.2 Optimizations results analysis

This paragraph compares and discusses the results of the optimal solutions selected at the end of each of the twenty optimizations. Data comparison is visually supported by charts obtained through the use of Microsoft Office Excel and maps created with QGIS (v3.24.3). The discussion is divided in three main topics (*genes*, *fitness* values and energy use/savings) for easier understanding. Results are displayed in full in the summary table provided in ANNEX 2. Considering the constraints placed on Octopus optimization process (limited number of generations), it must be remembered that the solutions presented in this work are just some of the infinite design options that could be considered optimal. The selection of the solution for each specific case was made independently from the others, considering only their energy and daylight performance (*fitness* values). Hence, it is not certain that a correlation between the individual variables measured in the twenty cases exists, neither a dependency of each variable on the climatic conditions. In fact, final performance in a given climate does not depend on individual parameters, yet on a combination thereof. Consequently, *genes* values are discussed briefly. Instead, comparison of comfort and

[24] The correctness of this result should be verified through other databases, which provide more reliable future climate projections obtained using regional downscaling models (Regional Climate Models or RCM).

energy results is more meaningful for the analysis purpose, as it gives evidence of the applicability and resilience of the presented tool under different climatic conditions.

4.2.1 *Genes* or parameters

Design variables in their optimized configuration for the ten locations are here presented and compared, trying to find a correlation with climatic variables (temperatures, winds, etc.). First parameter to be discussed is the orientation of the building, which is also strongly related to the WWR on each wall and window area operable for natural ventilation.

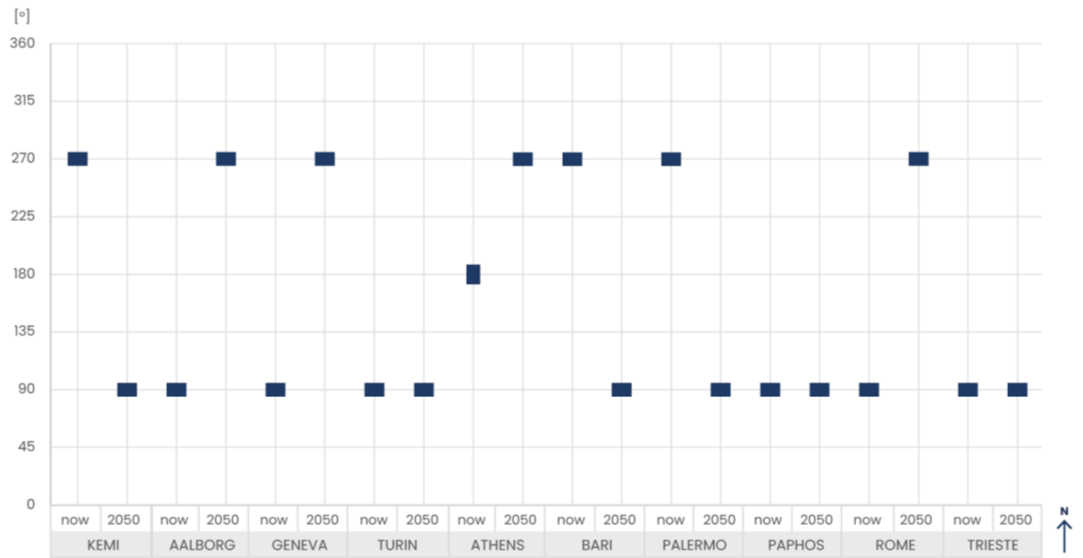

Figure 58 - Building orientation chart.

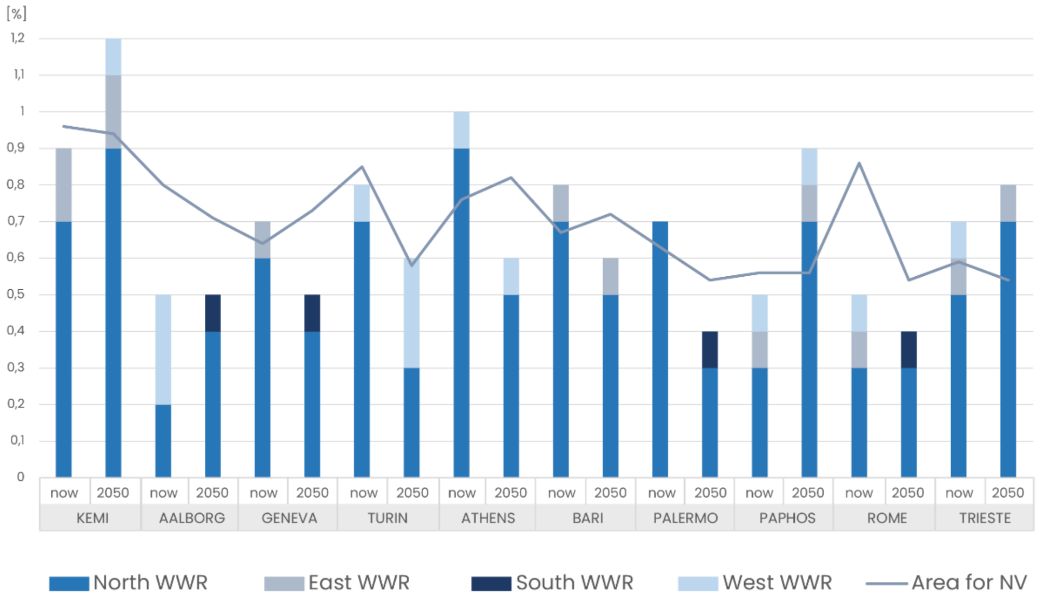

Figure 59 – Bar chart comparing WWR and glazed area for NV. Each bar contains the stacked WWR values for the four walls (colors are indicated in legend under the figure).

Figure 58 and Figure 59 display respectively building orientation and glazed ratios on the four walls (together with window area operable for NV). It can be observed that, in every location under both present and 2050 climatic conditions, the optimized zone has an east-west orientation, which means that it faces the north with its long side (90° and 270° rotation). The only exception is represented by Athens under present conditions, whose optimized zone has a north-south orientation, which means that it faces the north with its short side (180° rotation). In this case, north glazed aperture, for equal WWR, will be smaller than in the other cases. As far as windows are concerned, it can be noticed that glazed surface on the north wall is always present and is generally the largest. Although north-facing windows receive less amount of light during the year with respect to glazing exposed to other directions, they may bring several benefits. First, they receive diffuse light: not being exposed to direct sunlight prevents both overheating and glare problems. Then, to ensure an adequate amount of light indoors, northern glazing apertures' area is maximized. However, this could lead to an increase in thermal dissipation towards the considered direction, so a thicker insulation layer could be necessary. Looking at Figure 60, it can be seen that higher insulation thicknesses correspond to higher north WWR and vice versa. This happens in almost every location, except for Palermo, Paphos and Trieste. Total WWR[25] in 2050 solutions tends to decrease with respect to present configurations, and this may be a consequence of future temperatures' rise. Kemi, Aalborg, Paphos and Trieste represent exceptions to this trend. In Kemi 2050, total WWR increases. The reason could be that, due to Kemi's hash climatic conditions, the optimization process tries to maximize heat gains deriving from the already poor amount of available solar radiation, scarcer in 2050. A similar case can be made about Aalborg (another cold location) in 2050, where total WWR remains the same as the present one. However, north WWR increases and south-facing window is added as a replacement for present window placed on west façade, maybe to increase the amount of light and heat that enters the environment. For Trieste's case, the reason for the total WWR rise could be found in temperatures and wind. Air flows speeds and temperatures significantly

[25] Total WWR refers to the sum of WWR o each cardinal direction.

increase in 2050, so west window is closed (west is one of the prevailing wind directions for this location). But, probably for daylight threshold reasons, north window area needs to be increased, letting in diffused sunlight without excessive heat inflow. Moreover, due to 2050 temperatures' rise, insulation thickness decreases. Lastly, Paphos' WWR probably increases in 2050 for reasons of ventilation. Under equal insulation thickness and operable window area for NV, higher WWR is required to increase ventilation rate in response to higher outdoor temperatures.

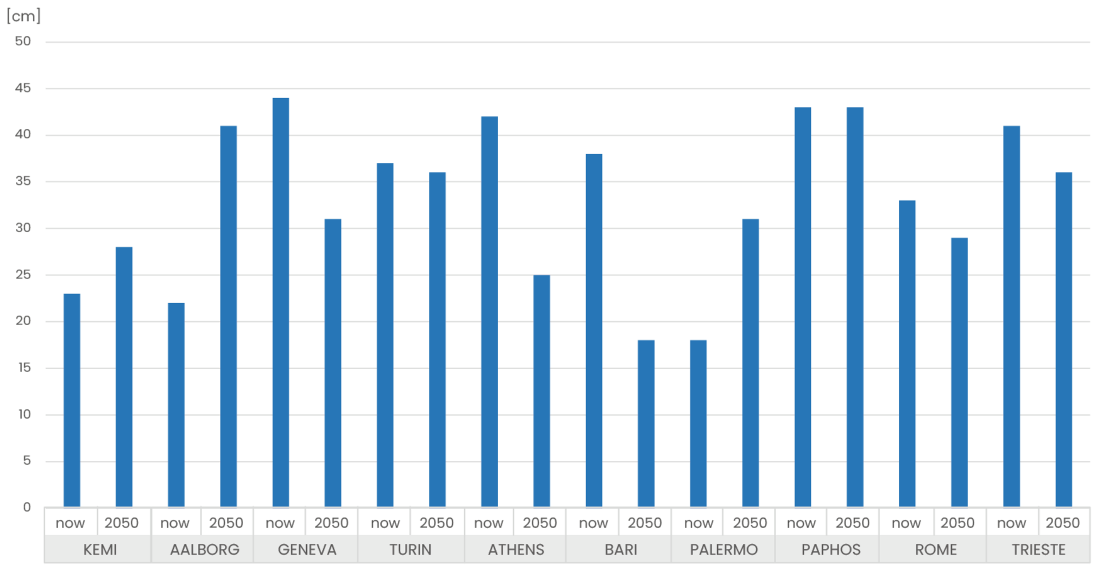

Figure 60 - Insulation thickness bar chart.

Additional considerations on WWRs could be made. Comparing Figure 59 with wind roses analyses carried out in §4.1, it can be stated that windows in optimal solutions are generally placed on walls facing the prevailing summer wind directions, in such a way that air flows enter the indoor environment perpendicularly or with an acute angle with respect to the inlet window surfaces. In Aalborg and Geneva's present optimal cases, windows are placed only on downwind walls (with respect to prevailing wind direction), which could mean that a strong NV is not required, probably due to their cool climate. In Turin (both under present and 2050 conditions) happens nearly the same thing: prevailing wind comes from the east, but windows are only north-facing and west-facing. However, this placement seizes other less predominant air flows coming from SW, west and NW directions (see Turin's wind roses - Figure 39). Broadly speaking and referring to what Grosso said in his book ([84], pp. 334-336), design conditions for an effective NV are achieved in almost every location, apart from the aforementioned cases. Glazing area operable for NV is highly variable.

Figure 61 compares the shades rotation angle for the twenty optimal solutions. It must be remembered that shading material is not completely opaque – see §3.3.2. In most of the cases, shading devices are positioned to block the solar radiation income (angles from 0° to +90°). Probably, these angles are chosen to reduce glare problems and to prevent overheating, especially in hot locations (Athens, Palermo, Paphos, Rome, Trieste). In Geneva and Kemi (present), shades are nearly horizontal (almost 0°). Shading devices rotated with this angle, as well as with angles below 0° (as for Turin and Bari's present cases and Athens 2050), let solar radiation in.

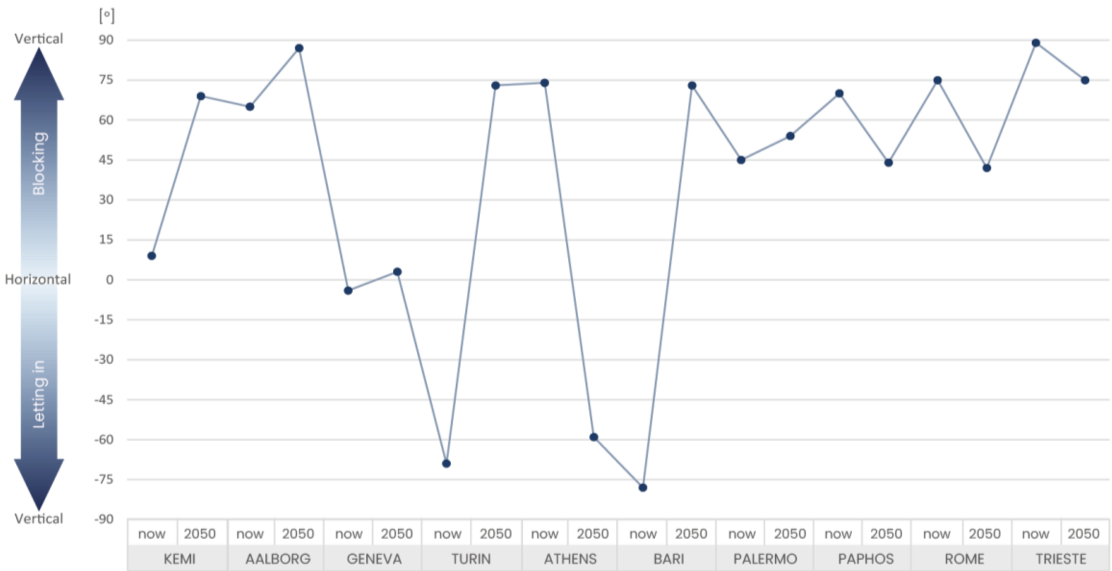

Figure 61 - Shading devices angle chart.

4.2.2 *Fitness* values or objectives

Before analyzing the *fitness* values, it should be remembered that, given the settings discussed in the previous chapter, the selected optimal solutions are the ones, among the 15 generation of individuals found by Octopus, that better balance all the four objectives. Figure 62 compares adaptive thermal comfort, DLA, $UDLI_{100-2000lx}$, and ASE obtained for the twenty optimal design options. Values for sDA are also taken into consideration.

As regards thermal comfort, the tool seems more efficient in reaching higher percentages of comfort in mild-to-hot climates than in colder and less irradiated climates (e.g., Kemi and Aalborg). Also Ginevra and Turin show lower comfort values with respect to other locations. Aalborg and Turin's 2050 cases are exceptions to this general trend. For locations that belong to climate zone IV 1 (from Athens to Trieste), the tool found design solutions that allow to reach very high levels of thermal comfort in free-running mode. For instance, in Bari, Palermo, Paphos and Rome, occupants feel comfortable for over the 90% of the analysis period. This should drastically reduce the energy use for those locations when applying the optimized HVAC schedules to the mixed-mode systems.

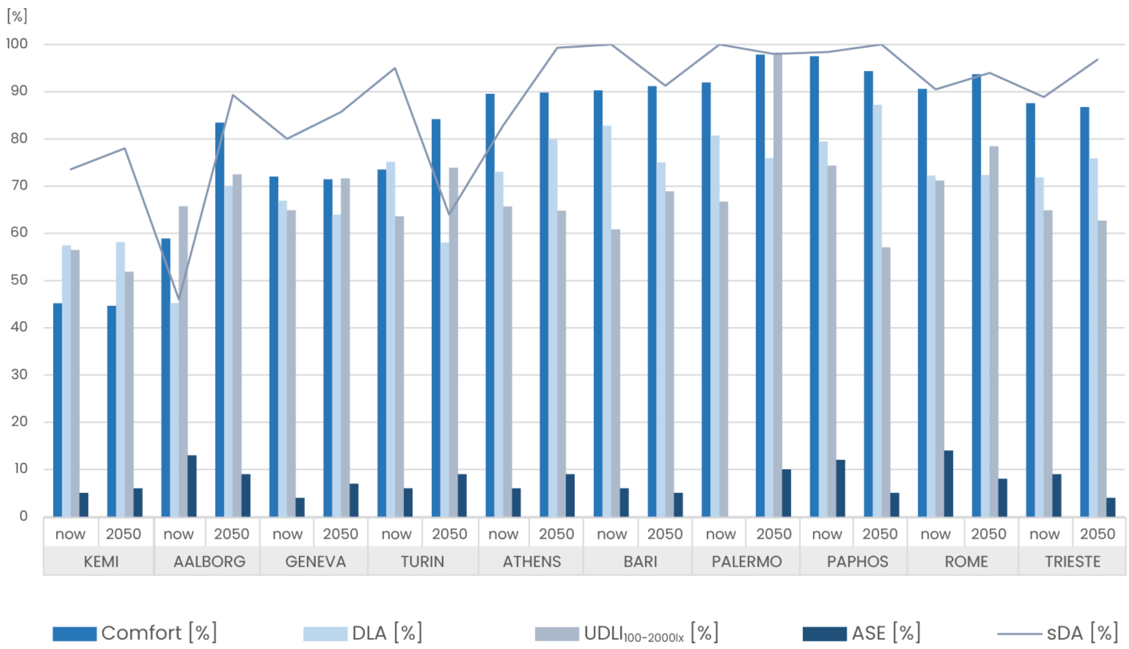

Figure 62 - Optimization objectives comparation bar chart.

Visual comfort is evaluated considering DLA, UDLI and sDA. Ideally, the higher the DLA and $UDLI_{100\text{-}2000lx}$ values, the smaller the energy use required throughout the year for artificial lighting. Averaged daylight autonomy (DLA) is always achieved for at least 50% of the time of the occupancy period, except in Aalborg's present case (DLA<50%). Illuminance threshold of 500 lx is reached for over 70% of the time only in more irradiated locations (under both present and 2050 climatic conditions), that is for locations that belong to climate zone IV 1 of Troll and Paffen classification. Turin's present case, where DLA is equal to 75%, represents an exception. With respect to averaged $UDLI_{100-2000lx}$, the daylight metric that represent the percentage of the time the working area receives effective illuminance (between 100 and 2000 lx), Figure 62 shows a high variability of this parameter. The lower the $UDLI_{100-2000lx}$ value, the higher the ineffective light (illuminance less than 100 lx – $UDLI_{<100x}$) or the excessive and undesirable light (illuminance over 2000 lx – $UDLI_{>2000lx}$). Apart from Kemi's case, where a low useful daylight illuminance is expected due to the poor available annual solar radiation, $UDLI_{100-2000lx}$ exceeds 60% in almost every location, except in Paphos 2050. Palermo's case under 2050 climate represents the ideal condition: averagely, the working plane receives useful daylight for nearly 100% of the time, thus requiring very little energy for artificial lighting during the active occupancy period.

Analyzing sDA (percentage of the working plane area that receives at least 300 lx for 50% of the analysis period), it can be seen that LEED target (55%) is achieved in all cases, except in Aalborg under present conditions. An ascending trend can be identified: in general, higher values of sDA are obtained in hotter climates.

As far as glare is concerned, ASE metric is successfully kept below 10%, as LEED suggests, almost in every location. In Palermo present case, ASE even reaches 0%, completely removing potential glare problems. In contrast, Aalborg, Paphos and Rome's present cases show ASE levels that exceed 10% threshold. These values result from an unavoidable choice when selecting the optimal solutions that balance all the four objectives. In some cases, it also happened that the optimization process did not identify design options with lower ASE, so the one with the lowest value was selected.

4.2.3 Energy use and savings

This paragraph discusses and compares the zone's energy use for the twenty optimal solutions. Figure 63 shows four Europe maps obtained through the use of QGIS which represent non-optimized and optimized zone's energy use under present and 2050 climatic conditions. On each map ten pie charts, representing the zone energy usage balance (CEUI, HEUI and LEUI), are displayed and positioned on the corresponding location. The bigger the pie chart, the higher the total Energy Usage Intensity.

It must be remembered that energy use results to which reference is made are the outcome of the two parallel simulations run for the optimal solutions with a mixed-mode conditioning (see §3.9). Non-optimized refers to the results obtained applying default Honeybee HVAC and lighting schedules, which provide a constant activation of the systems. In contrast, optimized results are generated applying custom optimized schedules to the systems, turning on heating, cooling and lighting only when strictly needed.

Looking at non-optimized maps (present and 2050), several considerations can be made. Under present climatic conditions, cooling energy need is almost absent in cold locations, such as Kemi and Aalborg, while becomes greater in hotter locations like Paphos and Athens, replacing heating energy needs. In 2050, energy balance changes: heating loads decrease while cooling loads increase as a consequence of higher outdoor temperatures. This is particularly evident for Aalborg, for example. Kemi's energy use almost maintains the same proportions, with a small decrease in heating energy demand and a little increase in cooling load. In both present and 2050 maps, it is clear that lighting load represents a large portion of the total EUI. Then, comparing non-optimized and optimized pie charts' size and EUI values, it can be observed that, by applying optimized schedules to the optimal solutions, total EUI experiences a reduction, which is greater for mild-to-hot climates. Hence, the tool seems more resilient in this type of climates rather than in cool or extremely cold cases (such as Kemi), where

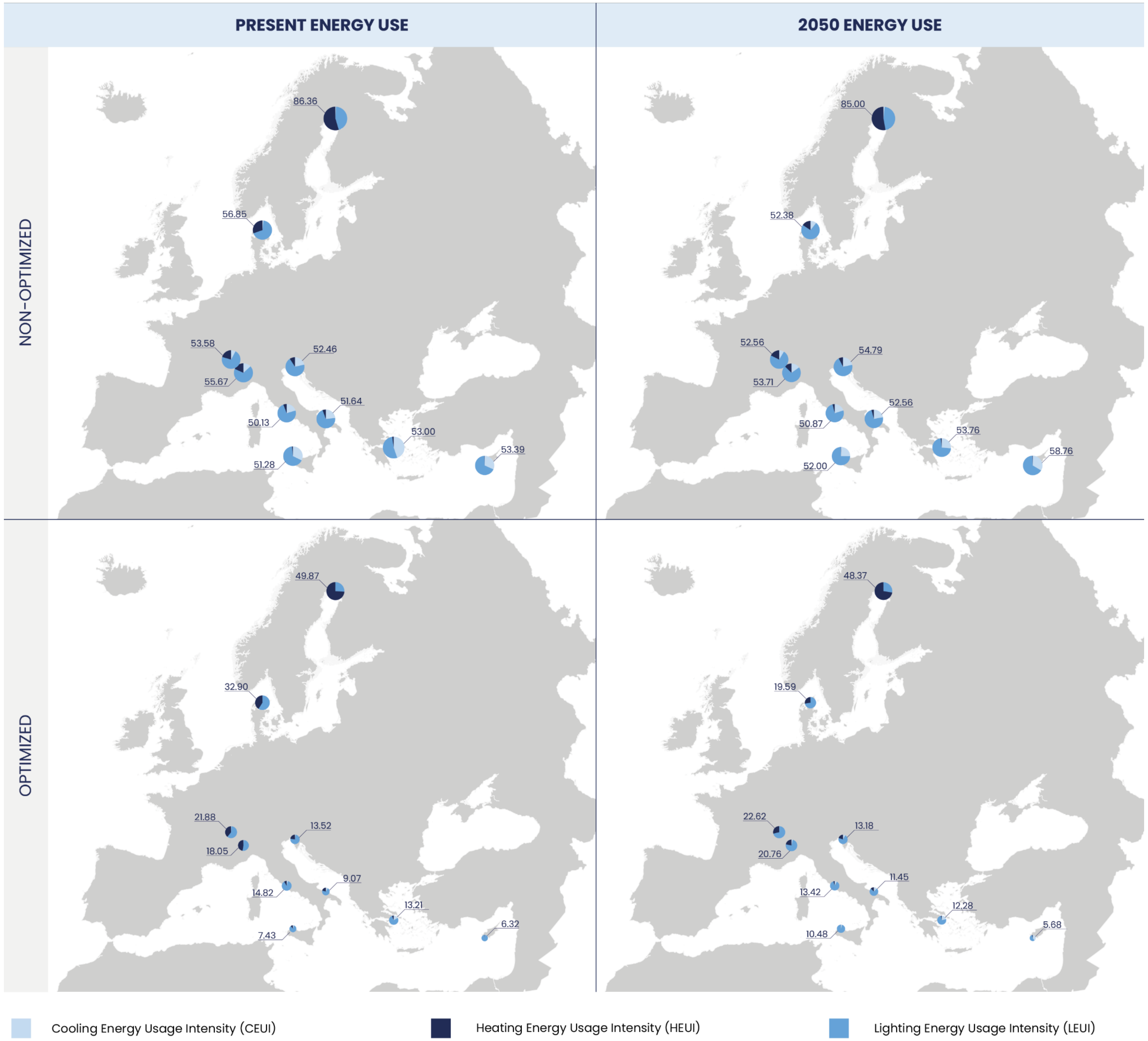

Figure 63 - Maps showing non-optimized and optimized zone energy use under present and 2050 climatic conditions. Numbers displayed on the pie charts represent total annual energy demand in kWh/m² for the corresponding location.

only a small decrease is noticeable. Cooling energy need is minimized in all locations and nullified in colder ones (Kemi, Aalborg). The same happens to heating energy need, which is reduced and nearly eliminated for locations in hotter climates. Energy required for artificial lighting is also decreased. Paphos present case is remarkable: cooling and heating energy needs are strongly minimized (around 0.10 kWh/m^2); lighting need is still present, but it is much smaller (from 38.64 kWh/m^2 to 6.13 kWh/m^2 – see ANNEX 2). However, as expected, in Kemi's case but also in Aalborg's present solution the tool failed to find a design option that allowed a substantial reduction of heating load.

Figure 64 shows TEUI and LEUI savings achieved in each location by applying custom optimized HVAC and lighting schedules. Energy saved for artificial lighting in optimized solutions seems homogeneous throughout the ten locations, ranging from 50% to 92%. Instead, TEUI savings are variable. The maps displayed here on the left validate what was previously mentioned: the optimization tool is more successful in reducing thermal energy use in mild-to-hot climates rather than in colder ones. In fact, TEUI saving dots are bigger for locations that included in climate zone IV 1, while are smaller for the others, especially for northern cities. For instance, Kemi corresponds to really small TEUI dots with respect to the other locations, both in present and 2050 conditions. Also Aalborg present case shows little thermal energy savings. Instead, Paphos (present), as expected, corresponds to the highest savings in terms of TEUI (99%).

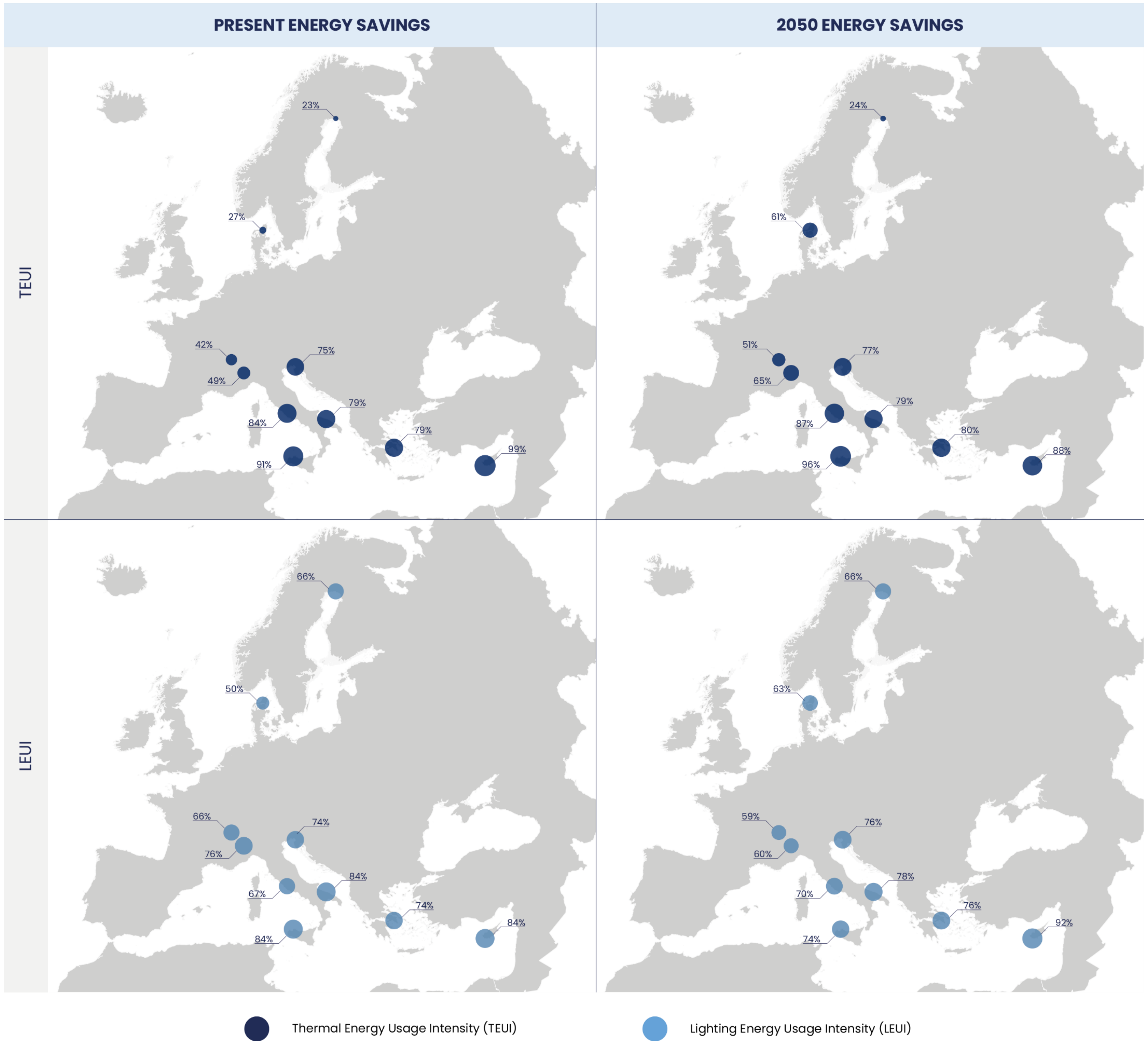

Figure 64 - Maps showing TEUI and LEUI savings under present and 2050 climatic conditions. Numbers displayed on the maps represent the percentage of energy saving obtained in solutions with optimized HVAC systems with respect to non-optimized solutions.

5. CASE STUDIES

5. CASE STUDIES

The optimization tool is applied to two real case studies placed in Italy. First case study is a school classroom located in Torre Pellice, while the second one concerns a residential apartment in Turin. Both buildings are subjects of innovative renovation interventions within the framework of EU funded projects EDYCE (school) and PRELUDE (apartment). Also in these cases, the optimization processes are run under present and future (2050) climatic conditions to compare the optimal design solutions.

Figure 65 - Localization of Torre Pellice and Turin within the Italian context.

5.1 CASE 1_school classroom in Torre Pellice

The school building considered for the analysis is the "Istituto Comprenstivo Gianni Rodari" located in the center of Torre Pellice, as shown in Figure 66. Torre Pellice is a small city in Piedmont, an Italian region located in the northern part of the country. As can be seen from Figure 65, Torre Pellice is about 45 km southwest from Turin (one of the ten locations already considered for the first part of the research).

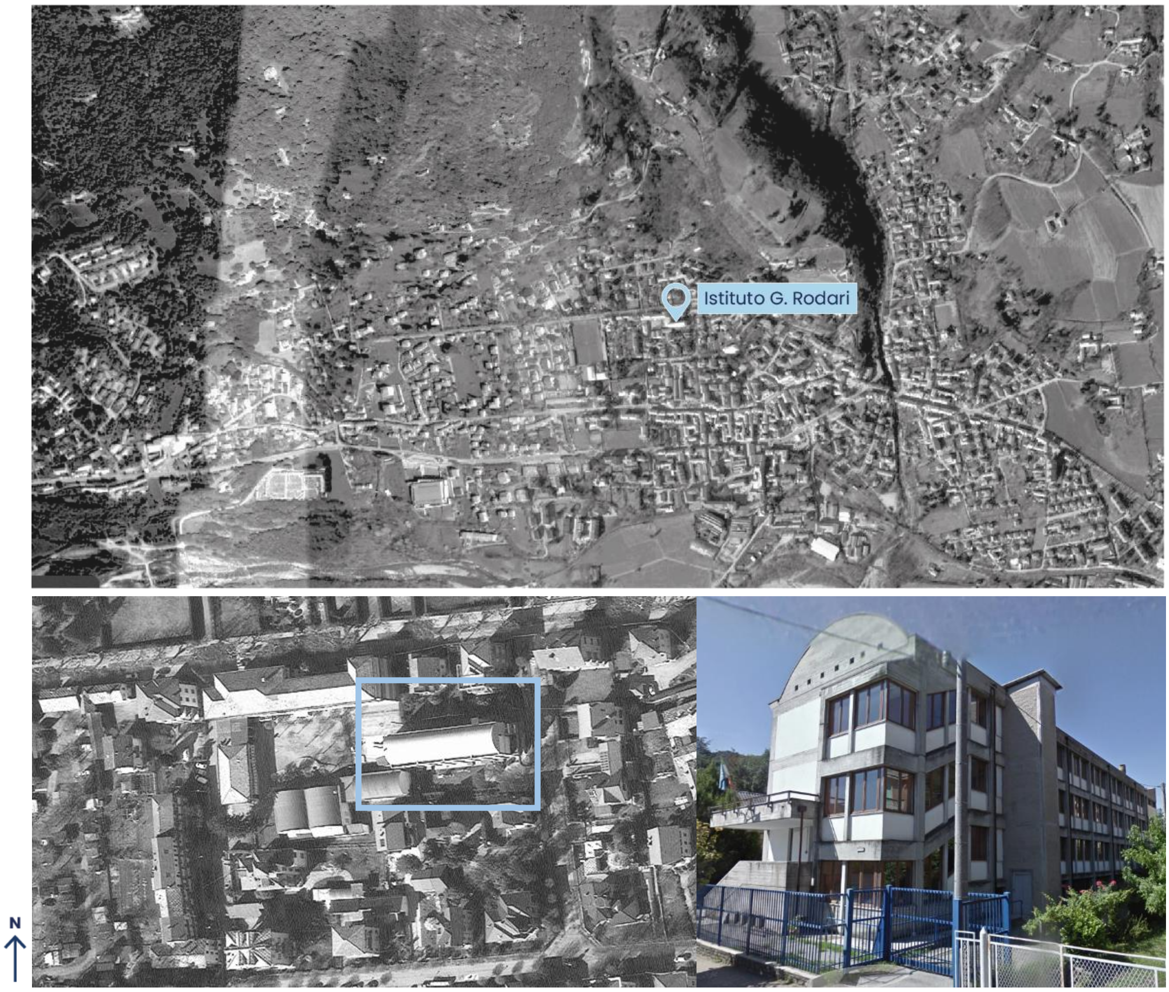

Figure 66 - Orthophoto from Google Earth pro of Torre Pellice. Localization of the school building. On the right, photo of the building from Google Maps Street View. Link to Maps: https://goo.gl/maps/DqYFNhywYhnLziTNA.

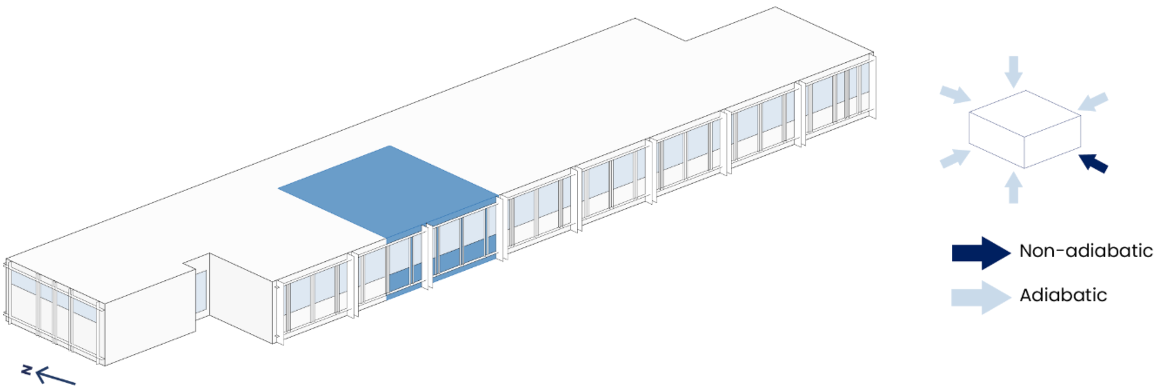

Figure 67 - Position of the reference classroom on the ground floor.

The reference classroom is located on the south side of the ground floor of the building, as displayed in Figure 67. Only the south wall is non-adiabatic, which means that is exposed to the outdoors, while the other walls, the ceiling and the floor are considered adiabatic as they face the indoors. The façade has six glazed openings, three with dimensions 1.42 m x 1.72 m and three with dimensions 0.61 m x 1.72 m, and a fixed shading system made of vertical elements.

5.1.1 Climate analysis

Torre Pellice is included in Troll and Paffen's climatic zone III 3 (submaritime climate): its winters are moderately cold and its summers are warm. Comparing todays and 2050 monthly average temperatures – see Figure 68 – it can be observed that hotter summers are expected in the future, with a temperature rise of over 3°C in July. During the rest of the year, temperatures are similar or slightly higher than present ones. As far as global horizontal radiation is concerned (Figure 69), 2050 radiation is more intense during summer period with respect to present conditions.

Prevailing wind directions are north and NE, but useful air flows come also from the south and the south-east directions. NV in the classroom can harness these winds to improve thermal comfort. In 2050, wind speed and temperatures increase.

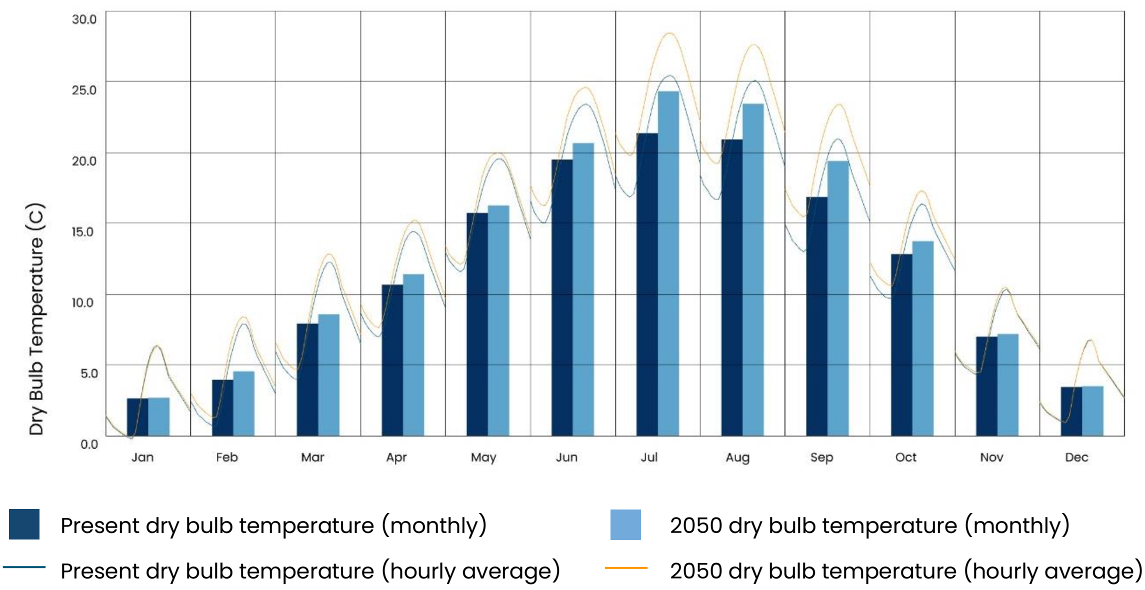

Figure 68 - LB bar chart showing Torre Pellice's monthly average dry bulb temperatures annual trend, comparing present and 2050 values.

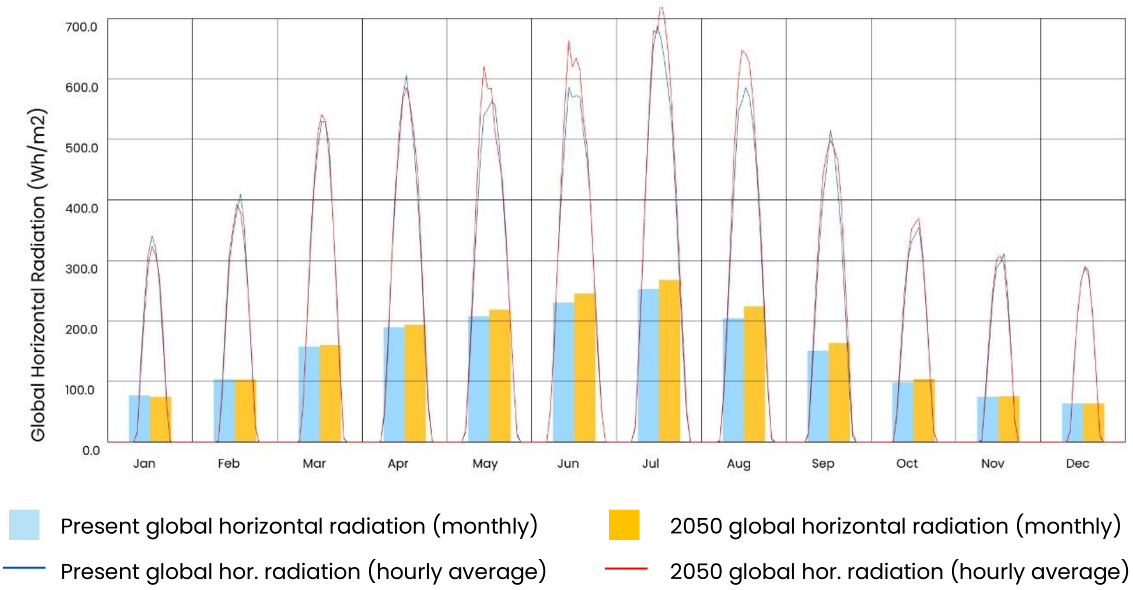

Figure 69 - LB bar chart showing Torre Pellice’s monthly average horizontal global radiation annual trend, comparing present and 2050 values.

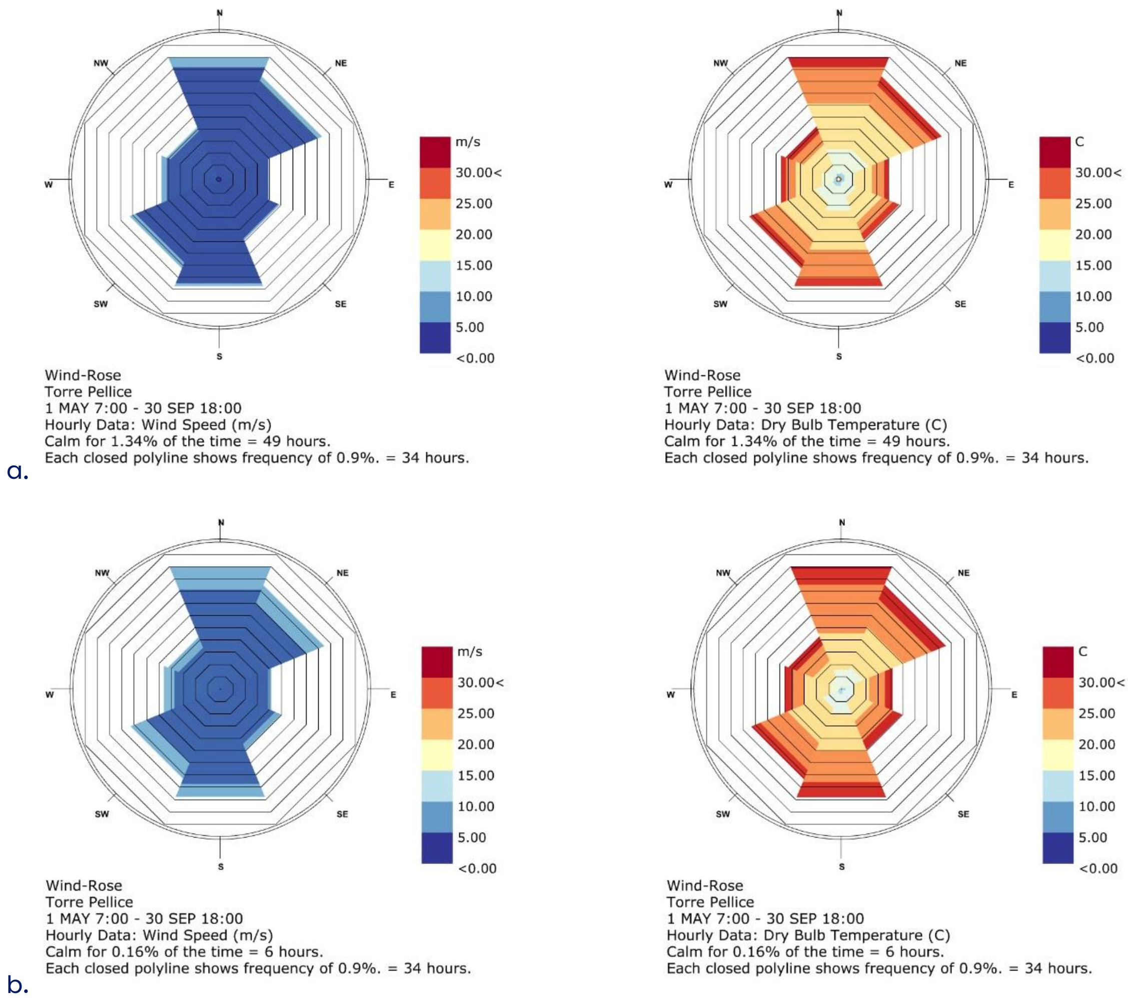

Figure 70 – Torre Pellice’s prevailing wind direction and speed (on the left) and temperature (on the right). 70a - present conditions; 70b - 2050.

5.1.2 Classroom definition

For the case study under discussion, the same workflow tested in the previous chapters is applied, with some differences due to the concreteness of the case. As far as the classroom model definition is concerned, a calibrated IDF file from EP of the ground floor of the school building was available. So, instead of creating the reference geometry from scratch, GH provides the possibility to import the building model by using the Honeybee component *importIdf*. However, several issues resulted from this method. First, HB was not able to read the glazed surfaces from the IDF file. Hence, the imported geometry of the whole floor was baked into Rhino environment to allow the selection of the six surfaces that define the reference classroom's space. These surfaces were then re-imported into GH as Honeybee surfaces through the *createHBSrfs* component, defining for each of them the name, the surface type (e.g. wall, ceiling, floor, etc.), the boundary condition (adiabatic or outdoors) and the EP construction. The HB zone was then created plugging the so-defined HB surfaces into the *createHBZones* component. A classroom (secondary school) program is then chosen from the HB List Zone Programs and assigned to the zone, which, at this stage of the workflow, is considered non-conditioned. The second problem resulted when defining the envelope constructions and the schedules. In addition to the geometry, the *importIdf* component gives the possibility to import EP materials, constructions and schedules from the IDF, which are automatically saved into the Honeybee library. Though, HB did not read all the constructions correctly, especially the window one[26]. So, for the avoidance of any doubt, EP materials were recreated into GH environment and then combined to generate the façade EP construction. Constructions of the other opaque surfaces (internal walls, ceiling and floor) were not considered, as they are adiabatic and do not affect the simulation. Table 8 indicates the stratigraphy and the U-value of the south façade. To overcome the impot issues, windows were generated using *addHBGlz* (add glazing) starting from child surfaces created from scratch in

[26] Materials that should have been transparent were not read as such. So, when running daylight simulation through Radiance, daylight metrics values were all 0 or even -1, which did not make sense. Furthermore, fiberglass layer in the façade construction had a very high U-value, impossible for an insulating material.

Rhino and then imported in GH as Breps. Dimensions of these apertures were measured from the building model available in Design Builder. For the actual zone simulation, the IDF window construction is recreated, as shown by Table 9. U-value of the windows in their current configuration is 2.369 W/m²·K.

FAÇADE EP CONSTRUCTION	LAYERS	THICKNESS (m)	CONDUCTIVITY (W/m·K)	DENSITY (kg/m³)	SPECIFIC HEAT (J/kg·K)
	Plaster	0.02	0.72	1860	840
	Perforated brick	0.08	0.38	740	1000
	Fiberglass	0.07	0.04	30	670
	Perforated brick	0.12	0.38	740	1000
	Plaster	0.02	0.72	1860	840
				U-VALUE (W/m²·K)	**0.429**

Table 8 – Current façade EP construction details.

WINDOW EP CONSTRUCTION	LAYERS	THICKNESS (m)	CONDUCTIVITY (W/m·K)	g-value (-)	τ_v (-)
	Glass pane	0.003	0.90	0.74	0.82
	Air gap	0.013	0.07	-	-
	Glass pane	0.003	0.90	0.84	0.90
				U-VALUE (W/m²·K)	**2.369**

Table 9 - Current EP construction for the windows.

Another issue related to the IDF import regarded schedules. Schedules imported from the file were written as EP compact schedules and HB was not able to read and translate them. Therefore, custom annual fractional schedules for occupancy, lighting and equipment were generated based on the school classroom schedules suggested by EN 16798-1:2019 standard [119, p. 65] and assigned to the zone. Occupancy period is defined between 9 a.m. to 5 p.m., from Monday to Friday, while fractional values were defined as shown in Table 10. In addition, equipment load per area (0.185 W/m²) and number of people per area (ppl/m²) are derived from the same European standard and applied to the zone through the HB *setEPZoneLoads*.

WEEKDAYS SCHEDULE	HOUR	VALUE
	9	0.6
	10	0.7
	11	0.6
	12	0.4
	13	0.3
	14	0.7
	15	0.6
	16	0.4
	17	0.2

Table 10 - Fractional values suggested by EN 16798-1 standard used for the definition of occupancy, lighting and equipment schedules on weekdays.

Natural ventilation is defined as discussed in §3.3.1. However, in this case cross ventilation is not possible as apertures are only placed on the south wall. Moreover, temperature constraints for NV were changed for this specific case: ventilation is now allowed only when outdoor temperature is above 10°C and indoor temperature is at least 23°C. Glazed area operable for NV is considered equal to 1 (100%) for double-leaf casement windows.

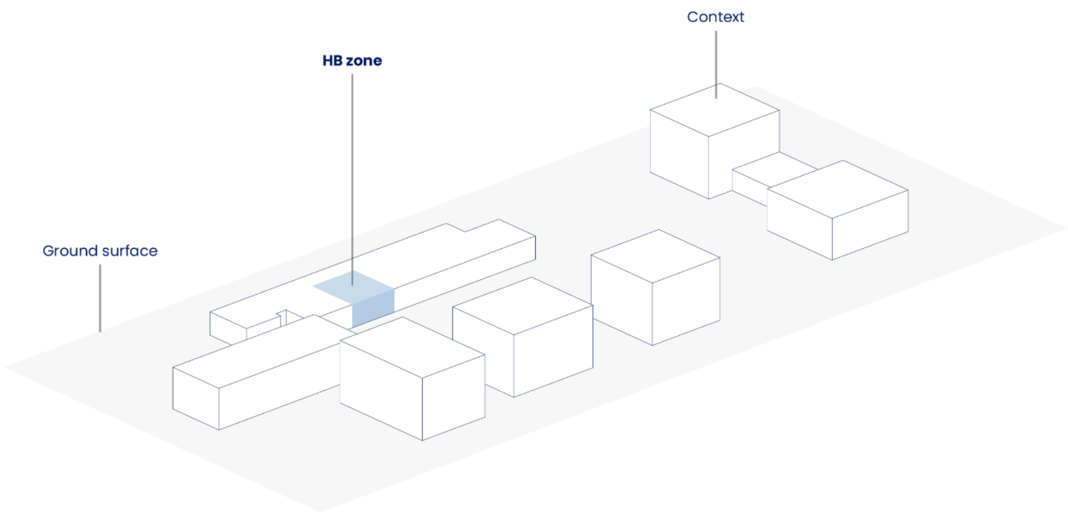

Figure 71 - Axonometric view from Rhino of the classroom context.

Defining boundary conditions for the school classroom, Torre Pellice EPW present and future files are used to consider its climatic conditions. Physical context has been modeled in Rhino environment based on Google Maps, as shown in Figure 71.

CLASSROOM DEFINITION FOR OPTIMIZATION

As building orientation, WWR and envelope constructions are fixed (except the window one), the conceived retrofit concerns the addition of an external thermal insulation layer, ranging from 0 m to 0.20 m, the installation of an additional shading system and the replacement of windows with more appropriate ones. Hence, the optimization process focuses on the transmittance of the façade elements (both opaque and transparent), on window characteristics (visual, such as g-value and τ_v, and dimensional, operating on the percentage of glazed area operable for NV) and on additional shadings configuration.

NEW FAÇADE EP CONSTRUCTION	LAYERS	THICKNESS (m)	CONDUCTIVITY (W/m·K)	DENSITY (kg/m³)	SPECIFIC HEAT (J/kg·K)
	Plaster	0.02	0.72	1860	840
	Additional XPS	Variable 0-0.20	0.035	100	1450
	Perforated brick	0.08	0.38	740	1000
	Fiberglass	0.07	0.04	30	670
	Perforated brick	0.12	0.38	740	1000
	Plaster	0.02	0.72	1860	840

Table 11 - New façade EP construction with the additional insulation layer.

As regards windows, in the GH workflow the glazing construction is not specified in all its layers, yet a generic window construction is defined through the HB *EPWindowMat* component, with variable U-value (between 0.50 and 3 W/m²·K), g-value (between 0 and 1) and visible transmittance (τ_v between 0 and 1). This facilitates the control over the glazed surfaces thermal and visual features for the optimal zone configuration. Glazed area operable for NV ranges between 0.50 (50%) and 1 (100%). As far as shadings are concerned, in addition to the existing fixed ones placed on the façade, a shading system made of horizontal external blinds is designed. It is similar to the one discussed in §3.3.2, but this time visual transmittance, depth, rotation angle and number of shades are parameters to be optimized. Transmittance can vary from 0 to 1, shades number from 0 to 10, their depth from 0 to 0.30 m and rotation angle from -90° to +90°.

5.1.3 Free-running simulations and optimizations

Once established the thermal zone and its context, EP and Radiance simulations are run. Simulation parameters are the same discussed in §3.5. Afterwards, thermal and daylight comfort metrics are calculated alongside ASE. Octopus optimization process is then launched: *genes* and *fitness* considered are listed in Figure 72 here below.

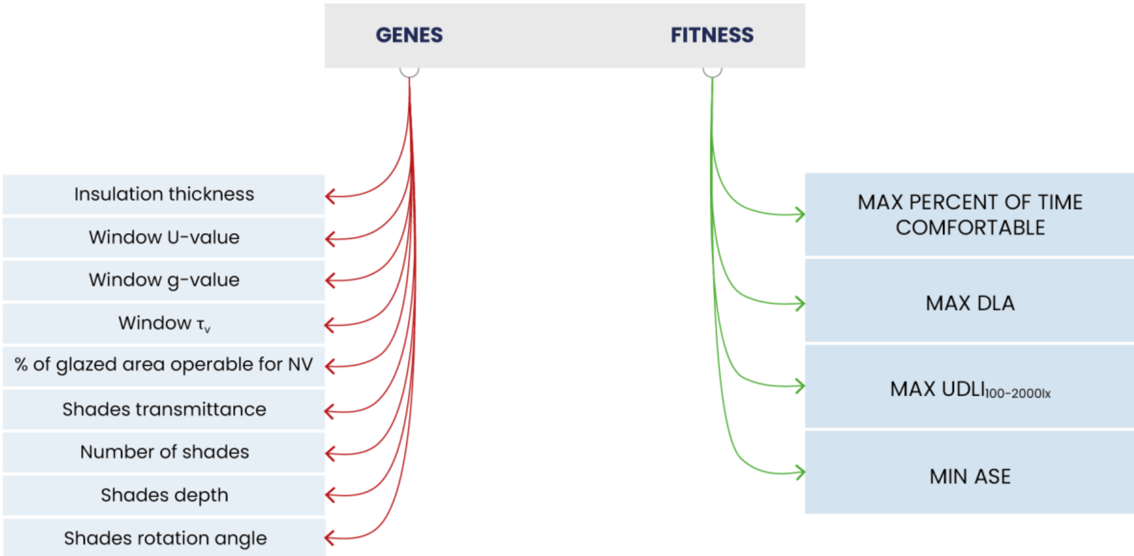

Figure 72 - Parameters and objectives for the classroom optimization.

For both present and 2050 optimizations, several optimal solutions have been identified, as displayed in Figure 73. Among these, a single option for each case is selected. The chosen solutions are the ones that, from a personal point of view, better balance the four objectives, improve sDA, provide higher energy savings and have reasonable genes values, especially for windows features. In fact, in particular in present options, g-values are too low (0.1, which means that nearly no heat from solar radiation is transferred through glazing), while τ_v is equal to 1 (which means that 100% of the incident light is transmitted into the environment) in most cases, also in 2050 options. Such values are very difficult to obtain with common windows, hence the solutions with the most realistic glazing features are selected.

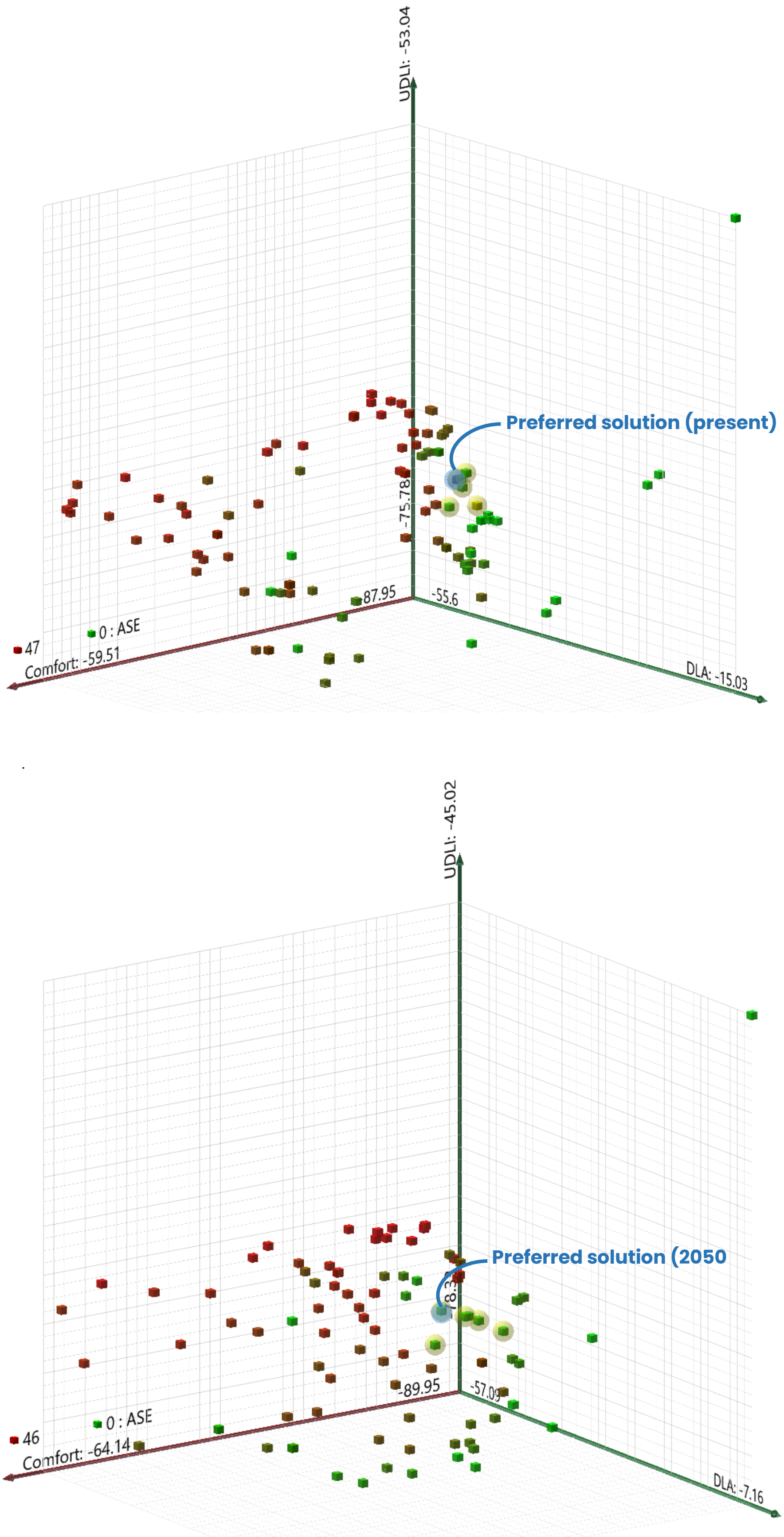

Figure 73 - Octopus cubeview of the classroom's optimizations under present (above) and 2050 (below) conditions. Optimal solutions are circled in yellow, while preferred solutions are highlighted in blue.

In both cases, as can be seen from Figure 74, optimal solutions do not require particularly high-performance windows in terms of thermal transmittance: U-values of the selected solutions are comparable to the actual one. G-values are equal to 0,5 and τ_v ranges between 0.9 and 1. In this respect, it is probable that real windows will have lower visible transmittance values (around 0.80), which could reduce a little the calculated daylight comfort metrics. Optimal glazed area for NV in present solution is half of the current one, while in 2050 increases a little (81%).

With respect to optimal shades, it can be seen that they let nearly half the light pass through. This could be obtained, for example, with metal devices that are 50% perforated. Rotation angle is almost the same and corresponds to a position of the shades that blocks the solar radiation income. In 2050, one horizontal blind is removed, but depth increases. Finally, the external insulation layer decreases the wall's U-value; in 2050 the layer is even thicker, reducing the façade transmittance by two-thirds.

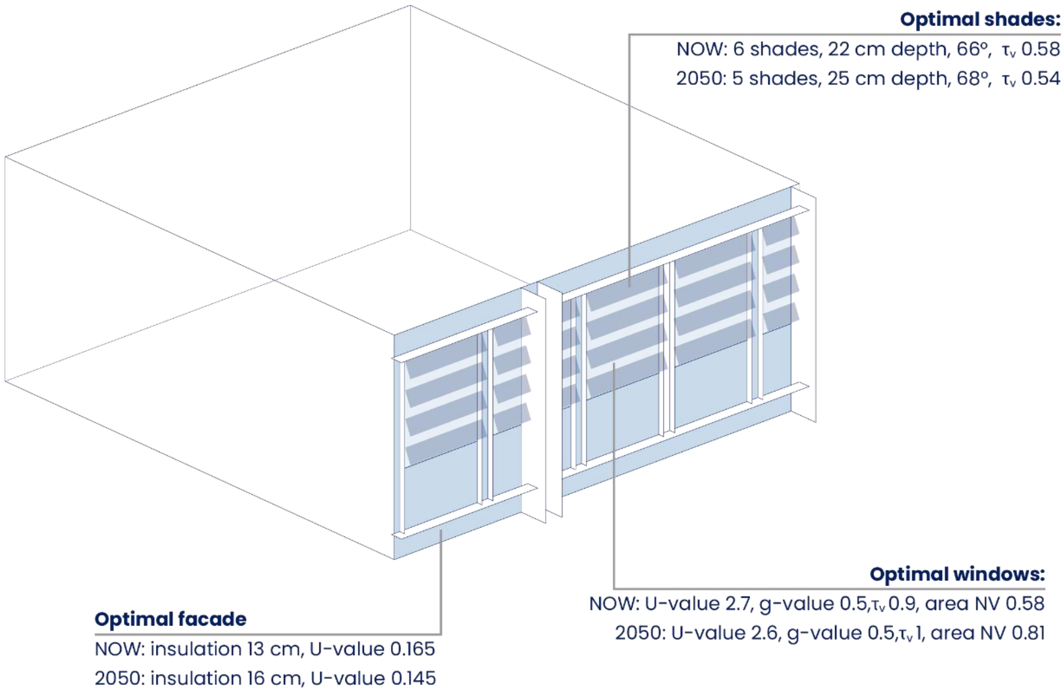

Figure 74 - Present and 2050 classroom's optimal genes values.

5.1.4 Results comparison

COMFORT METRICS

This part of the paragraph compares and discusses thermal and visual comfort metrics, calculated in free-running mode, of the actual classroom design and of the optimal design solution. The same approach is repeated under present and 2050 conditions. Results are provided in ANNEX 3. Figure 75 shows the adaptive comfort charts obtained through LB component of the four cases for the specified occupancy period. In the actual charts (present and 2050) it can be observed that indoor operative temperatures reach very high values, up to 40°C, and this happens especially when prevailing outdoor temperature is under 10°C. In contrast, when outdoor temperature is above 10°C, indoor operative temperatures fall mostly within the comfort range. This is due to the fact that the zone has very high internal gains, deriving from occupants and equipment, and the NV constraints set do not let the windows open even if indoor temperature rises over 23°C. This prevents from dissipating the heat towards the outdoors and discomfort conditions are experienced. The same issue happens in present and 2050 optimal classroom design solutions, although less pronounced. The two adaptive charts displayed at the bottom of the page demonstrate the effectiveness of the tool in improving free-running comfort: indoor temperatures remain below 32°C when outdoor prevailing temperature is under 10°C. It should be pointed out that the optimizations have been run considering these NV constraints (min. outdoor temp. 10°C and min. indoor temperature 23°C), as previously mentioned in §5.1.2. However, to avoid such high indoor

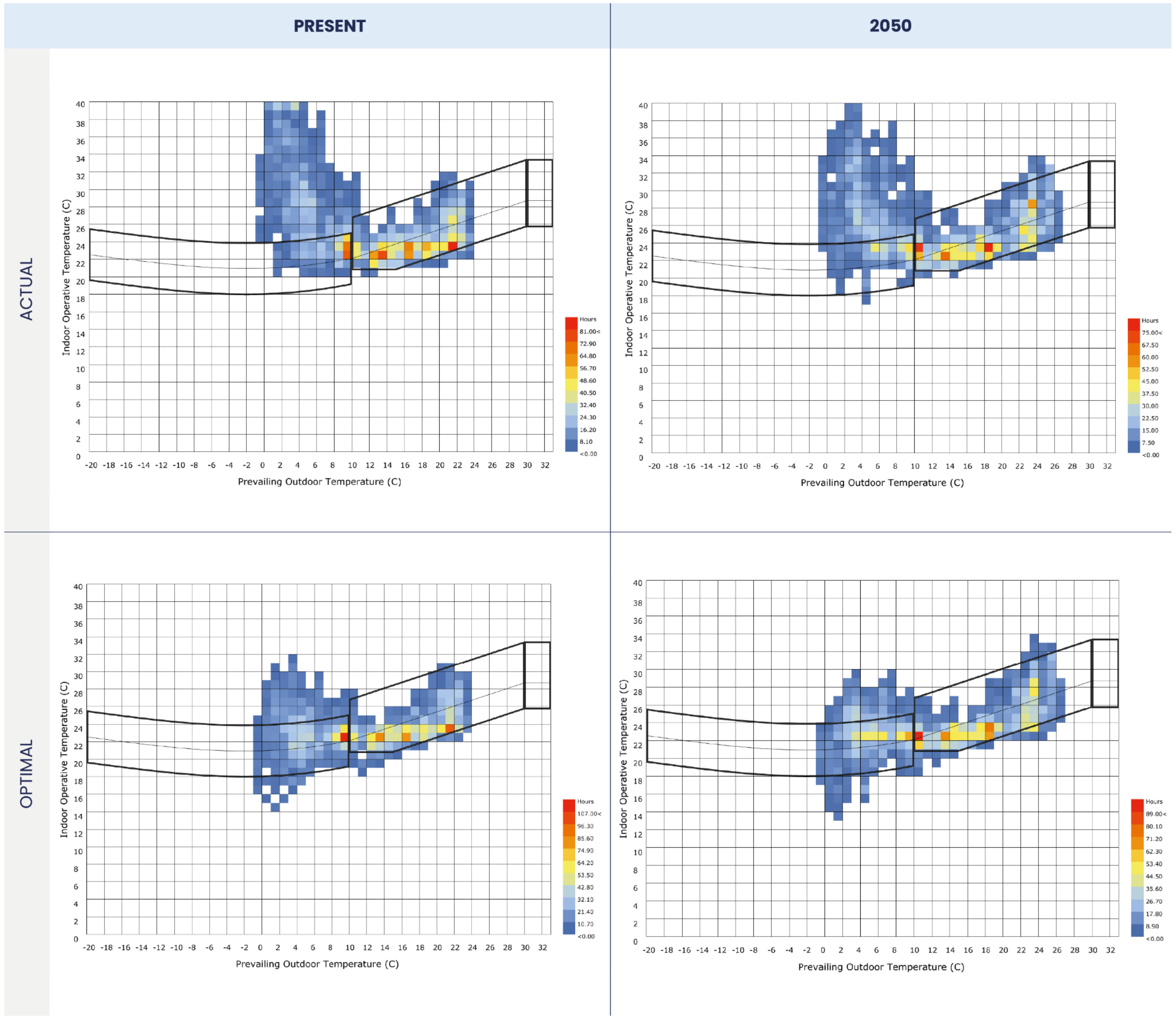

Figure 75 – Classroom's adaptive charts comparison.

temperatures, the simplest solution (and also the most realistic) is allowing the windows opening even when outdoor temperatures are below 10°C: e.g. setting the *minOutdoorTempForNatVent* of the *setEPNatVent* component to 2°C. This would consistently improve comfort during those critical periods.

The effectiveness of the tool is also deducible from Figure 76, which compares the condition of occupants during the active occupancy period in the four cases. As expected, percent of time comfortable is higher in optimal solutions than in actual ones, and the percent of time occupants feel hot is reduced up to one-third. In 2050 classrooms, both actual and optimal, percent of time cold is higher than in present cases. The reason for this could be found in the outdoor temperature rise expected in future climatic conditions. These higher temperatures allow the windows to be opened more frequently when needed, always taken into account the discussed NV constraints.

As regards visual comfort metrics, Figure 77 compares ASE values, while Figure 78 makes a comparison between averaged DLA and $UDLI_{100-2000lx}$ of the four studied cases. ASE values are clearly too high in the current classroom design, especially near the glazed apertures, which increases the probability of visual discomfort caused by glare. Adding a

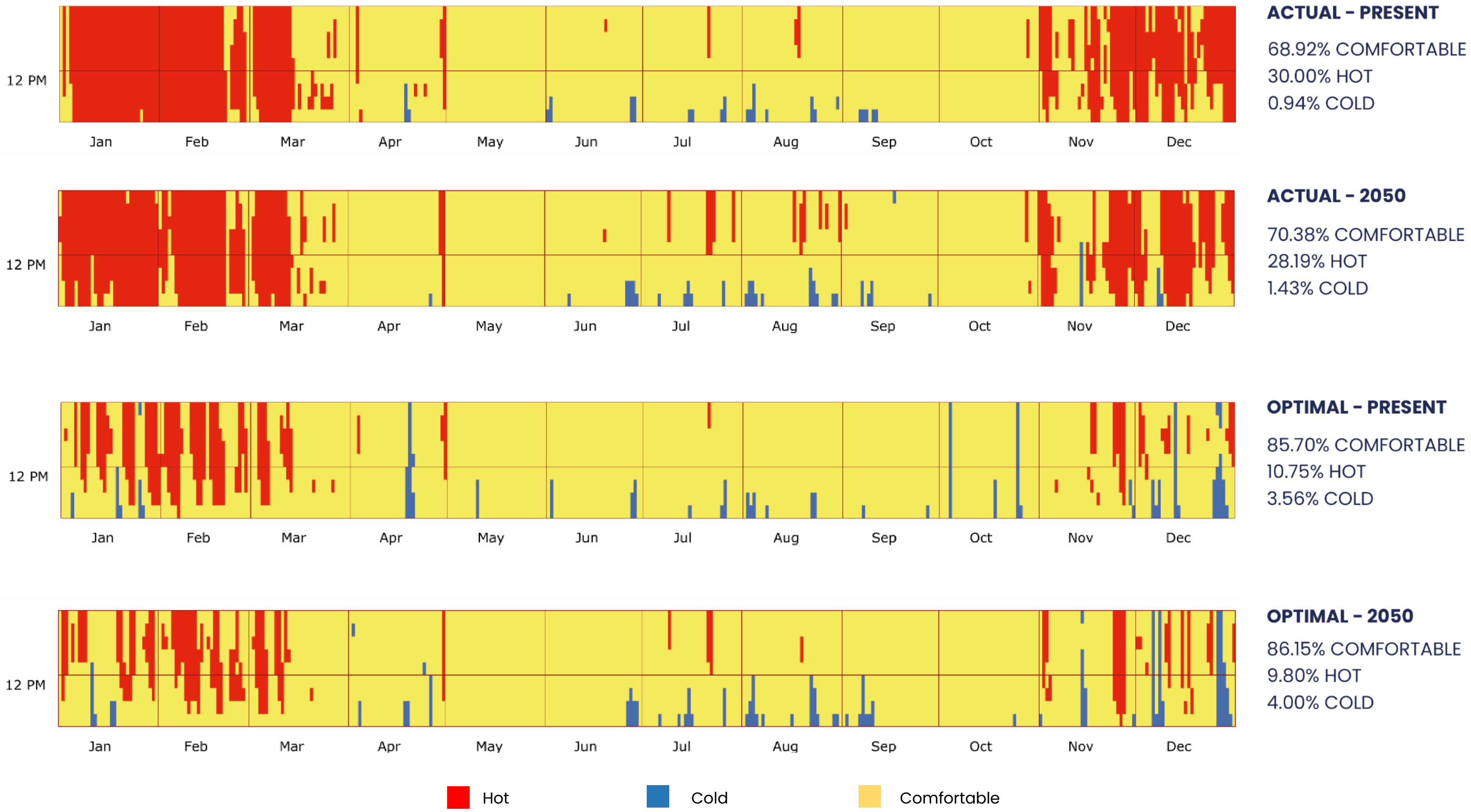

Figure 76 - LB 3D charts displaying the percent of time comfortable, hot and cold of the actual and the optimal classroom designs under present and 2050 climatic conditions.

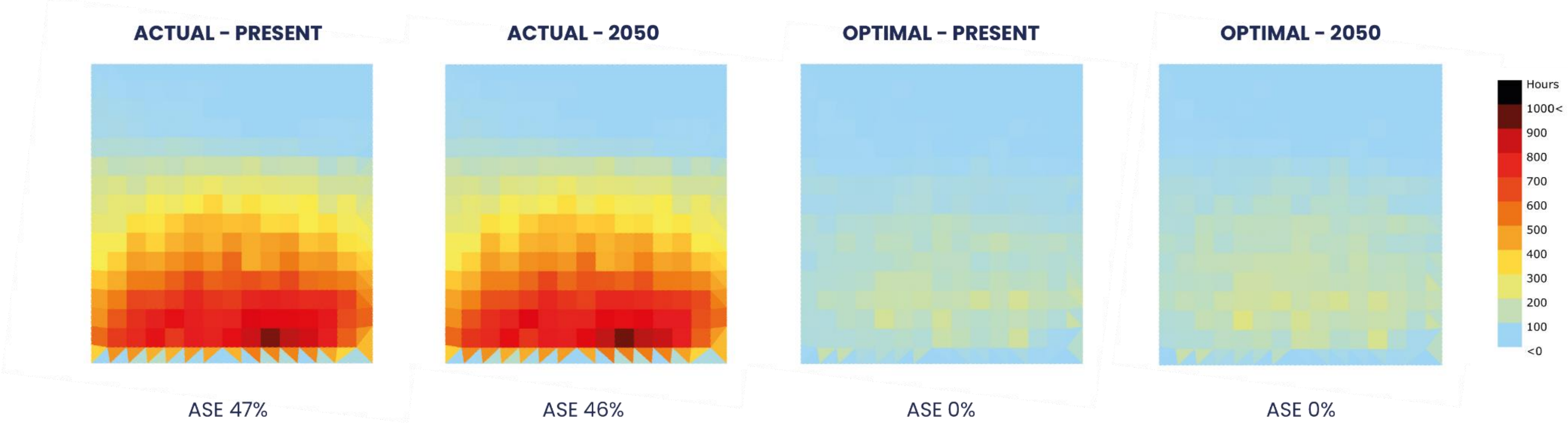

Figure 77 – Classroom's ASE comparison on plan visualization.

supplementary external shading system allows to nullify ASE and, consequently, eliminate the probability of glare problems. At the same time, the design shades let the solar radiation pass. With respect to the actual cases, in optimal solutions DLA and $UDLI_{100-2000lx}$ appear more uniformed on the analysis plane[27]. DLA is higher near the windows, while it gradually decreases towards the back of the room. Instead, the highest UDLI values are found in the center of the zone. The light blue region close to the façade represents an area in which higher values od useful daylight illuminance are reported ($UDLI_{>2000lx}$). The area close to the bottom of the classroom experiences lower $UDLI_{100-2000l}$ values, as it is more distant from the windows, which means that $UDLI_{<100lx}$ values are higher. In general, optimal solutions provide greater daylight performance.

ENERGY USE AND SAVINGS

EP energy simulations are repeated in mixed-mode, considering both NV and mechanical systems. The zone is now set conditioned and temperature set points are specified, as shown in Table 12. Demand controlled mechanical ventilation is allowed for IAQ reasons.

TEMPERATURE SETPOINTS		HEATING	COOLING
	SETPOINT	20°C	26°C
	SETBACK[28]	16°C	32°C

Table 12 - Heating and cooling setpoint and setback temperatures for Torre Pellice classroom.

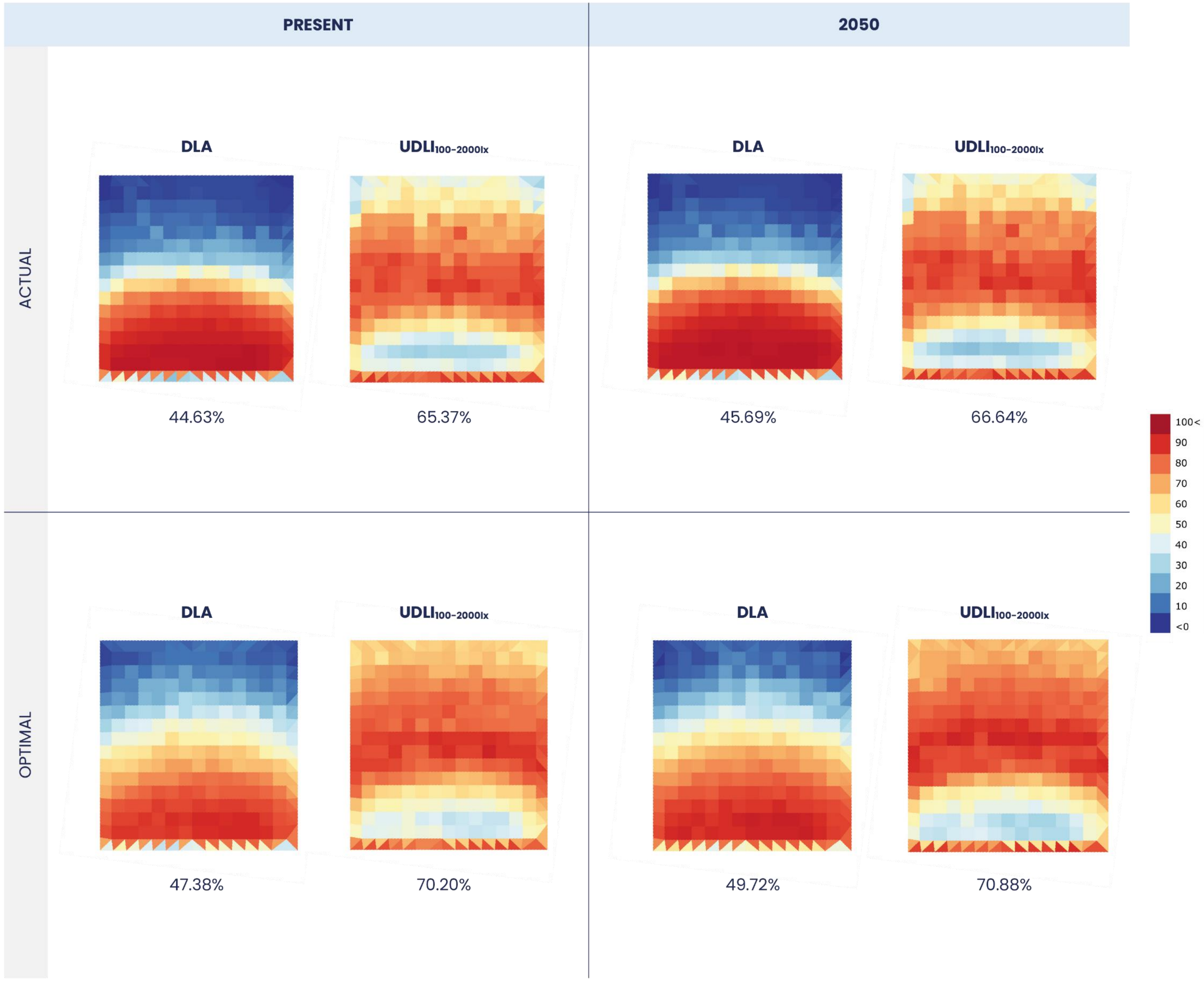

Figure 78 – Classroom's DLA and UDLI comparison.

[27] As in the previous simulations, the analysis plane is set at a height of 0.80 m from the zone floor.
[28] The temperature setback of a heating or cooling system is the temperature at which the space should be kept during unoccupied hours.

In addition, to avoid that cooling system is turned on while windows are open, maximum outdoor temperature for NV is set to 25°C. It must be pointed out that adding a mechanical ventilation component causes a decrease in the indoor temperatures calculated by EP in the conditioned simulation with respect to temperatures obtained in free-running mode, as colder outdoor air is introduced into the environment and mixed with indoor air. When using the ventilation rate suggested by the European regulation EN 16798-1 for school classrooms (equal to 0.0038 m³/s·m²), which is a very high rate [29], indoor temperatures of the conditioned space experience a consistent decrease with respect to unconditioned ones. This causes an evident discrepancy between the condition of occupants calculated by LB adaptive comfort component and the energy needs for heating and cooling of the zone with HVAC. Therefore, the outdoor air flow rate for mechanical ventilation is minimized and set at 0.0002 m³/s·m², with the aim of not changing too much indoor temperatures when running the simulation in mixed-mode. In doing so, occupants should feel comfortable with mechanical ventilation on during almost the same periods identified by the adaptive comfort model and, in general, should feel less hot. This little temperature difference, along with different set points (HVAC system setpoints are different from the

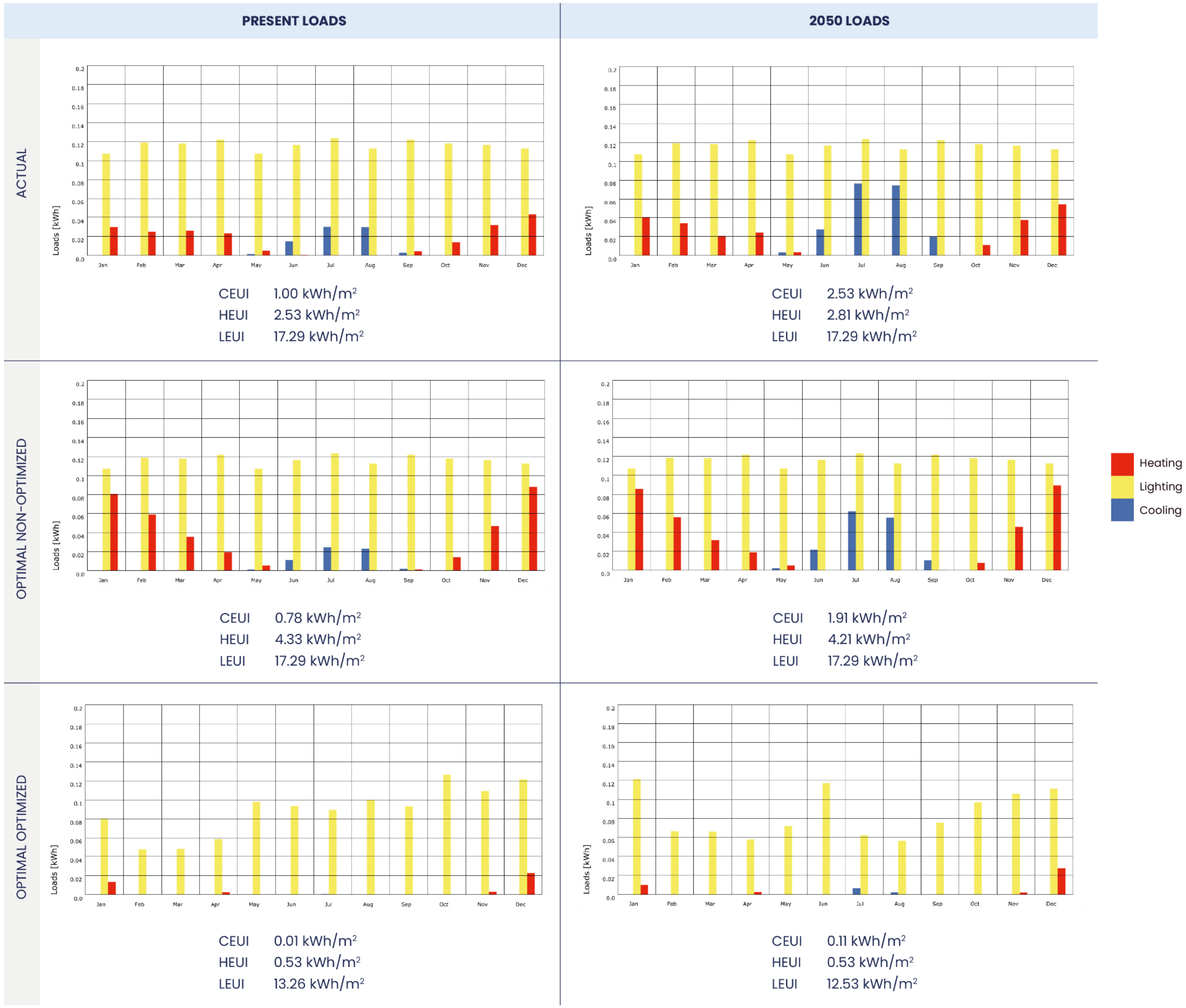

Figure 79 - LB bar charts comparing heating, cooling and lighting loads of actual and optimal classroom designs.

[29] HB component *setEPZoneLoads* suggests that outdoor air ventilation rate for laboratories and cleanrooms, where air must be kept clean without dust contamination, should be set at 0.0025 m³/s·m². Hence, a ventilation rate of 0.0038 m³/s·m² appears too high for a simple school classroom.

adaptive model comfort temperatures), imply that cooling and heating systems do not turn on during all the discomfort period when applying custom schedules, yet only when, during those periods of time, indoor air temperature is below or above the heating and cooling setpoints/setbacks respectively. This explains the difference between optimized heating and cooling loads displayed in Figure 79 and the hot/cold periods reported in Figure 76.

Ladybug bar charts has been chosen as the simplest and most immediate visualization method to compare energy uses deriving from actual and optimal classrooms designs under present and 2050 climates – see Figure 79. Table containing full energy use details can be found in ANNEX 3. As regards loads, optimal solutions in both climatic conditions successfully reduce cooling needs, even when non-optimized system schedules are applied. Optimized custom schedules, created from free-running discomfort periods, further minimize these loads (e.g. present optimized solution's CEUI is nearly zero). As expected, 2050 cooling loads are higher than present ones because of warmer outdoor temperatures. Heating loads appear higher in optimal (non-optimized) solutions with respect to actual ones. This is probably due to the fact that the tool tries to reduce the percent of time the occupants feel hot (which represents most part of discomfort period) and, in doing so, consequently increases the percent of time people feel cold in the indoor environment, thus incrementing the heating needs. Also in this case, the application of custom optimized schedules effectively decreases HEUI. As far as artificial lighting is concerned, LEUI values are only moderately decreased in optimized solutions. Since windows can only be optimized in their thermal and visual properties and not in their dimensions (WWR is fixed), it is difficult to reach large energy savings for artificial lighting.

Figure 80 finally summarizes the energy savings in terms of thermal and lighting energy needs that result from the comparison of the optimized optimal solution energy use with the actual and the optimal non-optimized ones. The comparison is repeated for present and 2050 conditions. From the bar chart, it can be observed that the application of customized schedules allows to reduce TEUI up to 90% with respect to both actual and non-optimized energy uses. Instead, as previously mentioned, the tool is not as successful in cutting lighting energy use. LEUI savings are limited below 30%.

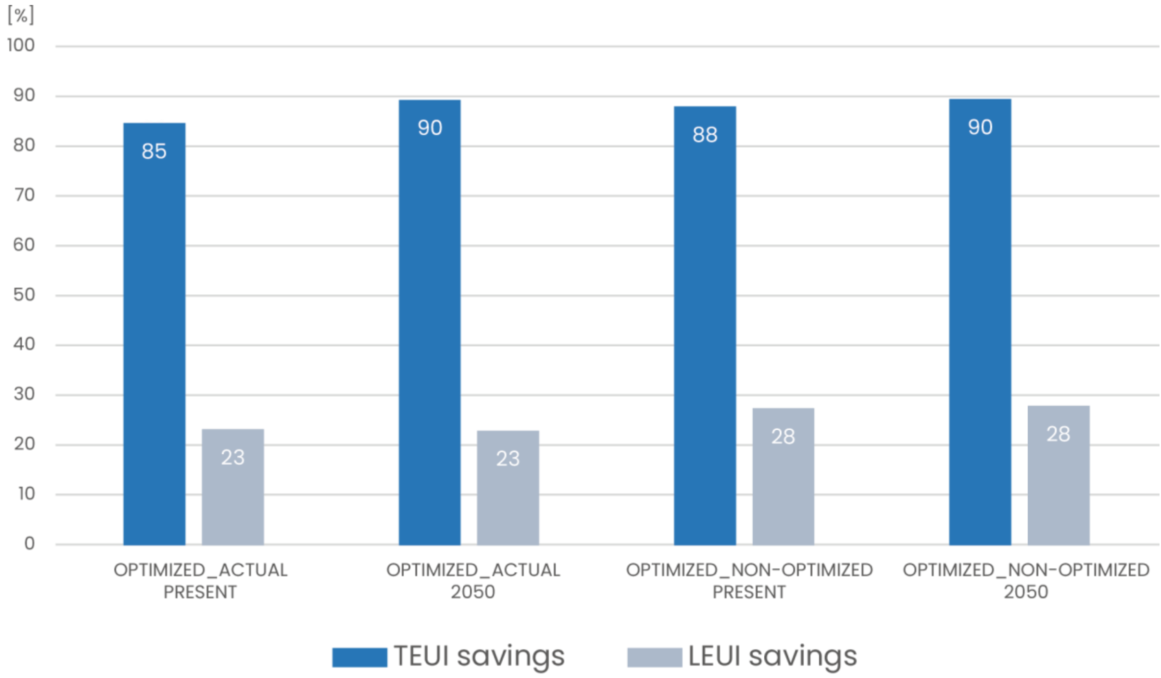

Figure 80 - Bar chart displaying the classroom energy savings obtained through the optimization. Optimized TEUI and LEUI are compared with actual and optimal but not optimized energy use.

5.2 CASE 2_residential apartment in Turin

The second case study to which the presented workflow is applied concerns an apartment placed in Corso Francia, in the western part of the city of Turin. As Turin is one of the ten European cities that have been considered in the first part of this paper, the analysis of its climate under present and 2050 conditions will not be repeated in this paragraph, as it can be found in §4.1.2.

The apartment is placed on the fourth floor of the building. It consists of three major spaces (a kitchen with a little entrance, a living room and a bedroom), in addition to a bathroom and a storeroom. Figure 81 displays the arrangement of these spaces on the plan and specifies their dimensions. The apartment floor area, inclusive of interior walls, is about 70 m^2 and ceiling height is 2.98 m. The flat has a balcony facing Corso Francia on the north side (accessible from the bedroom and the living room), while on the opposite side (kitchen and restroom), on the south, there is a closed veranda that faces the shared backyard. The veranda has been reported to be affected by overheating, due to the poorly insulated materials of which it is made (aluminum and single-glass pane windows).

5.2.1 Apartment definition

Starting from the plan made available by PRELUDE, the apartment is modeled in 3D into Rhino in environment considering its internal outline. The geometry is simplified and composed of basic surfaces or polysurfaces. Interior walls are placed on their centerline, as wall's thickness must not be considered in the geometry when working on energy modeling. Interior elements are not very meaningful for the analysis purpose, but they are considered anyway. Instead, interior doors are not taken into account, considering the doorway opened. Windows are modeled from the available dimensions, making sure that their surfaces are perfectly coplanar to the walls' ones. This is an essential requisite for the windows to be read by Honeybee and correctly imported into the GH model. The same method is followed for the veranda glazing. Balconies are modeled too, as they make up part of the context.

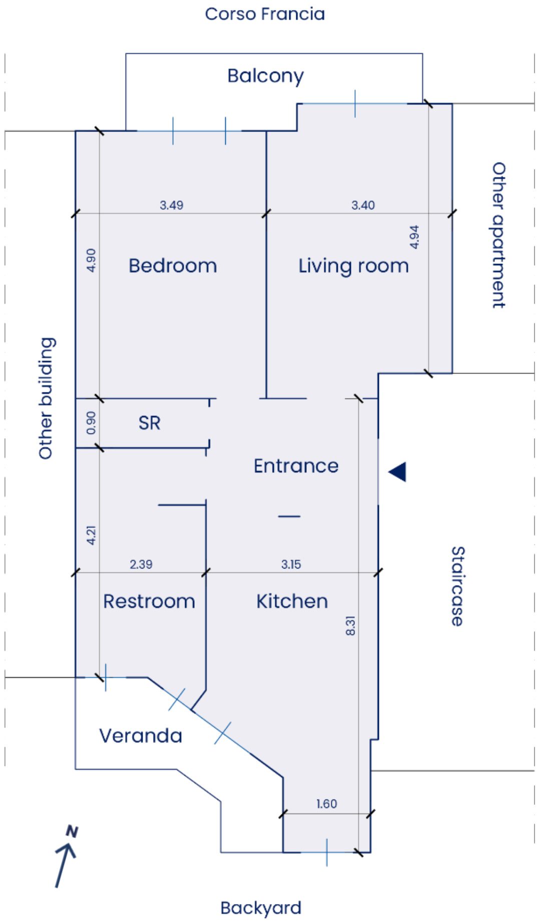

Figure 81 - Apartment plan with main dimensions (in meters).

Moving to GH environment, the apartment opaque surfaces are imported as Breps and HB surfaces are created using the *createHBSrfs* component, assigning for each type of building element a name, a boundary condition (outdoors or adiabatic) and an EP construction, as already done for the first case study. As can be seen from Figure

81, on the east side, the flat is adjacent to another apartment and the staircase, while on the west side, it confines with another building. Consequently, these walls are considered adiabatic (as well as the interior walls) while all the others and the veranda are exposed to the outdoors. As far as EP constructions are concerned, only the façades and the veranda are defined in their materials, given that constructions assigned to adiabatic surfaces do not significantly influence the simulation. Since the real stratigraphy of the façade is unknown, a construction similar to the one used for the classroom is assumed, replacing the internal insulation layer with an air space, as can be seen in Table 13. This construction is reckoned plausible having regard to the period in which the building was constructed.

FAÇADES EP CONSTRUCTION	LAYERS	THICKNESS (m)	CONDUCTIVITY (W/m·K)	DENSITY (kg/m^3)	SPECIFIC HEAT (J/kg·K)
	Plaster	0.02	0.72	1860	840
	Perforated brick	0.08	0.38	740	1000
	Air space	0.01	0.07	1.23	1005
	Perforated brick	0.12	0.38	740	1000
	Plaster	0.02	0.72	1860	840
				U-VALUE (W/m^2·K)	**1.367**

Table 13 – Current apartment facade EP construction.

VERANDA EP CONSTRUCTION	LAYERS	THICKNESS (m)	CONDUCTIVITY (W/m·K)	DENSITY (kg/m^3)	SPECIFIC HEAT (J/kg·K)
	Aluminum	0.015	204	2700	880
				U-VALUE (W/m^2·K)	**-**

Table 14 - Veranda material details.

VERANDA WALL EP CONSTRUCTION	LAYERS	THICKNESS (m)	CONDUCTIVITY (W/m·K)	DENSITY (kg/m^3)	SPECIFIC HEAT (J/kg·K)
	Plaster	0.02	0.72	1860	840
	Perforated brick	0.12	0.38	740	1000
	Plaster	0.02	0.72	1860	840
				U-VALUE (W/m^2·K)	**2.693**

Table 15 - Veranda wall construction layers.

The veranda is made of aluminum (Table 14). It leans on the south façade, on one side, and on another wall on the other side. This wall construction is considered different from the façade's, as it is only an exterior building element that defines the veranda space. A simple plastered brick wall is assumed for this element – see Table 15.

This case study was more challenging to model through Honeybee. As HB zones need to be closed Breps and both the veranda windows and the façade windows must open at the same time, it was necessary to create two separate thermal zones, one for the apartment and the other for the veranda. The final results of the simulation will however concern only the apartment zone. Both zones are set unconditioned for the first part of the simulation and a midrise apartment zone program is assigned to them. Differences in loads and schedules between the two zones will be specified later. Then, windows are created from Rhino child surfaces previously modeled and materials are assigned to them. The ones placed on the north and south façades of the building are currently double-paned, while the veranda windows are single-paned. Glazing constructions are reported in Table 16 and Table 17.

FAÇADE WINDOW EP CONSTRUCTION	LAYERS	THICKNESS (m)	CONDUCTIVITY (W/m·K)	g-value (-)	τ_v (-)
	Clear glass pane	0.004	0.90	0.86	0.89
	Air gap	0.013	0.07	-	-
	Clear glass pane	0.004	0.90	0.86	0.89
				U-VALUE (W/m²·K)	**1.537**

Table 16 – Current construction details of the windows placed on the facades.

VERANDA WINDOW EP CONSTRUCTION	LAYERS	THICKNESS (m)	g-value [-]	τ_v [-]	CONDUCTIVITY (W/m·K)
	Clear glass	0.004	0.86	0.89	0.034
				U-VALUE (W/m²·K)	**5.700**

Table 17 – Current construction details of the veranda windows.

APARTMENT SCHEDULES		WEEKDAYS			WEEKENDS		
	HOUR	OCCUPANCY	EQUIPMENT	LIGHTING	OCCUPANCY	EQUIPMENT	LIGHTING
	0	1	0.5	0	1	0.5	0
	1	1	0.5	0	1	0.5	0
	2	1	0.5	0	1	0.5	0
	3	1	0.5	0	1	0.5	0
	4	1	0.5	0	1	0.5	0
	5	1	0.5	0	1	0.5	0
	6	0.5	0.5	0.15	0.8	0.5	0.15
	7	0.5	0.7	0.15	0.8	0.7	0.15
	8	0.5	0.7	0.15	0.8	0.7	0.15
	9	0.1	0.5	0.15	0.8	0.5	0.15
	10	0.1	0.5	0.05	0.8	0.5	0.05
	11	0.1	0.6	0.05	0.8	0.6	0.05
	12	0.1	0.6	0.05	0.8	0.6	0.05
	13	0.2	0.6	0.05	0.8	0.6	0.05
	14	0.2	0.6	0.05	0.8	0.6	0.05
	15	0.2	0.5	0.05	0.8	0.5	0.05
	16	0.5	0.5	0.2	0.8	0.5	0.2
	17	0.5	0.7	0.2	0.8	0.7	0.2
	18	0.5	0.7	0.2	0.8	0.7	0.2
	19	0.8	0.8	0.2	0.8	0.8	0.2
	20	0.8	0.8	0.2	0.8	0.8	0.2
	21	0.8	0.8	0.2	0.8	0.8	0.2
	22	1	0.6	0.15	1	0.6	0.15
	23	1	0.6	0.15	1	0.6	0.15

Table 18 - Occupancy, equipment and lighting schedules for the apartment zone.

Schedules are created from scratch through the *AnnualSchedule* component. For the apartment zone, occupancy, equipment and lighting values for weekdays and weekends suggested by the EN 16798-1 standard for the residential category [119, p. 76] are used. Values are displayed in Table 18. Occupancy period is all day (24 hours).

As far as loads are concerned, equipment load per area is derived from the same European standard and it is equal to 3 W/m^2; number of people per area is calculated dividing the floor area per 2.5 people (two people and the dog), which is 0.0357 ppl/m^2. These loads are applied to the zone through the HB *setEPZoneLoads* component. As concerns the veranda zone, occupancy schedule and occupancy activity schedules are set 0 during all day every day, as it is a space that is not actively occupied. Number of people per area is 0, while equipment load is set to 2 W/m^2 as there is a washing machine on the veranda.

Before assigning passive strategies, as the two modeled HB zones are adjacent (they have four walls and three windows in common, it is necessary to solve adjacencies between them. If this step is skipped, EP will count the shared surfaces twice[30], thus affecting the accuracy of the simulation. For this reason, HB *Solve Adjacencies* component is used, plugging in the two separated zones and specifying to preserve the assigned EP constructions[31]. Only the window construction is changed, as they form part of the building envelope and not of the veranda. So, they must have the façade window construction assigned and not the veranda one. Once adjacencies are found and constructions fixed, the output from the *Solve Adjacencies* component is plugged into the *setEPNatVent* component to design natural ventilation of the zones. Window NV is allowed when minimum indoor air temperature is 25°C and outdoor air temperature is at least 12°C. Wind driven cross ventilation and inter zone air flow are permitted, so that the air that penetrates the veranda can also flow into the apartment zone. Glazing area operable for NV is set equal to 1 for the current apartment design.

Finally, before running the energy and daylight simulations, the building context is created. Surrounding buildings are modeled into Rhino environment starting from

[30] These shared surfaces have been imported twice, one time when defining the apartment closed Brep and another time when creating the veranda zone. This applies both to walls and windows.

[31] The component specifies that construction can be preserved only if the designer is sure that construction materials are assigned in reverse order on adjacent surfaces, otherwise EP will not read them correctly. Building the zones surface-by-surface, this is pretty easy to do. When building up the apartment zone, façade materials are assigned in the correct order, while when creating the veranda they are assigned in reverse order, as the innermost layer is the outermost layer for the apartment.

what can be seen from Google Maps. Only the buildings on the north and the south side are generated (see Figure 82), as they are the ones that could influence the most the solar radiation income. In addition to these Breps, also the balcony slab on the north façade is included into the apartment shading context.

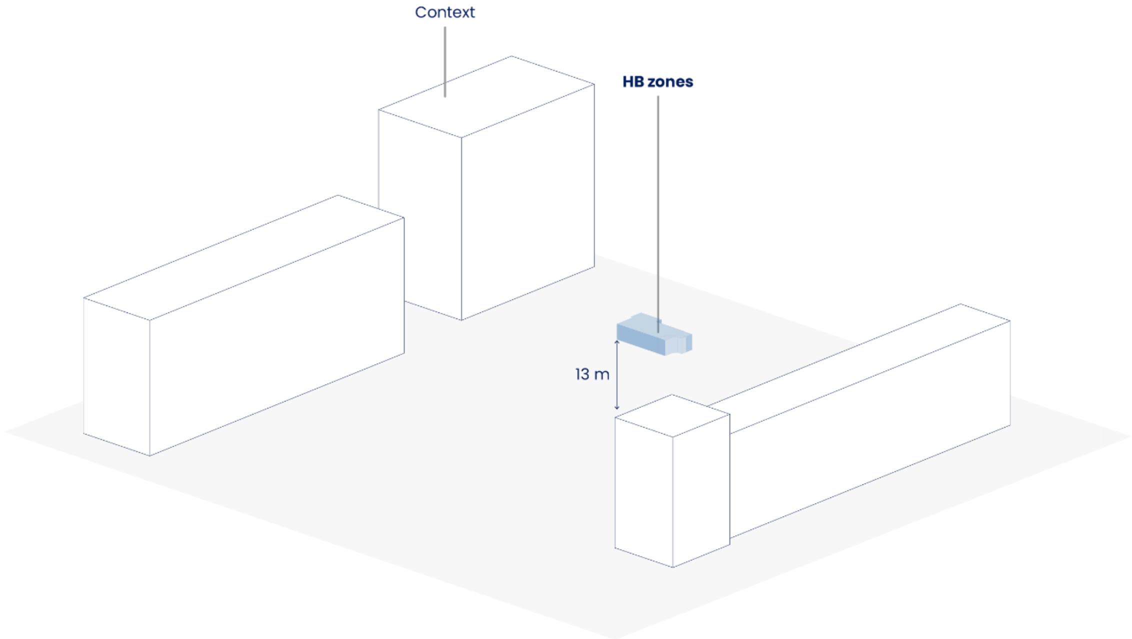

Figure 82 - Modeled context Breps surrounding the apartment. Axonometric view from SW.

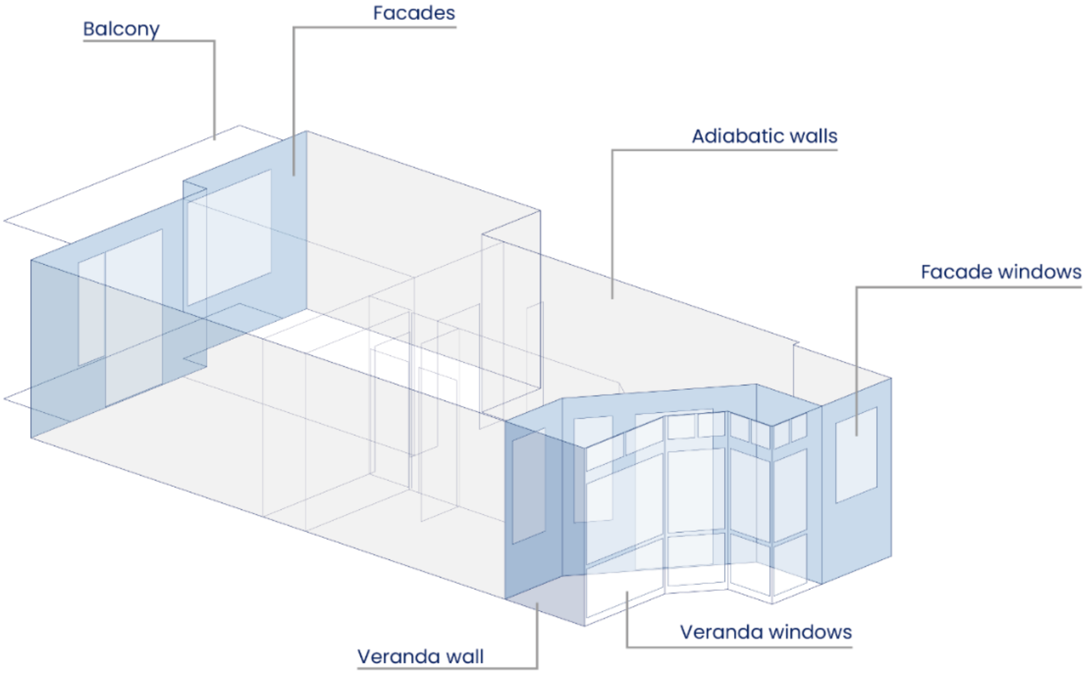

Figure 83 - Apartment and veranda axonometric visualization from Rhino-GH from SW direction.

APARTMENT DEFINITION FOR OPTIMIZATION

As for the classroom case study, the apartment retrofit takes into account the addition of an external insulation layer on the façades walls and the windows thermal and visual features improvement. The windows that are subjects of optimization are both the ones on the external apartment walls and the veranda ones. Due to the complexity of the case, shadings are not considered here but could be matter of further studies.

A new GH file where to perform changes in preparation for the optimization is created. As far as the external walls are concerned, an additional XPS layer is included in the existing EP construction, as displayed in Table 19. This regards the north façade as well as the walls facing the veranda on the south. The insulation layer thickness ranges from 0 to 0.20 m, thus changing the walls' U-value. For the optimization processes' purpose, façade and veranda's windows actual constructions are replaced by a generic window design, using HB *EPWindowMat* component as already discussed in §5.1.2. Glazing U-value can vary between 0.50 and 3 W/m^2·K, g-value between 0 and 1 and visible transmittance τ_v between 0 and 1. In addition, window area operable for NV can range between 0.50 (50%) and 1 (100%).

NEW FAÇADE EP CONSTRUCTION	LAYERS	THICKNESS (m)	CONDUCTIVITY (W/m·K)	DENSITY (kg/m³)	SPECIFIC HEAT (J/kg·K)
	Plaster	0.02	0.72	1860	840
	Additional XPS	Variable 0-0.20	0.035	100	1450
	Perforated brick	0.08	0.38	740	1000
	Air space	0.01	0.07	1.23	1005
	Perforated brick	0.12	0.38	740	1000
	Plaster	0.02	0.72	1860	840

Table 19 – EP construction of the apartment exterior walls with the additional insulation layer.

5.2.2 Free-running simulations and optimizations

First, energy and daylight simulations of the actual apartment design in unconditioned mode are carried out and free-running comfort metrics results are collected. The same actual design is tested using Turin's 2050 EPW file. Then, the same thing is done on the optimization GH files for both present and 2050 climatic conditions. It must be pointed out that in this case study, with respect to the other simulations performed until here, solar distribution calculation is set "full exterior with reflections" in the *energySimPar* component, as the apartment geometry is concave and messes up with interior solar distribution (this issue was already discussed in §3.5.1).

After calculating the required comfort metrics (percent of time comfortable - adaptive comfort, DLA, UDLI and ASE), the values referring to the apartment are selected [32] optimization processes are run. Objectives are always the same and parameters or *genes* whose optimal configuration must be searched are the ones discussed in the previous paragraph. Figure 84 lists these elements. Optimization algorithm settings are also kept the same as discussed in §3.7.2 (see Table 5).

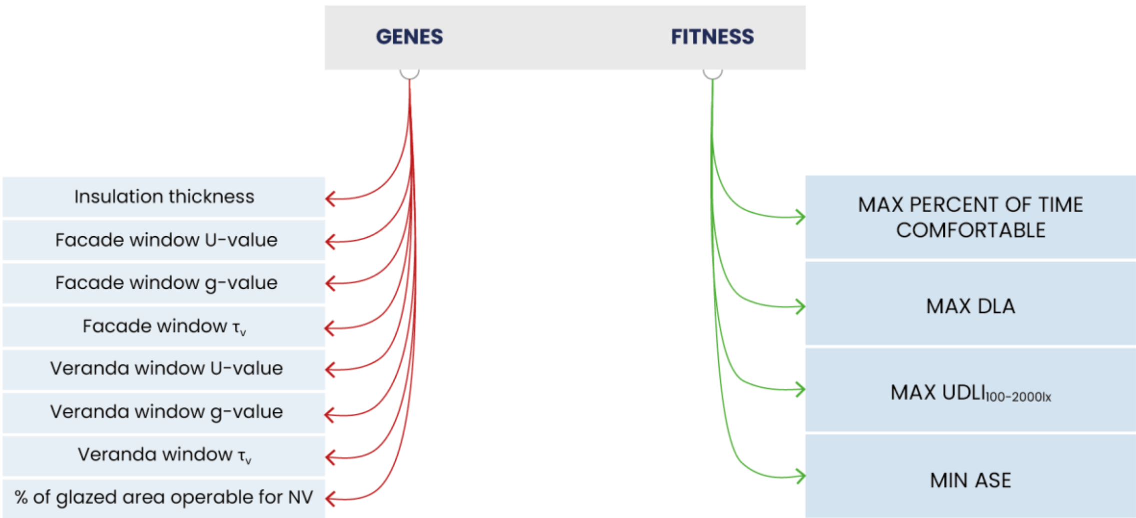

Figure 84 - Parameters and objectives for the apartment optimization.

[32] As energy and daylight simulations are run considering both the apartment and the veranda zones, output results are displayed in GH as trees composed of two branches. Only values referring to the apartment must be selected, so the GH *Explode Tree (BANG!)* component is used to separate the branches and extract only the relevant values.

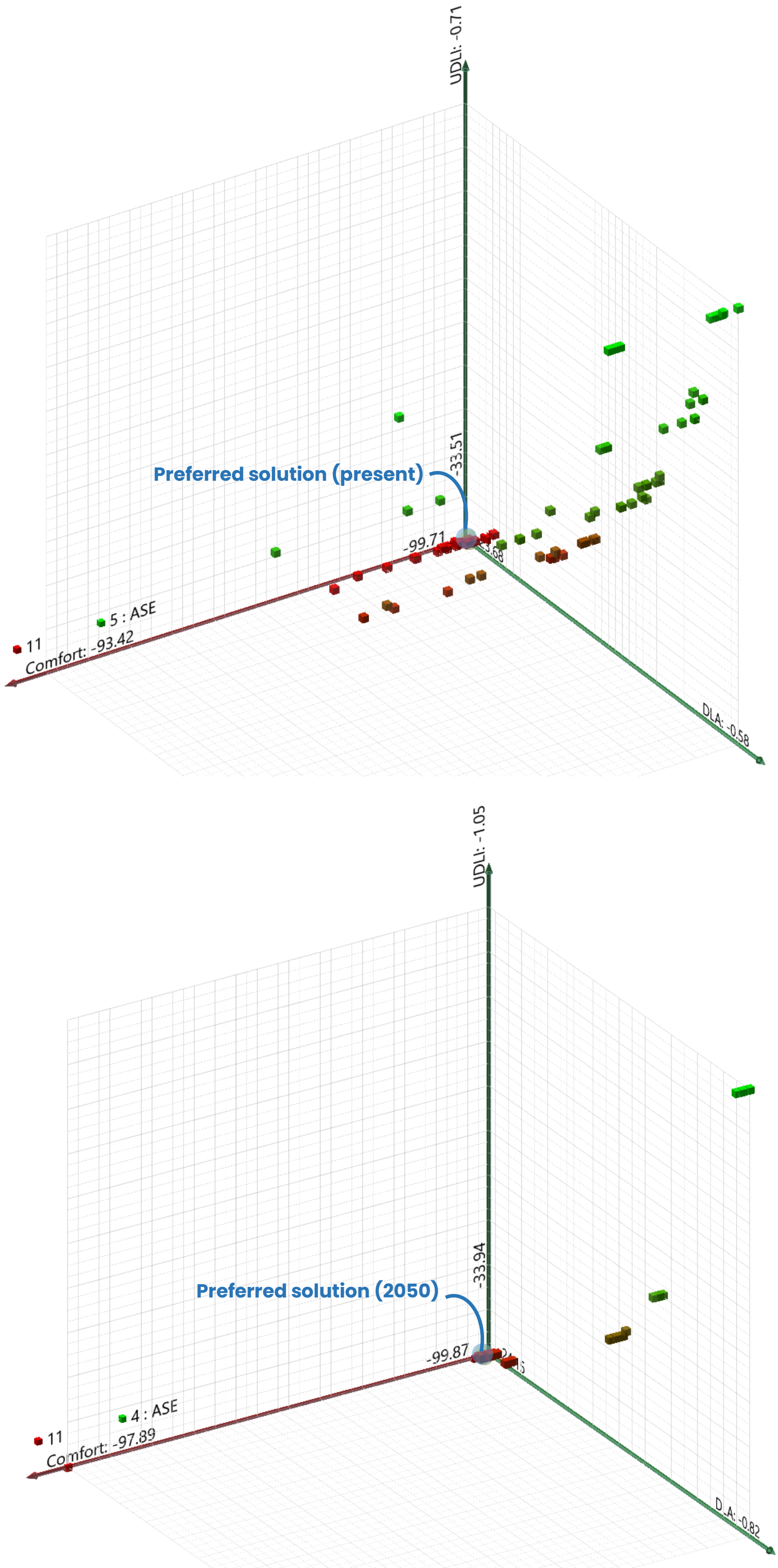

Figure 85 - Octopus cubeview of the apartment's optimizations under present (above) and 2050 (below) conditions. Preferred solutions are highlighted in blue.

Present and 2050 optimizations took about 3 days each to calculate the 15 generations of solutions. From the Octopus cartesian 3D graphs displayed in Figure 85 it can be seen that the lowest ASE values (in green) found by the optimization solver correspond to low DLA and $UDLI_{100-2000lx}$ values, while the highest thermal and visual comfort percentages correspond to the highest ASE values (in red). As the highest ASE is 11%, which is slightly over the LEED threshold of 10%, it is considered acceptable for the analysis purpose. So, preferred optimal solutions are chosen only based on the highest thermal and visual comfort metrics values, which means selecting the cubes that are the closest to the cartesian axes origin. The 2050 Octopus cubeview shows less cubes because, in the calculated populations of individuals, there were more dominated solutions with respect to non-dominated, which are the ones displayed on the graph.

Preferred solutions are reinstated into GH environment and optimal *genes* values are recorded. Figure 86 displays on the apartment's axonometric representation the optimal insulation and windows configurations corresponding to the selected optimal design solutions for present and 2050 cases.

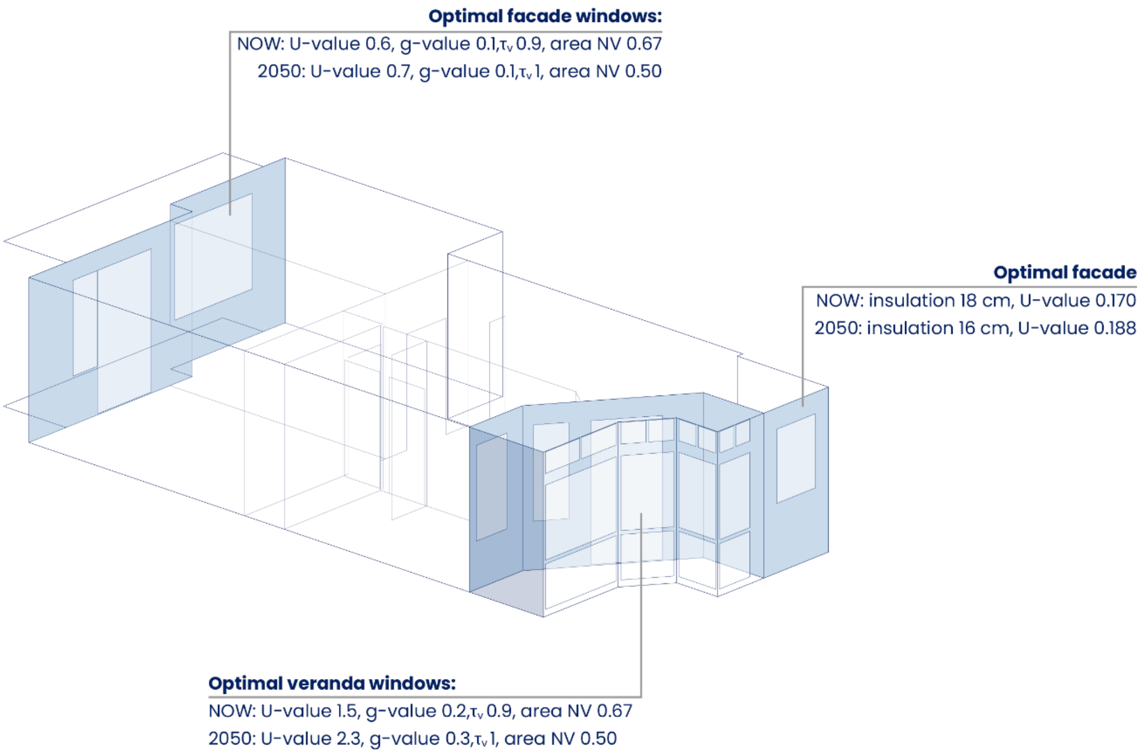

Figure 86 - Present and 2050 apartment's optimal genes values.

Optimal insulation thicknesses are quite high; in 2050, optimal thickness is lower than the present one (16 cm vs 18 cm in the present case). In both cases, the external walls' U-values dramatically decreases (from 1.367 W/m^2·K to 0.170-0.188 W/m^2·K). Optimal veranda windows generally have higher thermal transmittance with respect to optimal façade windows, yet still lower than the U-value of the single-pane glazing currently installed on the veranda (reader is referred to Table 17). Optimal configurations of the windows on the external walls have very low U-values, achievable using, for example, triple or quadruple-glazed windows with gas fillings and insulated PVC frames or wood/aluminum frames with thermal break. Examples of windows with such U-values are provided in [135, 136]. As concerns visible and solar transmittances, all optimal windows have very low g-values and very high τ_v (0.90 or 1), which means that nearly no solar energy or little energy must penetrate the indoor environment meanwhile light income must reach 90-100%. In real-life windows this is very difficult to achieve. To reduce g-values, solar control glazings with low-e coatings are usually employed. However, these coatings tend to decrease visible transmittances of the glazed surfaces, making it very challenging to balance the two values. Despite this, window features obtained through the optimization processes are considered to present the simulations' results, with the consciousness that, in real-life retrofits, comfort metrics values will be a bit different from the ones calculated in this research, which have the sole purpose of testing the developed tool effectiveness. To obtain more realistic values, it is possible to change the window features' ranges of variation, using more life-like boundaries. In the present research, it was chosen to consider the ranges of variation suggested by Honeybee components for g-values and τ_v (0-1). Operable glazing area for NV is equal to nearly 70% in the present case, while in 2050 it is reduced to 50%.

5.2.3 Results comparison

This paragraph compares and discusses comfort, energy use and savings results obtained from actual apartment design simulations under present and 2050 conditions and from the two optimization processes (present and future).

COMFORT METRICS

Thermal and visual comfort metrics results obtained through the free-running simulations are here discussed. Looking at the four adaptive charts displayed in Figure 87, it can be seen that the actual design of the apartment (no external insulation, poor facades and windows U-values) is not optimal, especially when outdoor temperatures are low. In fact, in present actual adaptive chart it can be observed that indoor operative temperatures lie below the comfortable range for numerous hours of the year. This happens also to the same actual design tested in 2050, despite the adaptive colored mesh is shifted to the right of about 4°C, due to the higher outdoor temperatures. Instead, in present and future optimal solutions found through Octopus optimizations almost all the indoor operative temperatures fall between the comfortable range of temperatures established by the European standard. Hence, in this second case study, the tool revealed to be very effective in maximizing thermal comfort in free-running mode (without any mechanical cooling and ventilation nor heating systems), only by adding an external insulation layer and improving windows' characteristics (especially U-value).

The tool's effectiveness is also visible from the four LB 3D charts displaying the condition of person throughout the year according to the adaptive comfort model grouped in Figure 88. As expected, the

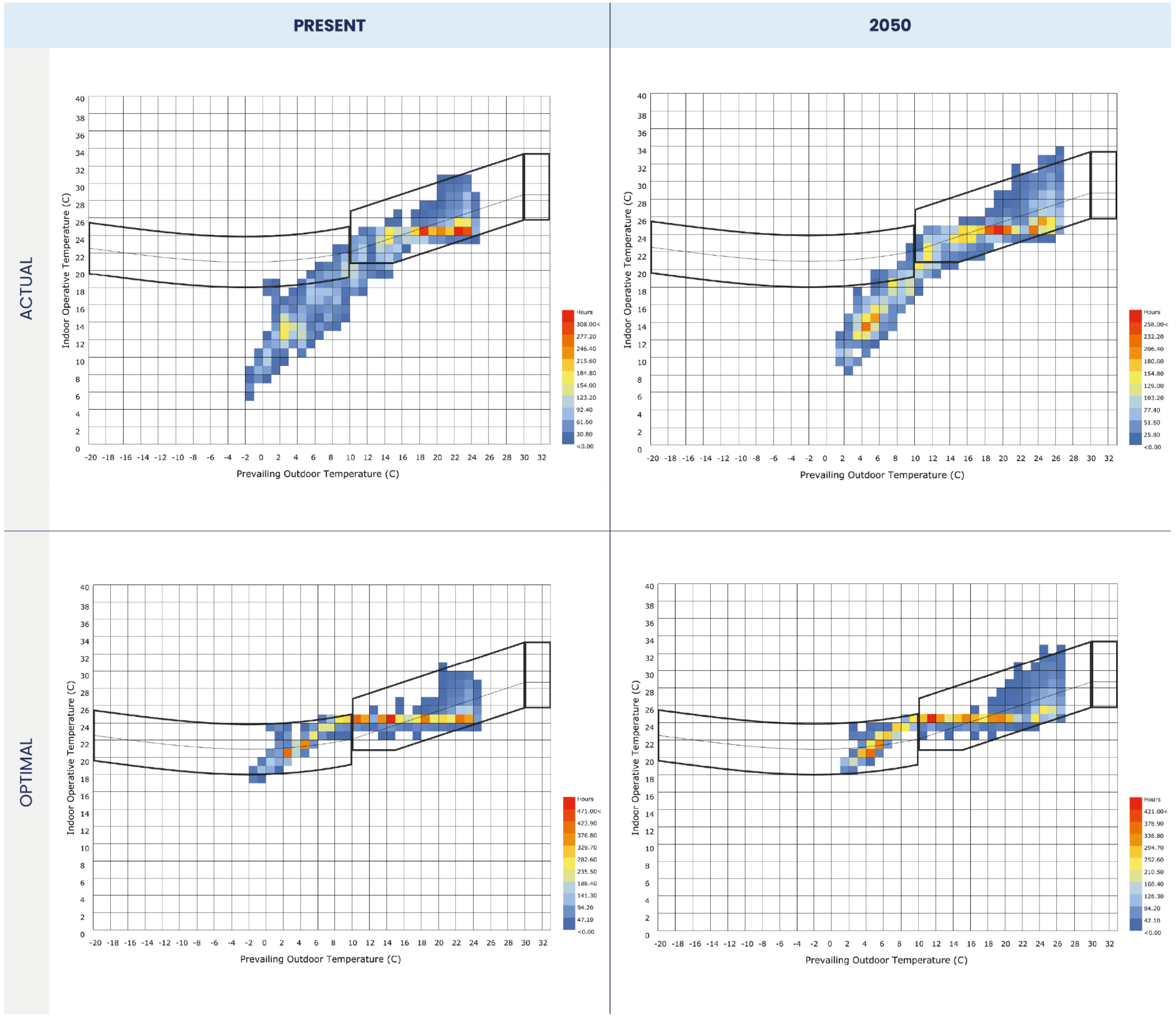

Figure 87 - Apartment's adaptive charts comparison.

accrual design configuration of the apartment makes occupants feel cold for nearly one-third of the year, especially during winter. Summer period is almost all comfortable, except for some hours in which occupants feel hot. Under 2050 climatic conditions, the percent of time hot increases, as does the percent of time cold. Indeed, optimal design solutions allow to reach nearly 100% of time comfortable without HVAC systems during the year, successfully minimizing the percentages of the time during which users fell hot or cold, values that reach nearly 0%. From these graphs it is clear that the retrofitted apartment could potentially function all the year in free-running mode, thus saving a lot of energy and nullifying GHGs emissions deriving from heating and cooling systems. These assumptions will be validated by the mixed-mode simulations that are presented in the next part of the paragraph.

As far as visual comfort metrics are concerned, the tool was not able to find better DLA and $UDLI_{100-2000lx}$ values or better light distribution with respect to the ones achieved with the actual design configuration. This is certainly because window-to-wall ratios on the two facades are fixed and visible transmittances of the optimal glazed surfaces do not differ greatly from the actual ones. The low daylight metrics values are legitimated from the fact that the apartment's plan is developed longwise and only has two views. In addition, considering internal walls does not allow the daylight to reach all the spaces of the flat, thus creating shadow

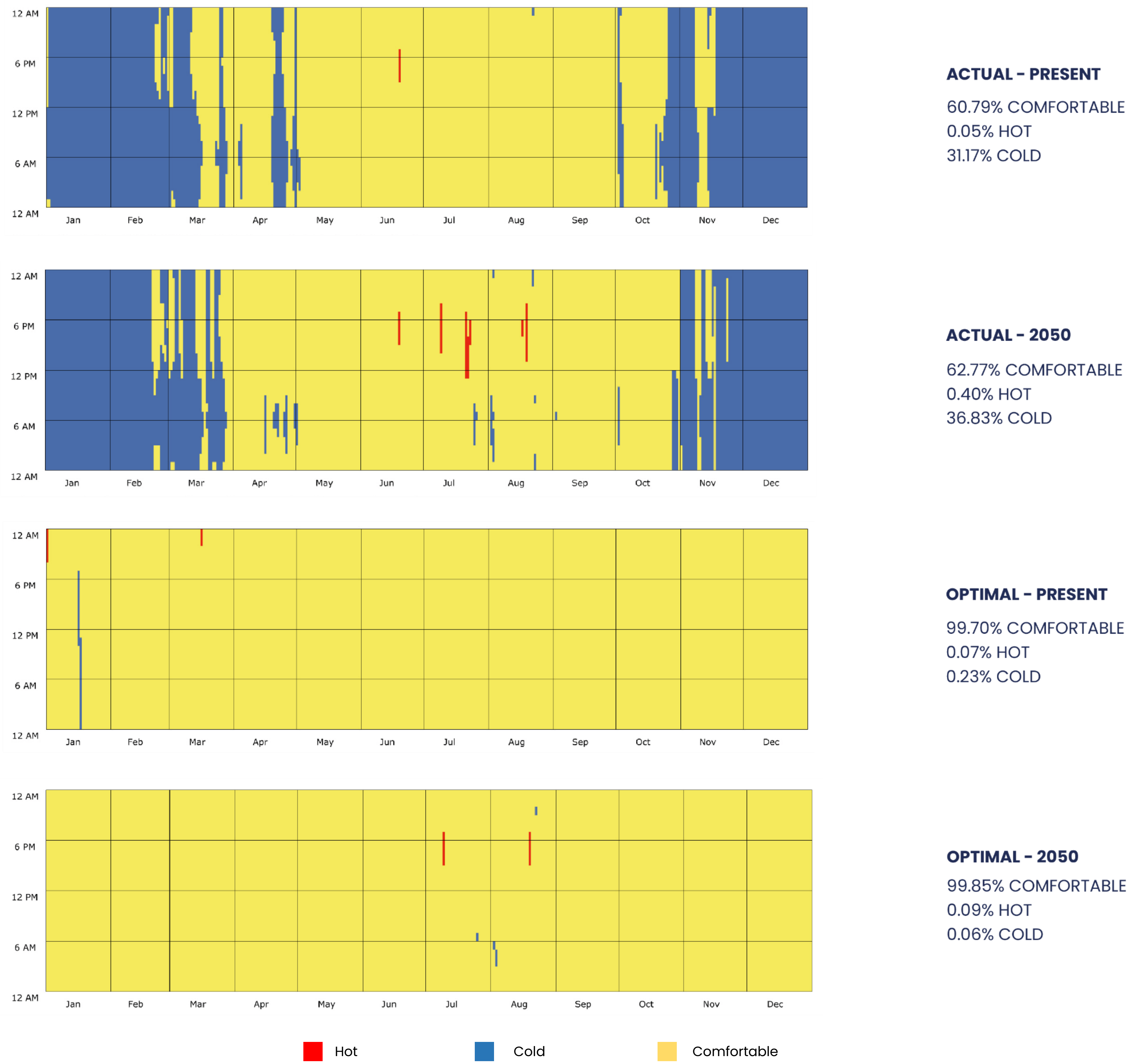

Figure 88 - LB 3D charts displaying the percent of time comfortable, hot and cold of the actual and the optimal apartment's designs under present and 2050 climatic conditions.

areas and decreasing the DLA and UDLI$_{100-2000lx}$ averaged values. The highest daylight autonomy and useful daylight illuminance values (30-50% of the hours of the year) are experienced near the windows, which means in part of the kitchen and the bathroom, of the living room and the bedroom. DLA is 0% in the center of the apartment, while UDLI$_{100-2000lx}$ is very low – see Figure 89.

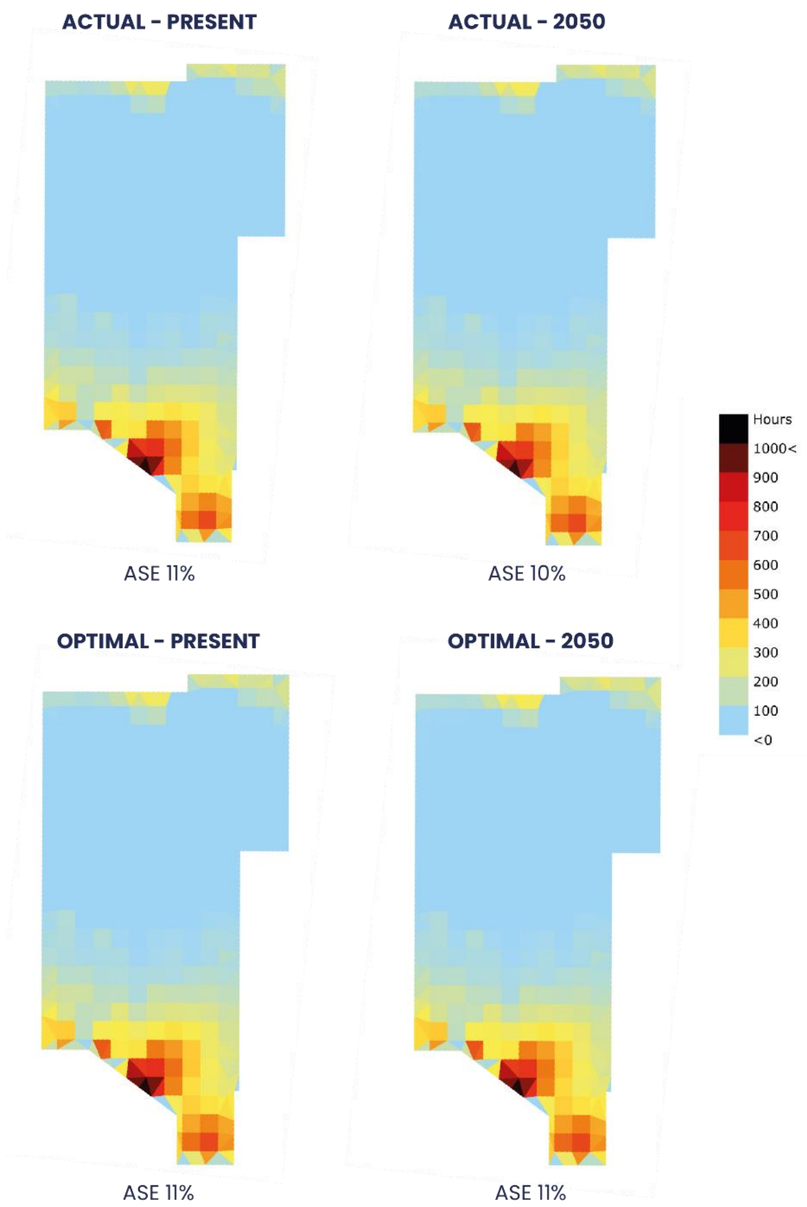

Figure 90 – Apartment's ASE comparison on plan visualization.

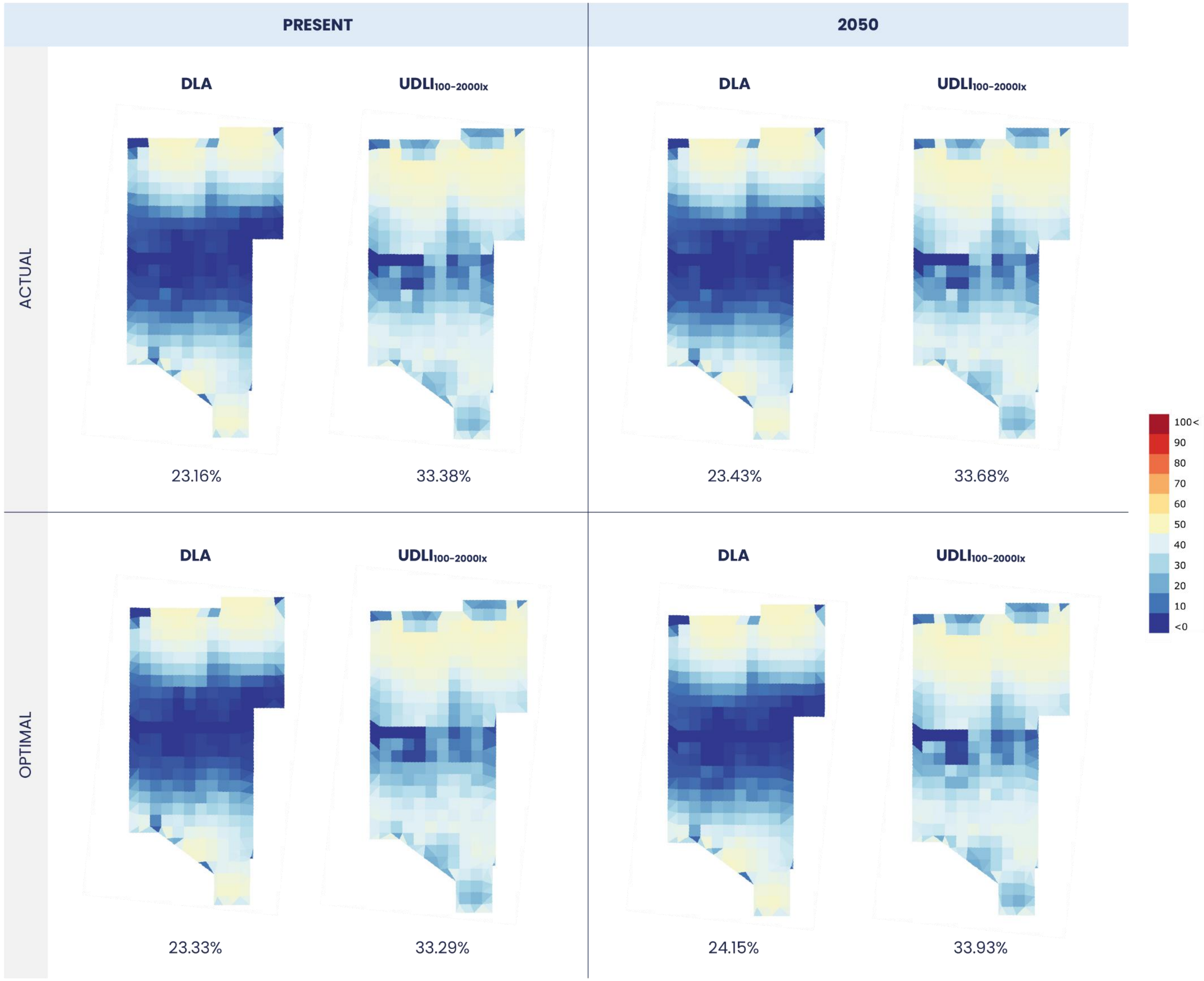

Figure 89 – Apartment's DLA and UDLI comparison.

ASE values are remains the same (see Figure 90), as optimal τ_v of the windows are similar to actual visible transmittance and no shading devices are placed on the glazed surfaces. The most critical area appears to be the one near the door-window in the kitchen that faces the veranda, as it is placed on the south. A shading system made, for example, of fabric rollers placed on the veranda windows (internal or external) could reduce ASE in that critical area but, as the same time, it would reduce the already scarce amount of daylight that penetrates the indoors. So it seems a good choice not having considered shadings in the optimization process.

ENERGY USE AND SAVINGS

Mixed-mode simulations are then run. The apartment zone is set conditioned, while the veranda remains unconditioned. Temperature set points for the apartment zone are specified (20°C for heating and 26°C for cooling), this time not considering setbacks since the occupancy period is 24 hours. No mechanical ventilation is taken into account because it is uncommon for residential units to have it. This way, the issue related to ventilation arisen in the classroom's case study is here avoided. As for the previous simulations, to avoid having cooling system turned on while windows are open, maximum outdoor temperature for NV is set to 25°C. Figure 91 displays the

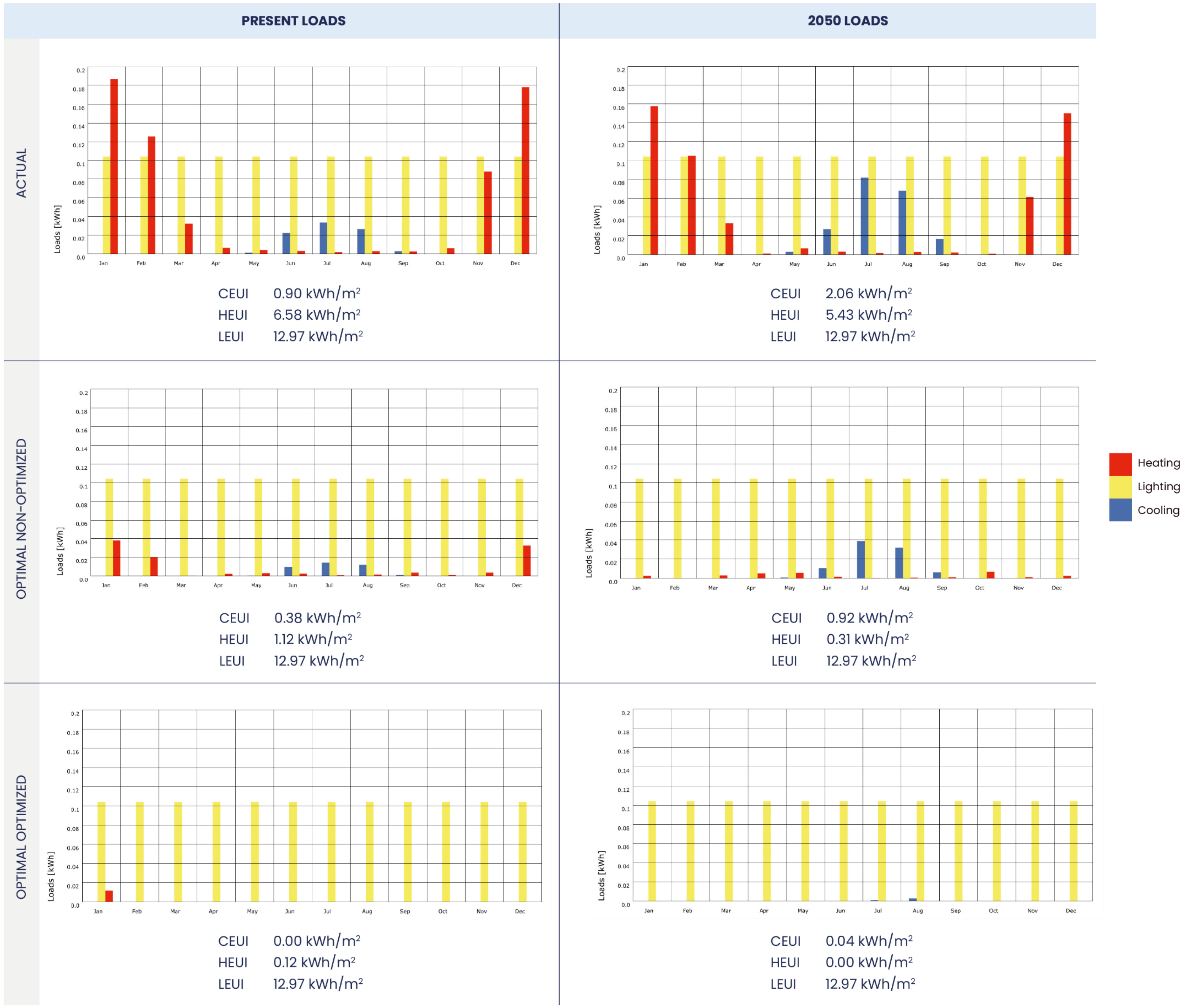

Figure 91 - LB bar charts comparing heating, cooling and lighting loads of actual and optimal apartment designs.

LB bar charts that show the apartment energy use when considering the actual design, the optimal solutions or the optimal solutions when custom HVAC schedules are applied. Optimized lighting schedules are not applied, since Daysim annual profiles produced a higher lighting load with respect to the one produced by the default schedule (over 71 kWh/m^2 for both present and 2050 solutions). For this reason, default EN 16798-1 lighting schedule is applied also to optimized optimal designs, considering LEUI savings equal to 0%. With respect to HEUI and CEUI, it can be clearly observed that in optimal solutions, even when applying default HVAC control schedules, heating and cooling loads are consistently reduced. Applying custom optimized HVAC schedules allow to nullify CEUI in the present solution and HEUI in 2050, while the other thermal loads are greatly minimized. Table containing full energy use details can be found in ANNEX 4. Optimized optimal solutions allow to reach TEUI savings over 90%. Present optimized optimal configuration can save 98% of the thermal energy that is currently used in the actual apartment under present condition, while under 2050 climate TEUI saved is equal to 92%. With respect to optimal non-optimized solutions, the application of custom schedules can save up to 99% of thermal energy in the present case, while TEUI savings reach 97% in 2050. LEUI savings are equal to 0% for the reasons mentioned above.

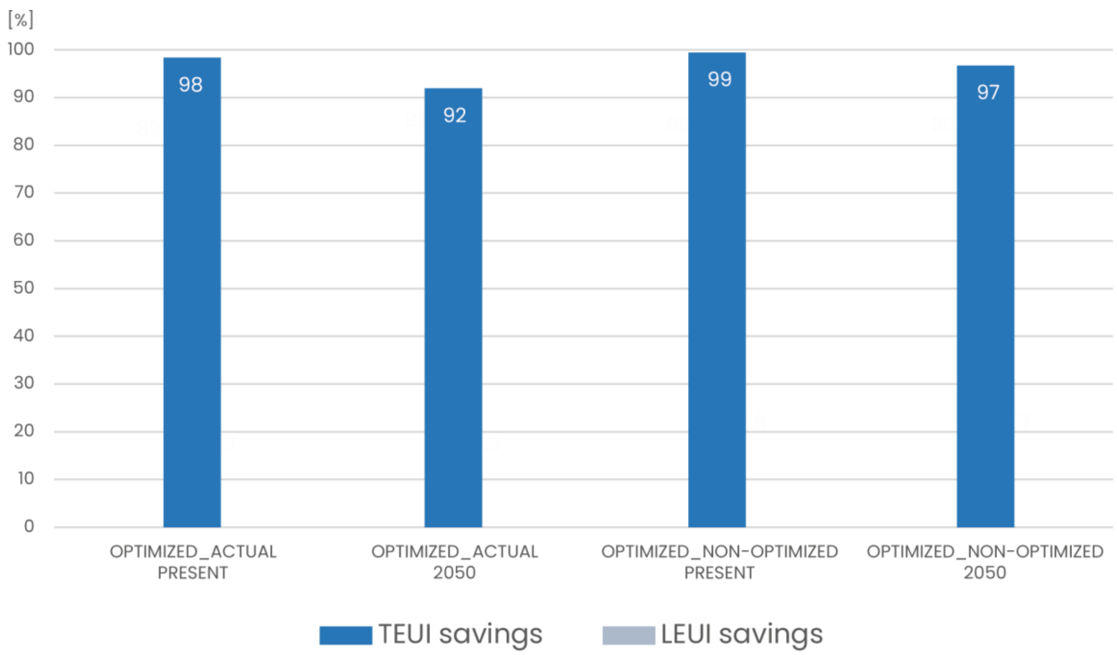

Figure 92 - Bar chart displaying the apartment's energy savings obtained through the optimization. Optimized TEUI and LEUI are compared to actual and optimal non-optimized energy use.

6. CONCLUSIONS

6. CONCLUSIONS

The presented parametric tool can be qualified as a valid instrument to drive a methodological change in the design process, seeking for improved occupants' comfort, higher energy savings and, consequently, lower GHGs emissions. The tool could become part of a sustainable project workflow that, starting from the optimization of the position of minimal functional space units (that differ in activity, needs and requirements) within their context, gets to analyze each of these units in terms of performance and indicates optimal technical solutions to define the building system. For instance, the workflow proposed in this research could complement Chiesa and Grosso's *site microclimatic matrix*[33] [84-85, 138-139]. The *microclimate matrix* tool derives adaptation/disadaptation values by analyzing sun and wind conditions and, based on these values, allows to define the building organization during the programming phase of design [85]. After this first stage, the proposed tool could be used to further improve comfort of the indoor environments based on their functions.

Due to the numerous opportunities that the tool offers, it is reckoned to be deserving of attention. However, as it is still at an embryonic stage, it needs to be further tested and developed. The presented research pointed out several potentialities as well as some limitations of the tool under discussion. First, it has proven to be capable of optimizing indoor comfort in free-running closed environments, a topic which is still poorly discussed in literature within the context of building performance simulations. The optimization processes drove to satisfying visual and thermal comfort levels in almost all the tested locations. As regards energy consumption for heating, cooling and artificial lighting in mixed-mode building usage, applying custom systems control schedules allowed to reach good energy savings results. The tool showed its resilience not only under present climatic conditions, but also under future ones (2050 A2 scenario, the most critical in terms of temperature rise). Though, the first twenty

[33] This tool was originally developed by American researchers Brown and Decay [137] in 2001.

optimizations identified one of the tool's limitations, finding that energy use is reduced the most in climates that are not too cold (Kemi's case), as reduction mainly affects cooling loads. Further applications of the tool in more diversified climates and contexts and with different HB model settings (e.g. envelope materials, type of shading, context, etc.) are required to validate these assumptions. Moreover, it was found very important for the mixed-mode simulation to set the maximum outdoor air temperature constraint for NV 1°C or 2°C below the cooling setpoint established for the HVAC, otherwise the windows will be open simultaneously to the cooling system functioning period, thus increasing dramatically cooling loads.

The implementation of the proposed tool in the two case studies, the school classroom in Torre Pellice and the residential apartment located in Turin, showed the effectiveness of the workflow when applied to concrete cases that have more constraints in terms of building orientation and geometric features (e.g. windows dimensions). TEUI savings achieved through the tool reach 90% for the classroom and nearly 100% for the apartment. As concerns the first case study, the mixed-mode simulation of the classroom pointed out the need to test the sensitivity of the optimized solutions under different ventilation rates. Since mechanical ventilation in EP simulation takes the air from the outside (which could be colder or hotter with respect to indoor air, depending on the site's climate), the introduction into the environment of these external air flows could significantly affect indoor temperatures, thus modifying the discomfort periods found through the adaptive comfort analysis. This would invalidate the effectiveness of custom schedules in reaching 100% of users' comfort in mixed-mode usage, so more studies on this topic are certainly needed. In addition to this, some issues showed up when importing the existing IDF file of the school. The impossibility for Honeybee plug-in to translate into readable objects some of the IDF elements (especially windows and schedules) weakened the potentially strong interoperability between the tool and the files outputted from EP, making it more difficult to switch from the classic text-based EP interface to the parametric and three-dimensional one proposed by the tool. Being aware of these difficulties, specific attention should be paid when the starting IDF file is created, e.g. making sure that schedules and other elements are written in a way that HB can read correctly. Alternatively, it is possible to translate manually each IDF object using HB components, although it could be more time consuming.

Overall, the proposed tool is quite simple to use. It does not require any specific EP or Radiance pre-existing know-how, yet only requires little knowledge of how Grasshopper and Rhino work. GH environment provides users with the possibility to easily change the workflow order, add HB zones to the simulation (thus switching from a single-zone to a multi-zone analysis, as in the second case study) and/or add new thematic sections. For instance, LCA analyses of the employed materials, GHGs emissions, intervention costs, design of renewable energy generation elements (photovoltaic or solar panels) and their integration within the architecture are just some of the topics that have not been considered in this research due to time constraints, yet that could be incorporated into the workflow and optimized to search for the best and most sustainable design alternative. In a personal opinion, the simulations that have been carried out through the use of the proposed tool within this paper have brought to very satisfying, even though further analyses and developments are required to investigate in greater detail more of its potentialities and overcome its limitations.

7. ANNEXES

ANNEX 1

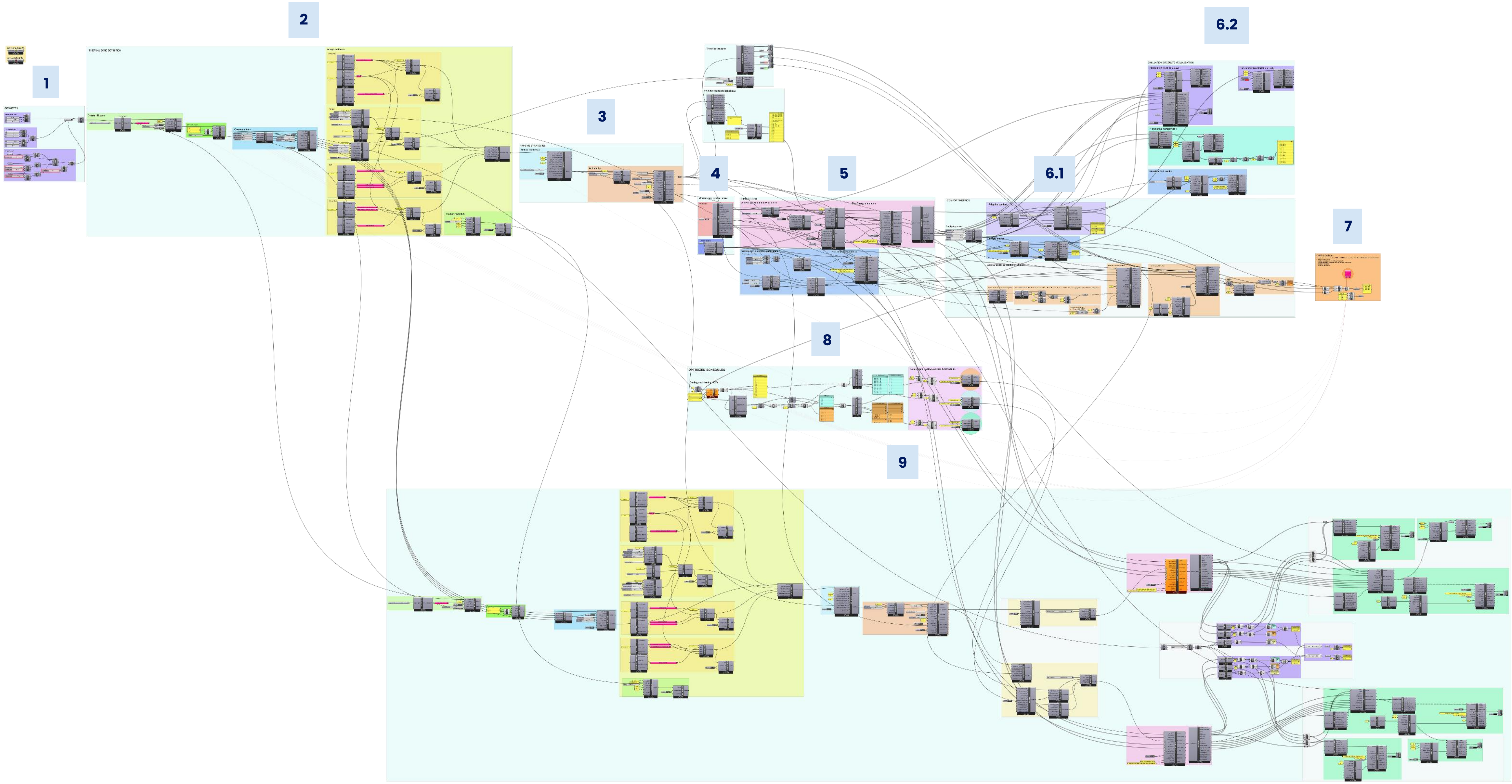

Figure 93 - Grasshopper workflow. (1) Geometry; (2) Thermal zone definition; (3) Passive strategies; (4) Boundary conditions; (5) EP and Radiance simulations in free-running mode; (6.1) Comfort metrics; (6.2) Visualize comfort metrics; (7) Optimization; (8) HVAC custom schedules creation; (9) Mixed-mode simulations and non-optimized/optimized energy use calculation + energy savings.

ANNEX 2

CITY	EPW	GENES								OBJECTIVES				ENERGY USE								ENERGY SAVINGS		
														NON-OPTIMIZED				OPTIMIZED						
		North WWR [-]	East WWR [-]	South WWR [-]	West WWR [-]	Building orientation [°]	Insulation thickness[cm]	Glazing area operable for NV [-]	Shading orientation [°]	Comfort [%]	DLA [%]	$UDLI_{100-2000lx}$ [%]	ASE [%]	CEUI [kWh/m²]	HEUI [kWh/m²]	TEUI [kWh/m²]	LEUI [kWh/m²]	CEUI [kWh/m²]	HEUI [kWh/m²]	TEUI [kWh/m²]	LEUI [kWh/m²]	TEUI [%]	LEUI [%]	sDA [%]
KEMI	NOW	0,7	0,2	0	0	270	23	0,96	9	45,21	57,46	56,48	5	0,66	47,11	47,77	38,59	0,00	36,88	36,88	12,99	23	66	74
	2050	0,9	0,2	0	0,1	90	28	0,94	69	44,66	58,11	51,87	6	1,47	44,94	46,41	38,59	0,00	35,08	35,08	13,29	24	66	78
AALBORG	NOW	0,2	0	0	0,3	90	22	0,8	65	58,88	45,24	65,74	13	1,07	17,31	18,38	38,47	0,00	13,49	13,49	19,41	27	50	46
	2050	0,4	0	0,1	0	270	41	0,71	87	83,47	70,01	72,47	9	5,59	8,23	13,82	38,56	0,06	5,39	5,45	14,14	61	63	89
GENEVA	NOW	0,6	0,1	0	0	90	44	0,64	-4	71,99	66,90	64,90	4	3,98	11,04	15,02	38,56	0,18	8,58	8,76	13,12	42	66	80
	2050	0,4	0	0,1	0	270	31	0,73	3	71,44	63,93	71,64	7	4,51	9,29	13,80	38,76	0,17	6,53	6,70	15,92	51	59	86
TURIN	NOW	0,7	0	0	0,1	90	37	0,85	-69	73,52	75,10	63,57	6	6,76	10,27	17,03	38,64	0,22	8,54	8,76	9,29	49	76	95
	2050	0,3	0	0	0,3	90	36	0,58	73	84,18	58,02	73,90	9	8,14	6,81	14,95	38,76	0,74	4,55	5,29	15,47	65	60	64
ATHENS	NOW	0,9	0	0	0,1	180	42	0,76	74	89,52	73,02	65,70	6	12,61	1,67	14,28	38,72	2,20	0,80	3,00	10,21	79	74	83
	2050	0,5	0	0	0,1	270	25	0,82	-59	89,79	79,92	64,80	9	14,19	0,93	15,12	38,64	2,59	0,42	3,01	9,27	80	76	99
BARI	NOW	0,7	0,1	0	0	270	38	0,67	-78	90,27	82,80	60,82	6	9,90	3,10	13,00	38,64	0,80	1,90	2,70	6,37	79	84	100
	2050	0,5	0,1	0	0	90	18	0,72	73	91,19	75,00	68,88	5	11,59	2,22	13,80	38,76	1,43	1,49	2,92	8,53	79	78	91
PALERMO	NOW	0,7	0	0	0	270	18	0,63	45	91,96	80,69	66,68	0	11,66	0,98	12,64	38,64	0,38	0,79	1,17	6,27	91	84	100
	2050	0,3	0	0,1	0	90	31	0,54	54	97,88	75,92	98,25	10	13,02	0,22	13,24	38,76	0,48	0,03	0,51	9,97	96	74	98
PAPHOS	NOW	0,3	0,1	0	0,1	90	43	0,56	70	97,51	79,44	74,37	12	14,45	0,30	14,75	38,64	0,09	0,11	0,20	6,13	99	84	98
	2050	0,7	0,1	0	0,1	90	43	0,56	44	94,36	87,20	57,03	5	19,69	0,31	20,00	38,76	2,27	0,20	2,47	3,21	88	92	100
ROME	NOW	0,3	0,1	0	0,1	90	33	0,86	75	90,59	72,21	71,19	14	8,42	3,08	11,49	38,64	0,60	1,28	1,88	12,94	84	67	90
	2050	0,3	0	0,1	0	270	29	0,54	42	93,70	72,31	78,44	8	10,19	1,92	12,11	38,76	1,01	0,61	1,62	11,80	87	70	94
TRIESTE	NOW	0,5	0,1	0	0,1	90	41	0,59	89	87,55	71,83	64,87	9	8,70	5,12	13,82	38,64	0,29	3,11	3,41	10,11	75	74	89
	2050	0,7	0,1	0	0	90	36	0,54	75	86,71	75,87	62,70	4	11,92	4,11	16,03	38,76	1,05	2,70	3,75	9,43	77	76	97

Table 20 - Genes, objectives and energy use data of the optimal solutions resulting from the twenty optimization processes.

ANNEX 3

CASE	EPW	GENES									OBJECTIVES				sDA [%]
		Insulation thickness [cm]	Window U-value [W/m²K]	Window g-value [-]	Window τ_v [-]	Glazing area operable for NV [-]	Shades τ_v [-]	Shades depth [m]	Shades number [-]	Shading orientation [°]	Comfort [%]	DLA [%]	UDLI$_{100-2000lx}$ [%]	ASE [%]	
ACTUAL	NOW	0	2,40	-	-	1,,00	-	-	-	-	68,92	44,63	65,37	47	44
	2050	0	2,40	-	-	1,00	-	-	-	-	70,38	45,69	66,64	46	45
OPTIMAL	NOW	13	2,70	0,50	0,90	0,58	0,58	0,22	6	66	85,70	47,38	70,20	0	47
	2050	16	2,60	0,50	1,00	0,81	0,54	0,25	5	68	86,15	49,72	70,88	0	54

Table 21 - Classroom design parameters and comfort metrics. Comparison between actual and optimal values for the present and the 2050 cases.

CASE	EPW	SCHEDULES	ENERGY USE				
			CEUI [kWh/m²]	HEUI [kWh/m²]	TEUI [kWh/m²]	LEUI [kWh/m²]	EUI [kWh/m²]
ACTUAL	NOW	NON-OPTIMIZED	1,00	2,53	3,53	17,29	20,82
	2050	NON-OPTIMIZED	2,53	2,81	5,34	17,29	22,63
OPTIMAL	NOW	NON-OPTIMIZED	0,78	4,33	5,11	17,29	22,40
		OPTIMIZED	0,01	0,53	0,54	13,26	13,80
	2050	NON-OPTIMIZED	1,91	4,21	6,12	17,29	23,41
		OPTIMIZED	0,11	0,53	0,63	12,53	13,16

Table 22 - Actual and optimal classroom solutions' energy use values under present and 2050 conditions.

ANNEX 4

CASE	EPW	GENES								OBJECTIVES				
		Insulation thickness [cm]	Façade window U-value [W/m²K]	Façade window g-value [-]	Façade window τ_v [-]	Veranda window U-value [W/m²K]	Veranda window g-value [-]	Veranda window τ_v [-]	Glazing area operable for NV [-]	Comfort [%]	DLA [%]	$UDLI_{100-2000lx}$ [%]	ASE [%]	sDA [%]
ACTUAL	NOW	0	1,54	0,80	0,82	5,70	0,88	0,90	1,00	60,79	23,16	33,38	11	0
	2050	0	1,54	0,80	0,82	5,70	0,88	0,90	1,00	62,77	23,43	33,68	10	0
OPTIMAL	NOW	18	0,60	0,10	0,90	1,50	0,20	0,90	0,67	99,70	23,33	33,29	11	0
	2050	16	0,70	0,10	1,00	2,30	0,30	1,00	0,50	99,85	24,15	33,93	11	0

Table 23 - Apartment design parameters and comfort metrics. Comparison between actual and optimal values for the present and the 2050 cases.

CASE	EPW	SCHEDULES	ENERGY USE				
			CEUI [kWh/m²]	HEUI [kWh/m²]	TEUI [kWh/m²]	LEUI [kWh/m²]	EUI [kWh/m²]
ACTUAL	NOW	NON-OPTIMIZED	0,90	6,58	7,48	12,97	20,45
	2050	NON-OPTIMIZED	2,06	5,43	7,49	12,97	20,46
OPTIMAL	NOW	NON-OPTIMIZED	0,38	1,12	1,50	12,97	14,47
		OPTIMIZED	0,00	0,12	0,12	12,97	13,09
	2050	NON-OPTIMIZED	0,92	0,31	1,23	12,97	14,20
		OPTIMIZED	0,04	0,00	0,04	12,97	13,01

Table 24 - Actual and optimal apartment solutions' energy use values under present and 2050 conditions.

8. REFERENCES

8. REFERENCES

1. EUROPEAN COMMISSION, *Special Eurobarometer 513: Climate Change*, Brussels, July 2021. https://data.europa.eu/data/datasets/s2273_95_1_513_eng?locale=en Accessed 06 April 2022.
2. HAIBACH H., SCHNEIDER K., "The Politics of Climate Change: Review and Future Challenges", in *Climate Change: International Law and Global Governance. Volume II: Policy, Diplomacy and Governance in a Changing Environment*, Nomos Verlagsgesellschaft MbH & KG, 2013, pp. 357-374.
3. CHIESA G., PAGANI R., *Biomimetica, tecnologia e innovazione per l'architettura*, Celid, Torino, 2010.
4. DRABICKA K. (edited by), *Climate action in the post-COVID-19 world. Insight from EU-funded project on how to build forward better*, European Commission, Directorate-General for Research and Innovation - Horizon 2020, Brussels, 2021.
5. NASA website accessible at https://climate.nasa.gov/ Accessed 03 April 2022.
6. NASA website, "Thawing Permafrost Could Leach Microbes, Chemicals Into Environment", NEWS, 09 March 2022. https://climate.nasa.gov/news/3153/thawing-permafrost-could-leach-microbes-chemicals-into-environment/ Accessed 28 June 2022.
7. CMCC, *Cambiamenti climatici: una minaccia al benessere delle persone e alla salute del pianeta. Agire ora può mettere al sicuro il nostro futuro* , Italian version of the IPCC official press release, Berlin, 28 February 2022, : https://ipccitalia.cmcc.it/cambiamenti-climatici-una-minaccia-al-benessere-delle-persone-e-alla-salute-del-pianeta-agire-ora-puo-mettere-al-sicuro-il-nostro-futuro/. Accessed 05 April 2022.
8. European commission website, *Paris Agreement*, https://ec.europa.eu/clima/eu-action/international-action-climate-change/climate-negotiations/paris-agreement_en. Accessed 28 June 2022.

9. UNITED NATIONS, *Paris Agreement*, Paris, 2015, https://unfccc.int/sites/default/files/english_paris_agreement.pdf. Accessed 09 April 2022.
10. Carbon Monitor project, https://carbonmonitor.org/ Accessed 04 April 2022
11. IEA, *Global Energy Review: CO2 Emissions in 2021*, IEA, Paris, 2022. https://www.iea.org/reports/global-energy-review-co2-emissions-in-2021-2 Accessed 04 April 2022.
12. EUROPEAN COMMISSION, *Questions and Answers on REPowerEU: Joint European action for more affordable, secure and sustainable energy*, Strasbourg, March 2022. https://ec.europa.eu/commission/presscorner/detail/en/qanda_22_1512. Accessed 04 April 2022.
13. EUROPEAN COMMISSION, *Factsheet - Energy Performance of Buildings*, Brussels, December 2021. https://ec.europa.eu/commission/presscorner/detail/en/fs_21_6691 Accessed 04 April 2022.
14. EUROPEAN COMMISSION, *Communication from the commission to the European parliament, the council, the european economic and social committee and the committee of the regions. A Renovation Wave for Europe - greening our buildings, creating jobs, improving lives*, Brussels, 14 October 2020. https://eur-lex.europa.eu/resource.html?uri=cellar:0638aa1d-0f02-11eb-bc07-01aa75ed71a1.0003.02/DOC_1&format=PDF Accessed 15 April 2022.
15. LAURENTI M., TRENTIN M., et al., *Ecosistema urbano: rapporto sulle performance ambientali delle città 2021*, Legambiente, 2021.
16. HORIZON 2020, "Secure, clean and efficient energy", in *Horizon 2020 Work programme 2018-2020*, European Commission Decision C(2020)6320, 17 September 2020. http://ec.europa.eu/research/participants/data/ref/h2020/wp/2018-2020/main/h2020-wp1820-energy_en.pdf Accessed 07 April 2022.
17. EUROPEAN COMMISSION, *Proposal for a DIRECTIVE OF THE EUROPEAN PARLIAMENT AND OF THE COUNCIL on the energy performance of buildings (recast)*, 2021/0426 – COM (2021) 802 final, Brussels, 15 December 2021.

https://ec.europa.eu/energy/sites/default/files/proposal-recast-energy-performance-buildings-directive.pdf. Accessed 06 April 2022.

18. EUROPEAN COMMISSION, *Questions and Answers on the revision of the Energy Performance of Buildings Directive*, Brussels, 15 December 2021. https://ec.europa.eu/commission/presscorner/detail/en/QANDA_21_6686 Accessed 06 April 2022.
19. EPB Center official website, holistic approach section, https://epb.center/epb-standards/background/holistic-approach/. Accessed 09 April 2022.
20. EUROPEAN COMMISSION, *Mandate M480 to the European Committee for Standardisation, CEN 2012-2017*, Brussels, 14 December 2010. https://ec.europa.eu/energy/sites/default/files/documents/2010_mandate_480_en.pdf. Accessed 01 May 2022.
21. CHIESA G., *Technological Paradigms and Digital Eras: Data-Driven Visions for Building Design*, PoliTO Springer Series, Springer International Publishing, 2020.
22. CARPO M., *The second digital turn. Design beyond intelligence*, The MIT press, Cambridge (London), 2017.
23. E-DYCE project official website https://edyce.eu/ Accessed 16/04/2022.
24. LEIRIA D. et al, “Using data from smart energy meters to gain knowledge about households connected to the district heating network: A Danish case”, *Smart Energy*, 2021, vol. 3, p. 100035.
25. PRELUDE project official website https://prelude-project.eu/ Accessed 14 April 2022.
26. CHIESA G., AVIGNONE A., CARLUCCIO T., “A Low-Cost Monitoring Platform and Visual Interface to Analyse Thermal Comfort in Smart Building Applications Using a Citizen–Scientist Strategy”, *Energies*, 2022, vol. 15 no. 2, p. 564. https://www.mdpi.com/1996-1073/15/2/564 Accessed 14 April 2022.
27. CHIESA G., “La prassi progettuale esplicito-digitale e l’approccio prestazionale”, in *Techne*, Firenze University Press, 2017, vol. 13, pp. 236-242.
28. CELENTO D., *Innovate or Perish. New technologies and architecture’s futures*, Harvard Design, 2007, no. 27, pp. 1–9.
29. HAUSLADEN G. et al, “Performative design and quality of architecture. Facade Engineering for IBM Headquarters in Rome”, *Techne*, 2019, n. 18, pp. 288-299.

https://www.proquest.com/docview/2359956574?parentSessionId=QWY73Z%2BwQof8fEfoI2Z%2BRs%2FW8nt8j6p%2BNMgxsDn8GnU%3D&pq-origsite=primo&accountid=28840 Accessed 10 April 2022

30. RATTI C., MATTHEW C., *Architettura Open Source verso una progettazione aperta*, Einaudi, Torino, 2014.
31. TURRIN M., VON BUELOW P., STOUFFS R., "Design explorations of performance driven geometry in architectural design using parametric modeling and genetic algorithms", *Advanced Engineering Informatics*, 2011, vol. 25 no. 4, pp. 656-675.
32. GEYMONAT L., *Storicità e attualità della cultura scientifica*, Insegnare 11:16, 1986.
33. TEDESCHI A., *AAD_Algorithms-Aided Design. Parametric strategies using Grasshopper*, Le Penseur Publisher, Potenza, 2014.
34. OZAKAYA I., AKIN Ö., "Requirement-driven design: assistance for information traceability in design computing", *Design studies*, 2006, vol. 27 no. 3, pp. 381-398.
35. SHI X., YANG W., "Performance-driven architectural design and optimization technique from a perspective of architects", Automation in Construction, 2013, vol. 32, pp. 125-135.
36. BENYUS J. M., *Biomimicry. Innovation inspired by Nature*, HarperCollins, New York, 1997.
37. ALEXANDER C., *Notes on the synthesis of form*, Harvard University Press, Cambridge, 1964.
38. ALEXANDER C., "A city is not a tree", *Architectural Forum*, 1965, vol. 122 no. 11, pp. 58–62.
39. CIRIBINI G., *Brevi noti di metodologia della progettazione architettonica*, Edizioni quaderni di studio, Politecnico di Torino, Torino, 1968.
40. CAVAGLIÀ G., CERAGIOLI G., FOTI M., MAGGI P.N., MATTEOLI L., OSSOLA F., *Industrializzazione per programmi. Strumenti e procedure per la definizione dei sistemi di edilizia abitativa*, Studi e Ricerche RBD, Piacenza, 1975.
41. CIRIBINI G., "Dal «performance Design» Alla Strategia Dei Componenti", *Casabella*, 1969, vol. 33 no. 342, pp. 40-44.
42. CHIESA G., ACQUAVIVA A., GROSSO M., BOTTACCIOLI L., FLORIDIA M., PRISTERI E., SANNA E.M., "Parametric Optimization of Window-to-Wall Ratio for Passive Buildings

Adopting a Scripting Methodology to Dynamic-Energy Simulation", *Sustainability* (Basel, Switzerland), 2019, vol. 11 no. 11, p. 3078.

43. WOODBURY R., BURROW A.L., "Whither design space?", *Artificial Intelligence for Engineering Design, Analysis and Manufacturing*, 2006, vol. 20 (Issue 2, Special Issue: Design Spaces: The Explicit Representation of Spaces of Alternatives), pp. 63-82.
44. KONIS K., GAMAS A., KENSEK K., "Passive performance and building form: An optimization framework for early-stage design support", *Solar Energy*, 2016, vol. 125, pp. 161-179.
45. EnergyPlus official website, https://energyplus.net/. Accessed 10 June 2022.
46. BigLadder software company official website (part of EP Development Team), https://bigladdersoftware.com/epx/docs/8-2/getting-started/energyplus-file-extensions.html#rdd. Accessed 10 June 2022.
47. EVINS R. et al., "EMI report: BESOS – an Expandable Building and Energy Simulation Platform", *Energy Systems and Sustainable Cities group*, University of Victoria, Victoria (BC), available at https://emi-ime.ca/wp-content/uploads/2020/03/UVic_Faure_BESOS.pdf. Accessed 11 June 2022.
48. BESOS official website, https://besos.uvic.ca/. Accessed 11 June 2022.
49. JEPlus on BEST, https://www.buildingenergysoftwaretools.com/software/jeplus. Accessed 11 June 2022.
50. YI ZHANG, "Use jEPlus as an efficient building design optimisation tool", *CIBSE ASHRAE Technical Symposium*, Imperial College, London (UK), 2012, http://www.jeplus.org/wiki/lib/exe/fetch.php?media=docs:072v1.pdf. Accessed 11 June 2022.
51. CHIESA G. (POLITO) et al., "Free running module", *E-DYCE D3.2*, 2022, https://edyce.eu/wp-content/uploads/2022/03/E-DYCE_D3.2_Free-running-module_28.01.2022_Final.pdf. Accessed 11 June 2022.
52. CHIESA G., FASANO F., GRASSO P., "A New Tool for Building Energy Optimization: First Round of Successful Dynamic Model Simulations", *Energies*, 2021, vol. 14, p. 6429, https://doi.org/10.3390/en14196429. Accessed 11 June 2022.
53. OpenStudio official website, https://openstudio.net/. Accessed 10 June 2022.

54. ROTH A., GOLDWASSER D., PARKER A., “There’s a measure for that!”, *Energy and Buildings*, 2016, vol. 117, pp. 321-331, https://doi.org/10.1016/j.enbuild.2015.09.056. Accessed 10 June 2022.
55. OpenStudio SDK User Docs, *About Measures*, https://nrel.github.io/OpenStudio-user-documentation/getting_started/about_measures/. Accessed 10 June 2022.
56. OpenStudio SDK User Docs, *OpenStudio Measure Writer's Reference Guide*, https://nrel.github.io/OpenStudio-user-documentation/reference/measure_writing_guide/#:~:text=In%20its%20most%20basic%20form,osm. Accessed 10 June 2022.
57. OpenStudio SDK User Docs, *Parametric Analysis Tool (PAT) Interface Guide*, https://nrel.github.io/OpenStudio-user-documentation/reference/parametric_analysis_tool_2/#algorithmic-mode. Accessed 10 June 2022.
58. DesignBuilder official website available at https://designbuilder.co.uk/ (UK version), https://www.designbuilderitalia.it/ (Italian version). Accessed 19 April 2022.
59. DesignBuilder UK website, *Parametric Analysis*, available at https://designbuilder.co.uk/helpv5.3/Content/Parametric_Analysis.htm. Accessed 11 June 2022.
60. DesignBuilder UK website, *Optimisation And Parametric Analysis Settings*, https://designbuilder.co.uk/helpv5.3/Content/OptimisationAnalysisSettings.htm. Accessed 11 June 2022.
61. Octopus plug-in manual, online resource available downloading the zip file from Food4Rhino website https://www.food4rhino.com/en/app/octopus or at https://pdfcookie.com/documents/octopus-manual-52e1g5jgw5v8. Both accessed 11 June 2022.
62. Solemma website, *ClimateStudio*, https://www.solemma.com/climatestudio. Accessed 11 June 2022.
63. ClimateStudio User Guide, https://climatestudiodocs.com/. Accessed 11 June 2022.

64. QINGSONG M., FUKUDA H., "Parametric Office Building for Daylight and Energy Analysis in the Early Design Stages", *Procedia, Social and Behavioral Sciences*, 2016, vol. 16, pp. 818-828. https://www.sciencedirect.com/science/article/pii/S187704281506259X. Accessed 29 May 2022.

65. TOUTOU A., FIKRY M., MOHAMED W., "The parametric based optimization framework daylighting and energy performance in residential buildings in hot arid zone", *Alexandria Engineering Journal*, 2018, vol. 57 no. 4, pp. 3595-3608, https://www.sciencedirect.com/science/article/pii/S1110016818301534. Accessed 29 May 2022.

66. FANG Y., *Optimization of Daylighting and Energy Performance Using Parametric Design, Simulation Modeling, and Genetic Algorithms*, PhD degree in Design, UC Berkeley, 2017, https://escholarship.org/uc/item/2zs2h81m. Accessed 29 May 2022.

67. KONIS K., GAMAS A., KENSEK K., "Passive performance and building form: An optimization framework for early-stage design support", *Solar Energy*, 2016, vol. 125, pp. 161-179, available at: https://www.researchgate.net/publication/289501910_Passive_performance_and_building_form_An_optimization_framework_for_early-stage_design_support#fullTextFileContent. Accessed 29 May 2022.

68. FANG Y., CHO S., "Design optimization of building geometry and fenestration for daylighting and energy performance", *Solar Energy*, 2019, vol. 191, pp. 7-18, https://doi-org.ezproxy.biblio.polito.it/10.1016/j.solener.2019.08.039. Accessed 12 June 2022.

69. ZHANG J., JI L., "Optimization of Daylight, Ventilation, and Cooling Load Performance of Apartment in Tropical Ocean Area Based on Parametric Design", *Advances in Civil Engineering*, 2021, vol. 2021, pp. 1-11, https://doi.org/10.1155/2021/6511290. Accessed 12 June 2022.

70. ZHANG A., REGINA B., VAN DEN DOBBELSTEEN A., SUN Y., HUANG Q., ZHANG Q., "Optimization of Thermal and Daylight Performance of School Buildings Based on a Multi-objective Genetic Algorithm in the Cold Climate of China", *Energy and*

Buildings, 2017, vol. 139, pp. 371-384, https://doi-org.ezproxy.biblio.polito.it/10.1016/j.enbuild.2017.01.048. Accessed 12 June 2022.

71. PILECHIHA P., MAHDAVINEJAD M., POUR RAHIMIAN F., CARNEMOLLA P., SEYEDZADEH S., "Multi-objective Optimisation Framework for Designing Office Windows: Quality of View, Daylight and Energy Efficiency", *Applied Energy*, 2020, vol. 261, p. 114356, https://doi-org.ezproxy.biblio.polito.it/10.1016/j.apenergy.2019.114356. Accessed 12 June 2022.
72. BAHDAD A.A.S., FAZDIL S.F.S., ONUBI H.O., BENLASOD S.A., "Sensitivity analysis linked to multi-objective optimization for adjustments of light-shelves design parameters in response to visual comfort and thermal energy performance", *Journal of Building Engineering*, 2021, vol. 44, p. 102996, https://doi-org.ezproxy.biblio.polito.it/10.1016/j.jobe.2021.102996. Accessed 12 June 2022.
73. KHIDMAT R.P., FUKUDA H., KUSTIANI, PARAMITA B., QINGSONG M., HARIYADI A., "Investigation into the daylight performance of expanded-metal shading through parametric design and multi-objective optimization in Japan", *Journal of Building Engineering*, 2022, vol. 51, p. 104241, https://doi-org.ezproxy.biblio.polito.it/10.1016/j.jobe.2022.104241. Accessed 12 June 2022.
74. KIM H., YANG C., MOON H.J., "A Study on Multi-Objective Parametric Design Tool for Surround-Type Movable Shading Device", *Sustainability (Basel, Switzerland)*, 2018, vol. 11 no. 24, p. 7096, https://www.mdpi.com/2071-1050/11/24/7096. Accessed 12 June 2022.
75. BAKMOHAMMADI P., NOORZAI E., "Optimization of the design of the primary school classrooms in terms of energy and daylight performance considering occupants' thermal and visual comfort", *Energy reports*, 2020, vol. 6, pp. 1590-1607, available at https://www.econstor.eu/handle/10419/244148. Accessed 29 May 2022.
76. SUN C., LIU Q., HAN Y., "Many-Objective Optimization Design of a Public Building for Energy, Daylighting and Cost Performance Improvement", *Applied Sciences*, 2020, vol. 20 no. 7, p. 2435, https://www.proquest.com/docview/2387092966?pq-origsite=primo. Accessed 29 May 2022.
77. MANNI M., LOBACCARO G., LOLLI N., BOHNE R.A., "Parametric Design to Maximize Solar Irradiation and Minimize the Embodied GHG Emissions for a ZEB in Nordic and

Mediterranean Climate Zones", *Energies (Basel)*, 2020, vol. 13 no. 18, p. 1, https://doi.org/10.3390/en13184981. Accessed 12 June 2022.

78. MANNI M., NICOLINI A., "Multi-Objective Optimization Models to Design a Responsive Built Environment: A Synthetic Review", *Energies (Basel)*, 2022, vol. 15 no. 2, p. 486, https://www.mdpi.com/1996-1073/15/2/486. Accessed 12 June 2022.
79. GIVONI B., *Passive Low Energy Cooling in Buildings*, John Wiley & Sons, NewYork, 1994.
80. Center for the Built Environment (CBE) website, "Mixed mode. Case studies and project database", College of Environmental Design, University of California, Berkeley. https://cbe.berkeley.edu/mixedmode/index.html. Accessed 28 April 2022.
81. ESTIA SA, *Dial + Version 2.5 User Guide*, Lausanne (Switzerland), 2017. https://www.dialplus.ch/_files/ugd/4e84bd_2b3ac031649c42ccb962f1a24953845b.pdf Accessed 11 June 2022.
82. JOHARI F., MUNKHAMMAR J., SHADRAM F., WIDÉN J., "Evaluation of simplified building energy models for urban-scale energy analysis of buildings", *Building and Environment*, 2022, vol. 211, 108684, https://doi.org/10.1016/j.buildenv.2021.108684. Accessed 29 April 2022.
83. DONALD R., WULFINGHOFF P.E., "Multiple-zone HVAC: An Obsolete Template", *Energy Engineering*, 2011, vol. 108 no. 2, pp. 44-56, https://doi.org/10.1080/01998595.2011.10389019. Accessed 29 April 2022.
84. GROSSO M., *Il Raffrescamento passivo degli edifici*, 3rd ed. Maggioli, Santargangelo di Romagna, 2011.
85. CHIESA, G., GROSSO, M., "Environmental and Technological Design: a didactical experience towards a sustainable design approach", *XV International Forum le Vie dei Mercanti*, Capri, 15-17 July 2017.
86. AGC Glass Configurator https://www.agc-yourglass.com/configurator/en. Accessed 01 May 2022.
87. IEA, *The Future of Cooling. Opportunities for Energy Efficient Air Conditioning*, International Energy Agency, Paris (France), 2018, https://www.iea.org/news/air-

conditioning-use-emerges-as-one-of-the-key-drivers-of-global-electricity-demand-growth Accessed 11 June 2022.

88. SANTAMOURIS, M., *Advances in passive cooling*, Earthscan, London (UK), 2007.
89. CHIESA G., GROSSO M., PEARLMUTTER D., RAY S., "Advances in Adaptive Comfort Modelling and Passive/hybrid Cooling of Buildings", *Energy and Buildings*, 2017, vol. 148, pp. 211-217.
90. IEA – EBC, *Ventilative Cooling. A state-of-the-art review*, Annex 62 Ventilative Cooling, Aalborg University, 2015.
91. BELLERI A., CHIESA G., "Ventilative Cooling potential tool. User guide - version 1.0", *IEA–EBC Programme Annex 62 Ventilative Cooling*, Eurac Research, 2016. https://venticool.eu/wp-content/uploads/2016/11/Ventilative-cooling-potential-tool_User-guide.pdf Accessed 17 April 2022.
92. BELLERI A., PSOMAS T., HEISELBERG P., "Evaluation tool of climate potential for ventilative cooling", 36th AIVC Conference *Effective ventilation in high performance buildings*, Madrid, Spain, 23-24 September 2015, https://www.aivc.org/sites/default/files/6_3.pdf Accessed 17 April 2022.
93. KAMAL M.A., "Shading: A Simple Technique For Passive Cooling And Energy Conservation In Buildings", *Architecture–Time, Space and People, monthly Magazine*, 2011, pp. 18-23. https://www.coa.gov.in/show_img.php?fid=100#:~:text=Shading%20can%20reduce%20the%20peak,dramatically%20affect%20building%20energy%20performance. Accessed 05 May 2022.
94. KUMAR R., GARG S. N., KAUSHIK S. C., "Performance evaluation of multi-passive solar applications of a non air-conditioned building", *International Journal of Environmental Technology and Management*, 2005, vol. 5 no.1, pp. 60 – 75. https://d3pcsg2wjq9izr.cloudfront.net/files/6471/articles/6268/f956437821121110.pdf. Accessed 05 May 2022.
95. GIVONI B., *Man Climate and Architecture*, Elsevier Architectural Science Series, Amsterdam, 1969, pp. 221-224.

96. JIA H., "Weather Converter Program", *Auxiliary EnergyPlus Programs*, http://bigladdersoftware.com/epx/docs/8-3/auxiliary-programs/energyplus-weather-file-epw-data-dictionary.html. Accessed 06 May 2022.

97. REMUND J., MÜLLER S., KUNZ S., SCHILTER C., *Meteonorm Version 7. Global Meteorological Database. Handbook part I: Software*, METEOTEST, Bern (Switzerland), 2012. https://www.energiehaus.es/wp-content/uploads/2015/06/manual-usuario-part-1-meteonorm.pdf. Accessed 07 May 2022.

98. REMUND J., MÜLLER S., KUNZ S., SCHILTER C., *Meteonorm Version 7. Global Meteorological Database. Handbook part II: Theory*, METEOTEST, Bern (Switzerland), 2012. https://www.energiehaus.es/wp-content/uploads/2015/06/manual-usuario-part-2-meteonorm.pdf. Accessed 07 May 2022.

99. TROLL C., PAFFEN K., *Jahreszeitenklimate der Erde*, Velhagen & Schroedel, Berlin, 1969.

100. HEYER E., *Witterung und Klima: eine allgemeine Klimatologie*, BG Teubner Verlagsgesellschaft, Stuttgard-Leipzig, 1988.

101. NAKICENOVIC, N., ALCAMO, J., GRUBLER, A., RIAHI, K., ROEHRL, R.A., ROGNER, H.-H., VICTOR, N., *Special Report on Emissions Scenarios (SRES), A Special Report of Working Group III of the Intergovernmental Panel on Climate Change*, Cambridge University Press, Cambridge, 2000. https://www.ipcc.ch/site/assets/uploads/2018/03/emissions_scenarios-1.pdf Accessed 07 May 2022.

102. IPCC, *Climate Change 2007: Synthesis Report*. *Contribution of Working Groups I, II and III to the Fourth Assessment Report of the Intergovernmental Panel on Climate Change* [Core Writing Team, PACHAURI R.K. and REISINGER A. (eds.)], IPCC, Geneva, Switzerland, 2007. https://www.ipcc.ch/site/assets/uploads/2018/02/ar4_syr_full_report.pdf Accessed 07 May 2022.

103. NARCCAP (North American Regional Climate Change Assessment Program) official website, *The A2 Emissions Scenario*, available at https://www.narccap.ucar.edu/about/emissions.html. Accessed 07 May 2022.

104.Radiance description provided by Radiance website at https://floyd.lbl.gov/radiance/framew.html. Accessed 08 April 2022.

105.Daysim software informer https://Daysim.software.informer.com/4.0/. Accessed 08 May 2022.

106.JACUBIEK J. A., REINHART C. F., *Overview and Introduction to Daysim and Current Research Developments*, Massachusetts Institute of Technology, Building Technology Program, September 2012, available at https://www.radiance-online.org/community/workshops/2012-copenhagen/Day1/Jakubiec/jakubiec%2Creinhart_radiance-workshop-presentation_Daysim.pdf. Accessed 08 May 2022.

107.WORLD GREEN BUILDING COUNCIL, *Principle 2: Prioritise comfort for building users*, online resource https://worldgbc.org/principle-2-prioritise-comfort-building-users. Accessed 14 May 2022.

108.ASHRAE, *ANSI/ASHRAE Standard 55-2013. Thermal environmental conditions for human occupancy*, Atlanta - GA, 2013.

109.VELLEI M., FOSAS D., HERRERA M., NATARAJAN S., "The influence of relative humidity on adaptive thermal comfort", *Building and Environment*, vol. 124, pp. 171-185, https://doi.org/10.1016/j.buildenv.2017.08.005. Accessed 12 May 2022.

110. FERGUS N., HUMPHREYS M., ROAS S., *Adaptive Thermal Comfort: Principles and Practice*, Routledge, Abingdon, 2012.

111. FANGER, P.O., *Thermal Comfort: Analysis and applications in environmental engineering*, Danish Technical Press, Copenhagen, 1970.

112. ISO 7730:2005, *Ergonomics of the Thermal Environment: Analytical determination and interpretation of thermal comfort using calculation of the PMV and PPD indices and local thermal comfort criteria*, International Standards Organization, Gneva, 2005.

113. DE DEAR R. et al., *Developing an adaptive model of thermal comfort and preference – final report on RP-884*, Macquaire University, Sidney, 1997.

114. DE DEAR R., BRAGER G.S., "Thermal comfort in naturally ventilated buildings: revisions to ASHRAE Standard 55", *Energy and Buildings*, 2002, vol. 34 no. 6, pp. 549-561.

115. HUMPHREYS M.A., “Field studies of thermal comfort compared and applied”, *J. Inst. Heat. and Vent. Eng.*, 1976, vol. 44, pp. 5–27.
116. HUMPHREYS M.A., “Outdoor temperatures and comfort indoors”, *Building Research and Practice (J CIB)*, 1978, vol. 6 no. 2, pp. 92–105.
117. HUMPHREYS M.A., RIJAL H.B., NICOL, J.F., “Examining and developing the adaptive relation between climate and thermal comfort indoors”, *Proceedings of Conference on Adapting to Change: New Thinking on Comfort, Cumberland Lodge, Windsor, UK, 9–11 April 2010*, Network for Comfort and Energy Use in Buildings, London, 2010.
118. CEN, *Standard EN 15251:2007. Indoor Environmental Input Parameters for Design and Assessment of Energy Performance of Buildings: Addressing indoor air quality, thermal environment, lighting and acoustics*, Comité Européen de Normalisation, Brussels, 2007.
119. CEN, *EN 16798-1:2019. Energy performance of buildings - Ventilation for buildings - Part 1: Indoor environmental input parameters for design and assessment of energy performance of buildings addressing indoor air quality, thermal environment, lighting and acoustics - Module M1-6*, 2019.
120. NICOL F., “Adaptive thermal comfort standards in the hot–humid tropics”, *Energy and Buildings*, 2004, vol. 36 no. 7, p. 628-637.
121. DE DEAR R.J., LEOW K.G., AMEEN, A., “Thermal comfort in the humid tropics – Part 1: Climate chamber experiments on temperature preferences in Singapore. Part 2: Climate chamber experiments on thermal acceptability in Singapore”, *ASHRAE Transactions*, 1991, vol. 97 no. 1, pp. 874–879; 880–886.
122. CEN, *Light and lighting – Basic terms and criteria for specifying lighting requirements*, European Committee for Standardization, Brussels, 2011.
123. BOUBEKRI M., CHEUNG I., REID K. et al., “Impact of Windows and Daylight Exposure on Overall Health and Sleep Quality of Office Workers: A Case-Control Pilot Study”, *Journal of Clinical Sleep Medicine*, 2014, vol. 10 no. 6, pp. 603-611. Available at: https://www.ncbi.nlm.nih.gov/pmc/articles/PMC4031400/. Accessed 14 May 2022.

124. Hydra website, ASE for LEED calculation method, available at http://hydrashare.github.io/hydra/viewer?owner=chriswmackey&fork=hydra_2&id=Calculate_ASE_for_LEED&slide=0&scale=1&offset=0,0. Accessed 09 May 2022.
125. IES, *LM-83-12. Approved Method: IES Spatial Daylight Autonomy (sDA) and Annual Sunlight Exposure (ASE)*, 2012.
126. USGBC, LEED v4: Daylight, https://www.usgbc.org/credits/healthcare/v4-draft/eqc-0?view=language. Accessed 15 May 2022.
127. IES – ILLUMINATING ENGINEERING SOCIETY, "Glare" definition in *ANSI/IES LS-1-21, Lighting Science: Nomenclature and Definitions for Illuminating Engineering*, available at: https://www.ies.org/definitions/glare/#:~:text=Jul%205%2C%202018,in%20visual%20performance%20or%20visibility. Accessed 14 May 2022.
128. DUTRA DE VASCONCELLOS G., "Evaluation of Annual Sunlight Exposure (ASE) as a Proxy to Glare: A Field Study in a NZEB and LEED Certified Office in San Francisco", Center for the Built Environment, UC Berkeley, 2017, available at https://escholarship.org/uc/item/3js1z0b8. Accessed 15 May 2022.
129. HENRIKSEN R., Optimisation vs. Adaptation: Multi-Parameter Optimisation, Unstudio, online resource https://www.unstudio.com/en/page/8629/optimisation-vs.-adaptation-multi-parameter-optimisation. Accessed 15 May 2022.
130. HOLLAND J.H., "Genetic Algorithms", *Scientific American*, 1992, vol. 267 no. 1, pp. 66-73, http://www.jstor.org/stable/24939139. Accessed 15 May 2022.
131. YANG X.S., "5. Genetic Algorithms", *Nature-Inspired Optimization Algorithms*, Elsevier, 2014, pp.77-87. Available at https://ebookcentral.proquest.com/lib/polito-ebooks/reader.action?docID=1637335. Accessed 15 May 2022.
132. VIERLINGER R., *Multi Objective Design Interface*, Master Thesis (advisor SCHRANZ C.), Technischen Universität Wien, faculty of Civil Engineering, 2013, https://www.researchgate.net/publication/283073414_Multi_Objective_Design_Interface/citations. Accessed 15 April 2022.
133. MOHANTY R., SUMAN S., DAS S.K., "Chapter 16 - Modeling the Axial Capacity of Bored Piles Using Multi-Objective Feature Selection, Functional Network and Multivariate

Adaptive Regression Spline", *Handbook of Neural Computation*, Academic Press, 2017, pp. 295-309.

134. Ladybug tools official website, *Honeybee*, available at https://www.ladybug.tools/honeybee.html. Accessed 16 May 2022.

135. Oknoplast website, *Winergetic premium passive*, https://www.oknoplast.it/finestre-pvc/winergetic-premium-passive. Accessed 27 June 2022.

136. Alfano serramenti website, *Star-One*, http://www.alfanoserramenti.it/public/File/Allegati/301_StarOne%20Italian%20Features.pdf. Accessed 27 June 2022.

137. BROWN G.Z., DEKAY M., *Sun, Wind & Light*, John Wiley & Sons, New York, 2001.

138. CHIESA G., GROSSO M., "Environmental indicators for evaluating properties", *Territorio Italia* (English Ed.), 2015, vol. 2/2015, Roma: Agenzia delle Entrate, pp. 59-70.

139. CHIESA G., GROSSO M., "Accessibilità e qualità ambientale del paesaggio urbano. La matrice microclimatica di sito come strumento di progetto", *Ri-vista. Ricerche per La Progettazione Del Paesaggio*, 2015, vol. 13 no. 1, Firenze: Firenze University Press, pp. 78-91.